UNIVERSITY OF SOUTHAMPTON

Faculty of Engineering and the Environment

School of Civil Engineering and the Environment

Long-term Pore Water Pressure Changes around Subsurface Structures

By

Clive Antonio Wiggan

Thesis for the degree of Doctor of Philosophy

December 2013

UNIVERSITY OF SOUTHAMPTON

ABSTRACT

FACULTY OF ENGINEERING AND THE ENVIRONMENT

SCHOOL OF CIVIL ENGINEERING AND THE ENVIRONMENT

<u>Doctor of Philosophy</u>

LONG-TERM PORE WATER PRESSURE CHANGES AROUND SUBSURFACE STRUCTURES

Clive Antonio Wiggan

Geotechnical engineering guidelines mandate the use of the most onerous hydraulic criteria for the design of earth retaining structures below the water table. Consequently, favourable local conditions, including the geometry of the structure, are not usually exploited. This means that retaining walls in particular are typically designed to resist hydrostatic pressures below the water table. Investigations have shown however that pore water pressures, axial stresses and bending moments reduce when groundwater seepage is allowed through the segmented linings of shallow tunnels. Contiguous pile retaining walls, by their nature, are also permeable. Allowing for groundwater seepage through the gaps in a retaining wall formed from contiguous piles could result in the pore water pressures on the active side of the wall being less than behind conventional impermeable retaining walls such as diaphragm walls.

Numerical simulations, laboratory flow tank experiments and long-term field monitoring were conducted to determine the impact of pile gaps on the hydraulic conditions around contiguous piles. A relationship between the resulting bulk permeability of the equivalent structure and the pile gap was derived from 2D numerical analyses and verified by flow tank experiments. This expression can be used to calculate bulk permeability values for uniform retaining walls representing circular piles in 2D numerical simulations. The permeability relationship was used to calculate and assign equivalent bulk permeability values for a continuous retaining wall of uniform cross-section during the back analysis of the hydraulic conditions around the contiguous pile retaining wall at CTRL, Ashford. Pore water pressures and horizontal total stresses from the back analyses were consistent with those from the field measurements but were much lower than behind retaining walls formed from secant piles in similar conditions.

Dimensionless charts were presented to estimate the groundwater level and the increased settlement observed behind contiguous pile retaining walls. The results demonstrated that the economic advantages of allowing through-wall seepage are greater than the perceived disadvantages.

Table of Contents

List of Tables

List of Figures

xii

xiii

DECLARATION OF AUTHORSHIP

I, Clive Antonio Wiggan declare that the thesis entitled "**Long-term Pore Water Pressure Changes around Subsurface Structures"** and the work presented in the thesis are both my own, and have been generated by me as the result of my own original research. I confirm that:

- this work was done wholly or mainly while in candidature for a research degree at this University;

- where any part of this thesis has previously been submitted for a degree or any other qualification at this University or any other institution, this has been clearly stated;

- where I have consulted the published work of others, this is always clearly attributed;

- where I have quoted from the work of others, the source is always given. With the exception of such quotations, this thesis is entirely my own work;

- I have acknowledged all main sources of help;

- where the thesis is based on work done by myself jointly with others, I have made clear exactly what was done by others and what I have contributed myself;

- parts of this work have been published as: Wiggan *et al.* (2013).

Signed: …………………………………………………………………..

Date:……………………………………………………………………….

Acknowledgements

NOMENCLATURE

Roman Symbols

A	area
c'	effective cohesion
C_H	Hazen's empirical coefficient
CO_2	carbon dioxide
d	pile diameter
D_{10}, D_{50}, D_{90}	soil grain diameter 10%, 50% and 90% finer respectively
D_{33}, D_{100}	days after construction of retaining wall at Ashford
D_s	thickness of soil layer
D_T	tunnel diameter
E	Young's modulus
E_0	one-dimensional stiffness modulus
EC7	Eurocode 7
E_{eq}	equivalent stiffness of the model wall
e_{max}	maximum void ratio
e_{min}	minimum void ratio
F_T	vertical distance from soil surface to tunnel crown
g	acceleration due to gravity
G	shear modulus
GL	ground level
G_s	specific gravity
h	hydraulic head
h_0	far field hydraulic head
h_1	hydraulic head at the distance of influence
h_{11}	hydraulic head at the back of the pile
h_2	hydraulic head at discharge surface
H_D	total head drawdown
h_l	hydraulic head on tunnel lining
H_m	model height
h_M	supply hydraulic head for flow tank simulations
HS	isotropic hardening
I	second moment of area

K	bulk modulus
K_0	coefficient of earth pressure at rest
k_h	horizontal component of soil permeability
k_l	tunnel lining permeability
k_p	bulk permeability of the equivalent structure
k_s	soil permeability
k_v	vertical component of soil permeability
k_w	wall permeability
l_l	distance of influence for numerical model
L_M	flow tank model length for numerical simulations
L_p	pile length
ms	millisecond
mV	millivolt
NAS	normalised analytical settlement
NNS	normalised settlement from numerical analyses
NPP	normalised pore pressures
PI	plasticity index
P_i	pressure transducer number
PSD	particle size distribution
Q	volumetric flowrate
Q_i	flowrates at different pile gaps
r_0	external tunnel radius including liner
r_i	internal tunnel radius
S_{av}	average drawdown
SC_i	spade cells number
S_f	seepage face length
S_{max}	maximum settlement from flow tank experiment
t	thickness of 2D element
U	pore pressure
U_0	in situ pore pressure
v	Poisson' s ratio
V_s	soil volume loss
w_M	model flow tank width
x	pile gap

x, y, z	Cartesian coordinate system
x/d	pile gap to diameter ratio
x_T	horizontal distance from tunnel springline
y	distance from soil surface to seepage face
Z	depth below ground level

Greek Symbols

γ	soil unit weight
γ_w	water unit weight
ρ	vertical displacement
ρ_{dry}	dry density
σ'	horizontal effective stress
σ_h	horizontal total stress
σ_{h0}	in situ horizontal total stress
σ_v	vertical total stress
ϕ'	effective friction angle

Subscripts

Est	estimated from linear seepage approximation
LT	long-term
m	model
max	maximum
min	minimum
p	pile
ST	short-term
Toe	toe of retaining wall

Chapter 1

1.0 Introduction

1.1 Groundwater flow around earth retaining structures

The installation of a substantial retaining structure, of low permeability, into the ground invariably alters the groundwater flow regime. Accordingly, one of the most critical factors when designing structures for service below the water table is the change in pore water pressures due to the impeded flow of groundwater and the influence that this has on the lateral loads acting of the structure. For example, in analysing the pore water pressure distribution behind a retaining wall, it is generally assumed that the phreatic surface intercepts the back of the retaining wall at a depth corresponding to the regional ground water level. Consequently, the usually accepted design practice is to treat the distribution of pore pressures around retaining walls as hydrostatic below the regional water table.

Recognition of the importance of the groundwater flow regime around subsurface structures has led to research into ways of controlling the hydraulic conditions surrounding shallow tunnels below the water table. It has been shown that tunnels with segmented linings allow groundwater seepage through the spaces in the linings and are known to act as sinks in fine soils. This supposition is based on extensive investigations into the hydraulic conductivity of segmented tunnel linings and research into other methods, based on groundwater seepage, which could possibly reduce the pore water pressures acting on tunnel linings. These research have established that the pore water pressure distribution around shallow tunnels is affected by whether or not groundwater is allowed to seep through the gaps in the tunnel linings (Shin *et al*., 2002; Nam and Bobet, 2006; Park *et al*., 2008; Arjnoi *et al*., 2009 and Shin, 2010).

Despite the evidence supporting the influence of segmented tunnel linings on the hydraulic conditions in the surrounding soil, there is still limited research into the hydraulic serviceability conditions of other leaky earth retaining structures below the water table and on how they impact the long-term groundwater flow regime. This means that there is scope for further research into how the geometry of subsurface structures affects groundwater flow and into ways in which this might be quantified and incorporated into design guidelines.

Retaining walls formed from contiguous piles are, by their nature, permeable unless considerable and usually expensive measures are undertaken to prevent groundwater seepage through the pile gaps. Thus, the hydraulic regimes around retaining walls formed from contiguous piles differ from those around continuous retaining walls and walls formed from secant piles where the bulk permeability of the equivalent structure, for design purposes, is extremely low. This means that the magnitude of pore water pressures and lateral loads behind retaining walls with gaps, such as those formed from contiguous piles, should be less than behind uniform retaining walls.

It is evident however, that design standards and guidelines do not generally differentiate between the hydraulic conditions around retaining walls formed from contiguous piles and those formed from secant piles, for example, in how the pore water pressures are treated. However, CIRIA 104 and CIRIA 580, which supersedes it, briefly acknowledge that economic advantages may be realized by designing a retaining wall to

facilitate through-wall seepage (Gaba *et al*., 2003). These reports, however, do not elaborate nor do they make it explicitly clear that the groundwater flow regime around retaining walls formed from contiguous piles differs from that around traditional impermeable walls by the fact that the former allow through-wall seepage.

The increasing prevalence of numerical applications for investigating groundwater flow problems has demonstrated that some retaining structures, based on their geometry, may be treated as being permeable. If a retaining wall in particular were to be treated as permeable, then it would be useful to have a relationship between the resulting bulk permeability, k_p, of the region affected by the introduction of the retaining structure and the pile gaps for 2D numerical analyses. This report presents the results of 2D numerical simulations of a laboratory flow tank, which were carried out to determine the impact of pile gaps on the hydraulic conditions around contiguous piles. An expression was derived relating the soil permeability, k_s, the pile gap to diameter ratio, *x/d*, and the bulk permeability of the region influenced by the low permeability pile section, k_p. The numerical results were verified by laboratory flow tank experiments. The derived bulk permeability expression was subsequently used to calculate the permeability of the uniform wall representing the contiguous piles in the back analyses of field data from Channel Tunnel Rail Link (CTRL), Ashford. The results from the plane strain analyses compared well with the field measurements.

1.2   Aim and objectives

Investigations were carried out with the aim of determining and quantifying the hydraulic regime around contiguous piles in fine soils.

The objectives of this thesis are to:

- Analyse the state of research into the effect of long-term pore water pressure changes around retaining structures below the water table.
- Review existing research in which two and three-dimensional numerical analyses were used to investigate the long-term hydraulic conditions around subsurface structures, with emphasis on retaining structures in fine soils.

- Investigate, using 2D plane strain analyses of a horizontal plane section, the influence of pile gaps on the groundwater flow regime around contiguous piles.
- Derive an expression for the bulk permeability, k_p, of the equivalent structure for the region influenced by the installation of the piles.
- Study the phreatic effects of applying calculated values of k_p, using the derived expression, to a uniform retaining wall representing contiguous piles in a vertical plane during 2D numerical simulations.
- Verify the permeability relationship derived from the numerical analyses by way of laboratory experiments of groundwater flow in a flow tank.
- Collect, process and analyse the long-term pore water pressure monitoring data from an instrumented section at the site of a contiguous pile retaining wall in overconsolidated clay.
- Identify and analyse the long-term pore water pressure changes around a retaining wall formed from secant piles.
- Use 2D numerical simulations to back analyse field data from the instrumented section of a contiguous pile retaining wall.

This report describes research conducted towards fulfilling these objectives and outlines suggestions for future work.

1.3   Outline of the report

Chapter 2 comprises a review of research into the hydraulic regime around subsurface structures. Existing design guidelines for the treatment of pore water pressure distributions around retaining structures are examined.   Emphasis is placed on research into ways of reducing pore water pressures around in-ground and belowground structures, drawing on the experiences gained from research into segmented linings for shallow tunnels.   Although the literature on the hydraulic conditions around retaining walls is scarce, efforts were made, where appropriate, to relate previous research on shallow tunnels to retaining walls. The chapter also includes a review of numerical analyses of groundwater flow problems with particular emphasis on the methods used to investigate retaining walls and shallow tunnels.

Chapter 3 describes numerical investigations carried out to determine the impact of pile gaps on the groundwater flow regime around contiguous piles in a horizontal plane. A relationship between the soil permeability, k_s, the bulk permeability of the equivalent structure, k_p, and the pile gap to diameter ratio, x/d, was determined. This relationship is useful in calculating the bulk permeability values for contiguous piles represented by continuous walls of uniform cross-sections in 2D vertical plane analyses. The expression was subsequently applied to a continuous retaining wall model to study the phreatic effects on the groundwater flow regime. Parts of this chapter were published as:

- Wiggan, C.A., Richards, D.J. and Powrie, W. (2013). Numerical modelling of groundwater flow around contiguous pile retaining walls. In *Proceedings, 18th European Conference on Soil Mechanics and Geotechnical Engineering*, Paris, September 2013.

In Chapter 4, the verification, by way of laboratory flow tank experiments, of the permeability expression derived from the numerical analyses in Chapter 3 is described. The experimental setup, procedures and results are discussed. Corresponding laboratory experiments to determine the soil properties and the calibration of pore pressure transducers are outlined. Parts of this chapter are currently under review for *Geotechnique*:

- Wiggan, C.A., Richards, D.J. and Powrie, W. (2013) Hydraulic changes around contiguous piles: Laboratory investigation.

A case study of the long-term pore pressure and horizontal total stress field data from an instrumented section of the cut and cover tunnel with retaining walls formed from contiguous bored piles at Channel Tunnel Rail Link, Ashford is presented and discussed in Chapter 5. The geology of the area, construction processes and sequence and the instrumentation of the construction site were previously described in detail by authors such as Clark (2006) and Richards *et al*., (2007). In this Chapter, the changes in pore pressures and horizontal stresses from the short-term conditions following construction, medium-term and long-term starting with the establishment of hydraulic equilibrium conditions are discussed.

In Chapter 6, two-dimensional simulations to back analyse the hydraulic conditions around the instrumented section of the contiguous pile retaining wall at Ashford are

described. The results of parametric studies conducted to determine the influence of the retaining wall and soil geometric properties are also presented and discussed. Monitoring data from the construction site at Ashford and the analyses in Chapter 5 were used to validate the numerical model.

Chapter 7 contains the conclusions arising from this research and recommendations for further research are made.

Chapter 2

2.0 Review of investigations into the hydraulic regime around retaining structures

2.1 Introduction

The laminar flow of groundwater through the inter-particulate spaces of a soil matrix is driven by the difference in hydraulic potential between two positions in the soil. Additionally, the rate at which groundwater flows through the soil depends on, among other things, the hydraulic conductivity of the soil. A consequence of this flow mechanism is that any activity, which disturbs the *in situ* soil state, could influence the groundwater flow regime. For instance, if a structure of lesser permeability than the surrounding soil, such as an impermeable retaining wall, is introduced into the ground, it may cause a damming effect resulting in pore water pressure (U) build-up on the retained side of the structure. This excess pore water pressure directly affects the ability of a saturated soil to resist a shearing force due to its influence on the soil effective

stress (σ') according to Terzaghi's equation (Equation 2.1). Engineering structures in fine soils are particularly susceptible to changes in pore water pressure. Therefore, an understanding of the long-term impact of hydraulic conditions around subsurface structures is important. Recognising this, Powrie (2008) draws attention to the medium and long-term failure of some engineering structures due to unforeseen high pore water pressures attained at equilibrium. The review reinforced the argument by Vaughan and Walbancke (1973) that the delayed failure of some engineering structures, in overconsolidated clay, was due to the gradual recovery of pore water pressures to their new equilibrium positions. Consequently, stability and serviceability checks conducted during the geotechnical engineering design phase of a construction project should be based on realistic estimates of equilibration times and the corresponding pore water pressures.

$$\sigma' = \sigma - U \qquad\qquad\qquad\text{Equation 2.1}$$

Anthropogenic activities to create more urban space further necessitate the introduction of various infrastructures into the natural ground. These actions range from the construction of deep basements and storage facilities to infrastructure work such as the construction of tunnels and roadways. One common feature, regardless of the size of the construction, is the removal or displacement of the *in situ* soil and its subsequent replacement with materials, which are usually of lower permeability. The inevitable consequence is the alteration of the groundwater flow regime and stress states in the soil. Other construction-induced changes to the soil conditions are manifest in the form of ground movements and volumetric changes, which may give rise to variations in pore water pressure. Research has shown, for instance, that as the soil within an area supported by diaphragm walls is excavated, the pore water pressures in the retained soil decrease (Clausen *et al.*, 1987; Ou *et al.*, 1998; Forth 2004 and Clark, 2006). This is due in part to stress relief in the surrounding soil and the movement of the wall away from the soil as posited by Gunn and Clayton (1992).

It is widely acknowledged that hydraulic conditions around earth retaining structures below the water table are perhaps the most critical and yet some of the most difficult design criteria to determine. This is particularly so in fine soils where small changes in the flow of groundwater can significantly affect the pore water pressure distribution and increase the lateral loads on earth retaining structures. Investigations into possible

mitigating measures are therefore required. One such option is the examination of the ways in which the geometry of civil engineering structures influences the pore water pressures in the surrounding soil.

This chapter presents a review of the hydraulic regime around subsurface structures, with emphasis on shallow tunnels and retaining walls below the water table. Investigations into the influence of construction activities on pore water pressure distribution, research into methods of mitigating pore pressure build-up and the use of numerical analyses to investigate the interaction of groundwater and subsurface structures are all considered.

2.2 Investigation of groundwater flow regimes around shallow tunnels

Pore water pressures and leakages are two of the fundamental considerations in the design of shallow tunnels below the water table. As a result, and due to the uncertainties surrounding the hydraulic conditions, tunnel designers tend to make overly conservative assumptions. These assumptions usually lead to the use of full hydrostatic pressures below the water table (Guilloux, 1994; Lee and Nam, 2001; Bobet, 2003; Fahimar and Zareifard, 2009 and Shin *et al.*, 2009). If a tunnel lining is treated as been impermeable, then the assumption is that there is no groundwater flow towards or through the tunnel lining. The lack of seepage paths through the tunnel lining can contribute to increased pore water pressures and the development of large axial forces and bending moments on the lining of fully waterproofed tunnels (Shin *et al.*, 2002; Fahimifar and Zareifard, 2009 and Shin *et al.*, 2010). This means that the ratio of the bulk soil-lining permeability to that of the surrounding ground permeability, k_l/k_S, is 0.

The use of impermeable linings for shallow tunnels is however deemed uneconomical and has led to increased research into the design of permeable linings for shallow tunnels located below the water table. Consequently, it is acknowledged that allowing groundwater to seep through the linings, as happens naturally with segmented tunnel linings, can cause a reduction in the hydraulic heads at the tunnel relative to the surrounding ground as shown in Figure 2.1. This reduced hydraulic head may be attributed to the drawdown of groundwater in the soil adjacent to the level of the tunnel spring line or to the level of the tunnel invert when a drainage blanket is provided. The higher hydraulic gradient induced by the permeable tunnel linings can cause greater groundwater flow towards the tunnel face at which the surface pressure is usually atmospheric. Some investigations into the impact of tunnel lining permeability on the hydraulic loadings and methods of reducing pore water pressures around shallow tunnels are described in the following sections.
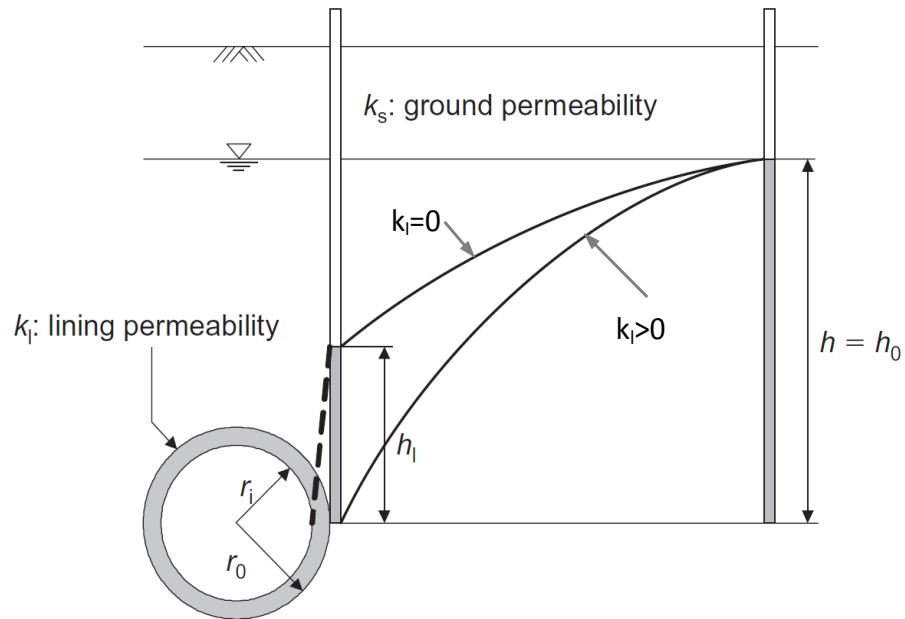
Figure 2.1: Influence of tunnel lining permeability on the hydraulic gradients in the surrounding soil (From Shin, 2010). Higher hydraulic head, h_1, observed with fully waterproofed tunnel lining.

2.2.1 Varying the hydraulic conductivity of tunnel linings

The presence of tunnels, particularly in fine soils, provides new hydraulic boundaries, which influence the direction of groundwater flow considerably. This is illustrated by field measurements performed by Ward and Thomas (1965) and Palmer and Belshaw (1980) who showed that the subsequent flow of groundwater depended on the hydraulic conditions of the tunnel linings. Further research concluded that, where segmented tunnel linings were used for shallow tunnels, groundwater flow was induced towards and consequently through the tunnel linings. Segmented tunnel linings may therefore be treated as permeable (Ward and Pender, 1981; Mair,1993 and Wongsaroj *et al.*, 2007). This recognition of the influence of segmented linings on the hydraulic conditions around shallow tunnels is in contrast to Atkinson and Mair's (1983) assertion that groundwater loadings do not change significantly in the presence of varying hydraulic boundary conditions and were therefore the same whether or not the tunnel lining was fully waterproofed. The assumptions made by Atkinson and Mair (1983) were however only valid where there was a constant head of water above a tunnel such

as for tunnels located in fine soils under a body of water. The seepage of water into a tunnel, under these conditions, would not be sufficient to affect the total head of water acting on the tunnel lining. It was further acknowledged that the advantages of reduced water pressures obtained by allowing seepage through linings into the tunnel would be lost by the development of significant steady-state seepage induced stresses on the soil grains and on the tunnel linings below, for example, a river. The use of advanced investigative techniques such as numerical analysis have however shown that for shallow tunnels without a constant head of water above, considerable reductions in the hydraulic loads acting on the tunnel linings may be realised by varying the hydraulic conditions of a tunnel lining.

The use of computer applications for geotechnical problems

Numerous investigations into the effect of varying the hydraulic conductivity of linings for shallow tunnels were reported in the literature. While these investigations were conducted by different researchers, geographically and chronologically separated, the preferred method, particularly for research conducted during the past three decades, seemed to be the use of two and three-dimensional numerical analyses. This increased research interests into the hydraulic conditions around tunnels were due in part to the ready availability of computer applications specifically designed for geotechnical engineering analyses. Hence, the paucity of data on investigations into the effect of hydraulic properties of segmented tunnel linings prior to about three to four decades ago.

In addition, there seemed to be a preference for 2D over 3D numerical simulations with predominantly 2D analyses reported in the literature. Two dimensional analyses usually produce satisfactory results with a fair degree of accuracy and are particularly suitable for tunnels in which the high ratio of out of plane dimensions to tunnel diameter made them ideal for plane strain analyses (Ghaboussi *et al*., 1978 and Sakurai, 1978). The default choice for the investigation of geotechnical problems in tunnelling therefore seemed to be 2D plane strain analysis. Benmebarek *et al*. (2008) posited that the prevalence of 2D simulations might also be due to the complexity, prohibitively high costs and amount of time needed to conduct 3D analyses. The availability of experienced modellers with the requisite skills to model subsurface structures in three-

dimensions might also be a factor. Consequently, several researchers modelled segmented tunnel linings in 2D plane strain analyses in which the ratio of the lining, k_l, to soil, k_s, permeability was greater than one, $k_l/k_s > 1$. For $k_l/k_s > 1$, the pore water pressures on the tunnel lining were zero and increased with distance away from the tunnel as might be expected in the presence of groundwater seepage towards the face of a tunnel (Shin *et al*., 2002; Lee *et al*., 2003; Yoo, 2005; Bobet and Nam, 2007; Kolymbas and Wagner, 2007 and Arjnoi *et al*., 2009). Arjnoi *et al*. (2009), for example, used field data to validate 2D analyses of the pore water pressures and lining stresses in a drained tunnel in medium dense sand using the finite element package, ABAQUS. Two drainage conditions were considered in the study;

i) A fully drained tunnel in which the pore pressures on the tunnel linings were equal to zero and

ii) A tunnel in which a constant head of water was maintained above the tunnel lining similar to the conditions examined by Atkinson and Mair (1983).

Figure 2.2 is a normalization and complete re-plot of the variation of pore pressures with horizontal distance from the tunnel spring line using data from Arjnoi *et al*. (2009). Pore water pressures were normalised using the product of the unit weight of water, γ_w and the vertical distance, F_T, from the soil surface to the tunnel crown ($U/\gamma_w F_T$). The horizontal distance, x_T, from the tunnel spring line was also normalised using the distance F_T.
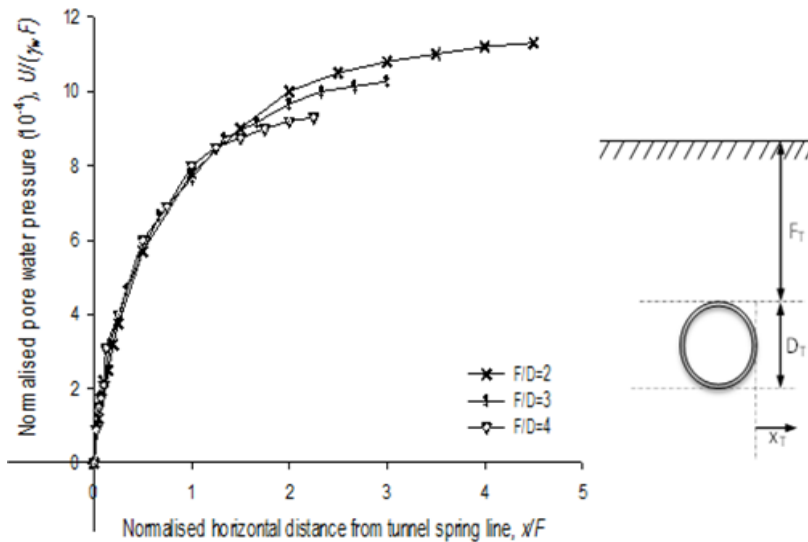
Figure 2.2: Variation of normalised pore water pressures, $U/(\gamma_w F)$, with normalised horizontal distance from tunnel spring line, x/F, using data from Arjnoi *et al*. (2009).

It is evident from Figure 2.2 that the normalised pore water pressures increased with normalised horizontal distance from the tunnel. This trend was consistent at various F/D ratios. It was further observed that at larger values of F/D the distance at which pore pressures continued to be affected by the lining permeability decreased. The results from Arjnoi *et al*. (2009) compared well with the analytical solutions for pore water pressure distribution around drained tunnels described by Lei (1999) and Park *et al*. (2007). The correlation of results from analytical, field and numerical analyses, in this instance, suggests that 2D analyses were adequate for investigation of the hydraulic conditions around shallow tunnels.

Influence of seepage on bending moments and axial forces

A major advantage of allowing seepage through tunnel linings, as demonstrated by the use of numerical analyses, is the reduction in axial forces and bending moments on the tunnel lining. The magnitudes of stresses and axial forces for permeable tunnel linings, although inconsistent, were shown to be significantly less than on watertight tunnel linings. For example, stresses and axial forces on the segmented tunnel linings with a permeability ratio of $k_l/k_s>1$ were lower than those on the watertight linings by, up to 30% Schweiger *et al*. (1991); 25% Lee and Nam (2001); 20% Arjnoi *et al*. (2009) and

14

by up to 70% Lee and Nam (2006). It was noted, however, that these reports did not seek to differential between the magnitudes of the changes in axial forces and bending moments but treated both together. This could be misleading unless both the axial stresses and bending moments changed by the same percentage amounts. Furthermore, the use of $k_l/k_s>1$ might be considered unrealistic as the bulk permeability of the equivalent structure (comprising lining and the soil in the spaces between) depends on the permeability of the soil in the spaces of the tunnel lining. Therefore, in the reported investigations, assuming that the liners were made of impermeable material, then groundwater seepage through the segmented linings was limited by the soil cross section in contact with the flow-tubes created by the lining. A more practical approximation of the bulk permeability ratio, k_l/k_s, might be in the range $0 \leq k_l/k_s < 1$ for linings made of impermeable material.

Influence of soil permeability

It was further recognised that for tunnels in fine soils such as clays to act as drains there need to be significant differences in the bulk permeability of the tunnel linings and the surrounding soil. For example, during investigations into the hydraulic conditions around a shallow tunnel, Gourvenec *et al*. (2005) showed that sandy fissures in the London Clay caused the differences in permeability of the soil and tunnel linings to be negligible. This was evident by the surprisingly small amount of localised seepage through the segmented linings, which did not provide the usual low-pressure boundary typical of segmented tunnel linings in fine soils. In addition, the observed pore water pressures were not influence significantly by the use of segmented instead of waterproofed linings. The lack of substantial differences in permeability, between the soil and lining, therefore resulted in the tunnel not acting as a drain as would be expected with segmented tunnel linings in fine soils. If a seepage or drainage path was provided by the tunnel lining, then the distance at which reduced pore pressures were observed would be considerably greater. The local geology can therefore influenced the usefulness of a tunnel lining to act as a drain. These have implications for the design of segmented tunnel linings for shallow tunnels in which pore pressure reduction methods are being considered.

2.2.2 Impact of tunnel lining permeability on soil displacement

Several authors investigated the impact that allowing groundwater flow through tunnel linings have on the vertical and horizontal displacements of the soil adjacent to shallow tunnels and at ground surface level. Two types of soil displacements were usually considered;

i) The size of the surface settlement trough or subsidence in the long-term and
ii) Instability at the advancing face of the tunnel.

For the purpose of this study, the former is of interest. The influence of tunnel construction on the development of surface settlement troughs was investigated extensively (Peck, 1969; O'Reilly and New, 1982; Mair *et al*., 1993; Sinclair and Norfolk, 2001; Shin, 2008; Yoo *et al*., 2008 and Lee *et al*., 2009). Attempts have been made to relate the amount of drawdown of groundwater levels caused by seepage through tunnel linings to the observed soil vertical displacement (Yoo, 2005; Park *et al*., 2008 and Lopez-Fernandez *et al*., 2013). Yoo (2005), for instance, investigated the interaction between tunnels and groundwater using 3D stress-pore pressure coupled finite element numerical simulations. The results showed that consolidation volume losses increased with increasing drawdown due to seepage into the tunnel as illustrated in Figure 2.3.
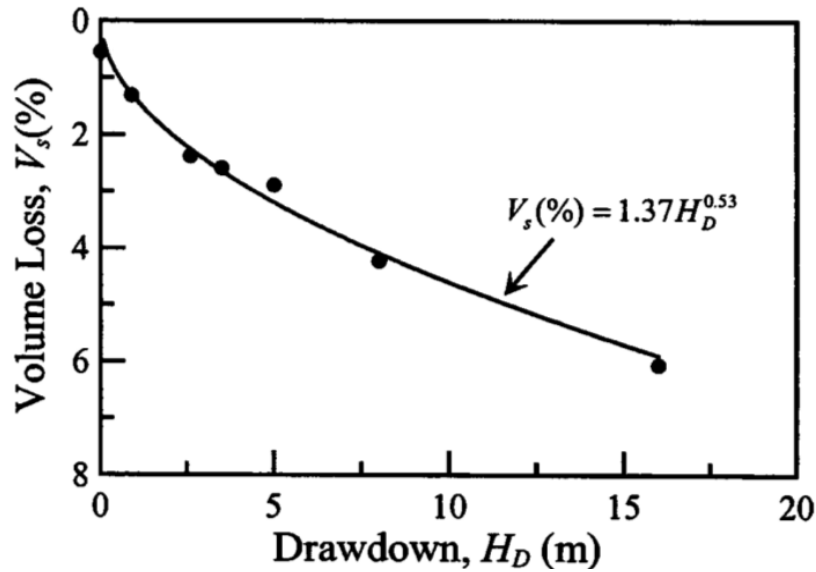
Figure 2.3: Relationship between consolidation volume loss and drawdown for tunnels (From Yoo, 2005).

A useful relationship between the volume loss and drawdown, shown in Equation 2.2, was proposed.

$$V_s = 1.37 H_D{}^{0.53} \qquad\qquad \text{Equation 2.2}$$

where V_s is the soil volume loss expressed as a percentage of the total tunnel volume and H_D is the total head drawdown in metres of water. The use of the term 'volume loss', in this context, deviated slightly from the conventional definition of soil volume loss due to tunnel over-excavation. Soil volume loss is usually defined as the volume of surface settlement expressed as a percentage of the theoretical volume of the excavated soil in the tunnel. Notwithstanding the slight difference in definitions, Lee and Ng (2002) made similar observations while conducting 3D simulations of ground settlement. Lee and Ng (2002) used a linear elastic perfectly plastic soil model to conduct 3D simulations of the tunnelling problem previously investigated in 2D by Addenbrooke *et al*. (1997). The study showed that the surface settlement troughs from the 3D analysis more closely represented field measurements and analytical solutions than the 2D simulations performed by Addenbrooke *et al*. (1997). Addenbrooke *et al*. (1997) however modelled the soil as a non-linear perfectly plastic model. Furthermore, the tunnel depths and diameters in the two investigations were different. These

fundamental differences could have contributed to the discrepancies between both results.

Hofle *et al*. (2009) also showed using 3D analyses that the magnitude of the settlement trough above a tunnel in soft soil increased with soil permeability. An increase in the soil hydraulic conductivity of an order of magnitude caused the maximum vertical displacement to increase by between 25% and 30%. This further suggests that soil settlement should increase as the lining permeability increased due to the explicit relationship between the soil and bulk permeability of the equivalent structure.

The observed differences in the magnitudes and shapes of the vertical displacement troughs obtained from numerical simulations may also be attributed to the influence of the constitutive soil models adopted for the analyses. For instance, Hejazi *et al*. (2009) used three soil constitutive models to investigate the impact of vertical displacement with distance from a tunnel. The results, shown in Figure 2.4, demonstrate that a Mohr Coulomb soil model produced unrealistic settlement magnitudes and profiles. An elasto-plastic soil model with isotropic hardening (HS) as described by Schanz *et al*. (1999) and a small strain stiffness model (HS-small) produced displacement profiles similar to those from empirical approximations and to those from field measurements. The wider settlement troughs observed from the Mohr Coulomb soil model were attributed to the inability of the soil models governed by the Mohr Coulomb failure criteria to simulate adequately changes in soil stiffness.
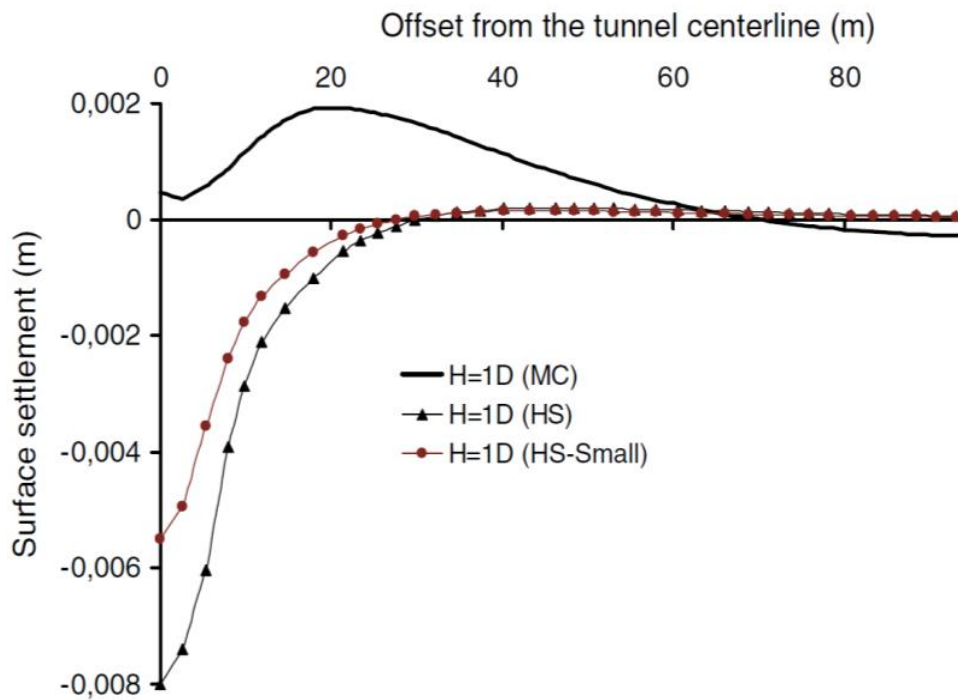
Figure 2.4: Effect of constitutive soil models on soil settlement troughs (From Hejazi *et al.*, 2009).

The investigations into the hydraulic conditions around shallow tunnels demonstrated that there were significant benefits to be derived from having tunnels in fine soils acting as drains. There were however negative implications which were manifest mainly as soil displacements. Consequently, a compromise is required between drainage and the amount of acceptable settlement for instance. This should be considered with respect to the higher pore pressures developed around impermeable structures. Similarly, the impact on the surrounding soil and the groundwater flow regime caused by semi-permeable structures must also be considered. Recognition of the possible deleterious effects of through-structure seepage has led to the recommendation of certain mitigating measures. These included, among other things, application of soil improvement techniques such as grouting to reduce soil volume losses caused by consolidation and tunnel excavation (Rowe *et al.*, 1983 and Yoo, 2005). These actions were meant to reduce the amount of soil instability and vertical displacement while exploiting the benefits of allowing seepage through the tunnel linings.

2.3 Investigation of hydraulic conditions around retaining walls

The influence of retaining wall construction on the development of soil stresses and pore water pressures in fine soils is well established. The techniques used to investigate these effects include, but are not limited to;

- i) Field observations,
- ii) Numerical analyses and
- iii) Laboratory investigations.

In the following sections, the effect that retaining walls have on the hydraulic regime in the surrounding soil was investigated. The influence of retaining wall construction on the *in situ* soil stresses and pore water pressures along with a review of numerical simulation of long-term groundwater flow regimes around retaining walls were all considered. Comparisons were also made between field investigation of conventional impermeable retaining walls such as those formed from secant piles and semi-permeable retaining walls made of contiguous piles.

2.3.1 Influence of retaining wall installation

Guoping *et al*. (2008) used 3D numerical analyses to investigate the impact on the groundwater regime of installing large foundations, idealised as blocks, into the ground. The influence on the groundwater flow was examined for soil/wall permeability ratios, k_s/k_w ranging in values from 1 to 10^3. The results showed that the presence of the low permeability foundations significantly alter the hydraulic conditions in the surrounding soil such that the bulk permeability of the flow region investigated decreased by up to 70%. This reduction in soil permeability was however, much less than that reported by Jiao *et al*. (2006) who suggested a decrease of between 14 and 20 times the soil *in situ* permeability when foundation blocks are installed. The differences between the results from Jiao *et al*. (2006) and Guoping *et al*. (2008) could perhaps be attributed to several factors including the boundary conditions adopted and the values assigned to the permeability ratio k_s/k_w during the numerical simulations.

20

Others have studied the effect of the installation of replacement type earth retaining structures on the *in situ* soil stresses and pore water pressures in fine soils. Kutmen (1986) for example, investigated the evolution of pore water pressures and horizontal stresses behind a diaphragm wall and a bored pile retaining wall using the finite element programme, CRISP. The diaphragm wall was modelled in 2D plane strain while the circular bored piles were modelled axi-symmetrically. An immediate reduction in pore water pressures due to excavation for the wall was observed as shown in Figure 2.5.
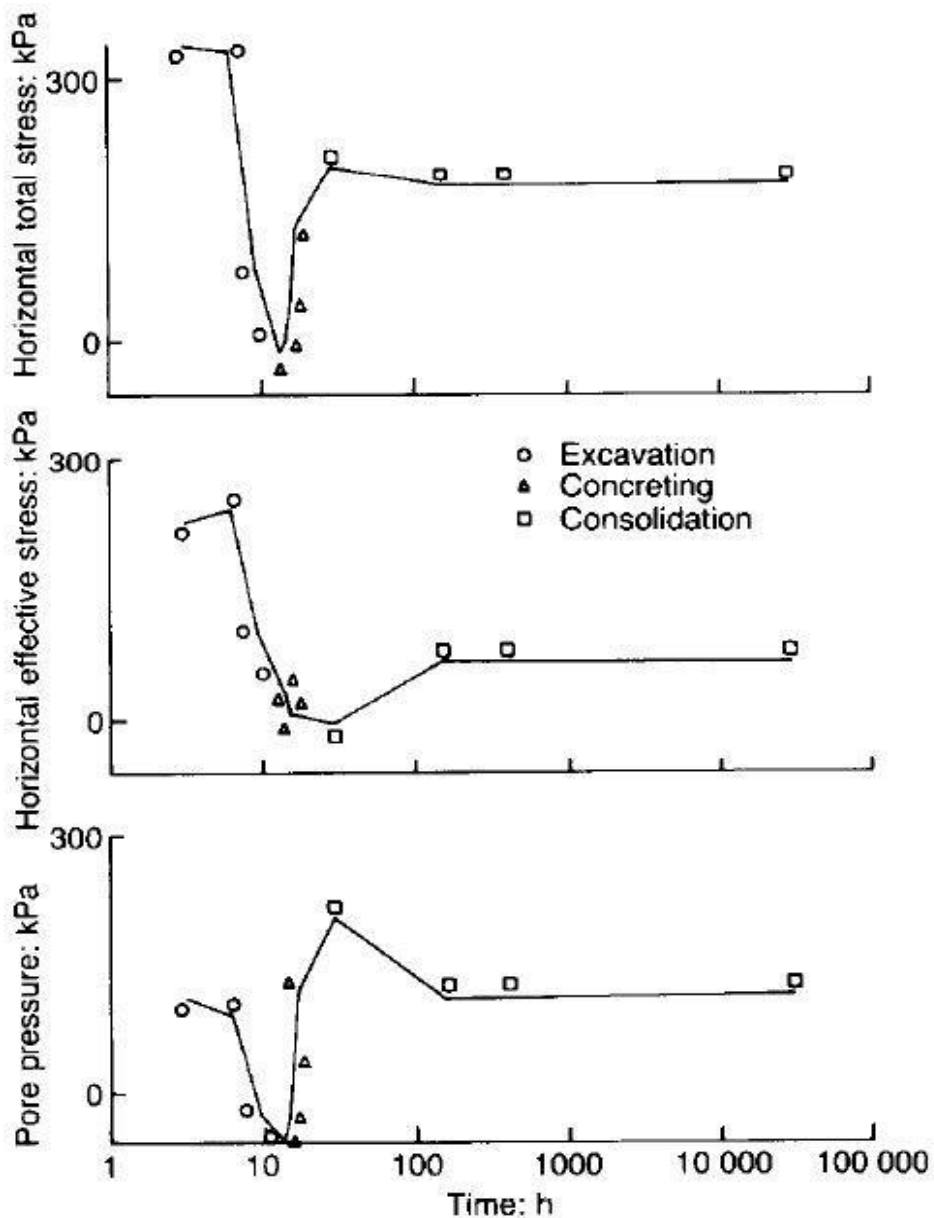
Figure 2.5: Horizontal stresses and pore water pressures calculated by finite element analyses for soils adjacent to bored piles (From Kutmen, 1986).

21

The water pressures increased to above their pre-installation values once concreting commenced. During the long-term consolidation phase, pore pressures fell to about the *in situ* values. Long-term horizontal total and horizontal effective stresses were also much less than the pre-installation values. These results corresponded to the generally observed trend of changes in pore water pressures induced by the installation of retaining walls and the subsequent long-term pore pressure distribution behind impermeable structures as obtained from numerical analysis (Fourie and Potts, 1989; Carder and Symons, 1989; Gunn *et al*., 1992; Ng, 1994; Rampello *et al*., 1998; Gourvenec and Powrie, 1999 and Benmebarek *et al*., 2006). Field investigations have also produced similar results in which a less than perfectly supported excavation of the soil caused a general decrease in pore water pressures and horizontal stresses (Gunn and Clayton, 1992; De Moor, 1994; Ou *et al*., 1998 and Richards *et al*., 2006). Subsequent concreting resulted in an increase in pore pressures and lateral stresses while the long-term conditions reverted to near their pre-installation values as would be expected for impermeable earth retaining walls.

Higgins *et al*. (1989) compared the numerically calculated and measured performance of a retaining wall embedded in London Clay at Bell Common using soil parameters obtained from an instrumented section of the wall. It was shown that installation of the secant pile retaining wall significantly influenced the build-up of soil stresses and pore water pressures behind the wall. The decrease and subsequent increase in pore water pressures during the installation of the retaining wall and the long-term pore pressure equilibrium observed by Kutmen (1986) and others are also evident from these investigations. Higgins *et al*. (1989) also demonstrated that modelling the retaining wall installation sequence properly and accurately provided closer approximation to field measurements.

Symons and Carder (1993) investigated the development of pore water pressures and horizontal stresses around a retaining wall formed of contiguous piles and around a diaphragm wall, both in London Clay. Pore water pressures were measured using pushed-in spade-shaped pressure cells fitted with high air entry pneumatic piezometers as described by Tedd *et al*. (1984). A similar trend in pore pressures as discussed for Higgins *et al*. (1989) was reported. Powrie and Kantartzi (1996) and Richards *et al*. (1998) conducted centrifuge tests which gave comparable results. The results from

Symons and Carder (1993) confirmed a previous investigation by Carder and Symons (1989). Closer examination of the results presented in Figure 2.6, which Symons and Carder (1993) indicated were the same for the contiguous pile retaining wall, however suggested that long-term equilibrium conditions were not achieved at the time. The piezometer readings at 14.5 m and 11 m were clearly still increasing and decreasing respectively. Furthermore, the indicated time of about 23 days was unrealistically short for complete dissipation of excess pore water pressures to take place in an overconsolidated clay. This was evident from the observation of approximately 95% dissipation of pore water pressures in similar soil after about 4 years as illustrated in the two dimensional numerical simulations performed by Powrie and Li (1991). However, Symons and Carder (1993) were more concerned with installation effects than long-term pore pressure conditions.
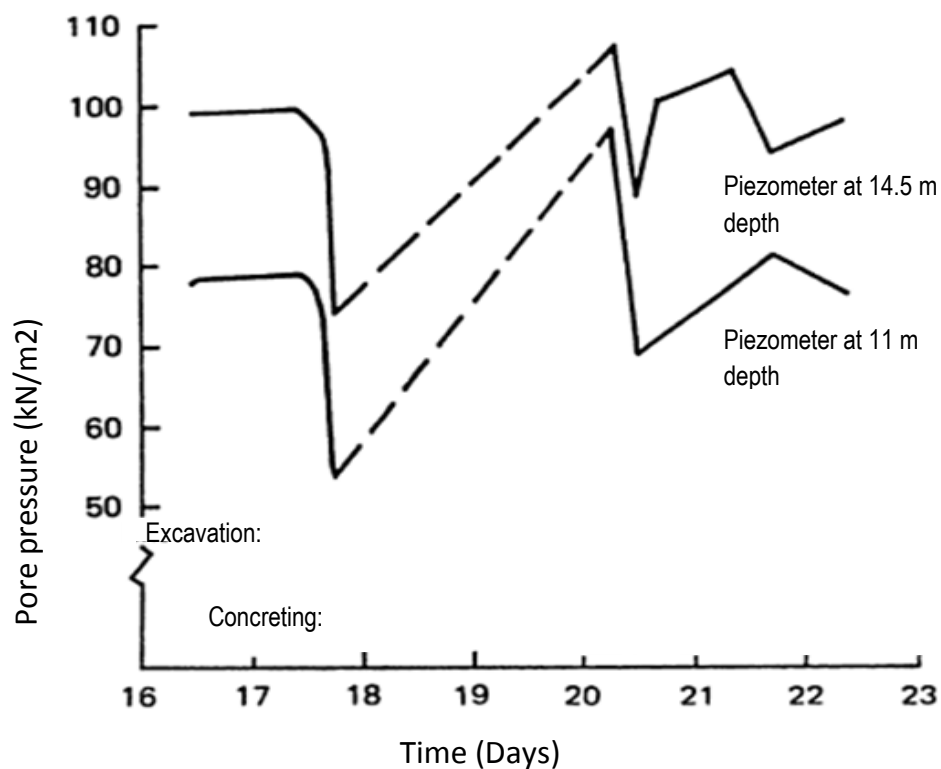
Figure 2.6: Variation of lateral stresses and pore pressures during the construction of an embedded retaining wall (From Symons and Carder, 1993).

23

It is apparent from the above that significant research has been conducted into the effect that construction activities have on the pore water pressures and lateral stresses around replacement type retaining walls. There is similar interest into the impact of the construction of displacement type retaining walls. From these works, it is noted however, that the type of soil also influences how pore water pressures and soil stresses change during wall installation. This is due in part to differences in the way various soils are displaced. For example, the soil displacement mechanism caused by driven piles differed between cohesive and non-cohesive soils. Rizkallah and Cunze (1987) submitted that in non-cohesive soils such as sands, compaction caused by driving a pile into the ground reduced the void ratio and soil volume. This explanation was perhaps far from what usually occurs in reality, as it did not account for shearing and dilation of the soil particles. At the extreme, pile driving could result in the crushing of the soil grains. The low permeability of cohesive soils causes reduced impact on soil volume, which was shown to remain relatively constant according to Rizkallah and Cunze (1987). This soil behaviour can result in surface heave, in cohesive soils, while excess pore pressures are usually generated near the driven piles as shown in Figure 2.7. Meaningful comparison of the effect of construction activities on displacement and replacement type retaining walls is difficult and would need to be conducted prior to dissipation of soil stresses and pore water pressures induced by the installation of the respective retaining walls.

Investigations of installation effects in soft clays and relatively coarse grain deposits, with low coefficient of earth pressure at rest (K_0) values, while showing similar trends to the above also demonstrated some noticeable increases in the contribution of each installation activity (Conti and Sanctis, 2012). This was due in part to the requirement to provide greater support to prevent collapse of the sides of the excavation in soft clays for example. Thus the pore water pressures still decreased during excavation for the piles but increased slightly due to the application of support, usually a bentonite slurry with unit weight much less than that of concrete. Further increases are observed approaching the hydrostatic pressure of the wet concrete. This mechanism was usually observed at least in the upper 5-10 m of an excavated bore or trench (Mayer and Gudehus, 2002 and Schafer and Triantafyllidis, 2004). Ground movement in terms of heave was also more pronounced in soft clay.
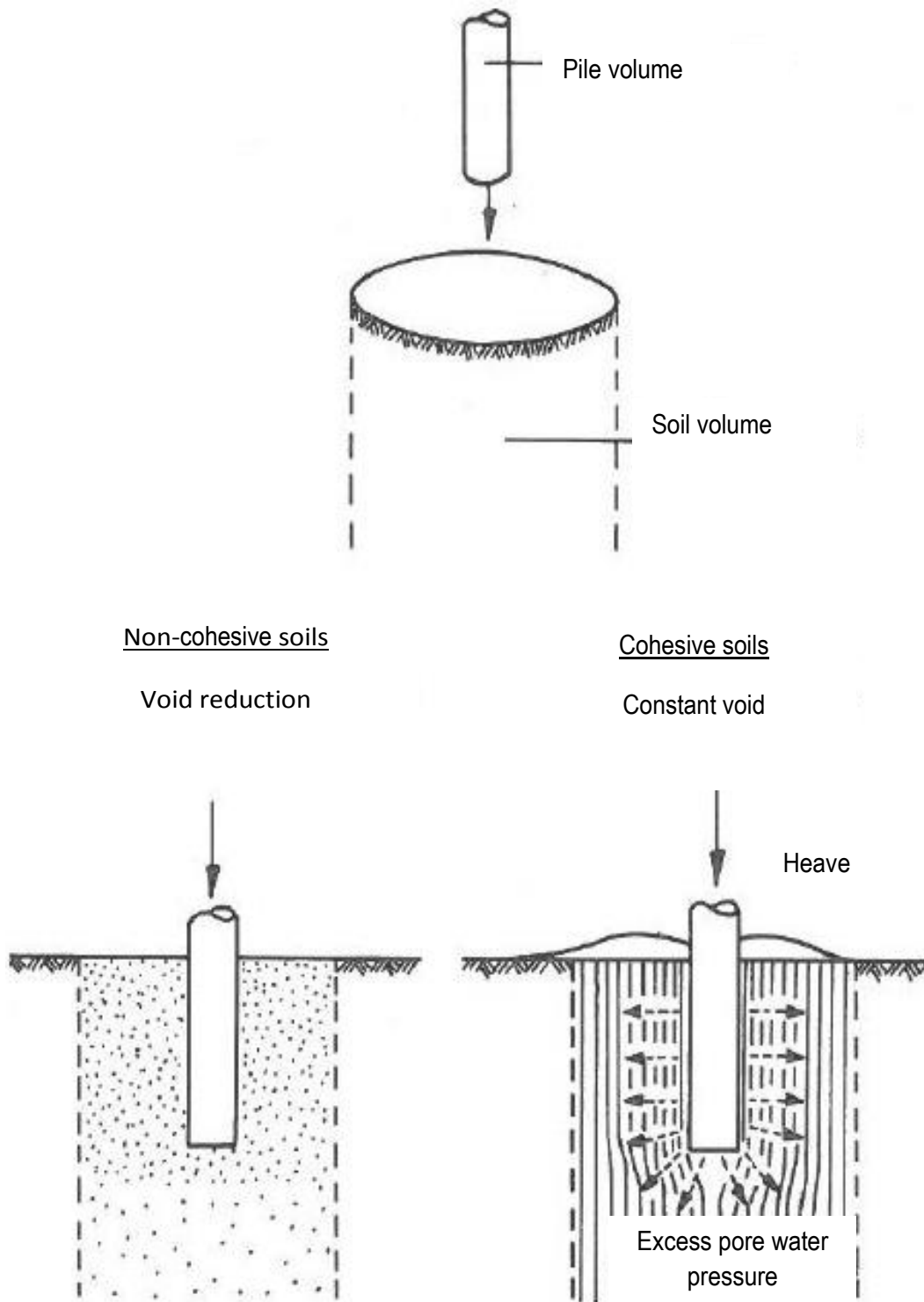
Figure 2.7: Effects of pile penetration on surrounding soils and the development of excess pore water pressures (From Rizkallah and Cunze, 1987).

2.3.2 Comparison of hydraulic regimes for secant and contiguous piles

Retaining walls are usually assumed impermeable and therefore designed to withstand full hydrostatic pressures below the water table. Eurocode 7 recommends that the most suitable pore water pressure distributions be adopted when selecting the hydraulic parameters for the design of retaining walls below the water table (British Standards Institution, 2004). This is invariably interpreted that the water table be taken at ground level without exploring potential benefits of other hydraulic regimes. Conversely, cursory mention is made in CIRIA 580 of the possible economic advantages of designing retaining walls with consideration of through-wall seepage (Gaba et al., 2003). However, the recommended approach in Eurocode 7 does not appear to support CIRIA 580.

Research have however shown that the pore water pressures behind earth retaining structures may be reduced by incorporating proper drainage systems (Harr, 1962; Wang, 2000; Wong, 2001 and Barros, 2006). This recognition of the usefulness of drainage systems to reduce pore pressure build-up behind earth retaining structures is the principle on which weep holes in retaining walls are based (Cedergren, 1989). Therefore, designing retaining walls to allow through-wall seepage can reduce the pore water pressures in the soil on the active side of the wall.

Contiguous pile retaining walls by their nature allow the seepage of groundwater through the pile gaps. It is reasonable to assume therefore that the pore water pressures behind a wall formed from contiguous piles would be less than behind conventional impermeable walls such as those formed from secant piles. Whereas for tunnels there is significant research into the use of segmented tunnel linings to achieve more efficient designs against pore water pressures, there seems to be no similar research interests into contiguous pile retaining walls. Hence, there is limited literature on the long-term pore water pressures behind retaining walls in general and contiguous pile retaining walls in particular.

Secant pile retaining walls at Bell Common

Hubbard *et al*. (1984) investigated the distribution of pore water pressures and lateral stresses around a propped retaining wall made of bored secant piles at Bell Common. The research showed that there was an overall decrease in horizontal total stresses and pore pressures measured behind the retaining wall in the period immediately following pile installation. The reduction in horizontal total stresses was attributed solely to construction-induced decreases in pore water pressures. Hubbard *et al*. (1984) noted however that, as would be expected of an impermeable structure, the pore pressures and horizontal total stresses behind the retaining wall gradually recovered, in the long-term, to near their pre-installation values. This increase in pore pressures and lateral stresses in the long-term occurred in spite of the presence of vertical drains behind the secant pile retaining wall.   It is apparent therefore that, in this instance, the impact of the retaining wall geometry on pore water pressures and horizontal stresses was more significant than the presence of the vertical drains behind the wall.

Contiguous pile retaining walls at Woodford

Similar investigations were conducted into the performance of an embedded retaining wall, formed from 1050 mm diameter contiguous piles at 1300 mm centres and with stabilizing base in an overconsolidated clay at Woodford.   Powrie *et al*. (1999) conducted back analysis of the performance of the retaining wall using a finite element method while Carder *et al*. (1999) investigated the long-term performance of the retaining wall with stabilizing base. Both report an overall decrease in pore water pressures immediately following installation of the piles similar to that observed at Bell Common. In this instance, however, the pore pressures behind the contiguous piles did not increase to near their pre-installation values in the long-term. In fact, measured long-term pore pressures were less than hydrostatic below a depth of about 7.5 m assuming the water table to be at 2 m below ground level as shown in Figure 2.8.
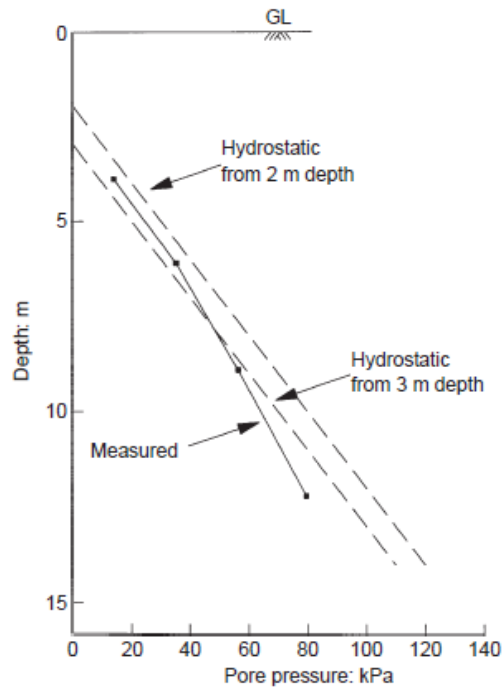
Figure 2.8: Measured pore water pressures compared with hydrostatic profiles in overconsolidated clay at Woodford (From Powrie *et al.*, 1999).

This decrease in pore water pressures behind the contiguous pile retaining wall was at the time attributed solely to the underdrainage of the upper Clay layer to the more permeable Chalk layer. The measured pore water pressure profiles indicate some amount of underdrainage, so the assumptions at the time, based on the evidence, were justified. In hindsight, comparison with a retaining wall formed from secant piles in similar soils would have probably indicate that the dominant influence on the hydraulic conditions was the geometry of the wall instead of the presence of underdrainage to the more permeable soil layer. It is not very clear therefore whether Powrie *et al.* (1999) or Carder *et al.* (1999) considered the possibility of through-wall seepage contributing to the decrease in long-term pore pressures as this line of investigation was not pursued any further.

Contiguous pile retaining wall at CTRL, Ashford

Similarly, the designers of the cut and cover tunnel formed of contiguous pile retaining walls at the site of the construction of the Channel Tunnel Rail Link, Ashford also assumed underdrainage of the Atherfield Clay to the more permeable Weald Clay. Whilst there was merit to the assumption of underdrainage at Ashford, it has since been shown that the geometry of the embedded retaining walls also influenced significantly the pore pressure distribution. For example, Clark (2006) and Richards *et al*. (2007) observed from monitoring data at the instrumented section at CTRL Ashford that the pore water pressure regime was very different from that assumed during the design of the retaining wall and much less than hydrostatic as shown in Figure 2.9.
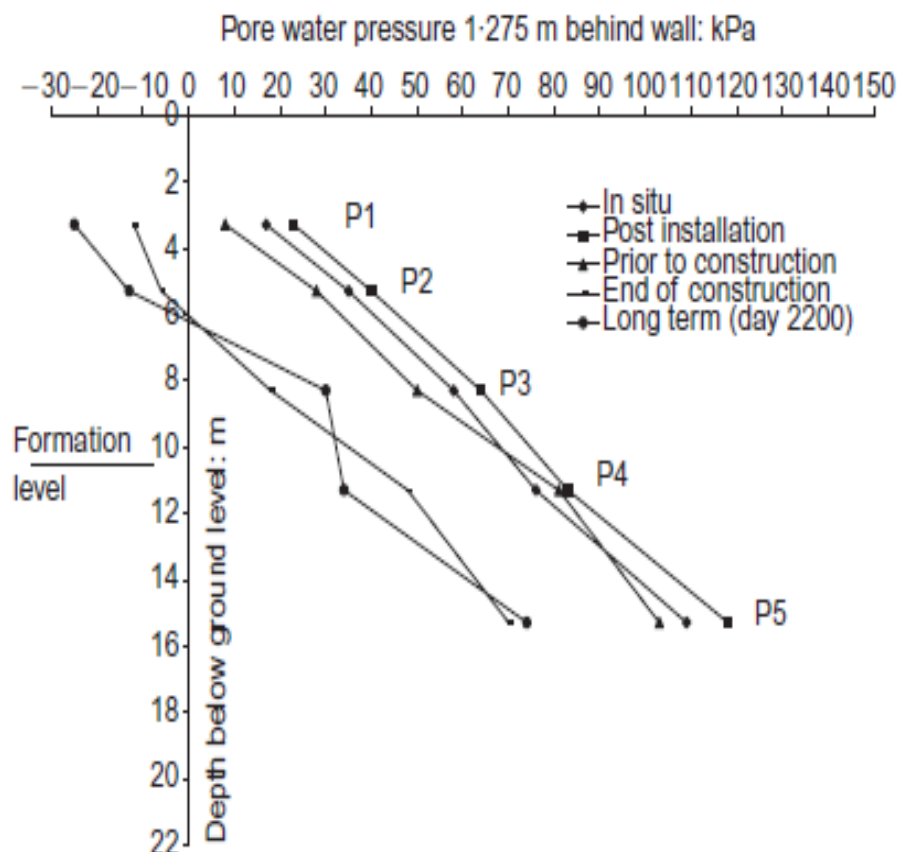
Figure 2.9: Pore water pressure profiles 1.275 m behind the retaining wall at CTRL, Ashford (From Richards *et al*., 2007).

Specifically, as expected, there was a reduction in the measured pore water pressures and horizontal total stresses behind the position of the wall during excavation of the bore. This was followed by increased pore pressures during the pouring of concrete for the piles. After pile installation, it would have been expected that the horizontal stresses and pore water pressures would return to their pre-installation values as illustrated for impermeable retaining walls by Hubbard *et al*. (1984). This was not observed however up to 6 years later, indicated that the long-term pore water pressures were much less than their design values. Furthermore, Richards *et al*. (2007) suggests that the observed reduction in total horizontal stresses was due solely to the reduction in pore water pressures as seen in Figure 2.10. Closer examination of Figure 2.10 however shows that whereas a decrease in pore pressures significantly reduce the horizontal stresses, other factors might have also contributed to the long-term stress reduction. Therefore, further investigation of the hydraulic conditions around contiguous piles is necessary.
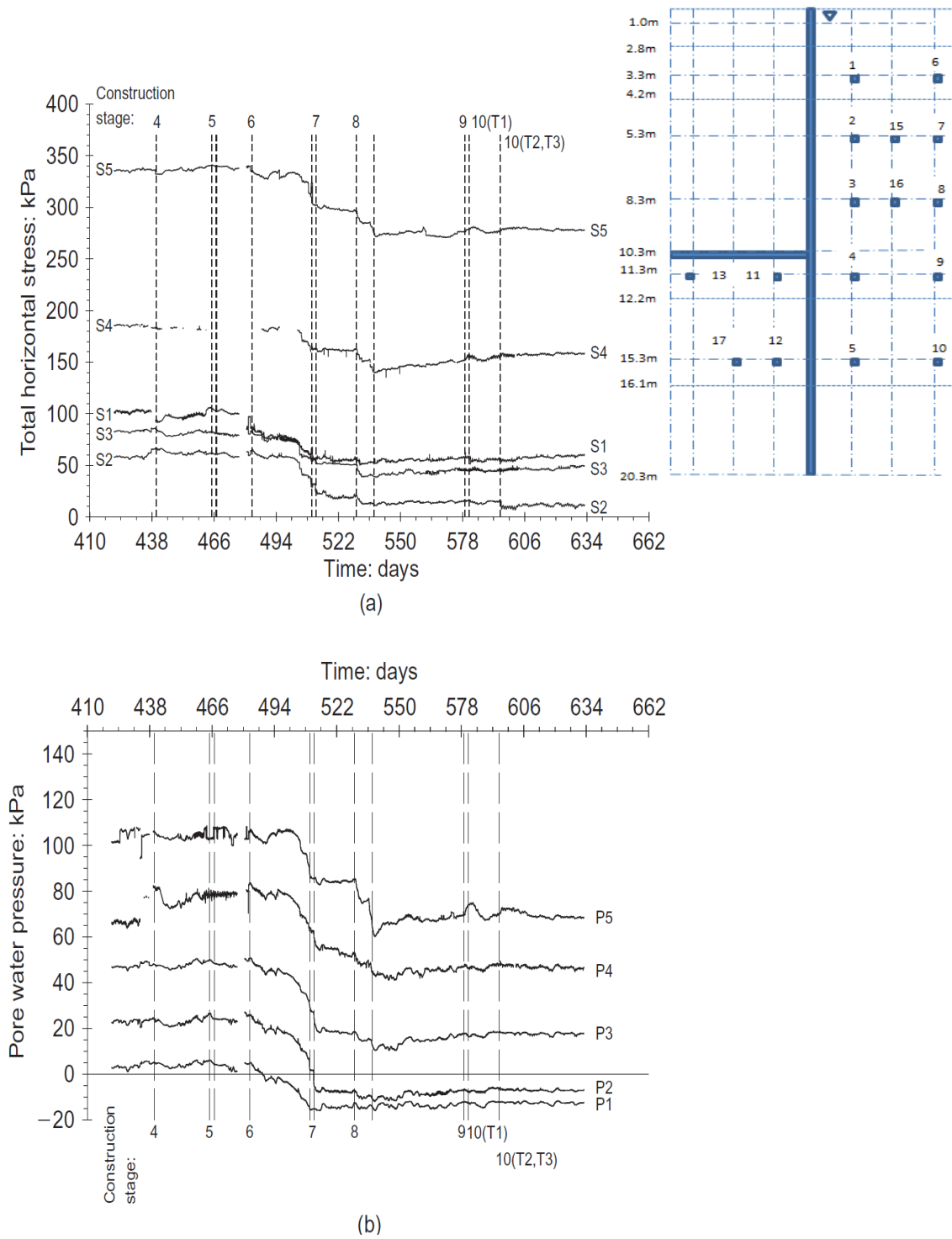
Figure 2.10: Variation of a) horizontal total stresses and b) pore water pressures 1.275 m behind the contiguous pile retaining wall at CTRL, Ashford (From Richards *et al.*, 2007). Instrument locations are shown inset.

Pore water pressure data at distances of 1.275 m, 2.375 m and 3.475 m behind the retaining wall, from the field measurements reported by Clark (2006) and Richards *et al*. (2007), were converted to hydraulic heads and presented as hydraulic head contours as illustrated in Figure 2.11.   Presenting the data as hydraulic head contours demonstrates more clearly the development of a hydraulic gradient towards the retaining wall in the long-term. This also shows that there was significant amount of underdrainage of the soil in front of the retaining wall beneath the reinforced concrete base slab. The hydraulic head contours also indicate that groundwater flow from behind the retaining wall was towards the face of the wall and not around the wall as is conventionally accepted for impermeable retaining walls. These results further supports the notion of through-wall seepage for retaining walls formed from contiguous piles.
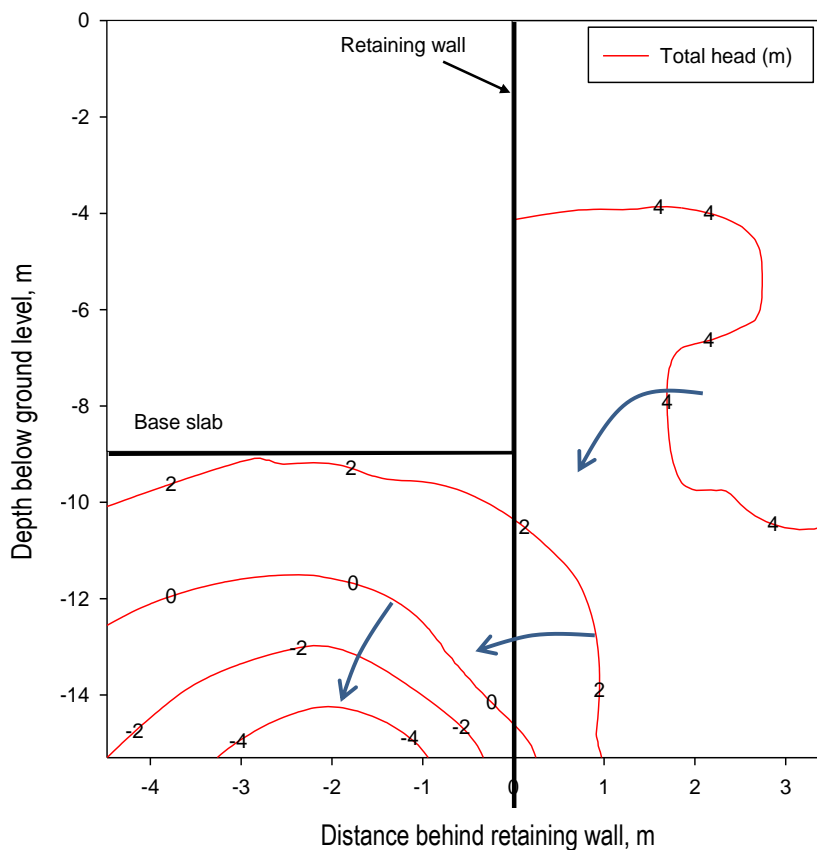
Figure 2.11: Plot of the long-term (2200 days) hydraulic head contours using data from Clark (2006). The arrows show the direction of groundwater flow.

The examples presented above suggest that, although there is plausible evidence that the hydraulic regime around retaining walls formed of contiguous piles differs from that of continuous retaining walls, including those formed of secant piles, there has been little investigation to quantify the hydraulic properties and pore water pressure distribution in particular. Consequently, the potential benefits of through-wall seepage have not been exploited in the design and construction of embedded retaining walls. This also means that possible negative impact of through-wall seepage has not been explored.

2.3.3   Soil displacement and retaining walls

The construction of subsurface structures in soft soils inevitably leads to ground movement. For retaining walls, soil displacement is typically manifest in the form of surface settlement or heave in the surrounding soil. This ground movement, in built-up areas, can cause damages to infrastructures and buildings with shallow foundations (Lee and Rowe, 1989; Lee and Rowe, 1991; Liu *et al.,* 2000 and Lee and Ng, 2002).

Effect of dewatering on soil settlement

Lowering of the groundwater levels for a proposed excavation causes the water table in the surrounding soils to fall and may induce settlement. Most of the construction induced soil settlement observed extending to greater distances from a construction site can usually be attributed to dewatering activities. This settlement can, and is known to, cause damage to buildings and infrastructures at relatively large distances away. The effect of construction dewatering on vertical displacement of the soil is therefore very relevant in any groundwater investigations. Roberts *et al.* (2007) explained the mechanism of soil surface settlement due to de-watering by considering the one-dimensional stiffness modulus or constrained modulus, E_0', of the soil as shown in Equations 2.3 and 2.4.

$$\rho = \frac{D_s \gamma_w S_{av}}{E'_{0,av}} \qquad \qquad \text{Equation 2.3}$$

and $\quad \frac{E'_0}{\Delta \sigma'_v} = 400 \qquad \qquad$ Equation 2.4

where ρ is settlement, D_s is the thickness of the soil layer, S_{av} is the average drawdown in the layer and E'_0 is the one dimensional stiffness modulus of the soil.

The approximation is based on the knowledge that for constant total vertical stress, σ_v a reduction in water level, by pumping for example, causes the pore water pressure, U, to decrease. The corresponding increase in the effective vertical stress, $\Delta\sigma'_v$ causes consolidation of the soil layers leading to increased settlement. This process usually takes longer in fine soils where the accompanying settlement is due to consolidation. The amount of settlement has been shown however, to be more significant for soil strata having layers of different bulk moduli. This is based on the compressibility of the different layers. Additionally settlement is increased if fines are removed by horizontal seepage if the dewatering system is not carefully designed (Preene *et al*., 2000). In contrast, settlement in coarse soils usually occurs in a relatively short time and is not dependent on consolidation.

If the reduction in water levels caused by seepage through a permeable retaining wall is approximated to the drawdown in a well due to pumping, then the one-dimensional stiffness modulus method for calculating settlement due to dewatering could be adopted to estimate the amount of settlement resulting from through-wall seepage. This simplification of the calculation of ground settlement is sufficiently robust to provide estimates of settlement profiles behind retaining walls in which there is through-wall seepage.

Effect of excavation on soil settlement

The other significant factor influencing soil displacement in the construction of retaining walls is the excavation process. Excavation of the soil in front of a retaining wall for instance, is usually responsible for the greater proportion of soil settlement near the wall. Similarly, ground movement during excavation for the installation of the retaining wall also accounts for some amount of construction induced soil displacement. Tedd *et al*. (1984) for instance, using results from an instrumented section of the retaining wall at Bell Common, demonstrated that ground movement during installation of the piles accounted for up to 30% of the total construction movement near the piles.

In contrast to construction induced movements, long-term ground movements are more difficult to predict and may be attributed to several factors including, but not limited to, soil type and condition and as illustrated in the following paragraphs, the geometry of the retaining wall.

Influence of retaining wall permeability on soil displacement

Retaining walls have traditionally been treated as impermeable in accordance with the guidance provided by various engineering standards. There are however, uncertainties regarding the waterproofness of most earth retaining walls due to their composition and nature of construction. This is particularly so for contiguous pile retaining walls where the soil in the pile gaps dominates the bulk permeability of the soil-structure. Even so, retaining walls are usually designed as impermeable. This means that research into the likely impact of wall permeability on ground movement is very limited. Nevertheless, Zdravkovic *et al*. (2007) conducted two-dimensional plane strain coupled (hydraulic and mechanical) numerical simulations to investigate the effect of through-wall seepage on the long-term ground movements adjacent to a deep excavation. The analyses were done using a finite element program and a typical soil profile for Central London. All the soils were modelled using a non-linear elasto-plastic Mohr Coulomb model except the made ground which was modelled using a linear elastic Mohr Coulomb soil model described by Potts and Zdravkovic (1999). The wall and props were modelled as linear elastic.

The investigations showed that the permeability of the retaining wall affected the long-term ground vertical displacement. As the ratio of the wall to soil vertical permeability, k_w/k_v increased the vertical displacements increased as shown in Figure 2.12.
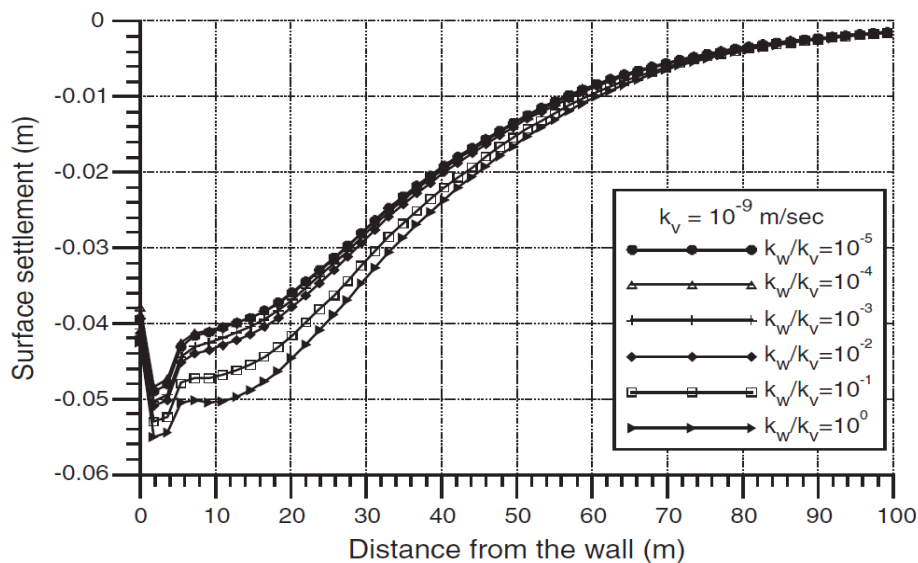
Figure 2.12: Variation of ground settlement behind the retaining walls due to changes in wall permeability (From Zdravkovic *et al.*, 2005).

The settlement behind the wall increased to about 25% for the limiting case of $k_w/k_v=1$ relative to the lower limit used for an impermeable wall, $k_w/k_v=10^{-3}$. The impact on soil displacement was more significant nearer to the wall as expected, with the observed displacement troughs typical of those for drawdown-induced settlement. It was observed that the increase in soil displacement was not particularly large as the wall permeability increased. This relatively small increase in vertical displacement is very important as it indicates that the reduced lateral hydraulic loads on the wall more than compensate for the inconvenience of increased vertical displacements.

The similarity in surface settlement profiles between drawdown induced and those due to the reduction in water levels caused by through-wall seepage suggests that the adopted method for calculating drawdown-induced displacement in the previous section was appropriate. It seemed though that the values of k_w/k_v used by Zdravkovic *et al.* (2007) were chosen arbitrarily with no attempt been made to assign realistic bulk permeability to the equivalent structure in the 2D analyses based on the pile gaps. Similarly, it was not entirely clear why only the soil vertical permeability was used. Zdravkovic *et al.* (2007), however, demonstrated that it was unrealistic and probably too conservative to model retaining walls formed from contiguous piles as being

36

impermeable. Clausen and Heimli (1987), although not entirely by design, made similar observations and showed that the accidental leakage of groundwater into an excavation caused a reduction in pore water pressures in the surrounding soils. The adverse effect however, was an increase in soil settlement at surface level near the excavation.

Selection of soil constitutive model for calculating displacement

Although the results from Zdravkovic *et al*. (2007) were very consistent at various distances from the wall, the displacement magnitudes should be viewed with caution. This is due to the fact that the Mohr Coulomb constitutive soil models, although commonly used in geotechnical engineering due to the ready availability of the required soil parameters, are known to produce unreliable surface settlement (Bolton *et al*., 1994; Addenbrooke *et al*., 1997; Dolezalova, 2002; Masin and Herle, 2005 and Bryson and Salehian, 2011). This uncertainty is based on observations of the calculated settlement troughs, derived from numerical analyses in which Mohr Coulomb soil models were used, being usually shallower and wider than those obtained from laboratory experiments and from field observations. Bolton *et al*. (1994) and Hicher and Shao (2008) attribute this drawback in part to the small strain section of the constitutive soil model. Hejazi *et al*. (2009) observed similar trends in soil surface settlement troughs while investigating the impact of constitutive models on the numerical analysis of underground constructions. Powrie *et al*. (1999) also notes that a Mohr-Coulomb plasticity model was relatively simple to implement but did not adequately represent changes in elastic stiffness modulus during effective stress analyses. The deficiencies of a Mohr Coulomb model is further evident when compared with a critical state (Cam Clay) soil model in the form proposed by Schofield (1980) and a brick model in which the soil stiffness varied with strain and average effective stress (Simpson, 1992). Burland and Karla (1986) however suggests that a Mohr Coulomb soil model would give reasonable approximation if the soil stiffness profile was selected carefully. This means that reasonable trends in soil behaviour can be established using a Mohr Coulomb soil model.

Mitigating against seepage induced settlement for retaining walls

Several methods exist that can be used to mitigate against the deleterious effects of through-wall seepage. For example, groundwater recharging and underpinning of existing foundations have been used to prevent settlement-induced damage to the surrounding building. Similarly, the use of compensation grouting to reduce settlement is common practice in ground improvement. A thorough understanding of the impact of through-wall seepage is therefore necessary to understand the likely negative impact in order that sustainable mitigating measures can be undertaken.

2.3.4 Adapting 3D parameters for 2D numerical analysis

Research has shown that two-dimensional numerical simulations are suitable for some investigations in geotechnical engineering. However, in order to represent adequately problems in 2D, which are ideally three-dimensional in nature, simple adjustments to the problem geometries are sometimes necessary. Modification of the load specifications may also be required to more realistically represent field conditions. Some aspects of retaining wall long-term behaviour can however be represented satisfactorily in 2D simulations without modification. However, the geometries of retaining walls formed from bored circular piles require alterations in order to be accurately characterised in 2D plane strain analyses. The following sections describe some geometric modifications to retaining walls, which were done to allow closer similarities in modelling 3D structures in 2D.

Calculating equivalent model wall thickness, t

Retaining walls formed from contiguous and secant piles are usually represented in 2D plane strain simulations by continuous retaining walls of equivalent thicknesses. While this geometric simplification is not always ideal, reasonable approximation to the 3D analysis can be obtained. A similar approach may be applied to sheet pile retaining walls which are essentially one-dimensional in geometry as Day and Potts (1993) demonstrates. Sheet pile retaining walls are usually modelled using 1D built-in structural beam elements in the numerical codes or by 2D grid elements to which the

equivalent wall properties are assigned. An equivalent wall thickness in the 2D simulations is therefore calculated by considering the geometric properties and stiffness of the material. Day and Potts (1993), for example, showed that the equivalent thickness of the wall elements in the numerical grid could be obtained by equating the bending and axial stiffness of the prototype wall to the numerical model and solving for the elastic modulus and thickness of the 2D elements using Equations 2.5 and 2.6 for axial and bending stiffness respectively. The assumption of negligible sheet pile stiffness was made in this analysis.

$$tE_{eq} = EA \qquad\qquad\qquad \text{Equation 2.5}$$

$$(EI)_{eq} = EI \qquad\qquad\qquad \text{Equation 2.6}$$

where t is the thickness of the 2D element, E_{eq} is the equivalent stiffness of the model wall, E is the material Young's modulus, A is the cross-sectional area and I the second moment of area.

Similarly, Powrie *et al.* (1999) used the second moments of area (Equation 2.7) of the model and retaining walls to calculate an equivalent wall thickness for a contiguous pile retaining wall in 2D plane strain analysis.

$$I_p = I_m \qquad\qquad\qquad \text{Equation 2.7}$$

where I_p and I_m are the second moments of area for the contiguous pile and the model wall respectively.

The analysis by Powrie *et al.* (1999) differs from that of Day and Potts (1993) by the absence of the material stiffness. The assumption by Powrie *et al.* (1999) was that the second moment of area, I per metre run was a property of the cross-section and was therefore comparable to other cross-sections of similar material. This implied that, if the materials have identical properties, then stiffness was irrelevant in the calculation of equivalent thickness for numerical simulations. Comparison of the equivalent wall thicknesses calculated for a contiguous pile of 1050 mm in diameter however, showed a difference of less than 11 mm between both methods. This implies that omission of stiffness is not that crucial for the analysis.

Additionally, Day and Potts (1993) demonstrates that beam elements in which stiffness was ignored were more suitable for modelling thin section walls such as sheet piles while 2D grid elements were better for modelling thick concrete walls. Caution should however be exercised as modelling a retaining wall with grid elements which are too large can produce unrealistic results. Furthermore, if the installation effects were of interest, then as suggested by Watson and Carder (1994), axi-symmetric analyses of a single bored pile may be more appropriate if 3D resources were not available.

Although 2D analyses of some engineering structures such as embankments and retaining walls might be appropriate, considerations of the time dependent nature of loading conditions is oftentimes required. This means that modifications to the geometry of some structural elements and the application of load adjustment factors might be necessary to represent adequately three-dimensional effects in 2D simulations.

Difficulties in adopting 3D simulations to 2D

Notwithstanding the possible adaptations, further studies have highlighted some shortcomings of conducting 2D instead of 3D analyses for some retaining wall problems. For example, Vrecl-Kojc and Skrabl (2009) suggests that the analysis of the failure mechanism of a cantilever retaining wall formed from a row of spaced piles was best investigated using 3D models. This assumption was based on the results from two-dimensional simulations which indicated that the failure of a retaining wall would be similar to that of a group of piles acting together. Comparable 3D analyses however, gave a more realistic failure mechanism similar to that observed in the field.

Equally, it has been shown that modelling retaining wall installation in 2D can over-predict soil displacement and the corresponding horizontal stress relief (Gunn and Clayton, 1992; De Moor, 1994; Ng *et al.*, 1995 and Rampello *et al.*, 1998). Gourvenec *et al.* (2002) modelled the installation and long-term conditions around a long retaining wall in 2D and 3D and compared the results. The calculated retaining wall movement in the 2D analysis was 6 times higher than from the 3D simulations. It was also noted that the 3D results were similar to the field measurements. The use of the same time scale during the excavation phase for the 2D and 3D simulations might have influenced the results base on the accuracy of the construction sequence. For example, an

excavation step in 2D analyses assumes removal of the soil for the full length (out-of-plane) of the structure without installing supports in a realistic time frame. The same step in 3D however, is more realistically done with added control over the excavation length and the steps at which supports, for instance, are installed.

The inconsistencies above were similar to the arguments previously made by Gourvenec and Powrie (1999) and Schafer and Triantafyllidis (2004). It might be argued however that, in some cases, the level of accuracy of the numerical results depends more on the geometry of the problem than whether 2D or 3D simulations are performed. For instance, Zdravkovic *et al.* (2005) notes that for retaining walls formed of bored piles, such as contiguous and secant piles, and for diaphragm walls made of large panels, the only isotropy was in the vertical direction. This meant that two-dimensional analyses of diaphragm walls do not consider the loss of isotropy in the horizontal direction as the model assumed zero thickness in the out-of-plane direction. Incidentally, vertical joints and connections can render the wall stiffness and other properties different from those of a truly continuous wall. Consequently, 3D simulations showed contrast in wall bending moments, displacements and soil deformations relative to the 2D analyses according to Zdravkovic *et al.* (2005).

It is apparent therefore that there are different views on the adequacy of using 2D simulations for geotechnical problems which are ideally 3D in nature. Nonetheless, it has been shown that reliable trends can be obtained from performing 2D plane strain analyses particularly when 3D simulations require much more resources.

2.4 Summary

Investigations into the hydraulic regime around earth retaining structures and the current methods of treating pore water pressure distribution were reviewed. Design guidelines generally recommend that pore water pressures be treated as hydrostatic below the water table. This has resulted in overly conservative design approaches in which retaining walls in particular were treated as impermeable. There is however significant research into the use of segmented linings to reduce the pore water pressures behind shallow tunnels located in fine soils. These investigations have shown that axial forces and bending moments on tunnel linings through which groundwater seepage is allowed

are lower than those behind waterproofed linings. The observed changes in hydraulic conditions caused by lining permeability are only valid however for shallow tunnels in which there is no maintained head of water above.

In contrast to investigations into the hydraulic conditions around shallow tunnels, there is scant research into adapting the geometry of retaining walls to reduce pore water pressures and lateral loads acting at the back of the wall. This is although it has been demonstrated by field monitoring that through-wall seepage could produce reduced pore water pressures and horizontal stresses behind earth retaining walls and that the use of weep holes are very effective in relieving hydraulic loadings on retaining structures. Contiguous pile retaining walls in particular, based on their geometry, allow seepage through the pile gaps and should be treated as permeable.

There are however, drawbacks to allowing through-structure seepage. Increased settlement and increased consolidation volume losses have been observed in the soil behind retaining walls and around shallow tunnels respectively. Consolidation volume losses were found to be proportional to the drawdown due to seepage through segmented tunnel linings. Similarly, the vertical displacement of the soil behind permeable retaining walls was shown to increase as the wall bulk permeability increased.

The methods of investigating the hydraulic regime around earth retaining structures include field and empirical investigations, analytical and numerical analyses and laboratory experiments. Two- and three-dimensional numerical analyses however, are very popular, with 2D plane strain simulations being the default numerical technique for structures with long geometries such as tunnels and retaining walls. There are however reported difficulties in conducting 2D analyses of structures that are ideally 3D in nature. Where it is thought however that 2D numerical simulations will suffice, modifications to applied stresses and geometries are sometimes required to represent more realistically field conditions.

The review of literature on the hydraulic conditions around retaining structures has shown that better understanding of the groundwater flow regime around retaining walls formed of contiguous piles could lead to more economical designs. This is evident by

the apparent gains from research into shallow tunnels with segmented linings and the observed reduced pore pressures reported behind contiguous piles.

Chapter 3

_____

3.0 Establishing an equivalent permeability relationship

_____

3.1 Introduction

As discussed in the preceding chapter, installing a civil engineering structure of relatively low permeability, such as an earth retaining wall, into the ground will alter the groundwater flow regime. This means that new hydraulic relationships will be established in which the soil/structure parameters are different from those *in situ*. Further research is necessary to properly quantify these relationships and to possibly exploit any potential benefits. Plane strain numerical analyses in two-dimensions were therefore conducted to determine the impact on the groundwater flow regime of inserting a low permeability circular pile section into a flow channel. Some of the numerical simulations were based on the geometry of a laboratory flow tank with appropriate adjustments made to facilitate parametric studies. In this chapter, the numerical procedures used to determine a relationship between the equivalent structure to soil permeability ratio, k_p/ks, and the pile gap to diameter ratios, x/d, for plane strain

analyses are outlined. The equivalent structure is taken as the pile section and the soil in the pile gap. The results are then discussed in terms of the impact of the low permeability pile section on the flowrates and the development of pore pressures around the model piles.

3.2 Method

The experimental flow tank simulated in these investigations is shown schematically in Figure 3.1. The analyses were conducted in two stages. During stage 1, horizontal plane analyses were used to investigate the effect of pile spacing on the groundwater flow regime and to derive a bulk permeability relationship. The equivalent bulk permeability derived during the stage 1 analyses was applied to a continuous wall of uniform cross-section in stage 2 in order to study the phreatic surface effects on the hydraulic conditions. Stages 1 and 2 analyses are described below:
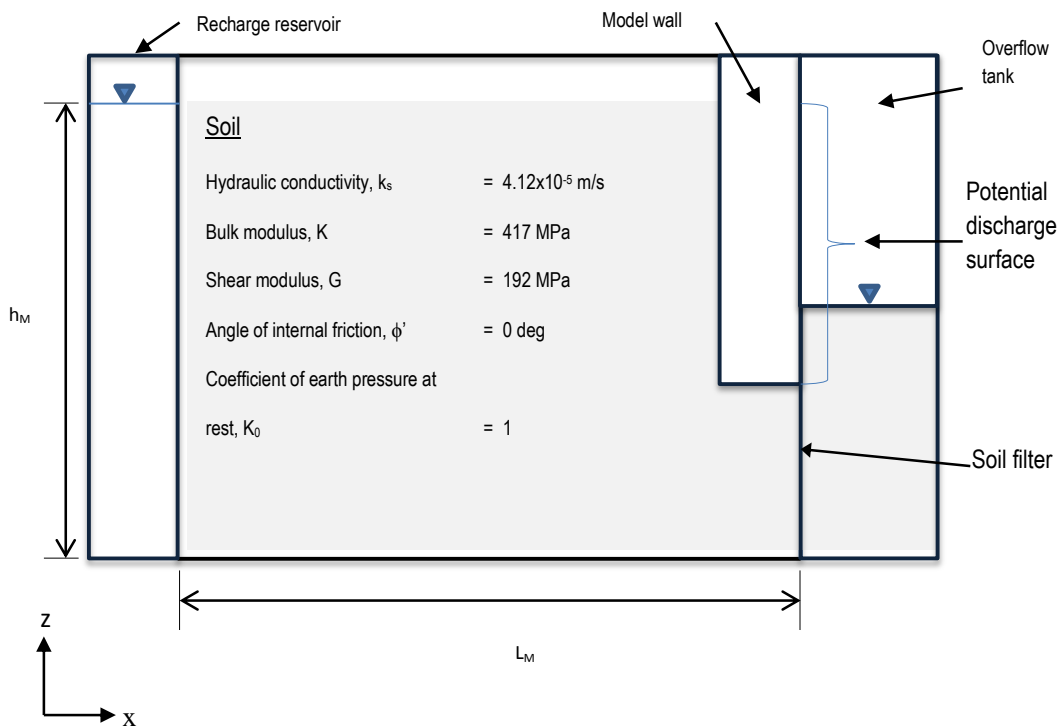
Figure 3.1: Schematic diagram of the flow tank. Soil properties are also shown.

3.2.1 Effects of pile spacing – stage 1

Two-dimensional numerical simulations of retaining walls formed from circular piles are usually carried out by representing the piles with a continuous uniform wall of equivalent thickness. There is no consistent established method to relate the equivalent bulk permeability, k_p, of the uniform model wall to the spaces between the piles. It is however customary to use the ratio of the equivalent structure to soil permeability, k_p/k_s, with a seemingly arbitrary value of k_p. A relationship between the pile gaps, diameter and the soil permeability is therefore necessary. Darcy's law for flow through porous media formed the basis of the stage 1 investigations. Groundwater flow through the spaces between piles was investigated using the hydraulic gradient between the distance of influence and the exposed face of the retaining wall. A cut through a retaining wall and the surrounding soil provided the necessary flow parameters on a horizontal plane. This horizontal plane analysis may be applied at levels above and below the phreatic surface. The impact of different pile gaps on the hydraulic conditions around the retaining wall could therefore be determined. To verify these assumptions, numerical simulations of an experimental flow tank were conducted. Groundwater flow through a horizontal (x-y) plane section cut through the flow tank, as shown in Figure 3.2, was investigated.
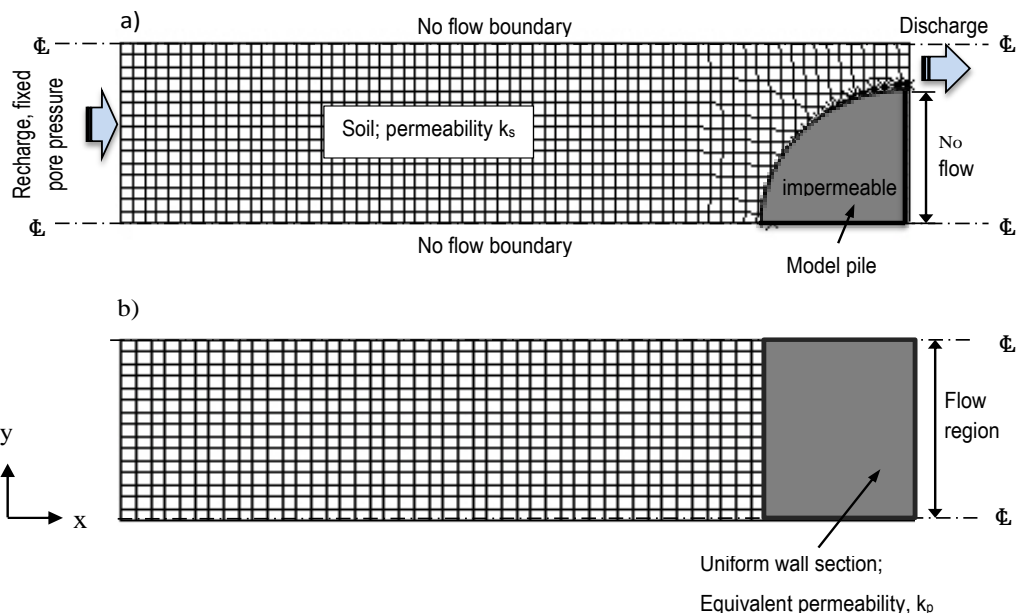
Figure 3.2: a) Horizontal (x-y) plane section cut through the flow tank. The model is fixed from movement in all directions. A horizontal section through the equivalent uniform

47

Two-dimensional horizontal plane flow was simulated by applying a pressure difference, ΔU_i between the recharge and potential discharge boundaries, which represented a reservoir of water and an overflow tank respectively. The base of the flow tank was taken as the reference datum for the calculation of hydraulic heads. The assumption was made that flow could take place at any point along the exposed face of the model pile and or through the soil in the spaces between piles. The flow of water between the recharge boundary and the potential discharge surface was therefore controlled by the pressure difference ΔU_i, the size of the inter-pile spaces, x and the hydraulic conductivity of the soil, k_s. The objectives of the stage 1 analysis were to:

1. Observe the influence of pile spacing on groundwater flow patterns around the low permeability pile section,
2. Determine the effect of pile gap to diameter ratios, x/d, on pore water pressures and steady state flowrates and
3. Derive a relationship between the bulk permeability, k_p, for the region constricted by the pile sections and the soil permeability, k_s, in terms of the ratio x/d. This relationship would then be used to calculate an equivalent bulk permeability value to the plane strain uniform retaining wall in stage 2 analyses.

3.2.2 Stage 2 - Phreatic surface effects

Stage 1 analyses proved the validity of the permeability ratio, k_p/k_s, for flow in the horizontal plane. Simulations were conducted in stage 2 to validate the application of the bulk permeability under conditions in which a phreatic surface was developing. Two dimensional plane strain simulations of groundwater flow in the vertical, (z-x) plane were therefore conducted. The problem geometry is illustrated by the vertical section through the flow tank shown as a typical FLAC[2D] grid in Figure 3.3. Flow was again simulated by applying a pressure difference, ΔU_i between the recharge and potential discharge boundaries as described for stage 1. A continuous retaining wall of equivalent thickness, t, was used to represent the circular pile sections in the 2D plane strain analysis. The permeability relationship derived in the stage 1 analyses was used

to assign bulk permeability values to the model walls in stage 2. This permeability was based on the size of the pile gap, x, the pile diameter, d, and the soil hydraulic conductivity, k_s. The flow of groundwater between the recharge and potential discharge boundaries in this stage was therefore controlled by the applied pressure difference, ΔU_i, the permeability of the soil, k_s, and the bulk permeability of the model wall, k_p.
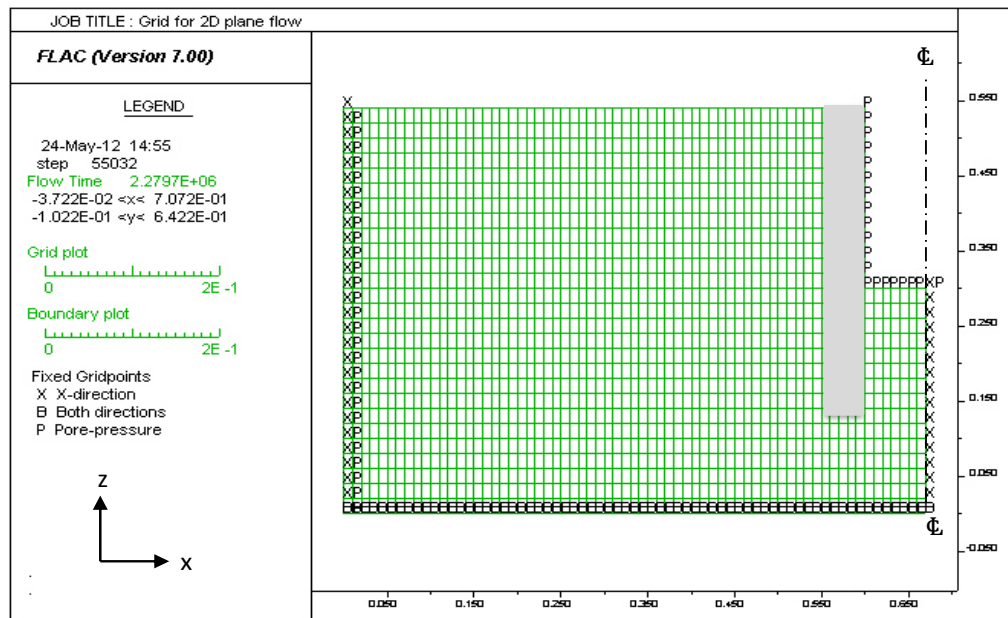
Figure 3.3: Typical FLAC2D grid, with boundary conditions, representing vertical section (z-x) through the flow tank.

3.2.3 Description of the numerical application

The numerical investigations were carried out using FLAC^{2D} (**F**ast **L**agrangian **A**nalysis of **C**ontinua in **2 D**imensions), a commercial geotechnical engineering finite difference programme developed by Itasca Consulting Group Inc. The explicit nature of FLAC^{2D} means that failure mechanisms are modelled accurately and the program is suited for modelling the behaviour of soils which undergo plastic flow when they have reached their elastic limits (ITASCA, 2012). Unlike some finite element packages, the numerical grid in FLAC^{2D} can deform in large-strain mode to give a more accurate description of soil failure mechanisms. The default mode of operation is however small-strain. Processing times in FLAC^{2D} are relatively fast because the program does not combine the element matrices into one large global stiffness matrix as is done in some finite element applications. The finite difference scheme employed in FLAC^{2D} instead regenerates the finite difference equations at each step, which means less computer memory is used. It is evident however, that although simulations involving non-linear problems (including large strain, physical instability) are routine in FLAC^{2D}, this level of efficiency is made redundant when modelling linear problems. This is due to the small time steps taken in the explicit methods employed by most finite difference program, which means that a large number of steps are taken for each solution. The implicit methods usually used by finite element programs, in contrast, utilise large time steps and are more suitable for modelling linear small-strain problems.

The soil models used in both stages of the simulations were represented by numerical grid elements or zones to which material properties were assigned. Similarly, the circular pile sections in the stage 1 and the continuous retaining wall in the stage 2 analyses were represented by grid elements as recommended for concrete sections by Day and Potts (1993). This is because 2D grid elements more accurately describe the geometry of the structure. Shear stresses and bending moments are also better represented using 2D grid elements than beam elements.

The following sections describe the numerical procedures adopted to investigate the groundwater flow regime around contiguous piles. The results are presented and

discussed and comparisons made with retaining walls in which there is no through-wall seepage.

3.3   Soil and model pile description

For all analyses in stages 1 and 2, the soil was assumed to be a homogeneous isotropic material. An elastic-perfectly plastic constitutive soil model was used throughout. To ensure consistency, mechanical properties for all analyses were the same and were kept constant throughout the simulations. Soil stiffness was assumed constant with depth and the ratio of *in situ* horizontal to vertical stresses, K_0 was set to 1. Elastic properties of bulk, K and shear, G moduli were used instead of Young's modulus, E and Poisson's ratio, v. Bulk and shear moduli are related to Young's modulus and Poisson's ratio by Equations 3.1 and 3.2.

$$K = \frac{E}{3(1-2v)}$$ Equation 3.1

And $$G = \frac{E}{2(1+v)}$$ Equation 3.2

Soil properties were obtained from published data and laboratory tests. The permeability of the soil used in the numerical analyses was obtained from constant head permeability tests as described by, for example, Powrie (2004). Actual permeability values were used so that the results of the numerical simulations could be verified by subsequent flow tank experiments. Preliminary numerical analyses were conducted to determine the effect of a wide range of soil permeability values on the numerical results. The investigations showed that the soil permeability did not significantly affect the ratio k_p/k_s.

An elastic isotropic material model, with properties listed in Table 3.1, was used to represent the pile section. This model was assumed sufficient to investigate the hydraulic properties as structural failure was not being investigated.

Model pile properties	Value
Dry density (ρ_{dry}), Kg/m^3	2500
Young's modulus (E), GPa	3.2
Poisson's ratio (v),	0.15
Moment of inertia (I)	varies

Table 3.1: Elastic properties of the pile sections used in the stage 1 simulations.

3.4 Stage 1- Analysis of flow in the horizontal plane

3.4.1 Initial and boundary conditions

The analyses in stage 1 were of typical horizontal sections through the flow tank at various elevations. Therefore the boundary conditions, as shown in Figure 3.2, consisted of fixed displacement and velocity boundaries in the x-y plane. The pile sections were restricted from movement in all directions. The hydraulic boundary conditions consisted of a prescribed upper pressure boundary at the recharge or far field boundary of the model. This was fixed at 5.4 kPa to simulate a full supply reservoir. The exposed face of the model pile and the adjacent soil surface were prescribed as a lower pressure boundary and modelled as possible discharge surfaces as seepage could take place if the equivalent permeability allowed. Pore pressures at the exposed surface of the wall and soil varied between 0 and 5.4 kPa corresponding to an empty and a full overflow tank.

3.4.2 Numerical procedure

The analysis commenced with a wished into place pile section. The geometry of the problem, a series of circular piles in a row, allowed for symmetry about the centre of a pile and about the midpoint of an adjacent pile gap. Similarly, for the uncoupled groundwater flow around circular piles in unexcavated ground, a condition of symmetry for flow conditions can also be assumed along the centre of a pile in the direction of the wall. Two cases were examined to determine the effect of different initial boundary conditions on the simulation results. For the case 1 simulations, the initial water levels were at the top of the model tank. The water level at the discharge surface was lowered incrementally for each step corresponding to pressure drops of ΔU_i relative to the pore pressure at the supply reservoir. This was achieved by applying pore pressure values corresponding to a full flow tank at the grid points representing the recharge surface. Pore pressures giving a difference of ΔU_i were subsequently assigned at the discharge surface. This was compared with the case 2 analyses in which the simulated water levels were initially at the base of the flow tank. For the subsequent case 2 simulations, the water levels at the recharge boundary were raised instantaneously to give pressure differences, ΔU_i while keeping the pore pressure at the discharge surface at zero. No significant differences were observed between the cases 1 and 2 simulations.

These procedures were repeated with the pile gap to diameter ratios, x/d, varying from zero, representing an impermeable wall, to a value at which the influence of x/d on the flowrates was negligible. The change in x/d was achieved by keeping the width of the model tank constant and varying the model pile diameter. The effect of keeping the model pile diameter constant while varying the model width was also investigated. There were no significant differences, at similar pile gap to diameter ratios, between the results of analyses with a fixed model width and those with a fixed pile diameter.

Steady state flowrates, Q_i at different pile gap to diameter ratios, x/d, were determined at the discharge surface for all simulations. The fluid flow paths were also tracked by 'injecting particles' at the recharge boundary and recording their direction of flow. This built-in facility in FLAC^{2D} is similar to the dye injection method used in laboratory experiments in which a dye is injected at various points at the upstream end of a physical model and the development of streamlines observed. Additionally, to

eliminate the impact of changing hydraulic gradients on the development of pore water pressures and steady state flowrates the simulations were repeated at various pressure differences, ΔU_i.

Convergence to steady state

Steady state flow conditions were determined by comparing groundwater inflow at the recharge boundary and the outflow at the discharge surface. This calculation was facilitated by a built-in feature, a FISH function in FLAC^{2D}, which is used to monitor the flowrates into and out of the model at grid points represented by fixed pore water pressure boundaries. The steady state convergence criterion used in the programme is Darcy's law for flow between the recharge and discharge boundaries. Initial hydraulic conditions corresponding to case 1 and case 2 as described above were compared. For case 1, the initial hydraulic conditions were that the water level was at the top of the model throughout. This meant that initial outflow quantities were greater than the inflow. Simulation of a lowered water level at the potential discharge surface introduced a hydraulic gradient, which induced outflow. Flowrates eventually converged and steady state was achieved when the volumetric inflow and outflow quantities for a specified time were equal. Convergence to steady state for the case 2, in which the initial water level was at the base of the model, varied slightly from the above. The process started with the initial inflow and outflow quantities being equal to zero. The water level at the recharge surface was raised instantaneously to a pore pressure, U_i corresponding to a difference in pressure, ΔU_i. The water level at the discharge surface remained at the base of the model throughout the analysis. Steady state convergence was reached when the inflow and outflow quantities were the same. The water level at the recharge surface was changed to simulate different values of ΔU_i. Convergence to steady state flowrates for both cases is shown in Figure 3.4. Both plots show that steady state flow was achieved with the inflow equalling outflow.

a) Case 1 – initial water level at the top of the model
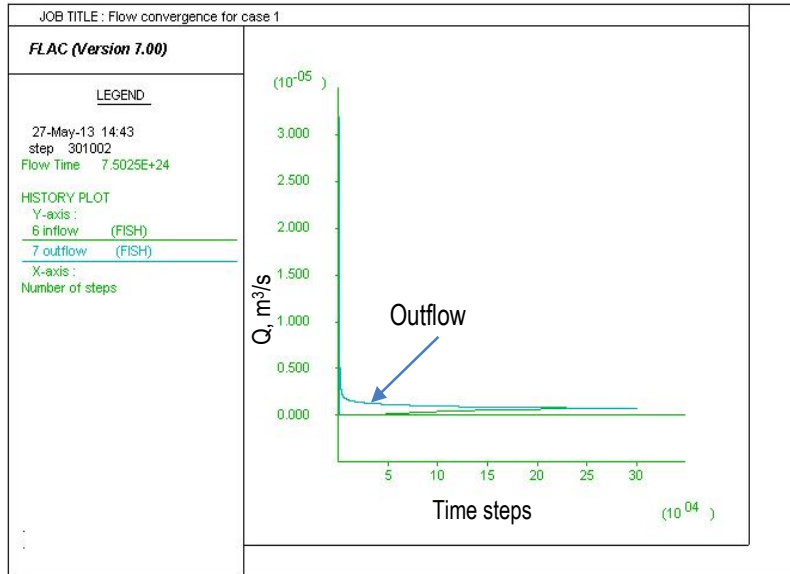
b) Case 2 – initial water level at the base of the model
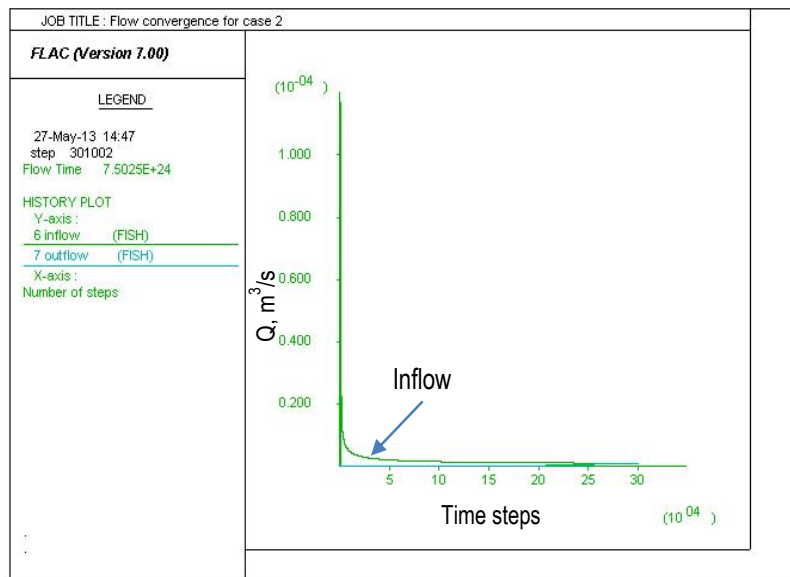
Figure 3.3: Convergence of inflow and outflow to steady state conditions for case 1 and case 2 analyses.

3.4.3 Parametric studies

The purpose of the stage 1 parametric studies was to validate the numerical model by testing the sensitivity of the results to different model geometric and soil hydraulic parameters. The technique adopted in stage 1 simulations was based on the manipulation of Darcy's equation using steady state flowrates under varying hydraulic conditions. This was also used in the calculation of the bulk permeability of the equivalent structure, which depended on the flowrates. Consequently, numerical simulations were conducted to determine the impact of model width and length on steady state flow and pore water pressures around the pile sections. Where the effect of soil parameters on the hydraulic properties was well established, further investigations were not conducted. However, where it was deemed that the effect, due to the presence of through-wall seepage, required more in-depth examination of a parameter, this was done. The analyses are presented and the results discussed in the following sections.

Effect of differences in hydraulic head

The difference in hydraulic head is one of the fundamental parameters driving the movement of groundwater between two points through the soil matrix. The theory governing the flow of groundwater through a homogeneous soil with isotropic hydraulic properties suggests that changing the difference in total head between the recharge and discharge boundaries, while keeping other factors constant, should have a proportional effect on the steady state flowrates. To validate the numerical model, simulations were carried out for hydraulic head drops, Δh between the recharge and discharge boundaries in the range 0 to 0.54 m for a fixed pile gap to diameter ratio, x/d=0.3. These were compared with flowrates calculated using Darcy's law at the same values of Δh and with the soil permeability of 2 x 10^{-5} m/s for a flow channel without any piles. The results, illustrated in Figure 3.5, show that increasing the hydraulic head difference, as would be expected, caused a corresponding increase in steady state flowrates. The flowrates calculated using Darcy's law were higher than the numerically derived values due to the reduction in flow caused by the presence of the pile in the numerical simulations.
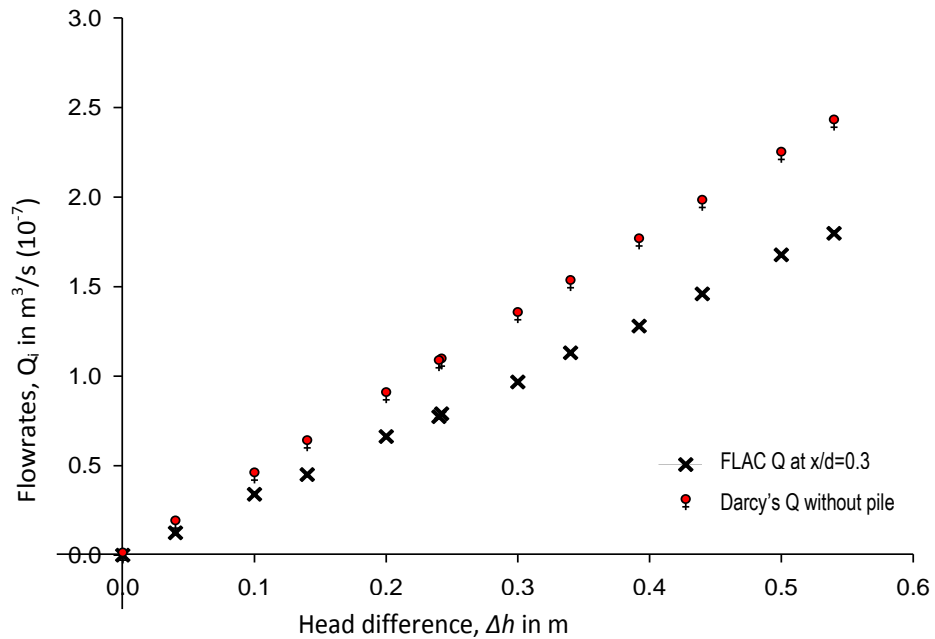
Figure 3.4: Variation of flowrates, Q_i, with head difference, Δh, at x/d=0.3. Flowrates were calculated using Darcy's law are plotted for comparison.

Effect of flow tank length, L_M

It is recognised that altering the length of a flow channel while keeping other parameters constant would cause an opposing change in steady state flowrates. This is due mainly to changes in the lengths of the flow paths along which each groundwater unit travels and the consequent inverse impact on the hydraulic gradient. Thus increasing the length of the numerical model, while keeping other factors constant, should cause a corresponding reduction in flowrates. Simulations were conducted to verify this supposition for the numerical model used. The length, L_M, of the model flow tank was increased by a factor of 2 and the numerical results compared. As illustrated in Figure 3.6a, increasing the model length to $2L_M$ caused a significant reduction in steady state flowrates as expected. The numerically calculated flowrates approached the asymptote of flow calculated using Darcy's law for lengths L_M and $2L_M$.

To enable further comparisons, flowrates were normalised using the product of the cross-sectional area and the hydraulic head difference between the recharge and discharge surfaces, ($Q/A\Delta h$). Figure 3.6b shows that the normalised pore pressures for lengths L_M and $2L_M$ both increased with x/d. The rate at which this change occurred is particularly significant for $x/d<0.5$ after which the impact of x/d diminishes.
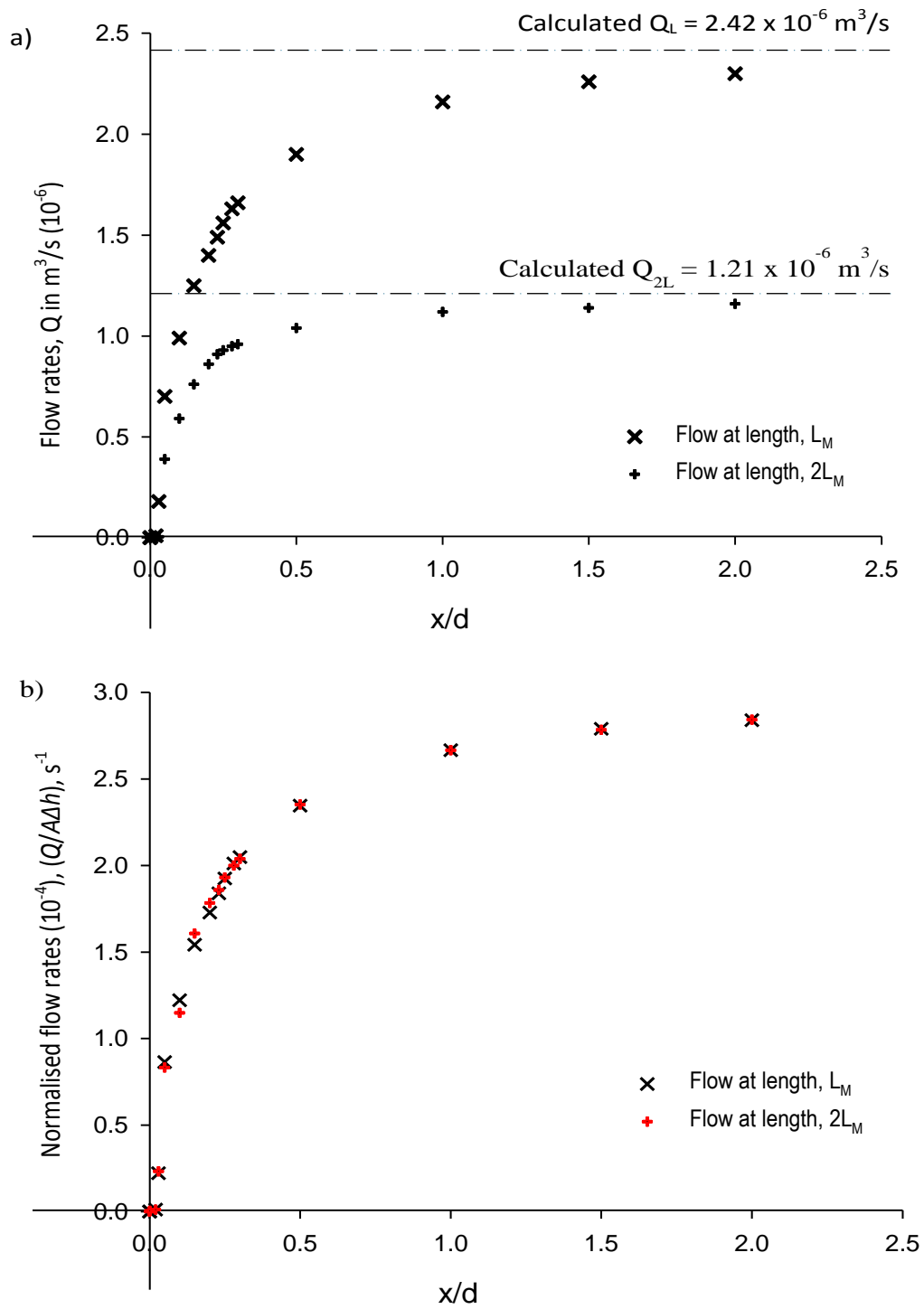
Figure 3.5: a) Comparison of flowrates for model lengths *L* and *2L* at a pressure difference of 5.4 kPa between the recharge and discharge surfaces. Normalised flowrates, $Q/(A\Delta h)$ in units of s^{-1} are shown at b).

Effect of flow tank width, w_M

Steady state flowrates, Q_i, are proportional to the width of the numerical model, $(x+d)/2$, in accordance with Darcy's law. The impact on pore water pressures behind the piles, in the presence of through-wall seepage, is however less certain. Numerical simulations were carried out at a constant pressure difference of 2.4 kPa between the recharge and discharge surfaces to determine the impact of the model width on steady state flowrates and pore water pressure near the pile section. Steady state flowrates, as would be expected, increased as the width of the numerical model increased. Flowrates were normalised using the product of the hydraulic head difference between the recharge and discharge surfaces and the cross-sectional area ($Q/\Delta hA$). Figure 3.7a illustrates that normalised flowrates were similar except for slight variations observed for x/d between 0.3 and 3. As x/d increased the normalised values of steady state flowrates converged.

Pore water pressures calculated on the back of the piles decreased with increased flow channel width as shown in Figure 3.7b. Pore pressures for the two model widths however converged at higher pile gap to diameter ratios.

Observations from parametric studies

The parametric studies extablished that the numerical model was adequate for simulations of flow in the horizontal plane. The flowrates calculated from the numerical analyses were consistent with those calculated using Darcy's law. Where variation of steady state flow occurred, these were usually attributable to the influence of the low permeability pile section which was not accounted for in the analytical solutions.
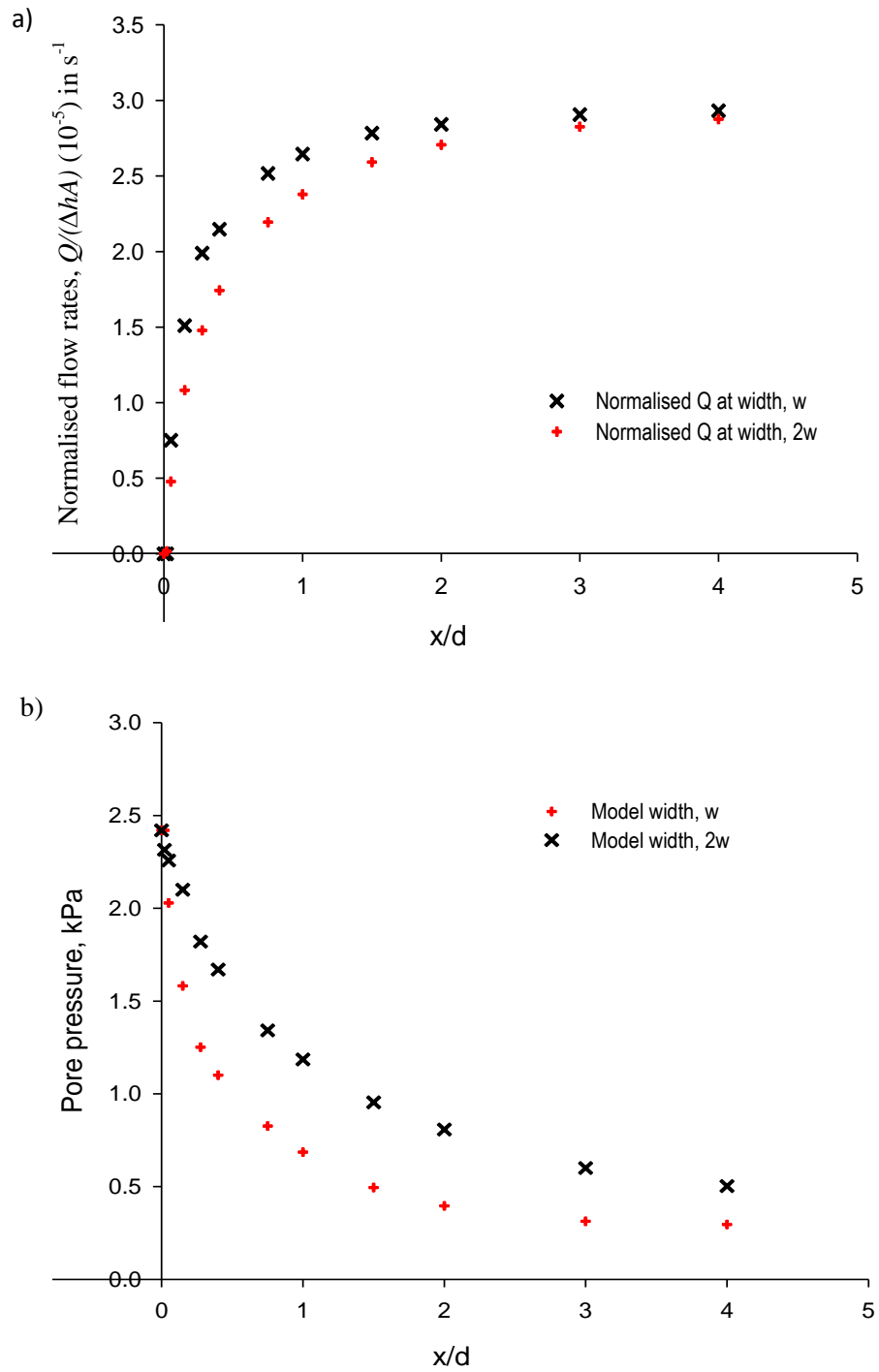
Figure 3.6: a) Comparison of steady state flowrates for model width w and $2w$ at varying pile gap to diameter ratios and b) pore pressures calculated behind the piles for the model widths investigated.

3.4.4 Results and discussion - Stage 1 horizontal plane analysis

The results of the numerical simulation of flow in the horizontal (x-y) plane, carried out in stage 1, are presented and discussed in the following sections. Where appropriate, comparisons were made between the numerical results and existing analytical solutions.

Groundwater flow around the piles

FLAC^{2D} has a built in feature which enables the movement of 'particles' representing groundwater to be tracked between two points in the numerical grid and for the resulting flow paths to be displayed graphically. The start point in the numerical grid is given in terms of the FLAC^{2D} coordinate system with the number of particles to be tracked stated. For example, the paths taken by a number of particles, *n*, may be tracked from the left hand side of a model. The particles are automatically distributed evenly at the recharge surface of the numerical grid and are then 'carried' along by the transporting fluid to the point of discharge. This is analogous to injecting a dye at various points in the upstream end of a physical laboratory model and observing the evolution of flow lines. Tracking flow paths in the numerical model therefore allows examination of the typical physical paths taken by a series of particles from the recharge boundary to the discharge surface and is useful in drawing groundwater flow patterns, which are similar to rudimentary flownets.

The installation of low permeability pile sections into the flow channel, as illustrated in Figure 3.8, restricted the groundwater flow paths. This contrasted with flow through a channel without any restrictive pile section and in which the flow paths were therefore simply linear, following the shortest distance from recharge to discharge surfaces. Figure 3.8 also shows, as would be expected, that as the pile diameter increased, the effect on the flow regime also increased with greater deflection of flow paths due to the low permeability pile sections.
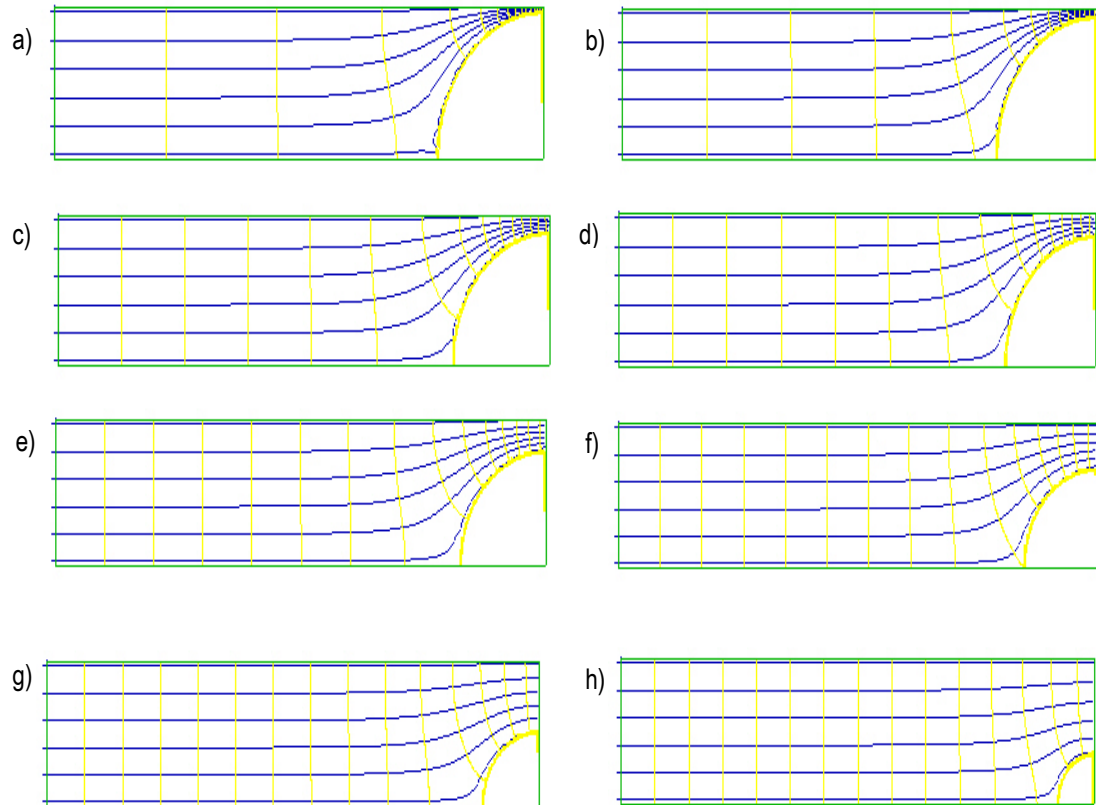
Figure 3.7: Flow paths (horizontal plane) for pile gap to diameter ratios of, a) 0.05, b) 0.1, c) 0.15, d) 0.2, e) 0.3, f) 0.5, g) 1.0 and h) 2.0.

Development of hydraulic gradient behind the piles.

The hydraulic gradient at the back of the pile was calculated using the difference between the pore water pressures at the distance of influence and at the discharge surface. The distance of influence, Δl_1, was taken as the point at which the impact of the impermeable pile section on the pore pressure contours, as shown in Figure 3.9, was negligible.
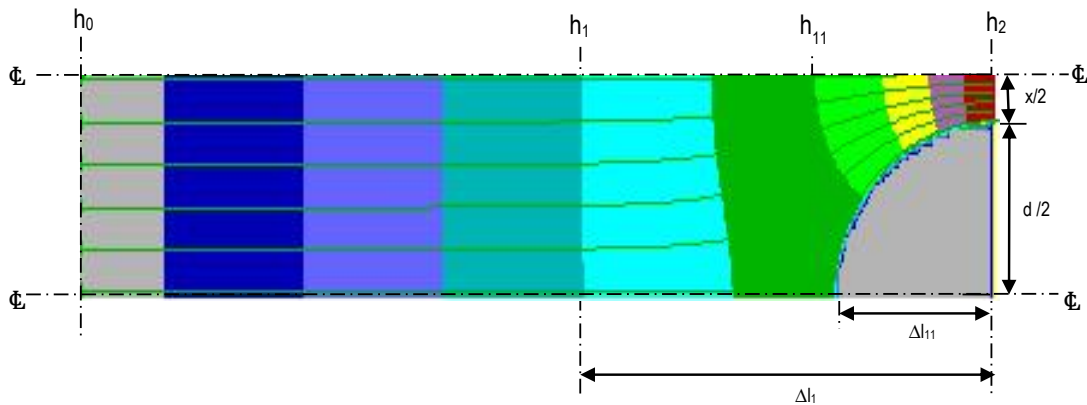
Figure 3.8: Plan of experimental flow conditions. The designation h_{11} represents the hydraulic head calculated at the back of the pile section.

The analyses were repeated for pressure differences ΔU_i between the recharge and discharge surfaces of 0.4 kPa, 2.42 kPa, 3.4 kPa and 5.4 kPa. Hydraulic gradients were normalised using the hydraulic head differences calculated from the value of ΔU_i for each simulation. The results, plotted in Figure 3.10, show that the normalised hydraulic gradients behind the piles decreased as x/d increased. This was consistent for various values of ΔU_i. The initial changes in hydraulic gradients were particularly large at small increases in pile gap to diameter ratios. This rate of decrease of hydraulic gradients reduced as x/d approached a value of about 0.5 after which reasonably constant values of hydraulic gradients were observed for the values of ΔU_i examined.
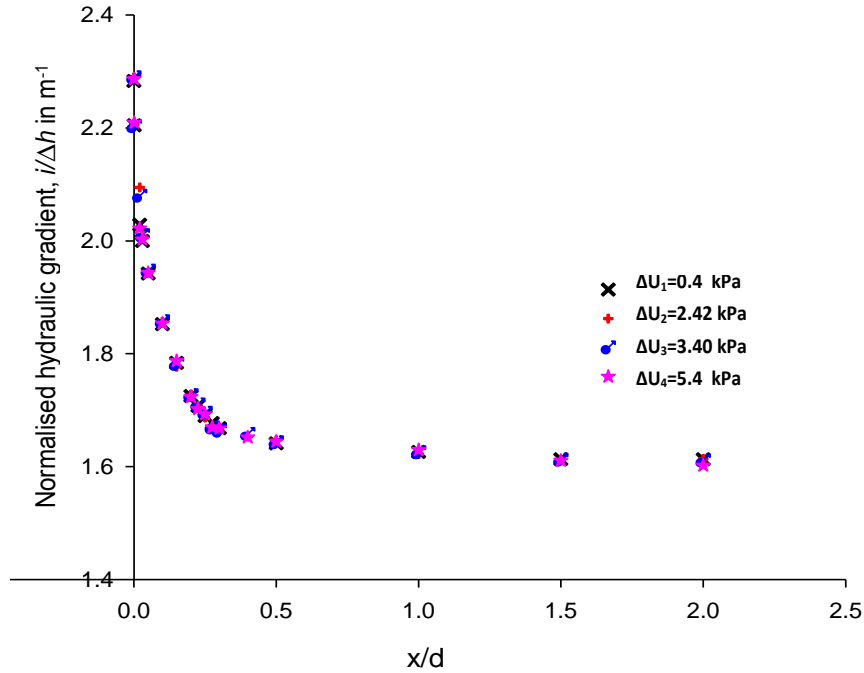
Figure 3.9: Variation of hydraulic gradient, i_j with pile gap to diameter ratio; where i_j correspond to hydraulic gradients at pressure difference, ΔU_j and the values increased from i_1 to i_4.

Calculating bulk permeability, k_p for the equivalent structure

The convergence criteria previously described were used to calculate steady state flowrates from the investigation of flow in the horizontal plane. The resultant bulk permeability, k_p, of the equivalent structure was calculated using Darcy's law for steady state flow in two dimensions, as in Equation 3.3:

$$Q = A_p k_p \frac{\Delta h}{\Delta l}$$

Equation 3.3

Volumetric flowrates, Q in Equation 3.3 were obtained directly from the numerical simulations at different pile gap to diameter ratios x/d. The other terms in the equation were obtained by considering Figure 3.9, which is a contour plot of the pore water pressure distribution around an impermeable pile section. The hydraulic head difference, Δh, was calculated from hydraulic head values, h_1, at the distance of influence and those at the discharge surface, h_2. It was assumed that the influence of the pile section on the pore water pressure distribution reduced as the distance from the

65

model pile increased. Consequently, scrutiny of the pore water pressure contours showed higher total head gradients near the impermeable pile as seen in Figure 3.9. Comparisons were made with Δh taken as the hydraulic head difference from the back of the pile to the discharge surface (h_{11}-h_2). Two distances were used, for comparison, in the calculation of the hydraulic gradient, Δl_1 and Δl_{11} as shown in Figure 3.9. It was observed that the results were similar for Δl_1 and Δl_{11}.

As previously noted, the pore pressure at the discharge surface was a boundary condition with a value of zero for the case 2 analyses. Therefore, h_2 was calculated from the value of the pore pressure contour at the face of the discharge region. Since it was the bulk hydraulic conductivity of the equivalent structure that was of interest, the area, A_p used in the calculations was taken as the total cross-sectional area per unit depth, $(x+d)/2$. The bulk permeability, k_p, of the equivalent structure was therefore calculated from steady state flowrates at different values of x/d by substituting into Darcy's law as shown in Equation 3.4.

$$Q = \frac{(x+d)}{2} k_p \frac{(h_1 - h_2)}{\Delta l} \qquad\qquad \text{Equation 3.4}$$

Steady state flowrates, Q_i, at three pressure differences, ΔU_i of 5.4 kPa, 3.4 kPa and 2.42 kPa, between the recharge and discharge surfaces were normalised using the product of the cross-sectional area, A, and the head difference calculated from ΔU_i, (Q_i/Ah_i) and are shown in Figure 3.11. The value of ΔU_i used throughout the investigation represented the difference in water levels at the top of the supply reservoir and at the two outlet levels of the overflow tank that will be used in subsequent laboratory experiments described in Chapter 4. Figure 3.11 shows that the normalised flowrates, which were similar, increased with x/d and converged onto the asymptote representing the normalised analytical flowrates calculated using Darcy's equation and the values of ΔU_i.
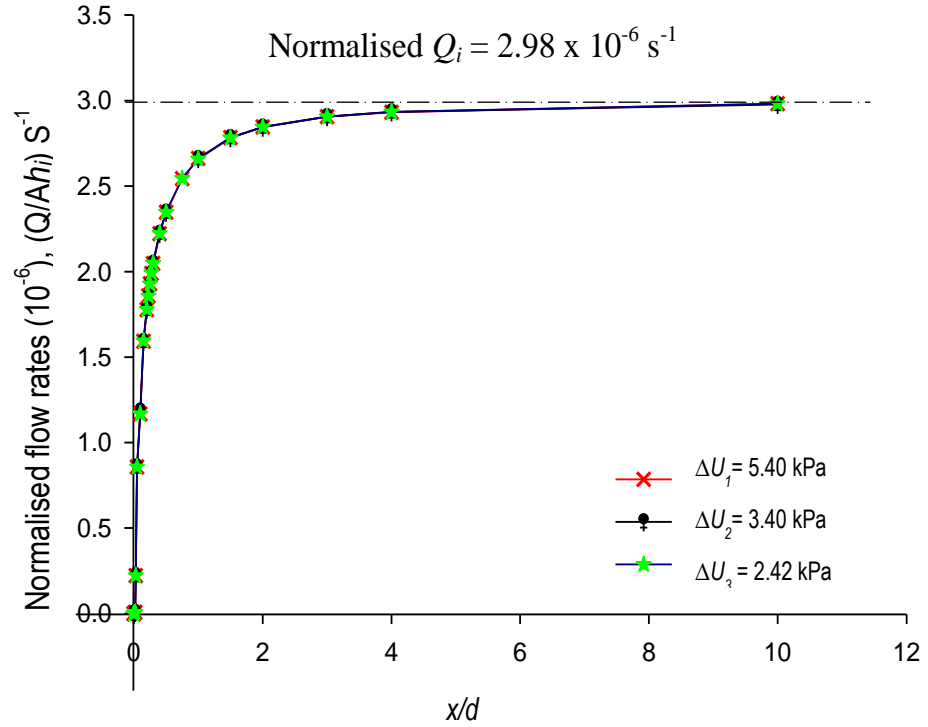
Figure 3.10: Normalised steady state flowrates at different pressure differences, ΔU_i. Flowrates, Q_i were normalised using the product of the flow area, A and the hydraulic head differences calculated from U_i.

The bulk permeability, k_p from the numerical simulations was calculated by rearranging Darcy's law as shown in Equation 3.5 for values of x/d. This was done for ΔU_i of 2.42 kPa, 3.4 kPa and 5.4 kPa. The hydraulic conductivity of the soil, k_s was taken as 2×10^{-5} m/s throughout. To establish a relationship between the soil permeability, k_s, the bulk permeability, k_p, the pile gap, x, and the pile diameter, d, the calculated values of k_p/k_s were plotted against the pile gap to diameter ratio, x/d as shown in Figure 3.12 and a relationship generated.

$$k_p = \frac{Q_i \Delta l}{\Delta h A}$$

Equation 3.5

67
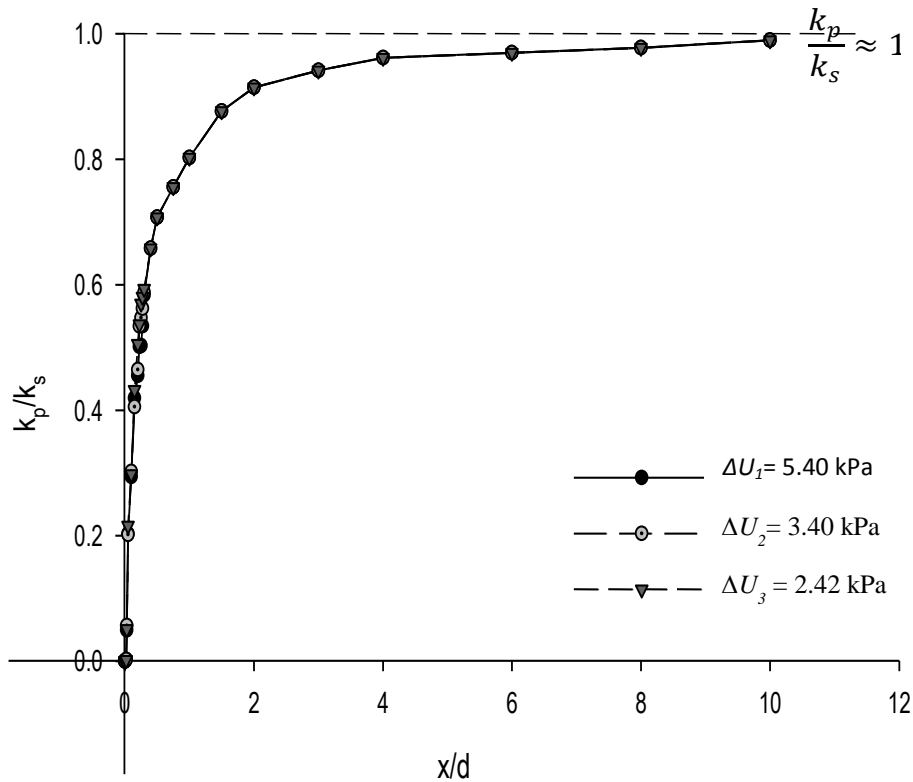
Figure 3.11: Calculated permeability ratio k_p/k_s for three pressure differences, ΔU_i used in the numerical simulations in FLAC^{2D}.

As illustrated in Figure 3.12, the resulting permeability expression was consistent at all value of ΔU_i. This level of consistency was expected because the analyses were based on Darcy's law, which ensured that the proportionality between the flowrates, for instance, and the hydraulic conductivity was maintained. Similarly, 3D phreatic surface effects were not active during the horizontal plane strain analysis.

After comparing the numerical results, an empirical hyperbolic relationship, of the form in Equation 3.6, which relates the permeability ratios to pile gap to diameter ratios, was derived.

$$\frac{k_p}{k_s} = \frac{4\frac{x}{d}}{1+4\frac{x}{d}}$$

Equation 3.6

This relationship may be used to calculate the equivalent bulk permeability of a continuous wall representing contiguous pile retaining walls in two dimensional plane strain analysis up to a pile gap to diameter ratio, *x/d* of about 0.5. Equation 3.6 was used to calculate the permeability ratios for various *x/d* and the results plotted as shown in Figure 3.13.
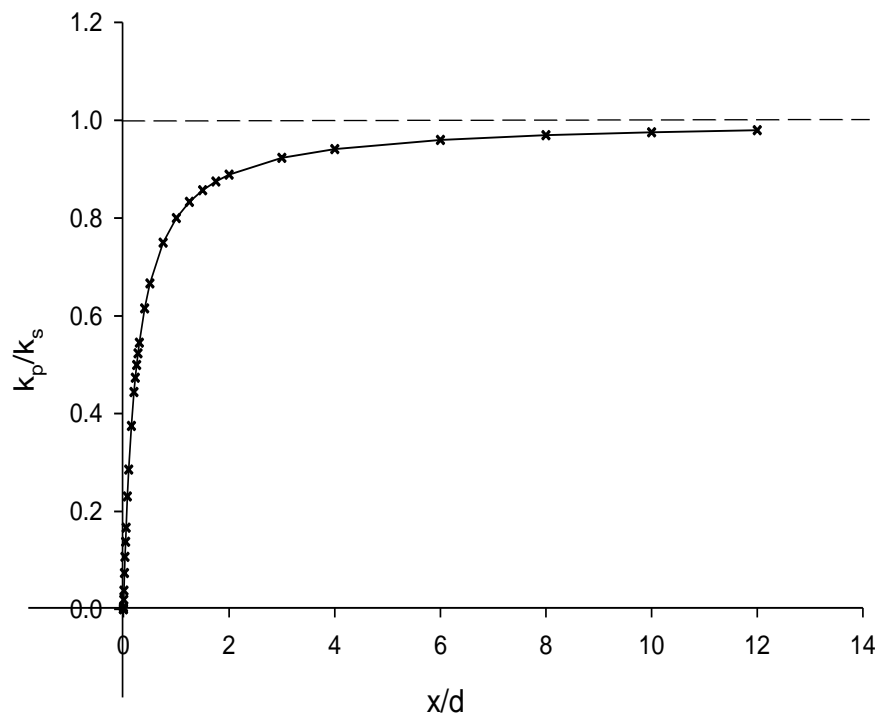
Figure 3.12: Plot of Equation 3.6. This relationship can be used to apply an equivalent bulk permeability to numerical simulation of contiguous pile in 2D plane strain analyses.

It is evident from the preceding discussion that the objectives of the groundwater flow analysis in the horizontal plane were fulfilled. The effects of changes in pile gap to diameter ratios and model geometric properties have been established. A useful expression for assigning equivalent bulk permeability to continuous walls representing contiguous piles in 2D plane strain was derived.

3.5   Stage 2- Phreatic effects: vertical (z-x) plane flow

Numerical simulations of flow through the vertical (z-x) plane were conducted to determine phreatic effects on the hydraulic conditions. The objectives of the analyses were to:

i)   Observe the flow paths taken by groundwater when a bulk permeability was applied to a continuous model wall representing a contiguous pile retaining wall in two-dimensional plane strain analyses,

ii)   Compare the development of pore water pressures at the back of the uniform wall with the pore pressures calculated at the same positions during the horizontal flow analyses and

iii)   Quantify the negative effects of allowing through-wall seepage.

The changes in hydraulic conditions around the permeable wall were also compared with those around an impermeable retaining wall, which was also represented in the 2D simulations by a continuous wall.

3.5.1 Initial and boundary conditions

The soil in the numerical grid was fixed from movements at the left, right and lower boundaries as shown in Figure 3.3. The model wall was restrained from rotation, translation and movement in the vertical direction. The soil adjacent to the model wall was however allowed to move in order to observe the effect of the developing hydraulic regime on soil displacement. The initial soil stresses were developed by allowing the unit weight of the soil to be automatically converted to vertical total stresses by the built-in facility in the numerical code. A hydrostatic distribution of soil stresses and pore water pressures were initially assumed for the analyses. All initial soil stresses and water pressures at the soil surface were assigned zero values. Gravitational acceleration of 10 m/s^2 was applied throughout the model while the coefficient of earth pressure at rest, K_0, was set to 1.

As before, two initial hydraulic boundary values, case 1 and case 2 were considered. For the case 1 analyses, the initial water level was assumed to be at the top of the model. Groundwater discharge was simulated by lowering the water level at the overflow tank to the level corresponding to a pressure difference of ΔU_i between the recharge and discharge boundaries. Likewise, case 2 simulations started with the assumption that the flow tank was empty with the pore pressures set to zero. The water level at the recharge surface was raised instantaneously to a level which corresponded to the pore pressure difference, ΔU_i, while the discharge water level was maintained at zero.

3.5.2 Numerical procedure

The investigations began with a wished into place model retaining wall. This was a continuous uniform wall representing the circular pile sections in 2D vertical plane strain analysis. The thickness (t) of the plane strain model wall at various pile gap to diameter ratios was calculated using the approach adopted by Powrie *et al*. (1999). In this method, the second moments of area (I) of the different cross-sections were equated using Equation 2.7 and the model wall thickness (t) calculated. The assumption made in this analysis was that different cross-sections of the same material have similar second moments of area. This enabled variations in geometric properties, such as wall thicknesses, to be calculated. Comparisons were made with the equivalent thickness calculated using the stiffness method adopted by Day and Potts (1993) (see Equations 2.5 and 2.6). This method is similar to that in Equation 2.7 with the additional inclusion of the material stiffness. The equivalent wall thicknesses calculated using both methods were very similar.

The model was brought to equilibrium with the simulated water level at the top of the flow tank corresponding to an applied pore pressure of U_0 for case 1 analyses. The overflow tank was 'turned on', which caused a reduction in the water levels consistent with a pressure difference, ΔU_i between the recharge and potential discharge surfaces. This induced groundwater flow. Flow through the model wall was achieved by applying a zero pore pressure boundary to the exposed surface of the model wall and

allowing the phreatic surface to develop automatically using the built-in facility in FLAC^{2D}. The equivalent permeability of the continuous retaining wall was assigned using the bulk permeability relationship, Equation 3.6, derived in the horizontal flow analysis. At this stage in the investigations, flow around the model wall was dominated by the applied equivalent bulk permeability. The procedure was repeated for different values of ΔU_i. The model wall thickness and bulk permeability were then changed to reflect different pile gap to diameter ratios, x/d, and the procedure repeated. Steady state pore water pressures at various positions behind and in front of the model wall were measured and the results discussed in the following sections. The simulations were repeated for case 2 hydraulic conditions. No significant differences between the cases 1 and 2 hydraulic conditions were observed in the results.

Effect of wall geometric properties on the numerical results

Orr (1987) suggested that the basic parameters of interest in geotechnical engineering designs are the soil strength, the load conditions and the geometric parameters including the groundwater level. As the focus of this study was on the development of the hydraulic conditions due to through-wall seepage, the soil and wall strength parameters, as far as they do not directly influence the hydraulic regime, were largely ignored. The effects on hydraulic loadings have so far been studied. Therefore, the following sections mainly describe investigations into the effect of the wall and model geometric properties on the hydraulic conditions adjacent to the retaining walls. Thus, parametric studies were conducted to determine the sensitivity of the numerical results to different soil and wall geometric properties not considered in the horizontal plane flow analysis. Additional modifications were made to the flow tank geometry during the simulations to establish how the geometric properties of the flow tank affected the results of groundwater simulation. The results of the analyses are presented and discussed in the following sections.

Effect of model wall embedment length

It is well established that, for impermeable retaining walls, increasing the depth of embedment causes a corresponding increase in the length of the flow paths around the wall. For instance in order to reduce the uplift due to water pressures in front of a retaining wall, the length of embedment may be increased. This causes a reduction of the critical hydraulic gradient in front of the wall (CIRIA 104). This assumption is based on the linear seepage approximation method, which is valid for an impermeable monolithic retaining structure in a homogenous soil. However, it was not previously reported how the flow paths would behave in the presence of through-wall seepage. In the 2D numerical analyses conducted in these studies two types of model walls with identical material properties but varying geometries were compared. Type 1 walls extended to the base of the numerical grid while type 2 walls stopped short of the base. If these were impermeable retaining walls, then there would be a build-up of groundwater behind the type 1 wall and groundwater would flow, in the classical sense, around the type 2 wall.

During these investigations into semi-permeable retaining walls, pore water pressure profiles behind and in front of the model walls were calculated and comparisons made between the types 1 and 2 walls. The results in Figure 3.14 show that pore pressures for the type 1 and type 2 walls were identical. This indicates, importantly, that once through-wall seepage was allowed, the lengths of the retaining wall did not significantly affect the hydraulic loads acting on the wall. Pore pressures were also compared with the hydrostatic distribution in front of and behind the model walls. As expected, the pore pressures measured behind both walls were less than hydrostatic while those in front were higher. This is typical of the pore pressure distribution from the well-established linear seepage approximation of pore pressures around impermeable retaining walls.
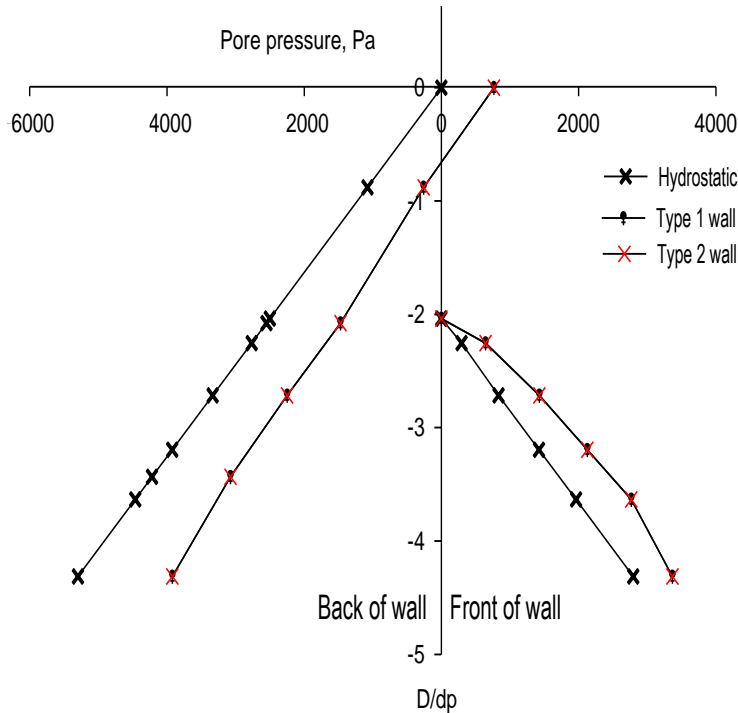
Figure 3.13: Pore pressure profiles for type 1 walls extending to, and type 2 walls stopping short of, the base of the model. Hydrostatic profiles are shown for comparison.

Flow patterns were investigated by 'injecting a set of particles' at the recharge boundary. The developing flow paths were tracked to determine the direction of flow of the fluid especially in the presence of the semi-permeable wall. The results, illustrated in Figure 3.15, show that increasing the depth of embedment, for the semi-permeable model wall, did not affect significantly the direction of the flow paths. In fact, steady state flow patterns for the types 1 and 2 walls are identical. Therefore, groundwater flow was simply through the walls. Similarly, comparison of the equipotential heads around both model walls showed no discernible differences. Again, the plots for the two embedment depths seem very similar. This reaffirms the earlier observation that once the retaining wall in the numerical simulations is considered permeable, then the length of embedment does not affect the hydraulic distribution. This is significant for geotechnical designs of contiguous piles used for their reduced pore pressure characteristics. It was however noted that the definition of relative permeability for the uniform model wall differs. Zdravkovic *et al*., (2007) suggested that a model wall can be considered permeable for $k_s/k_w > 1000$ whereas Powrie (2013) suggested a less conservative $k_s/k_w > 400$ as the lower limit of wall permeability.
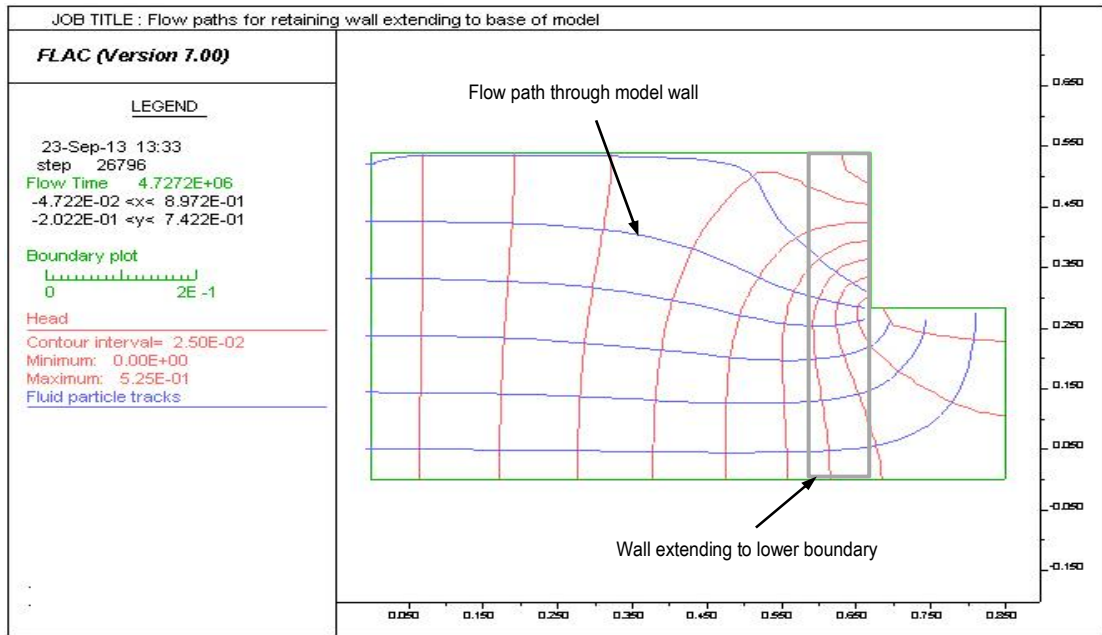
a)
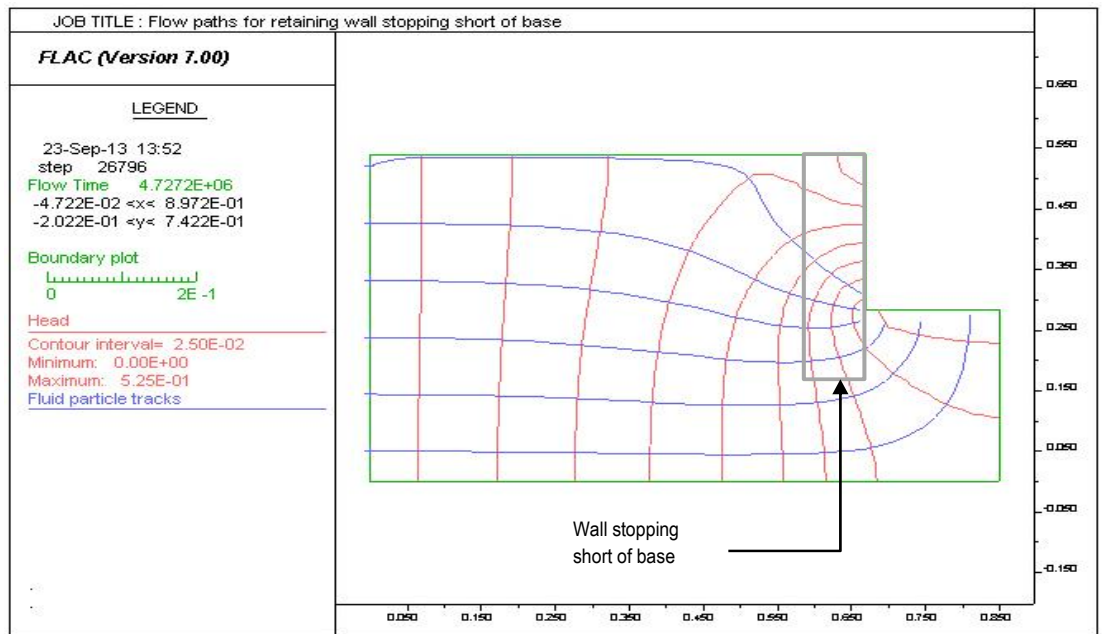
b)

Figure 3.14: Comparison of flow paths (at *x/d*=0.25) for the model wall a) extending to and b) stopping short of base of flow tank. There is negligible difference in flow paths and head contour distribution. The plots are not intended to be flownets hence the flow elements are not curvilinear.

Effect of flow tank length, (L_M)

The impact of varying the flow tank length, L_M, was investigated in the horizontal flow analyses in stage 1. It was thought however, that the distance over which the hydraulic head is dissipated might have an impact on the phreatic effects of flow in the vertical plane. Consequently, *2D* numerical simulations of flow in the vertical plane were conducted to study the variation of hydraulic properties with model length, L_m. The model lengths of interest were measured from the recharge boundary to the back of the retaining wall. All other parameters were kept constant during these analyses. The results were then compared in terms of the development of groundwater flow paths, pore pressure distribution adjacent to the model wall and steady state flowrates. A pile gap to diameter ratio, *x/d,* of 0.5 was used throughout.

Figure 3.16 shows a slight difference in flow patterns between the model walls of lengths L_M and $2L_M$. Specifically, it was noted that the flow paths for the model of length $2L_M$ were pulled down by the action of gravity on the fluid particles over the length of the model. The effect on flow path direction might also be attributed to the greater dissipation of potential energy over the increased length of the flow tank. The result however, was that the flow paths for the longer model appeared to be closer to the lower boundary of the model. This is particularly evident closer to the wall. Additionally, the positions of the hydraulic head contours adjacent to the model wall were also different, albeit not significantly so.
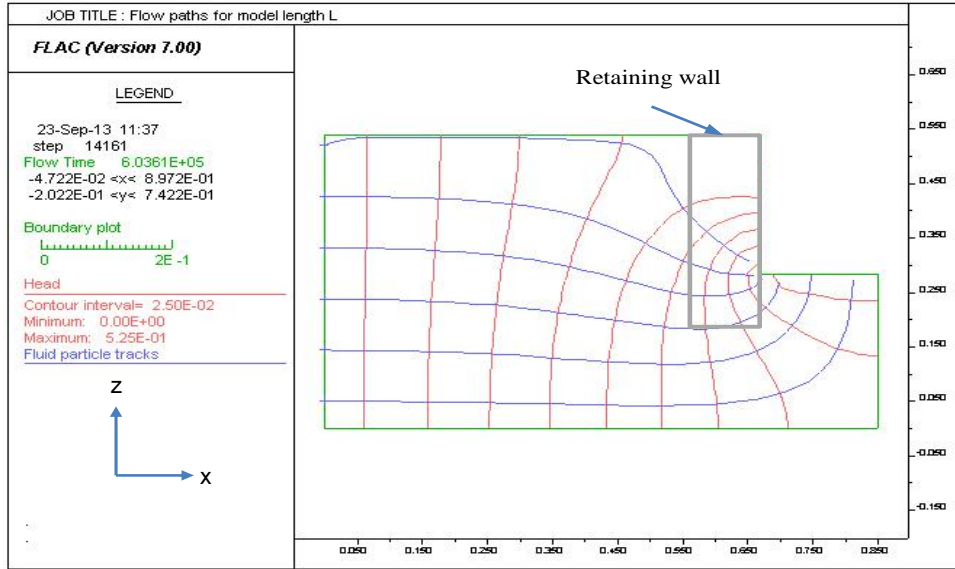
a)
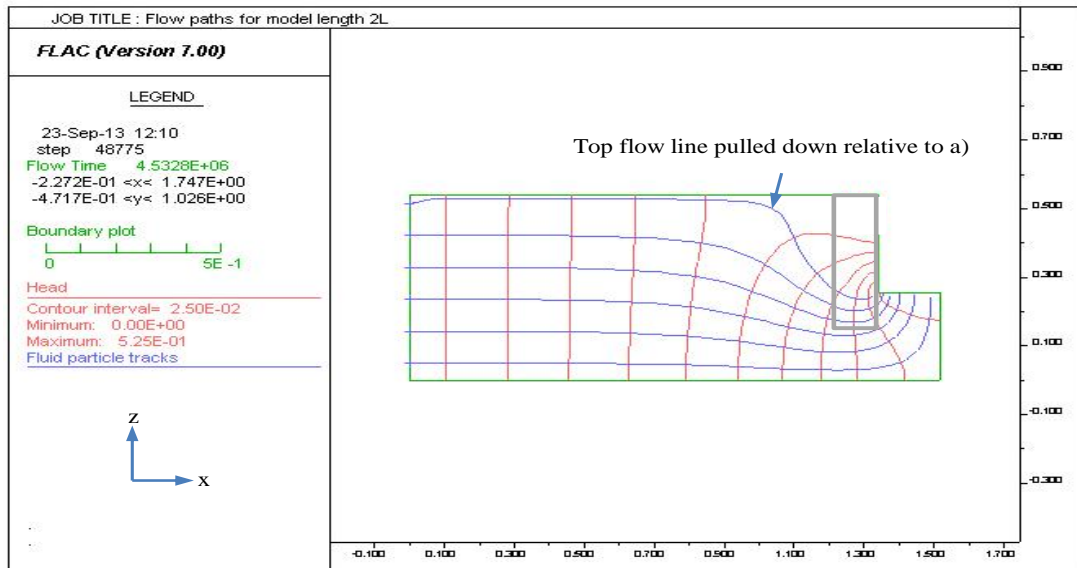
b)

Figure 3.15: Comparison of flow paths for models of lengths L_M and $2L_M$. Slight variation of flow patterns was observed.

Pore water pressure distribution around the model walls for lengths L_M and $2L_M$ were also compared. As illustrated in Figure 3.17, pore pressures at the front and back of the model of length, $2L_M$, were marginally less than those observed for model length L_M. This was consistent behind and in front of the model wall. The reduction in pore pressure due to model lengths may be attributed to the loss of energy as the water particles travel over a longer path and the maintained constant head at the supply reservoir. The differences in pore pressures observed from the profiles appeared to be increasing with depth. Similarly, both models in the presence of seepage had pore pressures lower than hydrostatic behind but higher than hydrostatic in front of the model wall.
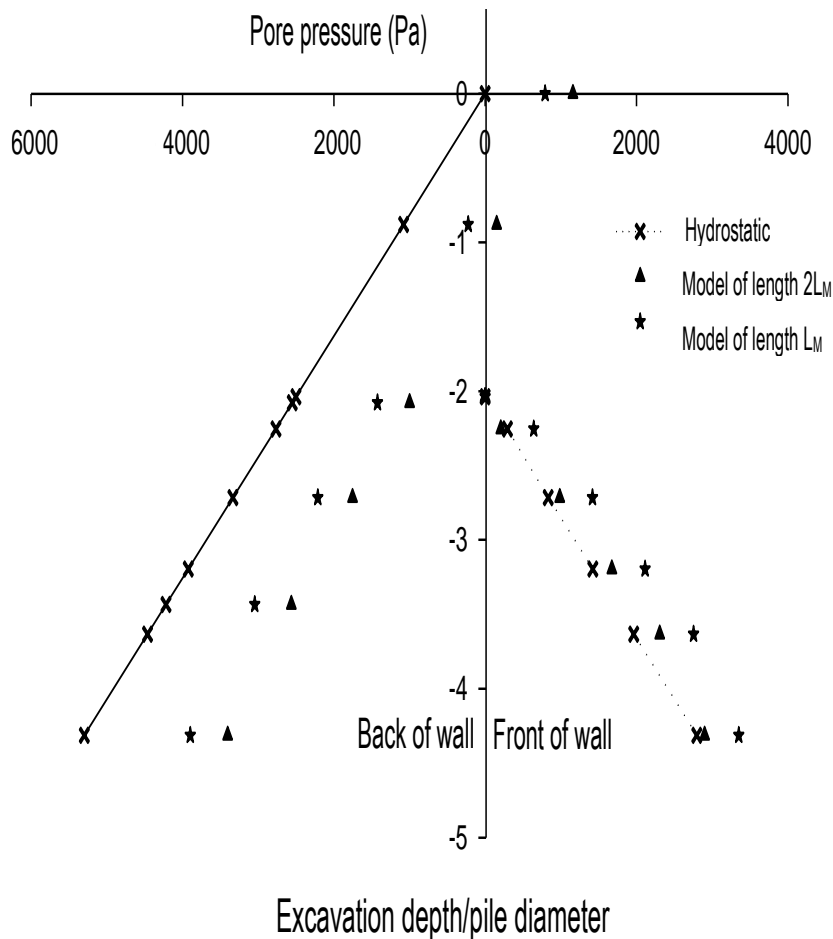
Figure 3.16: Variation of pore pressures measured in front of and behind model retaining walls of lengths L_M and $2L_M$. Hydrostatic pressures at the back of and in front of the wall are included for comparison.

Further comparisons were made between flowrates calculated for a channel without a pile using Darcy's law, flowrates calculated using the bulk permeability, k_p at x/d=0.5 (Equation 3.6) and the numerically calculated (FLAC[2D]) flow for x/d=0.5. Figure 3.18 shows that, at a constant pressure difference between the recharge and discharge surfaces of 5.4 kPa, as would be expected, steady state flowrates decreased as the model length increased. Flowrates calculated using Darcy's law, without any pile, were consistently higher at the model lengths investigated. Flowrates calculated using Equation 3.6 with k_p for x/d=0.5 was slightly less than the FLAC[2D] results for phreatic surface effects.
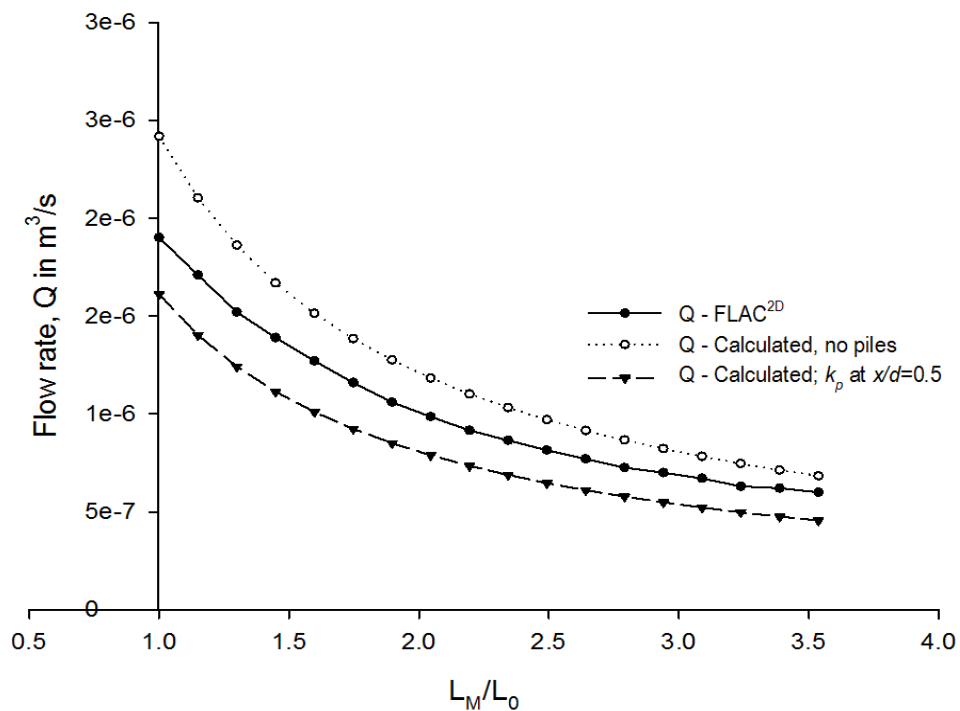
Figure 3.17: Variation of steady state flowrates, Q with model lengths, L_M.

It can be assumed therefore that the length of the flow tank had a slight impact on the development of flow patterns around the model wall, the pore pressure distribution near the wall and steady state flow quantities. This result, although not significant for the model lengths investigated, could have considerable influence on the results for numerical simulations involving much larger geometries.

Effect of model flow tank height, H_m

Investigations were carried out to determine the effect of model height, H_m, on the numerical results. Two model heights, H_M and $2H_M$ were investigated. Pore water pressures for each model height were normalised with respect to the corresponding hydrostatic pressures. The depths below surface level were also normalised against the wall length for both cases. Normalised pore pressures were then plotted against normalised depths below ground level and the results compared in Figure 3.19.

It was observed that the normalised pore water pressures behind the model retaining walls increased slightly with model height as illustrated in Figure 3.19. The water pressures however converged unto the hydrostatic pressure with increasing depth. The impact of model height was however more pronounced in front of the model wall. Normalised pore pressures in front of the wall were much higher than, but seemed to approach the, hydrostatic pressure with increasing depth. Normalised pressures in front of and behind the retaining wall are also higher for model height $2H_M$.

It is evident from the above discussion that, in the presence of through-wall seepage, the geometric properties of the wall do not significantly influence the results of numerical simulations. Some considerations however need to be made for the lengths and heights of the model selected for numerical investigations.
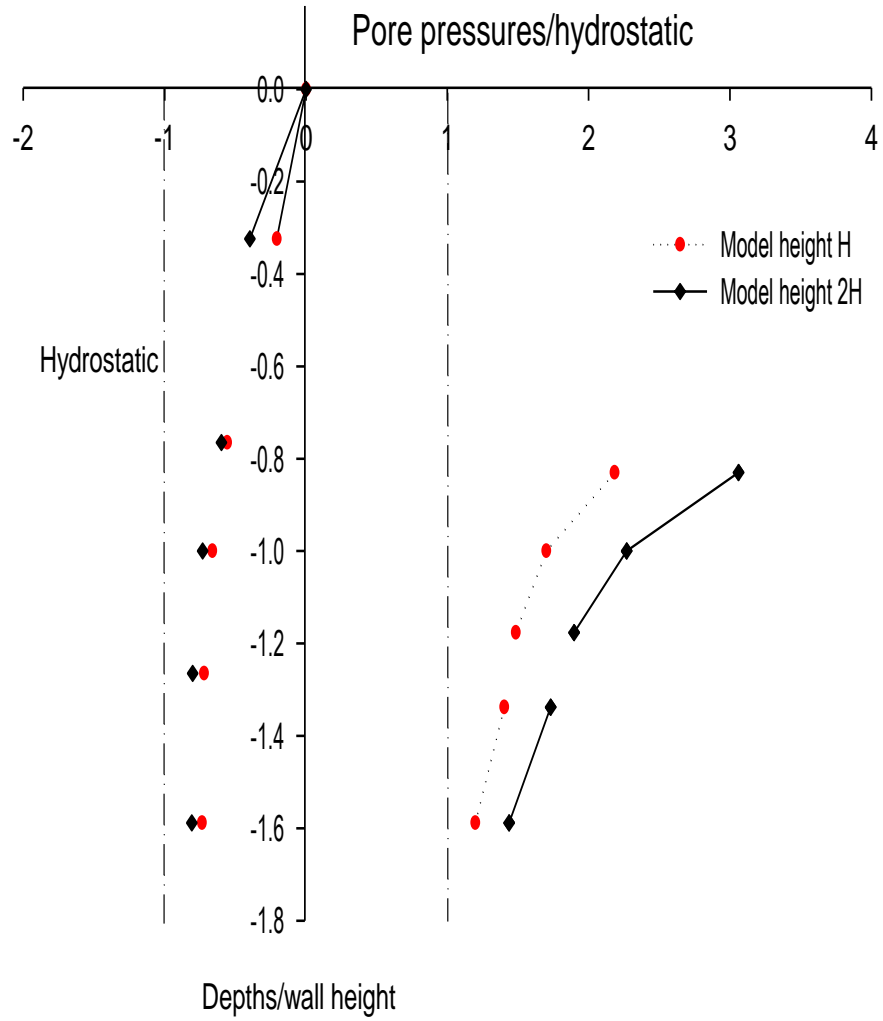
Figure 3.18: Comparison of normalised pore water pressures behind and in front of the wall for numerical models with heights H_M and $2H_M$.

3.5.3 Results and discussion of stage 2 vertical plane analysis

The results of the investigations into the vertical (z-x) plane flow are presented and discussed in the following sections. The results were analysed in terms of:

    i. The influence of the equivalent retaining wall bulk permeability on the groundwater flow regime,

    ii. The observed pore water pressure distribution in the vicinity of the model walls and

    iii. Vertical displacement of the soil behind the retaining walls.

<u>Flow behaviour around the equivalent retaining wall</u>

Flow patterns obtained from the tracking of groundwater flow were compared for various values of x/d as illustrated in Figure 3.20. The development of the conventional flow pattern for a low permeability retaining wall was observed as shown in Figure 3.20a for a pile gap to diameter ratio of x/d=0.0. At lower values of x/d, but greater than 0.0, similar profiles were observed. For example, the flow paths for x/d=0.001 are not much different to those for the impermeable wall. One notable difference between the two flow paths was however the development of a hydraulic gradient across the width of the wall with x/d=0.001. This indicates that through-wall seepage was possible although in this instance the flow was predominantly around the wall. There are significantly less pressure contours across the model wall for x/d=0.0, which indicates no flow conditions. The absence of significant flow quantities through the wall with x/d=0.001 corresponds to previous observation of semi-permeable retaining wall. For example, Zdravkovic *et al*. (2007) recommended that retaining walls in numerical analysis be considered impermeable if the wall permeability is more than three orders of magnitudes less than that of the surrounding soil. Using Equation 3.6, a value of x/d=0.001 gives a bulk permeability which borders on the suggested threshold for impermeable retaining walls in numerical simulations. Hence, the low flow quantities through the wall with x/d=0.001 were consistent with an impermeable retaining wall.
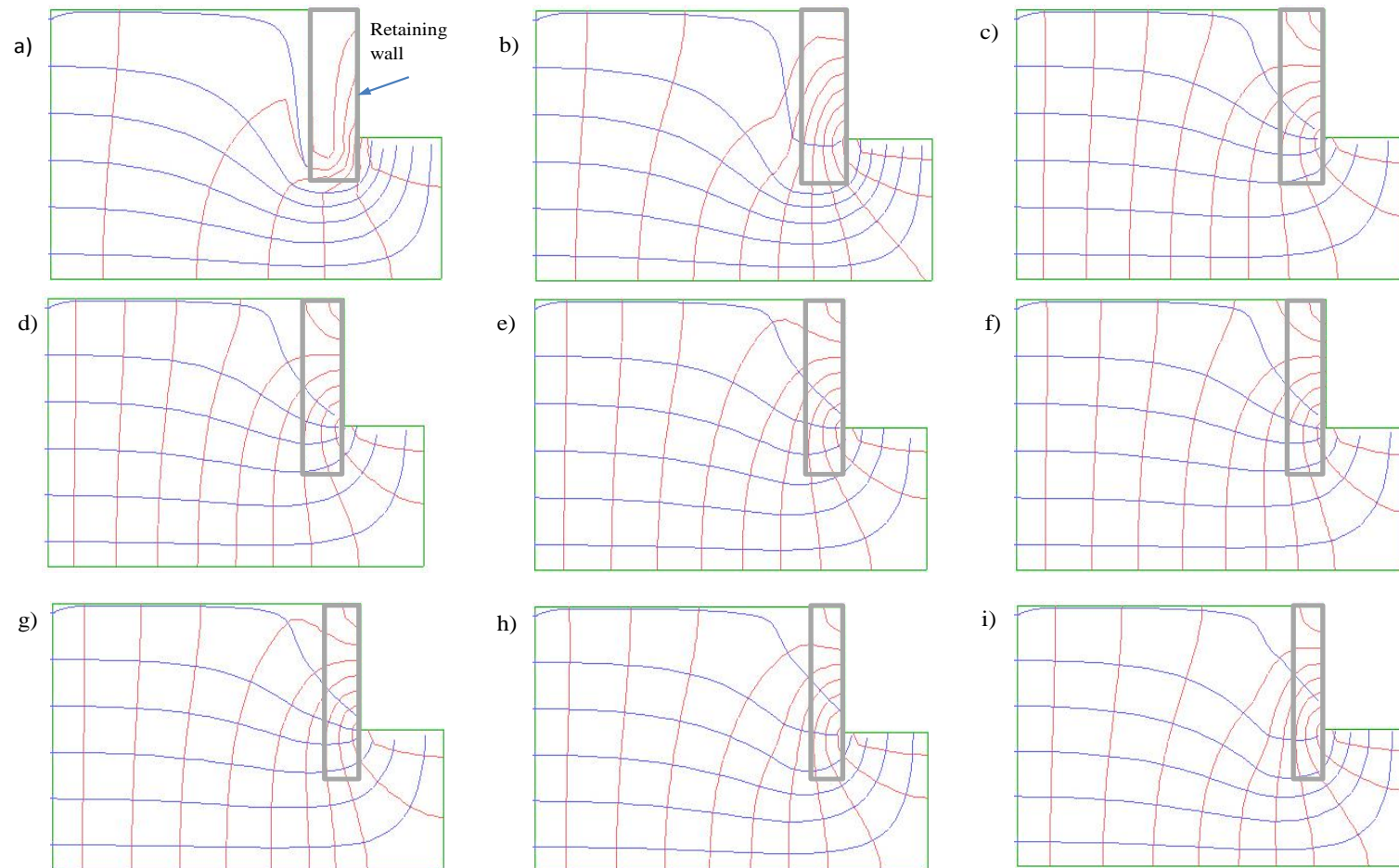
Figure 3.19: Development of flow patterns for pile gap to diameter ratios, *x/d* of; a) 0.0, b) 0.001, c) 0.05, d) 0.1, e) 0.2, g) 0.5, h)1.0 and i) 2.0.

Additionally, it was noted that as the permeability of the model wall increased, the flow regime changed causing the flow of groundwater to become predominantly through the retaining walls. Consequently, at larger values of x/d, the flow paths near the wall became more horizontal. For $x/d>0.1$ the flow paths were almost identical although there were slight differences in the distribution of hydraulic head contours around the model walls.

Pore pressure distribution

The distribution of pore water pressures was calculated at various distances behind the model wall and depths below the soil surface level. Pore water pressures at various pile gap to diameter ratios, P_i, were normalized against pore pressure for $x/d=0$, P_0. Normalized pore water pressures (P_i/P_0) were plotted against the normalized distances, (L/d) behind the model wall for various values of x/d as shown in Figure 3.21.
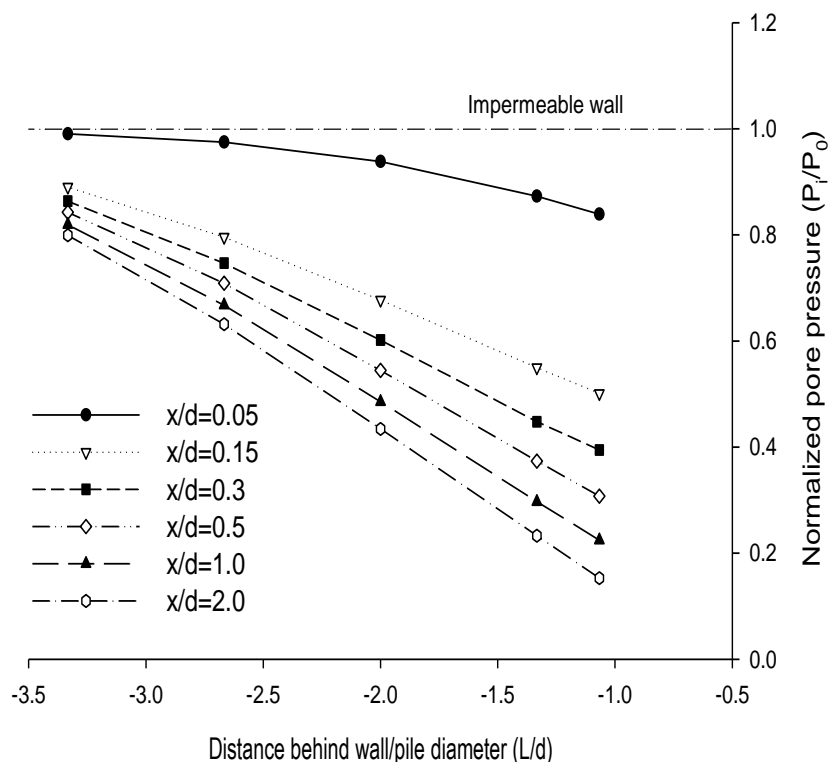
Figure 3.20: Normalised pore pressures at a depth of 0.14 m below ground level for $0 \leq x/d \leq 2$. P_i and P_0 represent pore water pressures for semi-permeable, $x/d>0$, and impermeable, $x/d=0$, walls respectively.

Calculated pore pressures at each position behind the model walls decreased as the pile gap to diameter ratios, *x/d*, and consequently the equivalent bulk permeability, increased. The reduction in pore pressures with increased *x/d* is very significant in practical terms. For example, a 50 mm gap between 1000 mm diameter contiguous piles, based on this analysis, could cause a reduction of approximately 20% in pore pressures at a distance of one pile diameter behind the wall relative to a similar retaining wall formed from secant piles. The implication for economic benefits becomes more attractive as the pile gap increases as illustrated by the inverse relationship between the normalised pore pressures and the permeability ratio, k_p/k_s, in Figure 3.21.

Further analyses showed that there was a reduction in pore water pressures and hence reduced hydraulic heads toward the model walls at various depths below the soil surface, at the back of the wall. This is illustrated more clearly by the normalized pore pressure profiles plotted in Figure 3.22, which also shows that there was a consistent overall reduction in pore pressures as *x/d* increased.
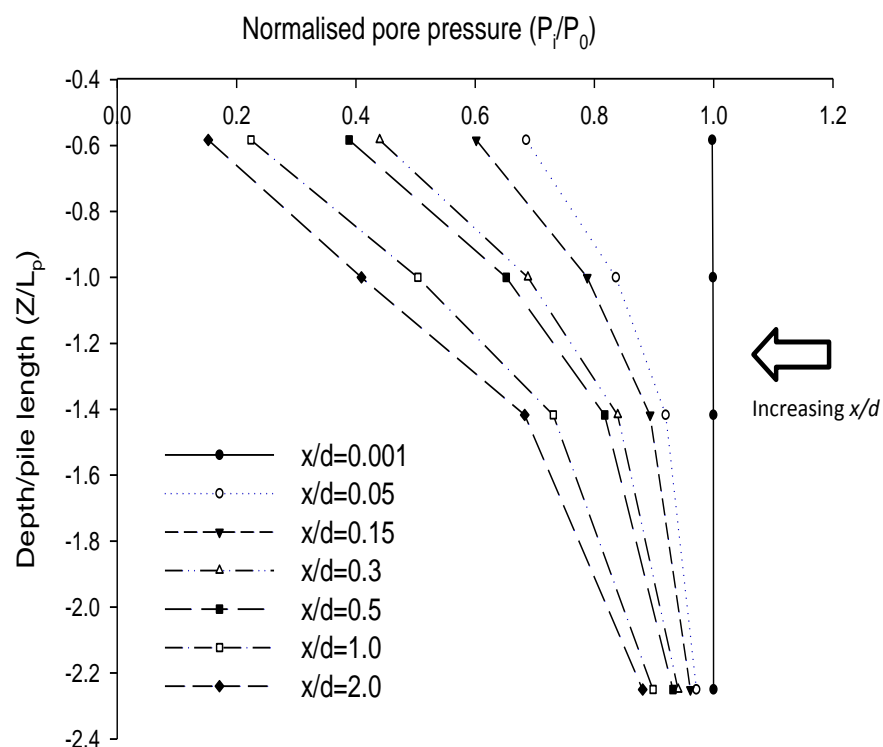
Figure 3.21: Normalised pore water pressures versus normalised depths below soil surface for different values of *x/d*. Depths, *Z*, below soil surface were normalised against pile length, L_p. Normalised pore pressures show that *x/d*=0.001 is almost impermeable.

Comparison of pore water pressures from stages 1 and 2 analyses

During the stage 1 horizontal flow analysis, pore water pressures were calculated at various distances, measured in pile diameters, behind the model pile section. This was done at different pile gap to diameter ratios, x/d. The pore pressures obtained represented steady state flow conditions in an infinitesimally thin horizontal layer through the flow channel at various elevations. Consequently, flow in the horizontal plane was not subjected to phreatic effects. Additionally, during the uncoupled hydraulic simulations in stage 1 analyses, the effects of mechanically induced pore water pressures were ignored. A similar approach was adopted for the stage 2 analysis but in which phreatic effects were introduced. The equivalent wall thicknesses were calculated based on the pile diameters as discussed previously. Thus, equivalent distances behind the model wall were related to the corresponding pile diameter from the stage 1 analysis. Pore water pressures were again calculated at equivalent distances behind the model wall. The pore pressures at similar distances behind the model wall and depths below soil surface in the horizontal (x-y) plane flow and vertical (z-x) plane analyses were compared at pressure differences, U_i, between the recharge and discharge boundaries.

Groundwater flow times for the horizontal only flow and for flow in the vertical plane analyses were normalised with respect to the flow time for an impermeable retaining wall in both planes. Pore pressures at various distances behind the model wall, expressed in numbers of pile diameters, d, were plotted against groundwater normalised flow times in both instances as shown in Figure 3.23.

The initial pore pressure distribution for the horizontal and vertical plane flow depended on the hydraulic boundary conditions at the recharge and discharge surfaces. The intermediate pore pressures were therefore calculated automatically by interpolation between the grid nodes. Consequently, Figure 3.23 shows that the initial pore water pressures at similar distances vary slightly between the two analyses. Stage 1 simulations commenced with pore pressures approximately 2.43 kPa whereas those at similar locations in stage 2 started at 2.67 kPa. This slight variation could account, in part, for the fact that the observed steady state pore pressures in the stage 2 analyses were slightly higher than those in stage 1.
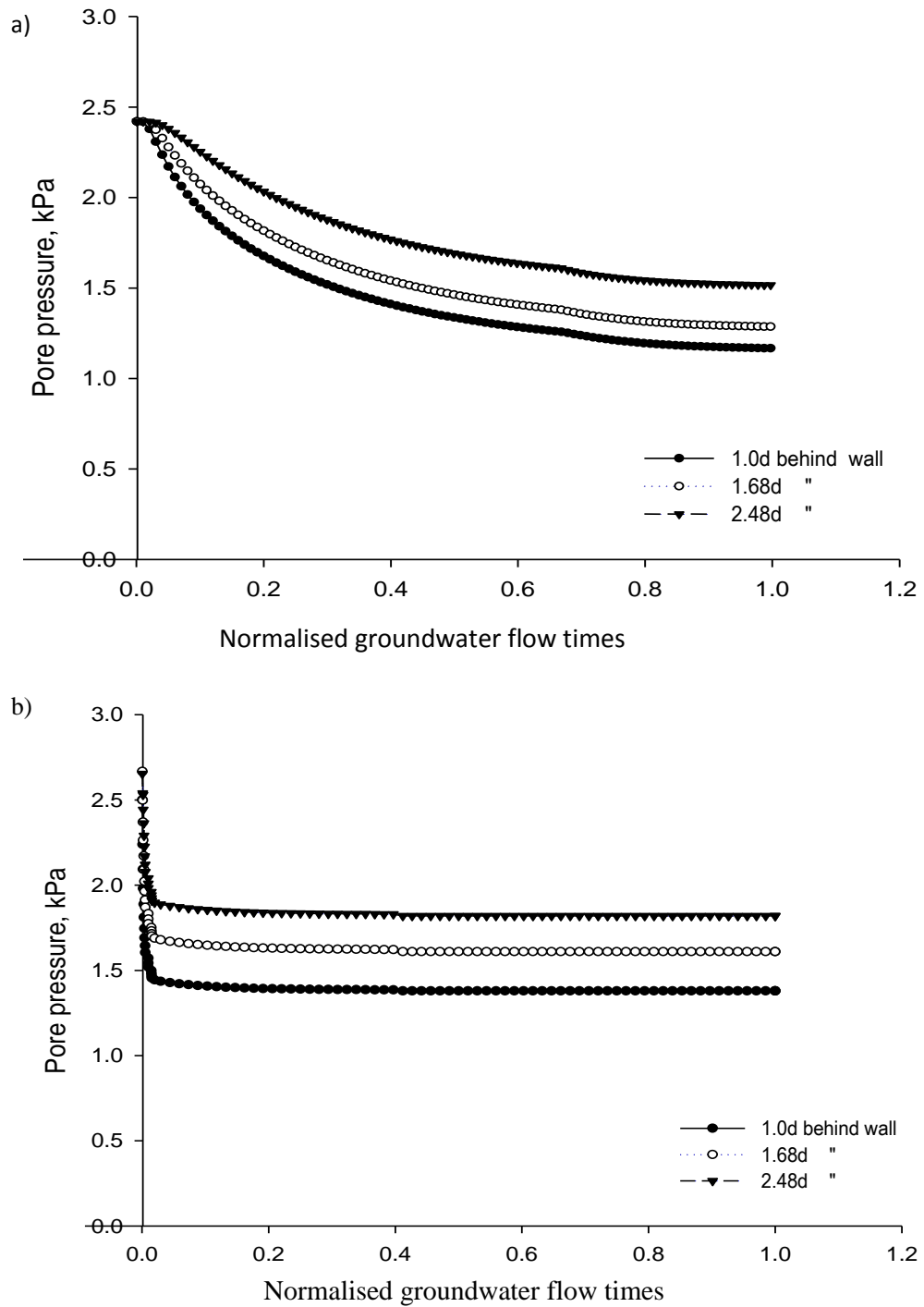
Figure 3.22: Pore water pressures for the horizontal (a) and vertical (b) plane flow at distances of 1*d*, 1.68*d* and 2.48*d* behind the retaining wall. For stage 2 analyses, *d* is taken as the equivalent thickness, *t*, of the continuous wall. Pore pressures were measured 0.24 m above the base of the model.

The omission of phreatic effects in the horizontal only flow during the stage 1 analyses in comparison with the vertical plane flow in stage 2 could have also been a factor. Even so, pore pressures at corresponding locations for flow in stage 2 compared well with those obtained from the horizontal plane flow analysis in stage 1. This demonstrates that the application of the equivalent permeability relationship, Equation 3.6, derived in stage 1 to 2D continuous model walls representing contiguous piles, is reliable.

The effect of wall permeability on soil surface settlement

Soil surface settlement caused by the drawdown of the groundwater level during extraction is well documented (Powers, 1985; Powrie and Preene, 1994; Preene *et al*., 2000 and Roberts *et al*., 2007). Drawdown induced surface settlement due to seepage into shallow tunnels is also well established (Yoo *et al*., 2008 and Lee *et al*., 2009). In this investigation, seepage through the semi-permeable equivalent retaining walls was treated as a form of drawdown of the water levels in the soil adjacent to the wall. During the stage 2 simulations, it was observed that soil surface settlement behind the retaining wall increased as the pile gap to diameter ratios, *x/d*, increased. Settlement troughs behind the equivalent wall for increasing values of *x/d,* from 0.0 to 1.0, are shown in Figure 3.24.
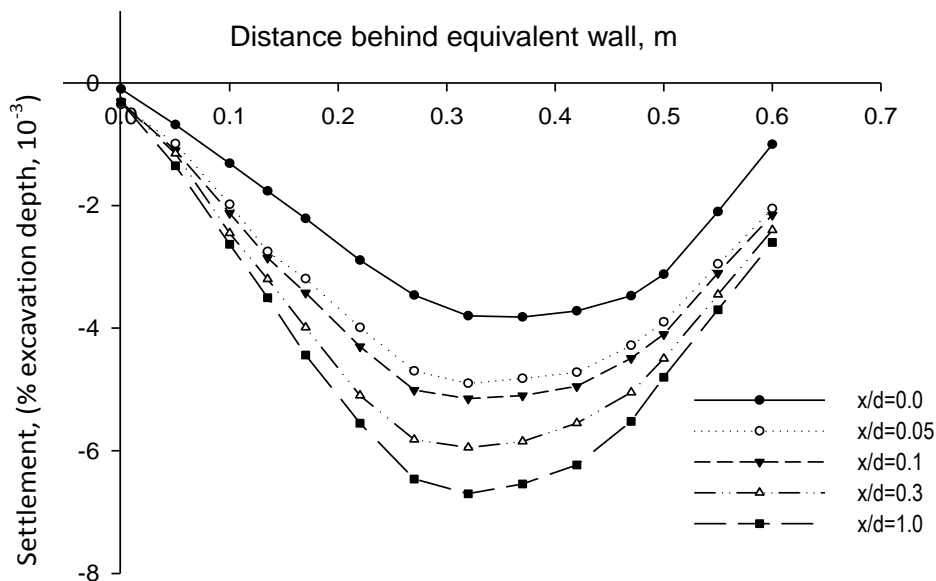
Figure 3.23: Settlement troughs behind the equivalent wall at various values of *x/d*. Settlement is represented as percentages of excavation depth.

Soil settlement values as percentages of excavation depth increased with *x/d*. Normalising settlement with respect to that for the impermeable wall as shown in Figure 3.25 demonstrates that, for example, at *x/d*=0.5 the increase in soil settlement at various distances behind the wall varies between 1.5 and 1.9 times that of the impermeable wall. This trend was consistent at all values of *x/d* and distances behind the model wall and is similar to the increasing soil surface settlement with retaining wall permeability observed by Zdravkovic *et al*. (2007) who conducted 2D numerical analysis of a retaining wall in London Clay.
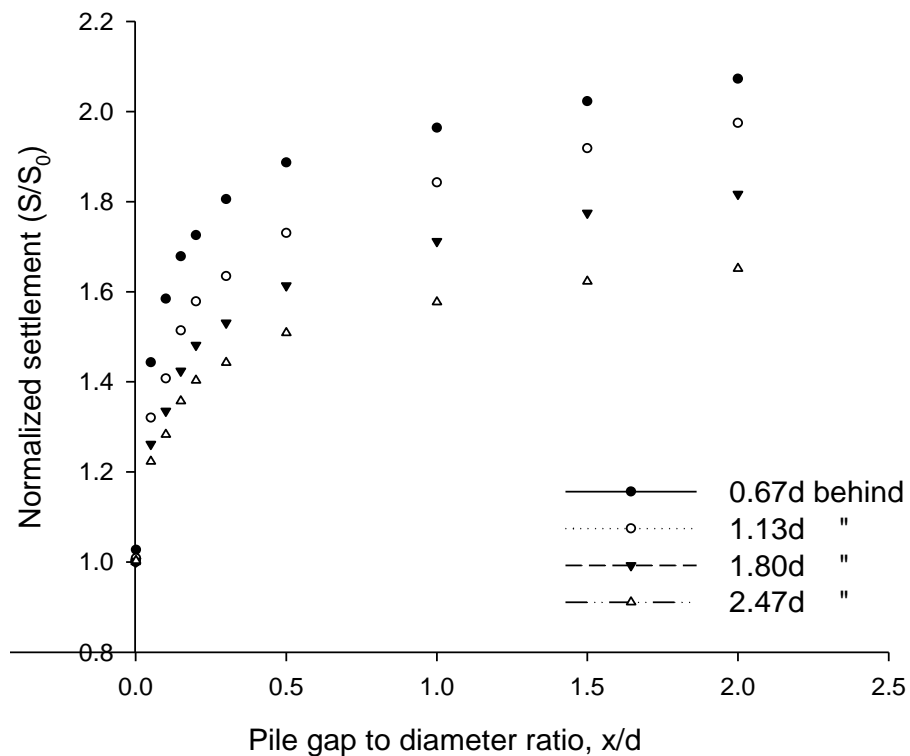
Figure 3.24: Variation of soil surface settlement with pile gap to diameter ratios at various distances, measured in pile diameters, d, behind the model retaining wall. Settlement, S_i, was normalised using soil settlement at *x/d*=0, S_0.

It is significant to note that the normalized settlement plotted in Figure 3.25 shows an initial sharp increase as the pile gap to diameter ratio increased to about 0.5. The influence of x/d seems to reduce after about x/d=0.5. A relationship, between the normalized settlement, S_i/S_0 and pile gap to diameter ratio, of the form in Equation 3.7 was derived from curve fitting exercises.

$$S_i = 1.8S_0 \left(\frac{x}{d}\right)^{0.1}$$ Equation 3.7

where S_0 and S_i are through-wall seepage induced settlement for an impermeable and a semi-permeable equivalent wall respectively. One apparent limitation of this relationship is that the permeability of the soil and hence the potential drawdown due to through-wall seepage is not included. This was however taken into consideration in the previously derived permeability expression (Equation 3.6) which provided a relationship between the bulk permeability of the equivalent structure and pile gap to diameter ratios. A further expression is needed to relate the amount of settlement to decreasing water levels due to through-wall seepage. This is addressed in Chapter 4 in a series of dimensionless charts.

Additionally, comparisons were made between the soil surface settlement derived from the numerical analyses and those obtained from an analytical solution. The solution used for comparison was based on the assumption that consolidation settlement due to dewatering may be calculated using the one dimensional stiffness modulus, E'_0 (Preene *et al*., 2000) according to Equations 3.8 and 3.9.

$$\rho = \frac{D_s \gamma_w S_{av}}{E'_{0,av}}$$ Equation 3.8

and $$\frac{E'_0}{\Delta\sigma'_v} = 400$$ Equation 3.9

where the terms were previously defined in equations 2.3 and 2.4.

The analytical solution was adopted to calculate settlement due to seepage through the semi-permeable retaining wall. This is a simple elastic approach with the assumptions that the one-dimensional stiffness modulus and the groundwater drawdown were linear with depth. For the purpose of these calculations, D_s the thickness or depth of the soil affected by seepage was taken as the soil depth in the numerical model for each value of x/d investigated. The average drawdown of groundwater, S_{av}, due to seepage through

the wall was taken as the difference between the original water level and the point at which the phreatic surface intersects the back of the retaining wall. Assuming that the vertical total stress remained constant, then changes to effective vertical stress are due solely to changes in groundwater level, $\Delta\sigma'_v = \gamma_w S$. Values for the one-dimensional stiffness modulus or constrained modulus, E'_0, were calculated at various x/d using Equation 3.9 and substituted into Equation 3.8 to calculate the corresponding soil settlement.

Figure 3.26 compares the normalized settlement calculated using the one-dimensional stiffness modulus method with settlement from the numerical analysis. It is evident that settlement values in both cases increased significantly as soon as through-wall seepage was allowed and continued to do so at a relatively high rate up to about x/d=0.5. Thereafter the influence of increasing x/d on soil settlement was low. It was also observed that the one-dimensional stiffness modulus method over-predicted the surface settlement particularly at higher values of x/d. This was hardly surprising as the nature of the investigations dictated that volumetric changes were displayed as vertical displacements.
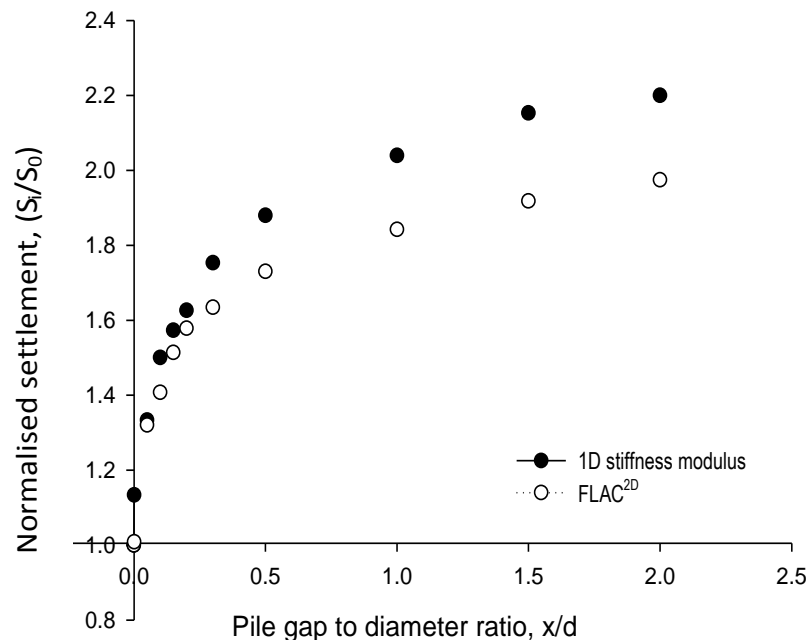
Figure 3.25: Comparison of soil surface settlement using a numerical (FLAC[2D]) solution and the 1D stiffness modulus method.

3.6   Summary

Numerical investigations to determine a relationship for the bulk permeability of the equivalent structure in 2D plane strain analyses were described in this chapter. The analyses comprised two stages. During stage 1, the effect of pile gaps on the hydraulic regime around contiguous piles was investigated for horizontal (x-y) plane flow only. The results were used to derive a relationship between the bulk permeability, k_p, of the equivalent structure, the soil permeability, k_s, and the pile gap to diameter ratio, x/d. The analyses showed that pore water pressures behind the piles were inversely proportional to increase in x/d. The bulk permeability of the equivalent structure increased with increasing x/d. The results also showed that there were no significant differences between the results for the case in which the experiments commenced with a full flow tank and that with an empty tank.

Phreatic surface effects were investigated in the phase 2 analyses. An equivalent wall thickness was calculated for continuous retaining walls used to represent the contiguous pile retaining walls for the analysis of flow in the vertical (z-x) plane. The equivalent wall thicknesses were calculated using the stiffness approach adopted by Day and Potts (1993). The values compared well with those calculated using the second moment of area (Powrie *et al*., 1999). The derived permeability expression, Equation 3.6, was used to calculate the bulk permeability of the continuous retaining wall in the 2D plane strain analyses. Results from the stage 2 analyses showed that an overall reduction in pore water pressures behind the model wall can be attributed to through-wall seepage. It was observed that once there was through-wall seepage, the length of the equivalent wall did not influence the hydraulic regime. The pore pressures at various positions in the stage 2 analyses were consistent with those in the stage 1 horizontal only flow simulations.

There were however some drawbacks to allowing through-wall seepage. These included increased surface settlement adjacent to the retaining wall during the vertical plane analyses. Soil settlement increased with x/d and hence with the bulk permeability of the equivalent wall. These observations were consistent with established research, which have shown that surface settlement above shallow tunnels with segmented linings were greater than those for waterproofed tunnels. The trends of increased settlement with x/d were also comparable to those reported by Zdravkovic *et. al.* (2007) who observed similar displacements as retaining wall permeability increased.

It is acknowledged however, that the possible advantages of allowing through-wall seepage are likely to be more significant than the drawbacks.

Chapter 4

4.0 Verification of groundwater flow regime by laboratory experiment

4.1 Introduction

Chapter 3 established, by way of numerical analysis, the groundwater flow regime for retaining walls, such as those made of contiguous piles, in which there is through-wall seepage. Laboratory investigations of a flow tank problem were subsequently conducted to verify the results of the numerical analysis. The flow tank experiments comprised the installation of circular model pile sections into a granular material contained within a fixed flow channel. The influence of various model pile diameters, and hence pile gaps, on the groundwater flow regime was determined. The flow tank experiments were based on Darcy's law for steady state seepage through a porous medium shown in Equation 4.1.

$$Q = kA \left(\frac{dh}{dl} \right)$$
<div align="right">Equation 4.1</div>

Volumetric flowrate, Q, in units of m^3/s from Equation 4.1, is proportional to the change in hydraulic gradient, *dh/dl,* over the length of the flow tank. During these experiments, the pile gap to diameter ratios, *x/d,* were varied and the corresponding steady state flowrates measured. The bulk permeabilities of the equivalent structure (pile and gap), k_p, at different values of *x/d* were then calculated from the experimental flowrates using Equation 4.1. In this chapter, details of the laboratory flow tank experiments and their results are presented and discussed. Where appropriate, comparisons are made between the results from the laboratory experiments and those from the numerical simulations presented in Chapter 3.

4.2   Flow tank experiments

The purpose of flow tank experiments, sometimes referred to as sand tank or sandbox experiments in the field of hydrology, is to carry out investigations involving the flow of groundwater through a porous medium in a controlled environment. This allows the advantages of having known experimental boundary and initial conditions to be exploited, albeit not to the degree of flexibility afforded by an advanced numerical method. Additionally, the properties of the porous materials used in these repeatable laboratory experiments may be determined separately from the main investigation. Owing to their low running costs, operational simplicity and adaptability, flow tanks of various sizes are also suitable for teaching purposes and are particularly useful in demonstrating otherwise complex flow phenomena. The usefulness of laboratory experiments to verify the results of numerical analyses is also well established. The reverse is also true; numerical simulations have been used to provide results that are comparable with those of laboratory experiments. For example, Rulon and Freeze (1985) investigated the development of seepage faces on slopes in a layered soil. The seepage face experiments were carried out using a laboratory sandbox in which precipitation was simulated by sprinkling water on the model slope. Subsequent numerical simulations of the sandbox problem using a finite element method, SEEP/W, provided results that were remarkably consistent with those of the laboratory investigations conducted by Rulon and Freeze (1985) (GeoStudio).

The laboratory flow tank experiments described in this chapter were used for two main purposes.

- First, quantitative data were recorded and analysed to determine how pile gap to diameter ratios, x/d, affected flowrates and pore water pressure distribution around the model pile in order to verify the relationship between k_p/k_s and x/d established by the numerical analyses in Chapter 3 (Equation 3.6).

- Second, qualitative comparisons of flow conditions were undertaken to verify, by flow visualisation, how the flow regime varied with x/d.

4.2.1 Description of experimental setup

The experimental setup is shown schematically in Figure 4.1. The experimental apparatus comprised a flow tank with a model pile installed at one end. A water supply reservoir and an overflow tank were positioned at the two opposite ends of the flow tank as shown in Figure 4.1. To capture the changes in pore pressures around the model piles, mini pressure transducers were connected to the tappings on the side of the flow tank. The pore pressure transducers were connected to a computer running the data processing software via a data acquisition unit. The setup, with a constant head of water at the recharge boundary, allowed investigation of the effects of different hydraulic gradients between the recharge and discharge boundaries.
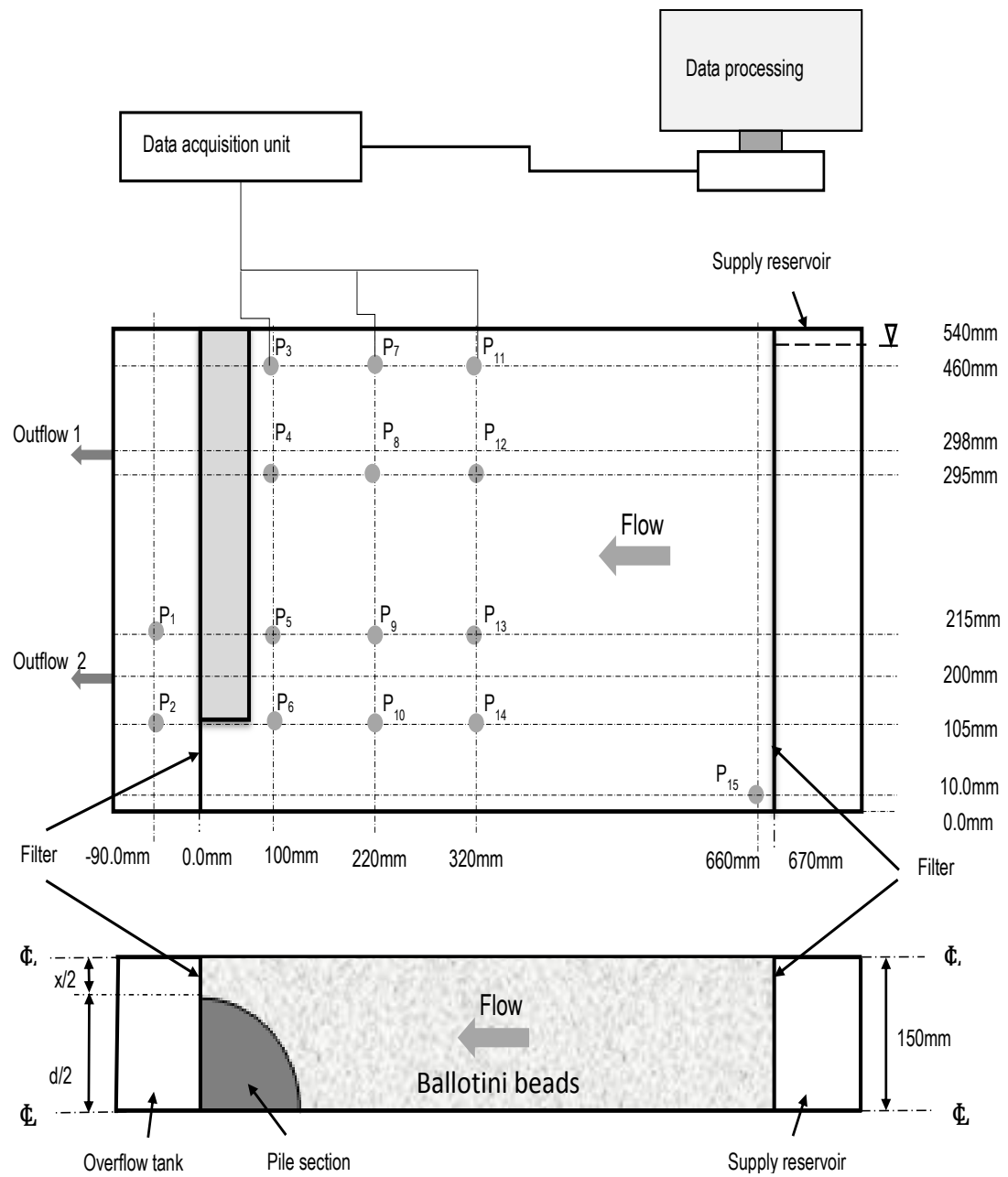
Figure 4.1: Schematic diagram showing flow tank with locations of pore pressure transducers. Plan view of the model pile section of diameter, d and pile gap, x, is also shown (not to scale).

Description of experimental flow tank

The flow tank used throughout the experiments consisted of a main section, into which the granular material was placed, with dimensions of 670 mm x 150 mm x 540 mm as shown in Figure 4.2.

The sides of the flow tank were made of 25 mm transparent Perspex sheets held together by 'I' beams resulting in a rigid structure. The water level at the overflow tank could be changed using outlets located at 200 mm and 298 mm above the impermeable base of the flow tank. The water levels represented idealisations of excavation depths although no attempt was made to carry out scale modelling of real retaining walls. The flow tank was designed to facilitate optimum visualisation of the groundwater flow around the model piles particularly on the side closer to the pile gap.
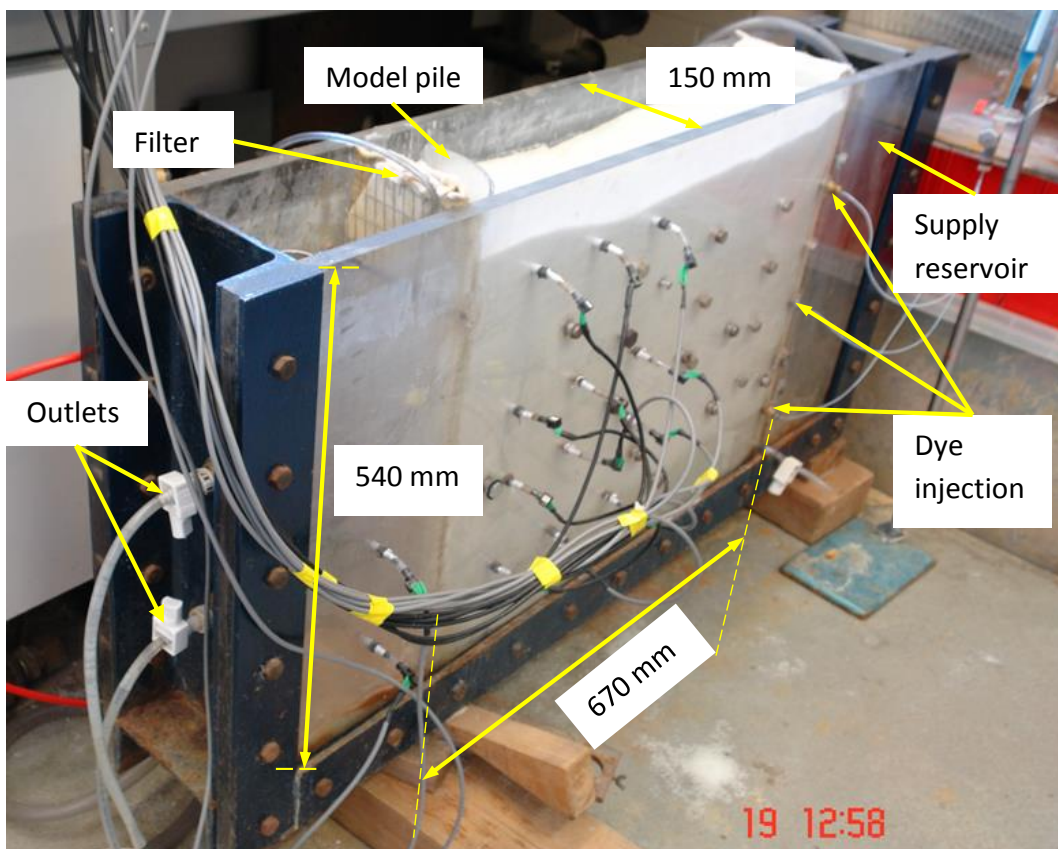
Figure 4.2: Flow tank used for the investigation of groundwater flow around contiguous piles.

Model pile

The model piles were made from circular Perspex tubes cut into quadrants each corresponding to a quarter pile section.   The model pile section was fixed and sealed onto the sidewall of the flow tank as shown in Figures 4.1 and 4.2. The base of the model pile was also sealed to prevent upward seepage into the pile. Particular care was taken to seal the side of the model pile onto the tank to prevent seepage along the sidewall. A membrane, fixed between the pile and the excavated region and extending to the base of the tank, was used as a filter.

Numerical investigations reported in Chapter 3 showed that, once through-wall flow was established, the embedment depth did not significantly affect the hydraulic head distribution or the flow regime around contiguous piles. Throughout the investigations, the distance from the pile toe to the base of the flow tank was therefore fixed at just over 100 mm.

Several model piles of varying diameters were tested to give pile gap to diameter ratios in the range 0 to 1.2. Significant amount of soil instability prevented investigation at higher pile gap to diameter ratios, x/d. Investigations at higher x/d, in the context of through-wall seepage, were also thought to be impractical for retaining wall applications.

Data acquisition equipment

Mini pore pressure transducers were used to observe and record the development of pore pressures due to changes in pile gap to diameter ratios, x/d. Druck mini transducers with a sensitivity range of 10 mV/psi and a response time of 1 ms were used for the duration of the experiments. The pore pressure transducers, numbered P_1 to P_{15}, were positioned along the side of the flow tank as shown in Figure 4.1. These were connected directly to the data acquisition unit, which supplied readings to the data processing software on a computer. The GDSLAB$^{©}$ v2 software used was supplied by GDS Instruments. The instruments detected changes in pore pressure through electrical excitement of sensors, which were then supplied in units of millivolts (mV). The electrical signals were then converted by the data acquisition unit, using the appropriate calibration factor, to kPa in these experiments.   All pressure transducers used in the

experiments utilized atmospheric pressure as a reference. This allowed the measurements of gauge pressure to be read directly without further processing. Prior to commencing the experiments, the pressure transducers were calibrated individually using an air pressure machine in a manner similar to that described by Trudeep et al. (2011). Calibration involved comparison of a known air pressure with those recorded by the instruments. To prevent finer particles clogging the pores of the transducers, soil filters were placed at the interface between the adapters and the granular material. Figure 4.3 shows the data acquisition unit, pore pressure transducers and accessories.
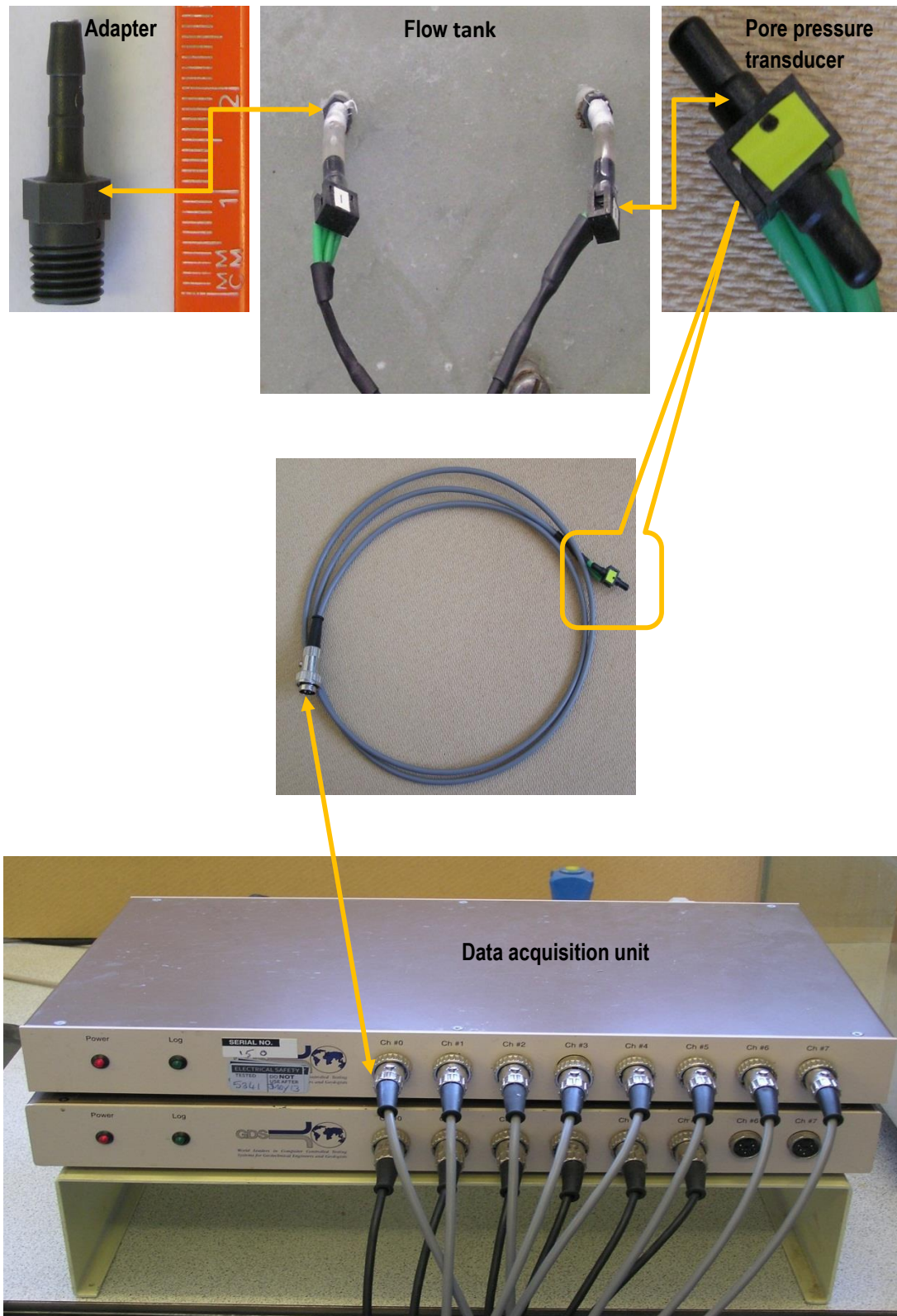
Figure 4.3: Data acquisition unit, pore pressure transducers and accessories used for flow tank experiments.

4.2.2 Soil description

The ballotini (glass beads) used throughout the experiments may be described as a dense white rounded poorly graded medium granular material free from organic matter and debris. Ballotini are highly spherical and are made of high quality and pure soda-lime glass (Ou and Liao, 1995). The material used was supplied by Sigmund Lindner with the properties listed in Table 4.1.

Property	Value	Source
Dry density, Mg/m^3		
$\rho_{d\ min}$	1.540	BS 1377: Part 4, 1990
$\rho_{d\ max}$	1.620	Miura and Toki, (1982); BS1377: Part 4, 1990
Specific gravity, G_s	2.500	BS 1377, Part 2, 1990
e_{max}	0.610	"
e_{min}	0.570	"
D_{10}, mm	0.320	PSD test
D_{50}, mm	0.500	"
D_{90}, mm	1.000	"
Permeability, k, m/s	2 x10^{-5}	Constant head test (Head, 1992) (average minimum k at maximum density)

Table 4.1: Properties of the ballotini beads used for flow tank experiments.

Laboratory tests were carried out to determine the hydraulic properties and classify the material. The particle size ranged between 0.25 mm and 1 mm with a mean (D_{50}) of 0.5 mm as shown in Figure 4.4.
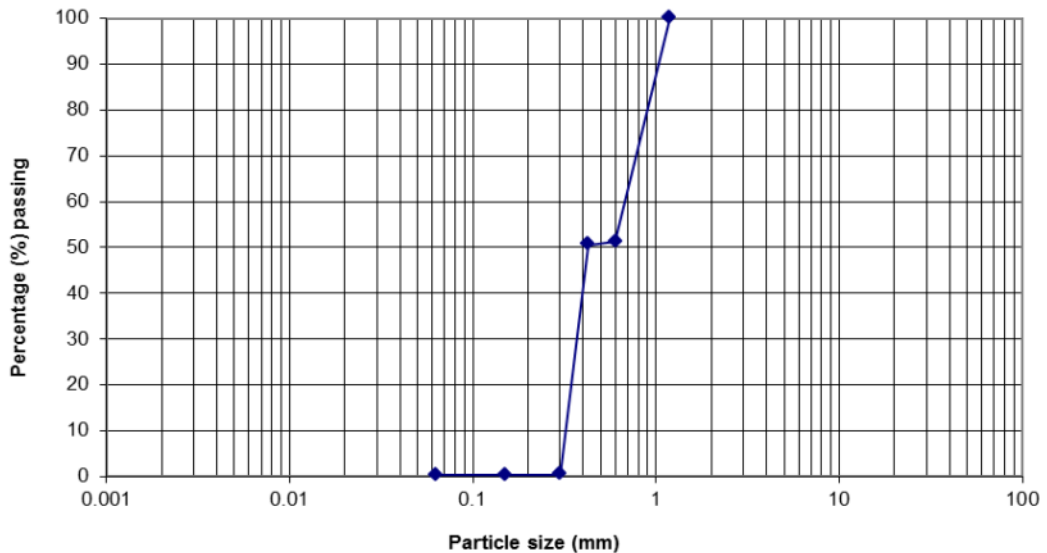
Figure 4.4: Particle size distribution of ballotini used throughout the experiments.

The minimum dry density was found to be 1.54 Mg/m^3 using the measuring cylinder method (BS 1377: Part 4 1990). The maximum dry density was determined to be 1.62 Mg/m^3 using the air pluviating tube method described by Miura and Tuki (1982). The hydraulic conductivity of the material was measured using the constant head method as outlined in most soil mechanics books. For consistency and in accordance with BS 1377, four or more permeability tests were conducted on each of five material samples and an average minimum permeability of 2×10^{-5} m/s obtained at maximum density. The hydraulic conductivity measured from the constant head experiments was compared with that calculated using the empirical formula, shown in Equation 4.2, which was developed to estimate *in situ* permeability of clean granular soil by Hazen (1892).

$$k(cm/s) \approx C_H(D_{10})^2 \qquad \text{Equation 4.2}$$

where k is the soil permeability (cm/s); C_H is Hazen's empirical coefficient; and D_{10} is the size of the sieve, measured in centimetres, through which 10% by mass of the soil particles will pass (Powrie 2004). Hazen's (1892) formula was derived for loose, clean

sand with a coefficient of uniformity of less than 2 (Terzaghi and Peck, 1964). The uniformity coefficient was described as the ratio D_{60}/D_{10}, where D_{60} is the sieve size through which 60% of the soil particles by mass will pass. The material used throughout these experiments had uniformity coefficient of 2.125, which was just over the suggested upper limit for valid use of Equation 4.2. The use of the equation was also limited to soils in the range 0.01 cm$<D_{10}<$0.3 cm (Hazen, 1982). The ballotini used in these experiments have $D_{10} \approx 0.032$ cm, which is well within the recommended range. The range of values adopted for Hazen's empirical coefficient varies between 1 and 1000 according to Carrier (2003), although the use of a value of C_H=100 was prevalent as suggested by several soil mechanics books. For comparisons with the laboratory-derived permeability in these experiments, C_H was taken as 100. The empirical solutions for hydraulic conductivity were found to be two orders of magnitude higher than the laboratory derived average minimum permeability. This is unsurprising based on the amount of uncertainty that have been shown about the empirical formula and the fact that the selected value of C_H could contribute to at least two orders of magnitude of errors.

4.3 Experimental Methodology

The experiments began with the model pile in position, fixed along one sidewall of the flow tank and against the soil filter as shown in Figure 4.2. The ballotini were placed in the flow tank in layers of approximately 10-15 mm from a maximum height of about 500 mm above the soil surface using the air-pluviation method to achieve a maximum dry density of about 1.62 Mg/m^3. Carbon dioxide was then flushed from the base of the flow tank through the granular material to ensure greater levels and rates of saturation. This is a modification of the de-airing method used in experiments by Lacasse and Berre (1988) in which it was noted that the solubility of CO_2 in water under pressure enabled greater saturation of a soil sample. The carbon dioxide was supplied at less than 10 Pa through a series of 'air stones' typically used to aerate aquariums for fish (Figure 4.5). The use of the air stones ensured that the carbon dioxide was evenly dispersed while displacing the air in the voids as it moved to the surface of the soil. The flow tank was then slowly filled with water using the supply reservoir, which once full was maintained at an elevation head of 0.54 m relative to the base of the tank for the

duration of the investigation. The CO_2 supply was kept on while the flow tank was being filled with water.
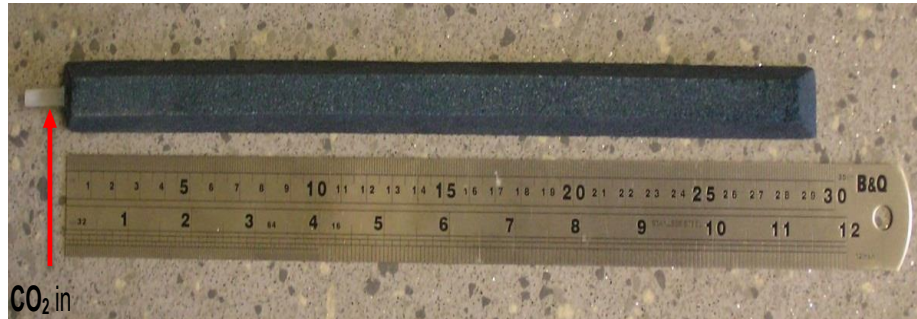
Figure 4.5: Typical air stone (porous) used for flushing flow tank with carbon dioxide.

Numerical investigations conducted in Chapter 3 showed that no significant differences in the flowrates and pore water pressure distribution would be expected between those when the initial water level is raised from the base of the flow tank and those when the experiment commenced with the water level at the top of the tank. In the experiments described herein, the water level was raised from the base of the tank by slowly filling from the supply reservoir. Volumetric flowrates at the overflow tank were measured to determine when the system had attained steady state conditions, which were taken as being when consistent flowrates were obtained. Static pore pressure measurements were taken once the material was fully saturated with the water level at the top of the flow tank. The water level in the overflow tank was then lowered to the first outlet while a constant head of water was maintained, as best as physically possible, at the recharge reservoir. Steady state flowrates and pore water pressures were recorded. The water level was subsequently reduced to the lower outflow position, again maintaining the elevation head at the supply reservoir. Steady state flowrates and pore pressures were measured. The flow tank was emptied and a model pile of different diameter installed. The procedure was repeated for different pile gap to diameter ratios, *x/d*.

4.3.1 Visualisation of groundwater flow paths

The dye injection method, as described by Wolfgang (1987), was used throughout the laboratory experiments to observe the development of flow patterns around the model pile sections. This technique, although unsophisticated, is incomparable as a means of assessing the groundwater flow regime through a porous medium in a practical manner. The dye injection method, if applied conscientiously, can provide useful information on the development of flow patterns around a solid object in a flow medium, such as an engineering structure in a soil. Hence, its wide application in several engineering disciplines including civil engineering and the geosciences.

To achieve consistent results from flow visualisation methods, some basic criteria should be fulfilled. Wolfgang (1987) recommended that the density and composition of the dye should be similar to that of the working fluid, water in this instance. Similarly, the flowrates at which the dye is injected into the flow channel should be slightly less than, or similar to the flowrate of the working fluid in the tank to prevent disturbance to the flow regime. The dye injection is usually done with small diameter (d<1 mm) tubes or by way of hypodermic needles. In these experiments, the dye was injected using 0.5 mm diameter tubes positioned at tappings to the side of the flow tank as shown in Figure 4.2. Conventional food dyes were deemed of sufficient quality to be used throughout the experiments as they were considered 'robust' enough and would not generally dissociate into their constituent parts. The dye was injected at a constant flowrate controlled by the total head of dye solution in the supply tube and the flowrate of the water at the supply reservoir in the flow tank. Further injection of the dye, at surface level just in front of the recharge boundary, was done manually to observe the development of the phreatic surface for different pile gap to diameter ratios.

The results of the dye injection procedure were captured using regular cameras. Only two dimensional plane flow images were obtained during the process. The main areas of interest in the flow visualisation were the variation of path lines and time lines and the evolution of a seepage face as x/d changed.

4.4 Results and discussion

The results of the flow tank investigations are presented and discussed with reference to the effect that varying the pile gap to diameter ratio, *x/d*, had on the steady state flowrates and pore water pressure distribution around the model piles. Qualitative analyses of the changes in flow patterns as the bulk hydraulic conductivity increased are also presented and discussed using results from the dye injection method.

4.4.1 Influence of *x/d* on steady state flowrates

Flowrates, Q_1 and Q_2, at hydraulic gradients, i_1 and i_2 are shown in Figure 4.6.
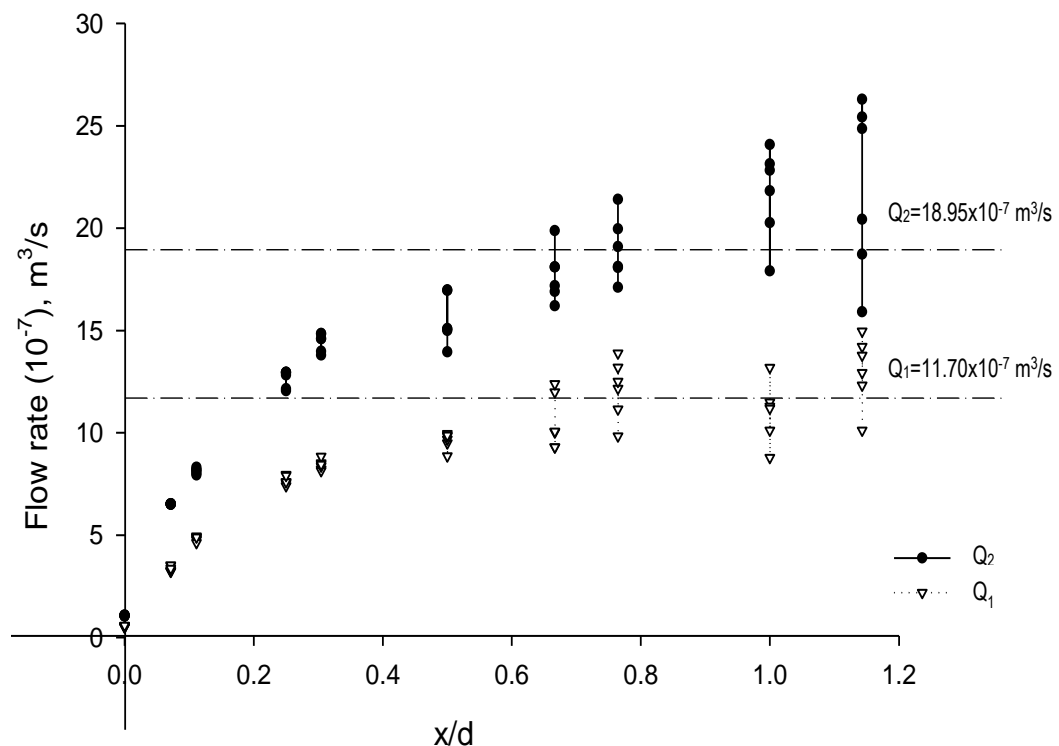
Figure 4.6: Measured flowrates, Q_1 and Q_2, at hydraulic gradient i_1 and i_2 corresponding to head differences between the recharge and discharge surfaces of 0.242 m and 0.34 m respectively. Calculated flowrates Q_i using constant head permeability results are shown at each hydraulic gradient.

109

The measured flowrates, as would be expected, increased with pile gap to diameter ratio at both i_1 and i_2. At lower values of x/d, up to about 0.3, the trends in flowrates from the experiments were very similar at the two hydraulic gradients investigated. As x/d increased however, the results became increasingly scattered. This could perhaps be attributed to the onset of soil instability observed behind the model wall for values of x/d above about 0.4.

Further investigations were conducted to compare the measured flowrates with existing analytical solutions. Darcy's equation was used to calculate steady state flowrates using the average minimum hydraulic conductivity of the ballotini beads obtained from the constant head permeability tests. Two flowrates, corresponding to the hydraulic gradients i_1 and i_2, were calculated. These were plotted as flowrates Q_1 and Q_2 superimposed in Figure 4.6. It was anticipated that the measured flowrates would have approached the asymptotes of Q_1 and Q_2 as x/d tended to infinity. This did happen as shown in Figure 4.6. It was observed however, that at higher pile gaps the flowrates from the laboratory experiments bracketed the calculated flowrates, particularly at the lower hydraulic gradient, i_2. It must be noted however that the value of k used in Darcy's law was the average minimum at the maximum soil density. Therefore, measured flowrates would be expected to bracket the calculated average values.

To eliminate or at least reduce the effect of the two hydraulic gradients on flowrates, the measured flows Q_1 and Q_2 were normalised against the product of the cross-sectional area, A and the hydraulic head drop, dh for the two hydraulic gradients investigated. Figure 4.7 shows the variation of normalised flowrates (units of s^{-1}) with x/d. It can be seen from Figure 4.7 that the normalised flowrates were very similar, particularly at low x/d. The persistent divergence of the steady state flowrates, in both their natural and normalised form, however indicates that the onset of soil instability adjacent to the model pile at higher x/d has a significant impact on the hydraulic regime around the model wall. This further demonstrates the need for additional investigation into the drawbacks of allowing through-wall seepage.
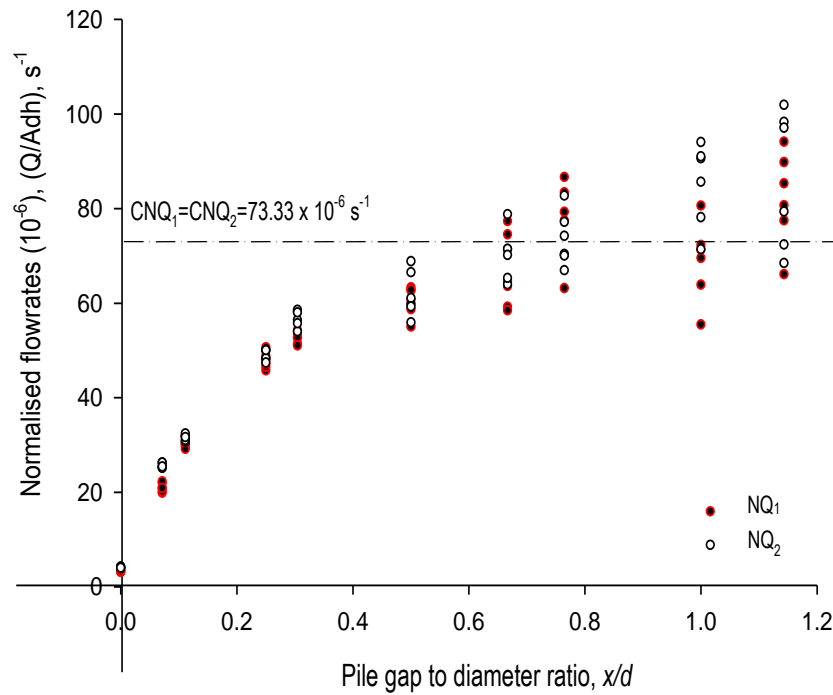
Figure 4.7: Comparison of normalised flowrates, NQ_1 and NQ_2 at hydraulic gradients i_1 and i_2 for various values of x/d. Calculated normalised flowrates, CNQ_i are also shown.

4.4.2 Influence of pile gap to diameter ratios on the bulk permeability, k_p

Darcy's equation was used to back-calculate the bulk permeability, k_p, from the measured flowrates. This was done by substituting hydraulic gradients and flowrates for h_1 and h_2 into Equation 4.1. The procedure was repeated at different pile gap to diameter ratio, x/d. For consistency and to ensure simplicity in the approach used, the flow area, A, in Equation 4.1, was taken as the width of the wall and the excavated depth for simulations at hydraulic gradients i_1 and i_2. The calculated bulk soil/structure permeability, k_p, was normalised using an average minimum permeability for the ballotini beads of 2×10^{-5} m/s, which was obtained from constant head experiments. The permeability ratios k_p/k_s were then plotted against the pile gap to diameter ratios,

x/d as shown in Figure 4.8. The permeability relationship derived from numerical analyses in Chapter 3 (Equation 3.6) was plotted for comparison.
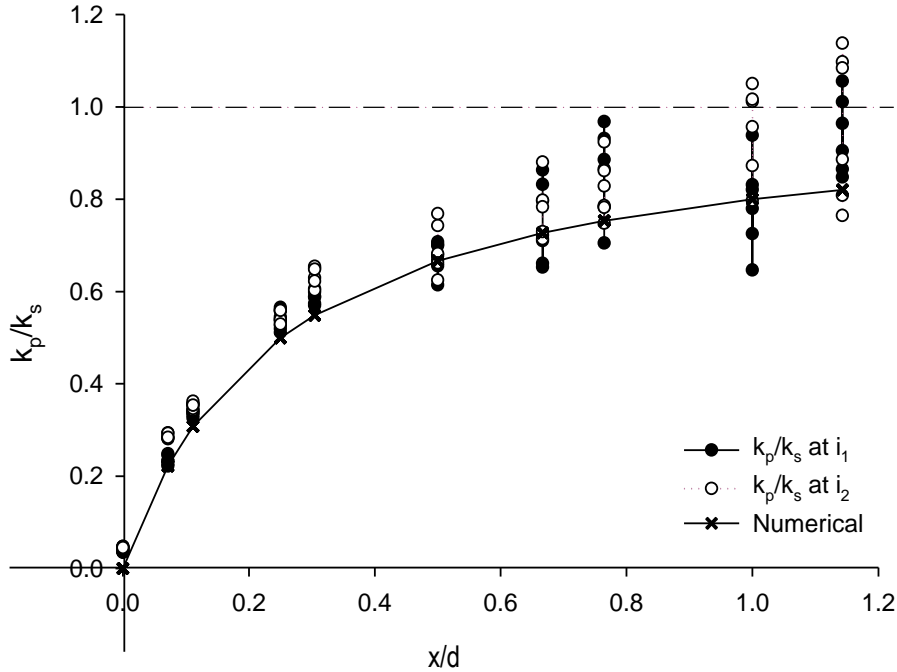
Figure 4.8: Variation of k_p/k_s with *x/d* at hydraulic gradients i_1 and i_2. The plot of k_p/k_s calculated from Equation 3.6 is shown for comparison.

It can be seen from Figure 4.8 that at low values of *x/d* the laboratory flow tank results are consistent and compare well with the permeability ratios derived from the numerical analysis. The laboratory results however became more scattered as *x/d* increased. This is particularly evident for *x/d*>0.3 and may be attributed to the previously discussed increased spread of experimental flowrates observed at higher *x/d*. Notwithstanding the scattering of data at higher *x/d*, k_p/k_s calculated from the experimental flowrates were very similar to the numerically derived values.

Throughout the investigations, it was also observed that, the average measured flowrates and subsequent calculated bulk permeability ratio, k_p/k_s, were consistently higher than the numerical calculated values. This might be due in part to the onset of soil instability in the laboratory model which was not fully represented in the numerical simulations. The laboratory experiments also represented three-dimensional flow

quantities, which as expected would be higher than flow through a 2*D* domain. This, to some extent, highlights the difficulties of investigating groundwater flow problems using two-dimensional numerical analysis. Notwithstanding the drawbacks noted above, the trends displayed by the laboratory flow tank results were very consistent with those from the numerical simulations particularly at lower values of *x/d*.

4.4.3 Effect of *x/d* on pore pressures around the model piles

Pore water pressures were measured at various positions behind and in front of the model pile sections corresponding to P_1-P_{15} in Figure 4.1. All horizontal distances were measured from the face of the model wall. Transducers P_1 and P_2 monitored changes in pressure at a distance of 90 mm in front of the piles. Transducers P_3 to P_6, P_7 to P_{10} and P_{11} to P_{14} measured water pressures at distances of 100 mm, 220 mm and 320 mm respectively behind the wall. The depths at which the transducers were located are also shown in Figure 4.1. Transducer, P_{15} was located 10 mm from the base of the tank and 10 mm in front of the supply reservoir to monitor the expected constant head of water.

Steady state pore pressure profiles (against depth below surface level) were plotted at different pile gap to diameter ratios, *x/d*. Hydrostatic pressure was also plotted for comparison as illustrated in Figure 4.9.
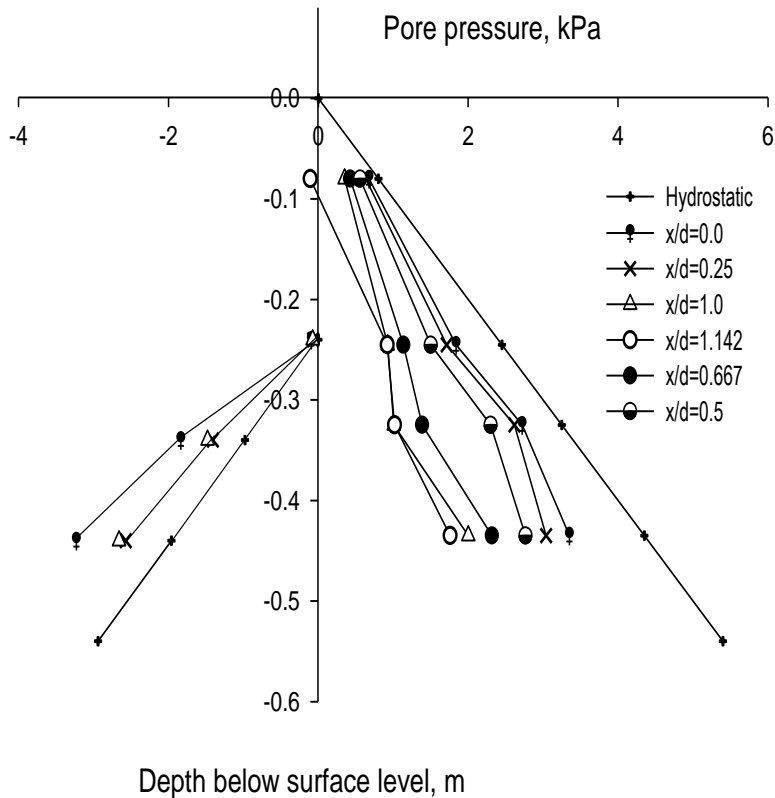
Figure 4.9: Pore pressure profiles behind and in front of the model wall at different pile gap to diameter ratios, *x/d*.

It was observed that the pore pressure profiles behind the model walls were all less than the calculated static pressure as would be expected in the presence of groundwater flow. Additionally, a noticeable decrease in pore pressures was measured behind the model pile as the pile gap to diameter ratios, *x/d*, increased. Consequently, the pressure profile for *x/d*=0.0 was closest to, while that for *x/d*=1.142 was furthest away from the line representing hydrostatic pressures. This trend is more consistent at lower values of *x/d*. At larger pile gaps, the pore pressure results were less reliable and the profiles seemed to diverge from the expected smooth linear variation with depth for *x/d*>0.5. This unpredictability of pore pressures measured at higher values of *x/d* was consistent with that observed for the variation of steady state flow quantities previously discussed. It also supports the notion of the significant influence of higher pile gaps on soil stability adjacent to the model piles and on the hydraulic regime.

The reduction in pore pressures due to through-wall seepage as the bulk permeability of the equivalent structure increased is similar to the reduction in hydraulic head calculated around shallow tunnels with segmented linings during numerical simulations (Shin *et*

114

al., 2002; Lee *at al*., 2003; Bobet and Nam, 2007 and Arjnoi *et al*., 2009). The changes were also consistent with those observed during numerical analyses of the flow tank problem described in Chapter 3.

The development of pore pressures in front of the model wall was monitored throughout the experiment and the values also plotted as vertical profiles in Figure 4.9. Hydrostatic pressure in front of the wall is included for comparison. Pore pressure profiles in front of the model walls were slightly greater than hydrostatic, as would be expected. The results at the front were however less conclusive than those at the back of the wall. However, pore pressures for the impermeable wall were noticeably higher than for those with $x/d{>}0$. This was not that surprising as it is well established that seepage around impermeable retaining walls causes increased water pressures on the passive side of the wall. This has the effect of reducing the gross passive resistance. Through-wall seepage also caused some increase in pore pressures in front of the model wall, albeit not to the extent caused by an impermeable wall.

Additionally, the development of a region of negative pore pressures adjacent to the model pile sections was observed at higher pile gaps. The magnitude of the negative pore pressures observed behind the piles however depended on the water level in front of the wall. At higher water levels, no suction was recorded regardless of the size of the pile gaps. This may perhaps be attributed to the fixed supply head, which prevented the water levels in the soil from falling too low. Nonetheless, the region of suction observed at the greater hydraulic gradient was again very similar to that obtained from numerical simulations.

Pore water pressures at various values of x/d were normalised against those at x/d=0.0 for each of the hydraulic gradient investigated. It was observed that as x/d increased, the normalised pore pressures decreased as shown in Figure 4.10.
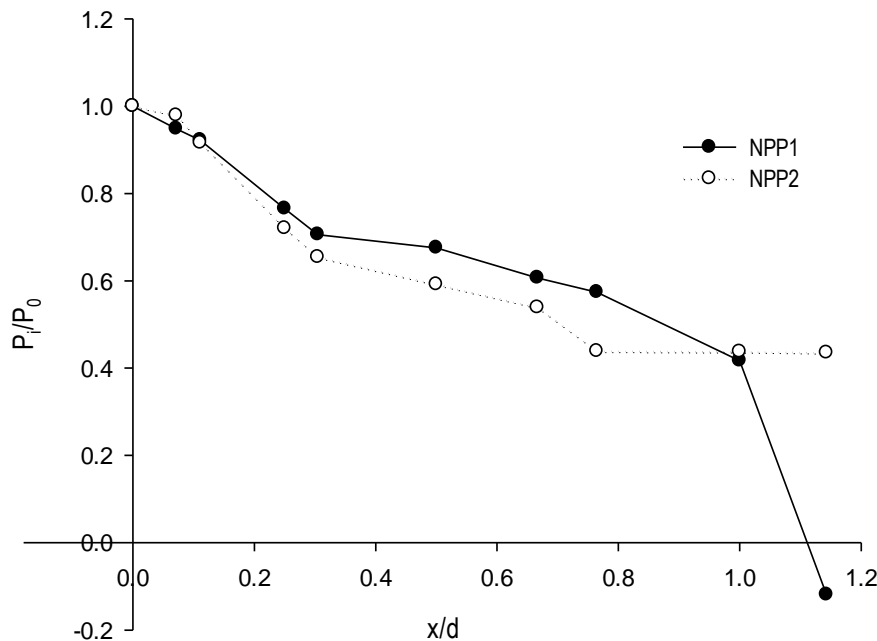
Figure 4.10: Variation of normalised pore pressures behind the model pile with x/d at hydraulic gradients i_1 and i_2 at P_3.

Comparison with linear seepage approximation

The pore pressures measured near the toe of the piles, U_{Toe}, were normalised with respect to those calculated using the linear seepage approximation method, U_{Est}, and plotted against x/d as shown in Figure 4.11. Linear seepage approximation allows the pore water pressures around a retaining wall at any point below the water table to be estimated without drawing a flownet for each case. For impermeable retaining walls, it is assumed that the head difference between the water level at the back of the wall and that on the excavated side is dissipated linearly around the wall (Padfield and Mair, 1984). Figure 4.11 shows that the measured pore water pressures are just under 80% of those calculated from the linear seepage approximation method for x/d=0.0. This represents a correction factor of 1.25. As x/d increases however, there is a marked decrease in the pore pressures from the experiment up to about x/d=0.7 after which the

effect of pile gaps was negligible. This could be useful in estimating pore pressures behind contiguous piles and for comparison with the hydraulic loads obtained from linear seepage approximation for similar impermeable retaining walls. For example, using Figure 4.11, pore pressures behind a retaining wall formed from contiguous piles with diameter 1000 mm and gaps of 300 mm is approximately 62% x 1.25 = 77.5% of those calculated using the linear seepage approximation method.
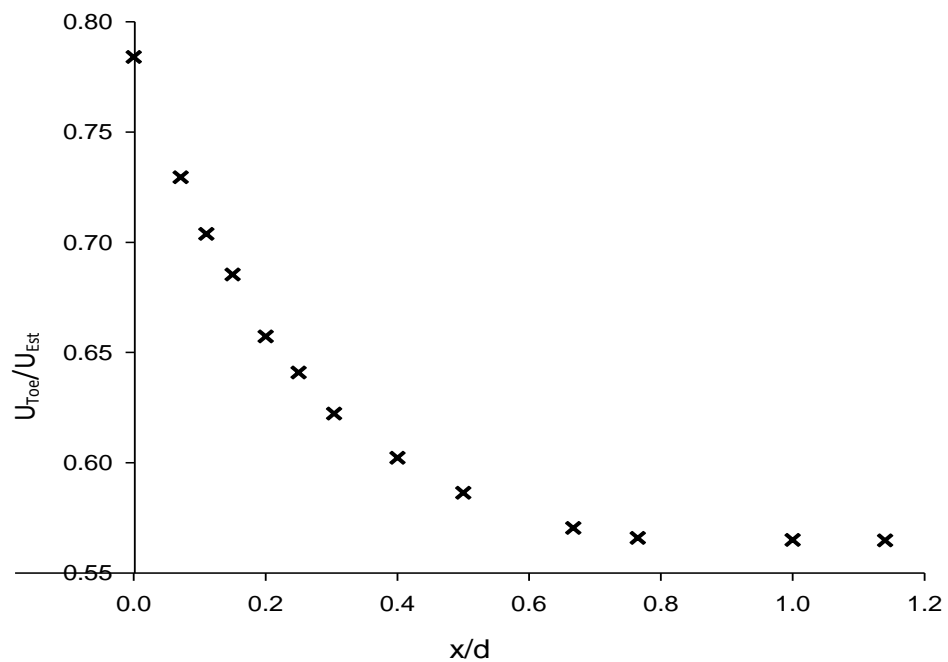
Figure 4.11: Normalised pore pressures at the pile toe. Pore pressure, U_{Toe}, were divided by those calculated using the linear seepage approximation method, (U_{Est}).

Further comparisons were made between the flow tank experiments and results from the numerical simulations conducted in Chapter 3. Results plotted in Figure 4.12 show remarkable similarities in the general trend between the numerical and experimental results, particularly behind the model wall. It was observed however that the pore pressure distribution in front of the wall was less well defined than those at the back as previously noted. This was more apparent for the flow tank experiments than in the numerical models.
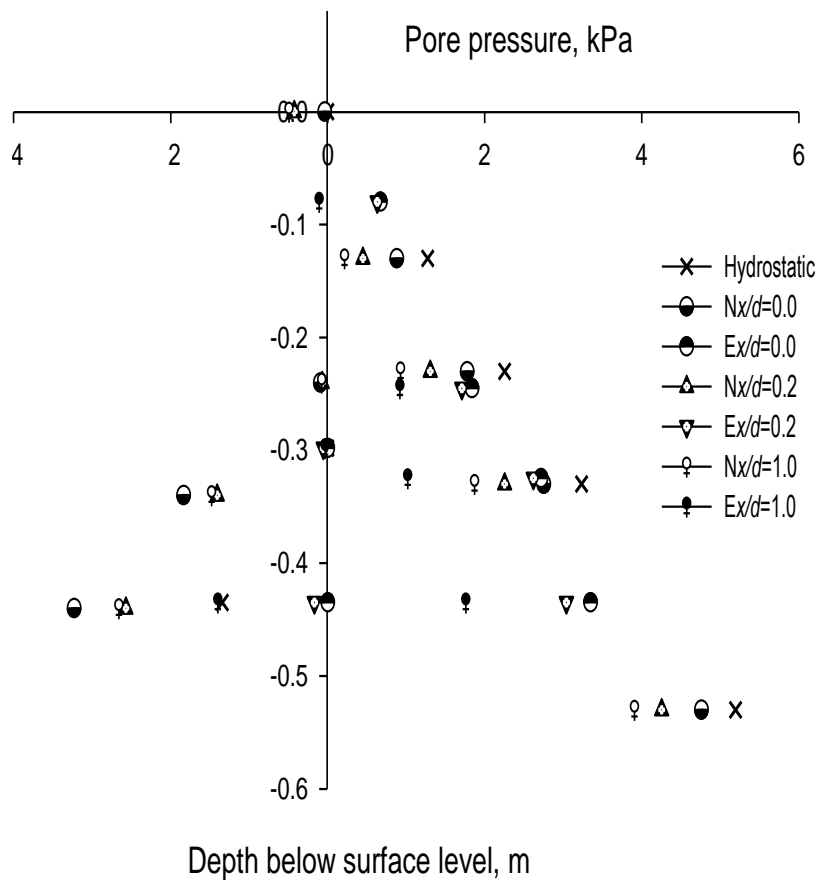
Figure 4.12: Comparison of numerical (*N*) and experimental (*E*) results for pore pressure profiles in front of and behind the model walls at different values of *x/d*.

4.4.4 Visualisation of groundwater flow

Flow paths were tracked by injecting a dye at various positions at the upstream end of the flow channel as shown in Figure 4.1. Since the distribution of streamlines formed by the flow of groundwater around an impermeable retaining wall is well established, the experiment for the case of *x/d*=0.0 was used to provide a flow tank standard against which the other permeability ratios could be compared. The development of flow patterns was subsequently compared for the different pile gap to diameter ratios, *x/d*, as shown in Figures 4.13 and 4.14. Flow paths for the case of *x/d*=0.0 were similar to flow channels for the conventional interpretation of flow around an impermeable retaining wall. The notable difference in this instance was that for the laboratory experiments, groundwater recharge was supplied from a constant head at the upstream end of the tank and that infiltration at the soil surface was not simulated. In contrast, typical investigations into flow around an impermeable structure by graphical methods, such as flownets, usually make use of a constant head of water ponded on the ground surface behind the wall. It is also apparent from Figures 4.13 and 4.14 that as the bulk permeability increased the flow direction below the phreatic surface, particularly closer to the model piles, became more horizontal. This suggests that the flow regime is increasingly dominated by lateral flow through the model wall as *x/d* increases. A similar observation was made from the numerical analyses conducted in Chapter 3.
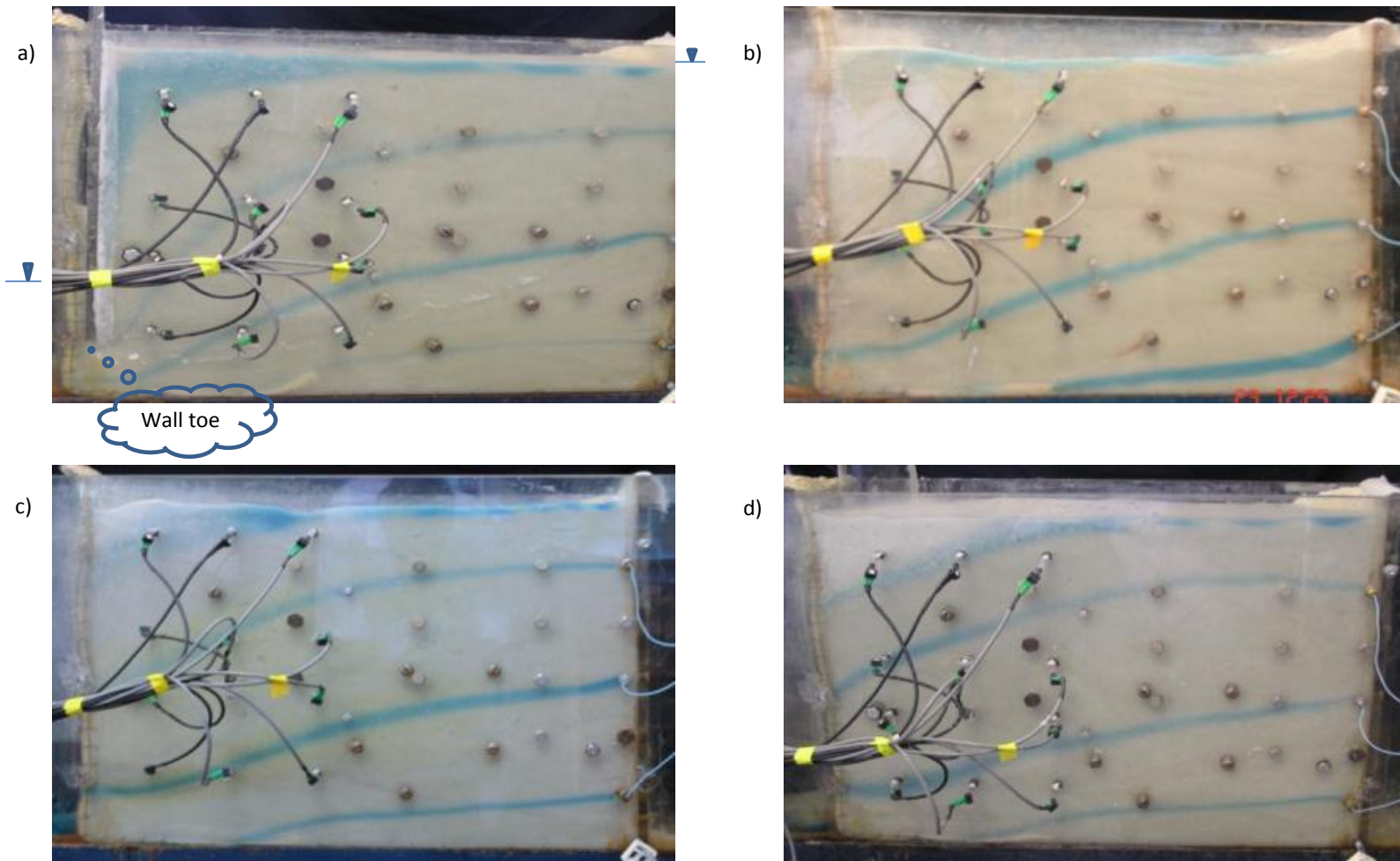
Figure 4.13: Experimental flow tank results for the visualisation of flow around the piles with $x/d=$ a) 0.0, b) 0.111, c) 0.25 and d) 0.667.
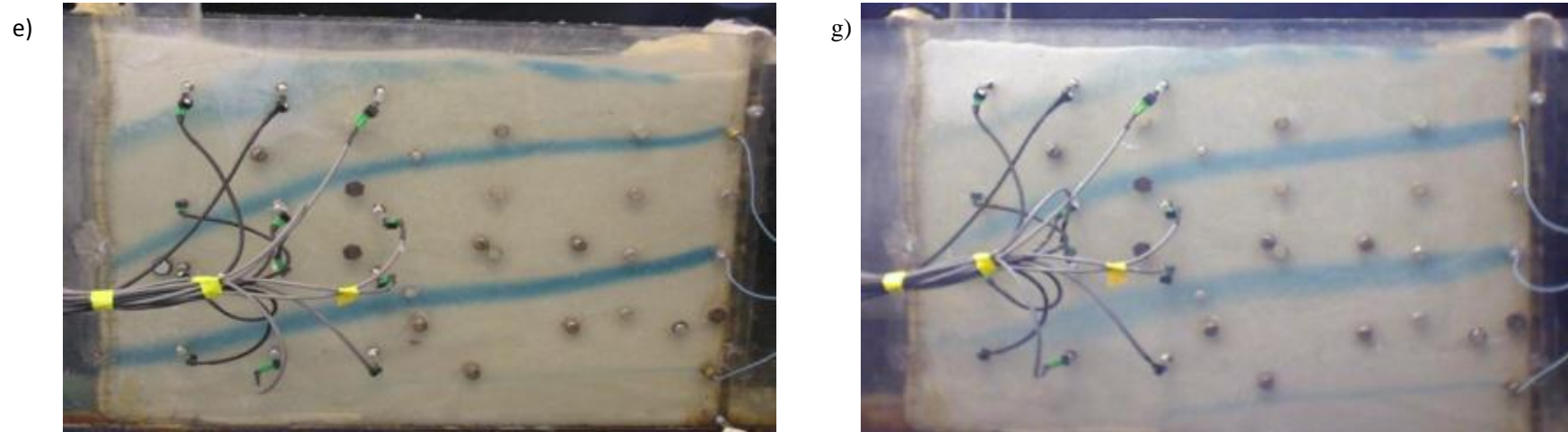
Figure 4.14: Experimental flow tank results for the visualisation of flow around the piles with *x/d*= e) 1.12 and f) 1.2.

Comparison of hydraulic head distribution

The distribution of hydraulic head around the model piles was calculated from the pore pressures recorded at transducers P_1-P_{15} for different pile gap to diameter ratios, x/d, and the elevation heads. To ensure consistency, the base of the flow tank was taken as the datum for the calculation of the elevation head throughout the investigations.   The total head values were then drawn as contour plots in metres against the lateral distance from the model pile and depths below ground level. The contour plots of hydraulic heads are shown alongside the diagrams of flow paths from the flow visualisation method. The resulting flow patterns and hydraulic heads are compared at various pile gap to diameter ratios, x/d, in Figures 4.15 to 4.19.

The results from an uncoupled groundwater flow analysis using $2D$ numerical simulations in SEEP/W are also included. The retaining walls in the SEEP/W analyses were modelled in a similar manner and with identical material properties as those in the FLAC^{2D} simulations described in Chapter 3. The bulk permeability of the continuous wall used to represent the circular piles in the SEEP/W simulations was again calculated using Equation 3.6, which was derived for this purpose.

a) Flow paths from experiments
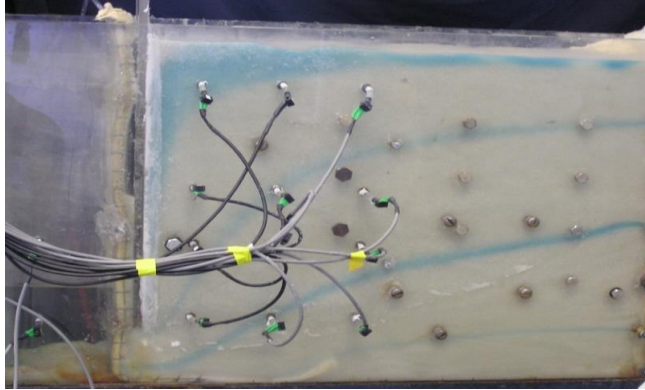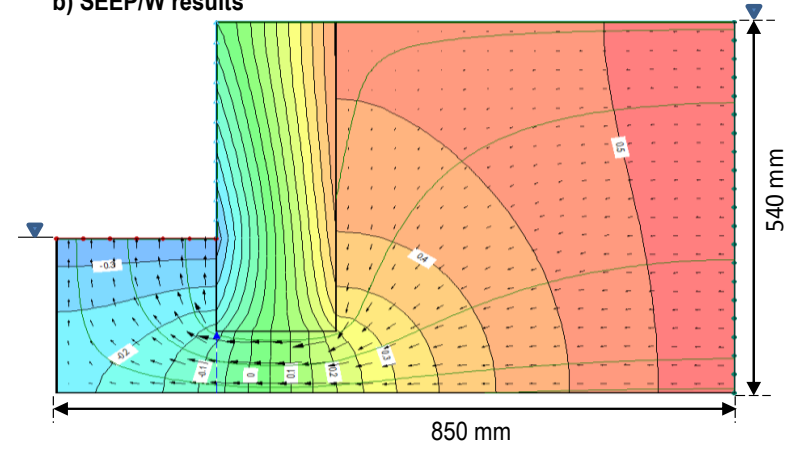
b) SEEP/W results

c) Hydraulic head contours from experiments
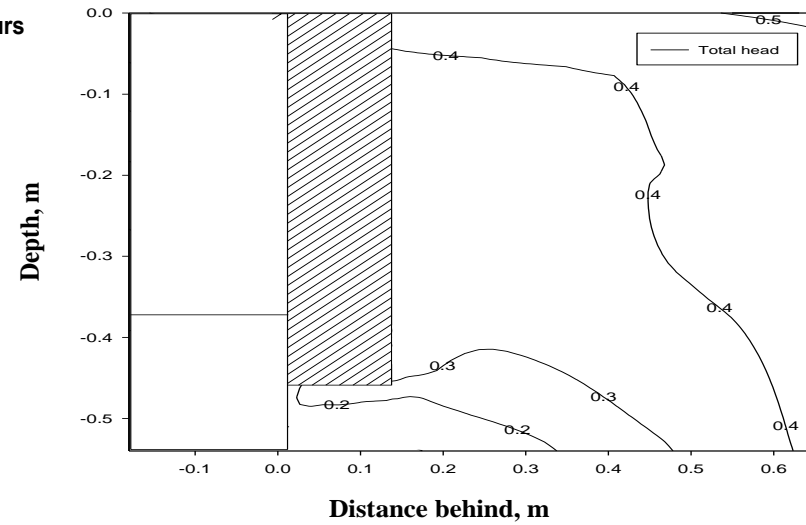
Figure 4.15: Comparison of flow paths for *x/d*=0.0. The three dimensions are equal.

123

a) Flow paths from experiments
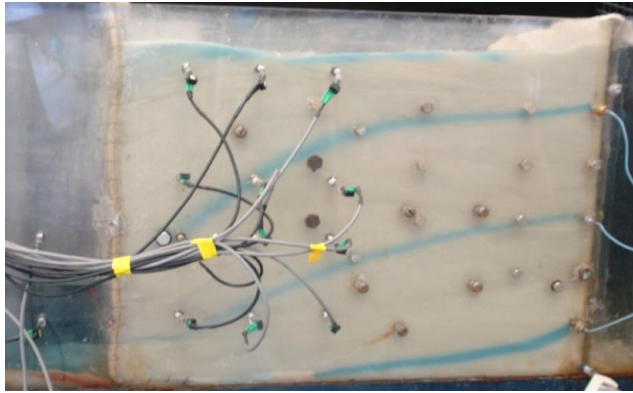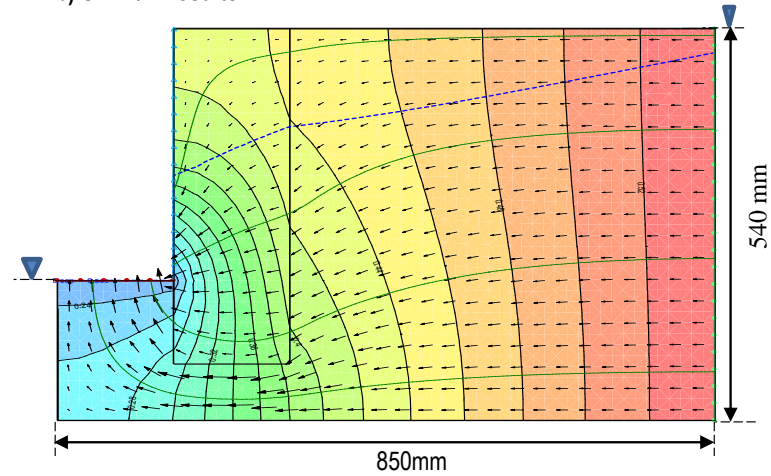
b) SEEP/W results

c) Hydraulic head contours from experiments
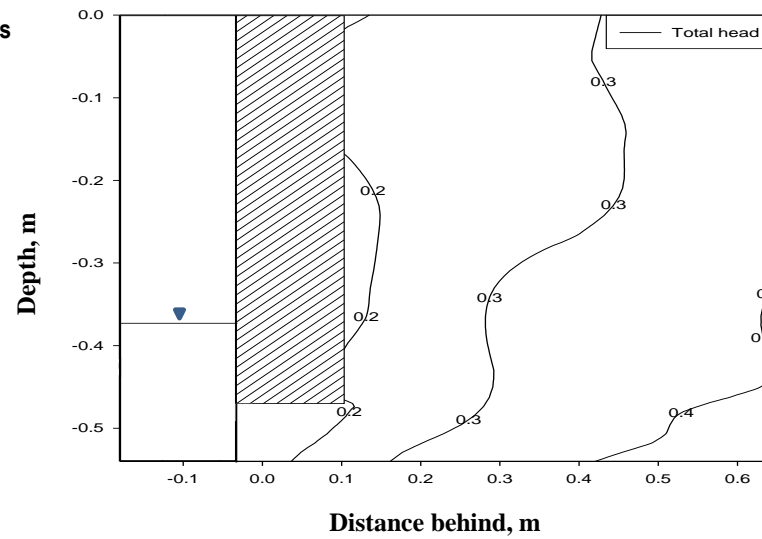
Figure 4.16: Comparison of flow paths *for x/d*=0.111.

a) Flow paths from experiments
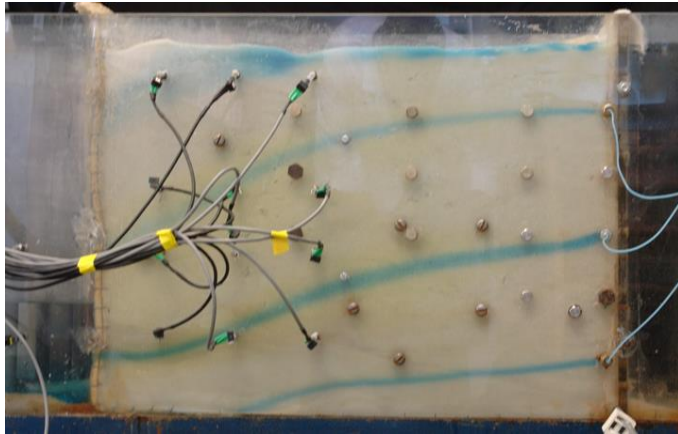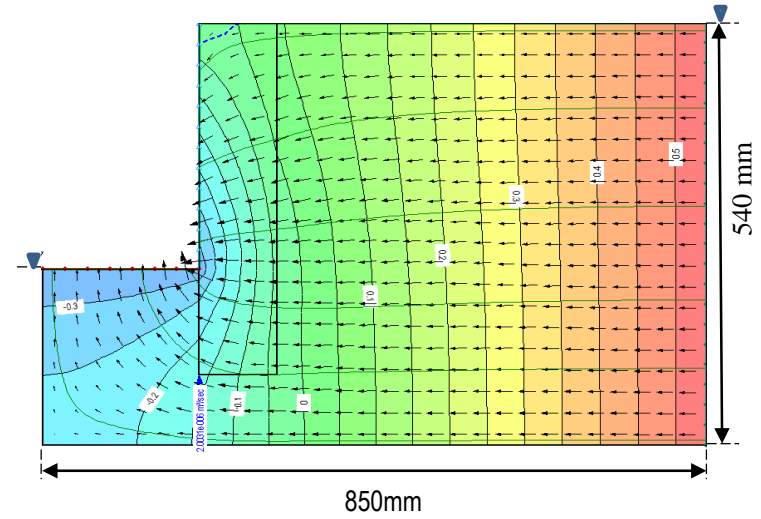
b) SEEP/W results

c) Hydraulic head contours from experiments
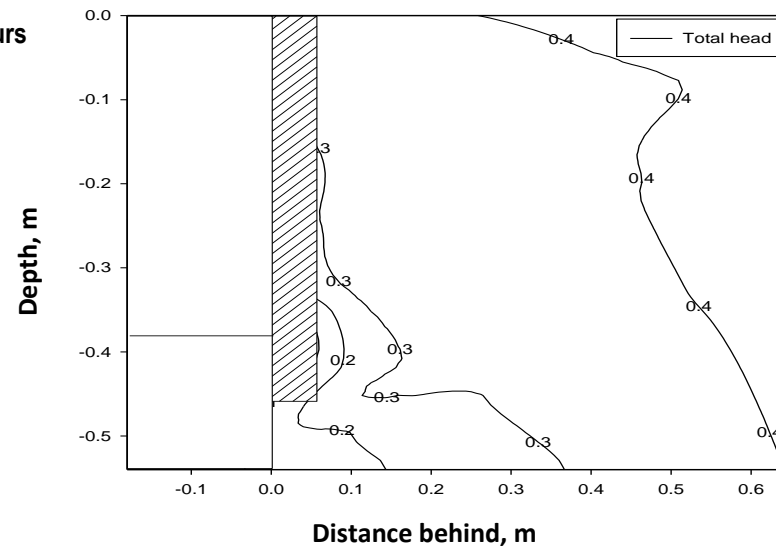
Figure 4.17: Comparison of flow paths for *x/d*=0.25.

a) Flow paths from experiments

b) SEEP/W results

540 mm

850mm
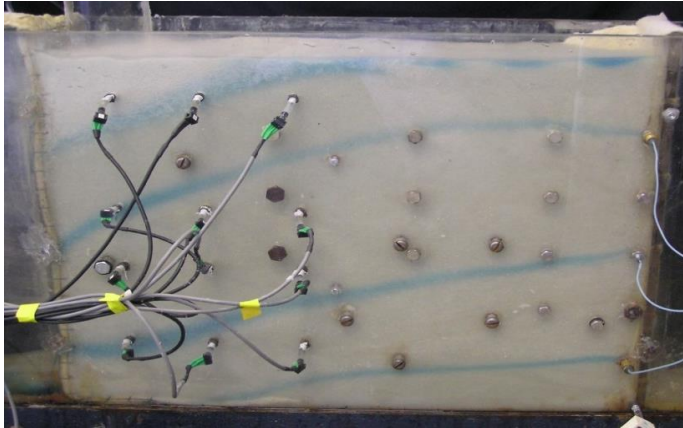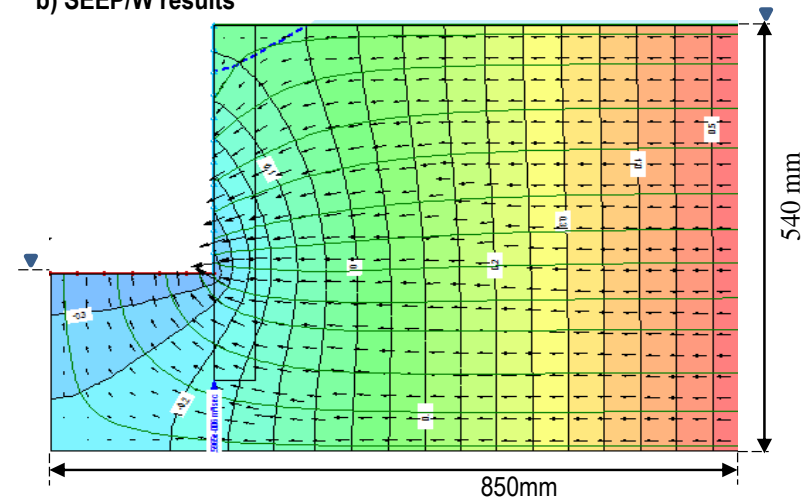
c) Hydraulic head contours from experiments
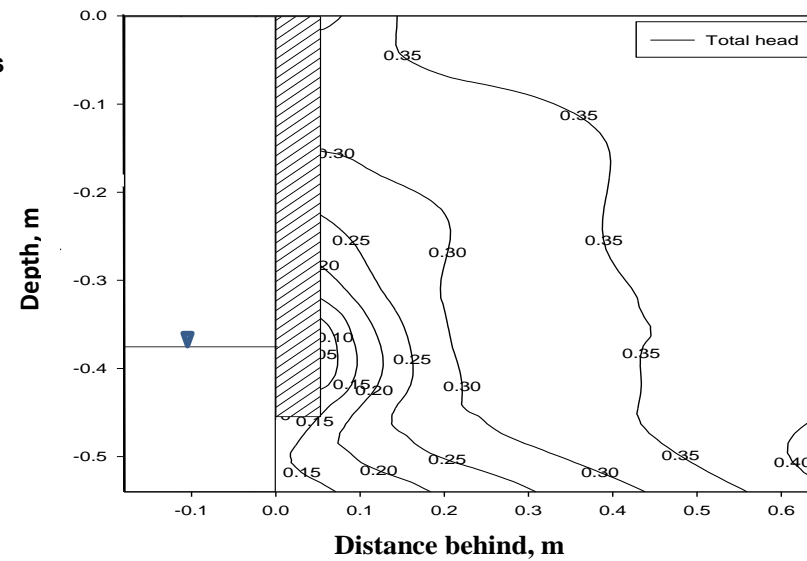
Figure 4.18: Comparison of flow paths for *x/d*=0.667.

a) Flow paths from experiments
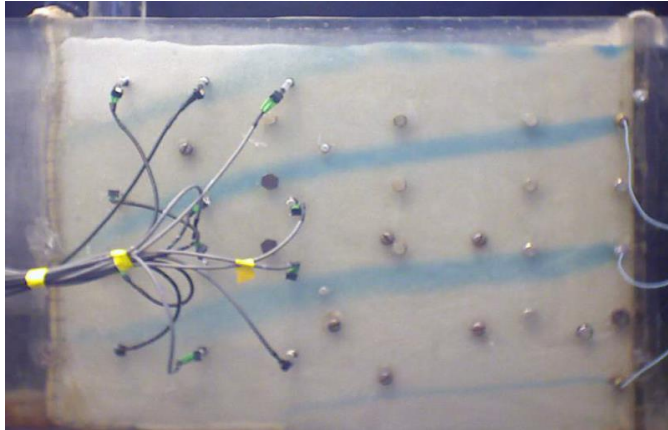
b) SEEP/W results
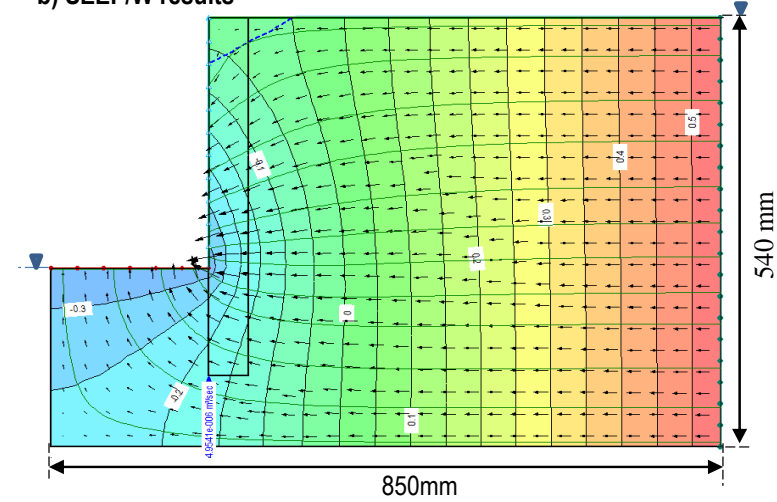
c) Hydraulic head contours from experiments
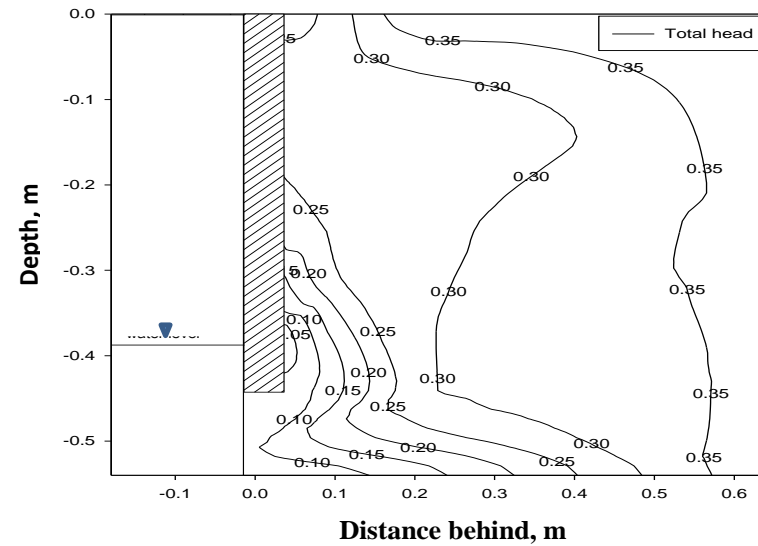
Figure 4.19: Comparison of flow paths for *x/d*=1.143.

Observations

1. The plots of flow lines and hydraulic heads from the laboratory experiments are consistent with those from the numerical simulations, particularly at lower pile gaps.

2. The flow paths for x/d=0.0 from the experiments were almost identical to the numerical results.

3. Slight differences between the hydraulic head distribution calculated from the experiment and those from the numerical simulations were observed. For instance, the values of head contours do not always fall in the same locations on the flow tank.

Minor deviations between the numerical and the laboratory results may be attributed to several factors as follows:

- The number of points at which the pore pressures were monitored, in retrospect, were insufficient to give more refined results.
- The disproportionate influence of the position of the transducers is apparent from the concentration of total head values in close proximity to the piles.
- The flow regime was dominated by a constant head of water at the supply reservoir and the imposition of discharge conditions at the outflows. These caused a higher head gradient than normal around the piles.

One disadvantage of this 'forced flow' regime was the difficulty in plotting flow nets by combining the measured hydraulic heads with the flow lines from the dye injection method. Thus, superimposing the plotted hydraulic head contours onto the flow line diagrams would not give a realistic approximation of the resulting flownets that would satisfy the rules governing the drawing of flownets. This is because the dye injection, in this instance, did not necessarily give uniform flow tubes and the spacing of the transducers is not conducive to getting equally spaced equipotentials. Additional errors could have also been introduced while measuring the pore pressures.

Development of seepage face

A seepage face when pumping from a well in an unconfined aquifer is the distance between where the water table intercepts the well face and the level of water in the well as shown in Figure 4.20.
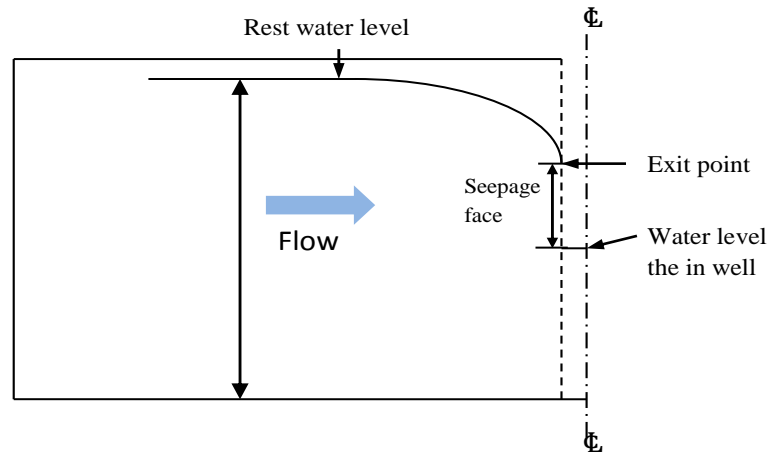
Figure 4.20: Definition of seepage face for unconfined flow to a well.

Several authors have researched the development of a seepage face due to the flow of homogeneous fluids through different types of porous media (Muskat, 1935; Chapman, 1957; Polubarinova-Kochina, 1962; Sakthivadivel and Rushton, 1989; Shamsai and Narasimhan, 1991 and Rushton, 2006).   Most seemed to use Dupuit's formula and an integration of Darcy's (1856) law for steady state flow to obtain the height of the free surface. This might lead to significant errors because Dupuit's formula represents flow below the free surface and does not really account for any vertical flow (Shamsai and Narasimhan, 1991 and Rushton, 2006). Shamsai and Narasimhan (1991) examined the solution for calculating the seepage face length in an open trench through a semi-confined aquifer similar to the work of Polubarinova-Kochina (1962) with the notable exception that no assumptions were made about the length of the seepage face. It was observed however that the presence of the free surface makes determining the seepage face lengths more difficult. Notwithstanding the influence of the free surface, the most commonly used analytical method for calculating the length of seepage face due to flow through homogeneous porous media with vertical faces seemed to be empirical charts presented by Polubarinova-Kochina (1962).   These charts were based on the volumetric

flowrates, the width of the structure and the head of water behind and in front of the structure respectively.

Throughout this investigation, it was apparent that previous analytical solutions could not be adopted to calculate the length of the seepage face developed as a result of through-wall seepage. This was due in part to the fact that existing methods were applicable to relatively thick structures in which the low permeability caused significant head loss as water flowed from the retained side to the front of the structure. Retaining walls are however thin relative to the other dimensions. Additionally, the existing solutions were developed for homogeneous structures resting on impermeable strata, a situation which differed slightly from the laboratory flow tank experiments. For the experiments described herein, the piles did not extend to the impermeable base of the flow tank as numerical analyses reported in Chapter 3 showed that the existence of through-wall seepage negate the impact of embedment depth on flow parameters.

In the absence of a suitable existing solution, the development of the seepage face due to changes in pile gap size was examined visually using the dye injection method. The uppermost streamline, which was analogous to the phreatic surface, was used throughout the analysis. The seepage face length, S_F, was taken as the distance between the point at which the uppermost streamline intersect the face of the wall and the water level in front of the wall as shown in Figure 4.21. This characterization is an adaptation of the seepage face definition used in well pumping by Sakthivadivel and Rushton (1989). The seepage face lengths were therefore measured at different pile gaps as shown in Figure 4.22.
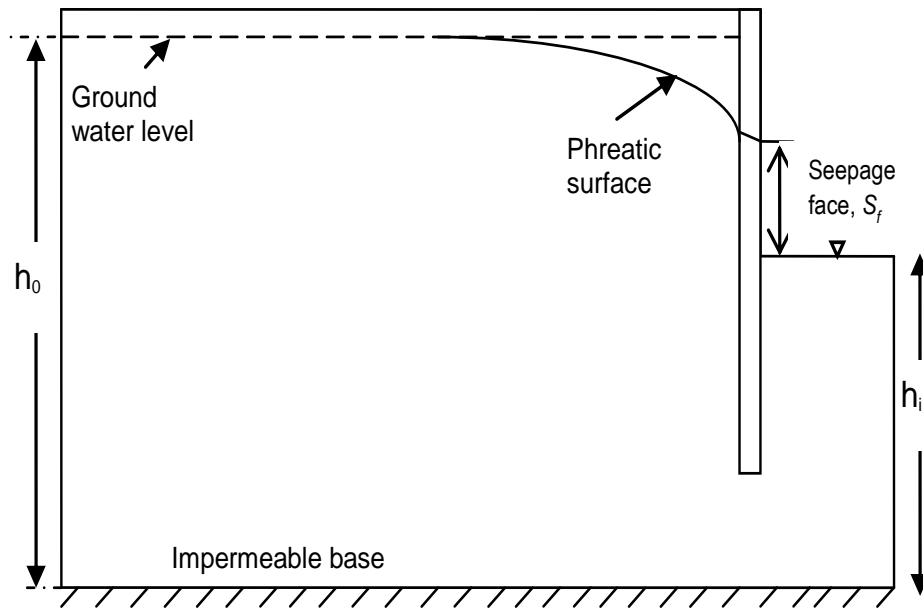
Figure 4.21: Schematic diagram of a permeable retaining wall showing the seepage face.
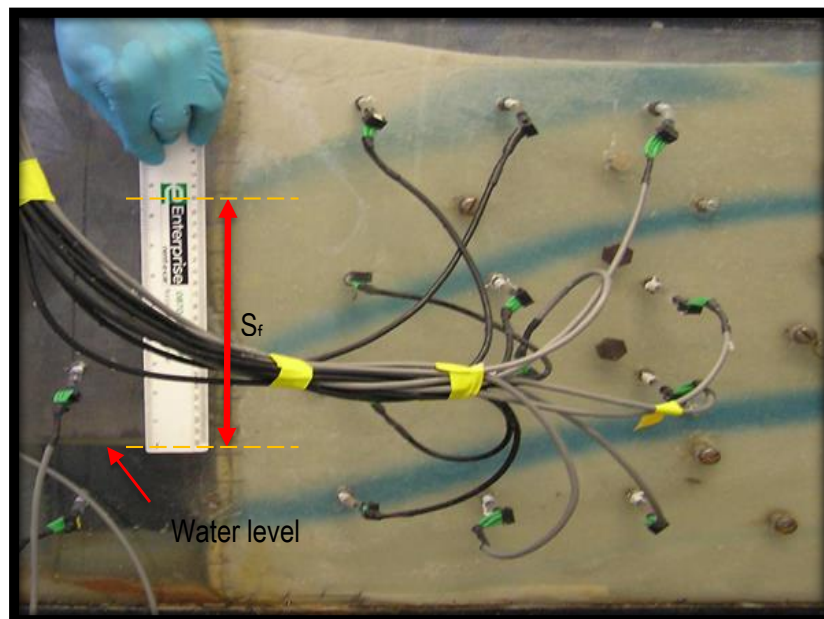
Figure 4.22: Measuring the seepage face lengths developed due to through-wall seepage. The size of the desaturated region, of lighter colour, just behind the model pile was also noted to be increasing with x/d.

Two major features of the influence of pile gap size on the emergence of seepage face were the rapid development of a de-saturated region behind the model wall and the increasing prevalence of horizontal flow. As the pile gap size increased, the depth below surface level to which the de-saturated region behind the model pile extended also increased. This caused the free surface to be 'pushed' further downwards to greater depths with increasing x/d as illustrated in Figure 4.23. It meant therefore that the length of the seepage face, ignoring seepage through the de-saturated region, decreased with increasing pile gaps. As the experiments were not configured to monitor flow conditions above the phreatic surface, it is not possible to comment on the proportion of seepage face length that was not accounted for. Further investigation into the contribution that flow above the phreatic surface makes to the length of the seepage face in retaining walls is therefore necessary. However, unsaturated flow was likely negligible in this instance.
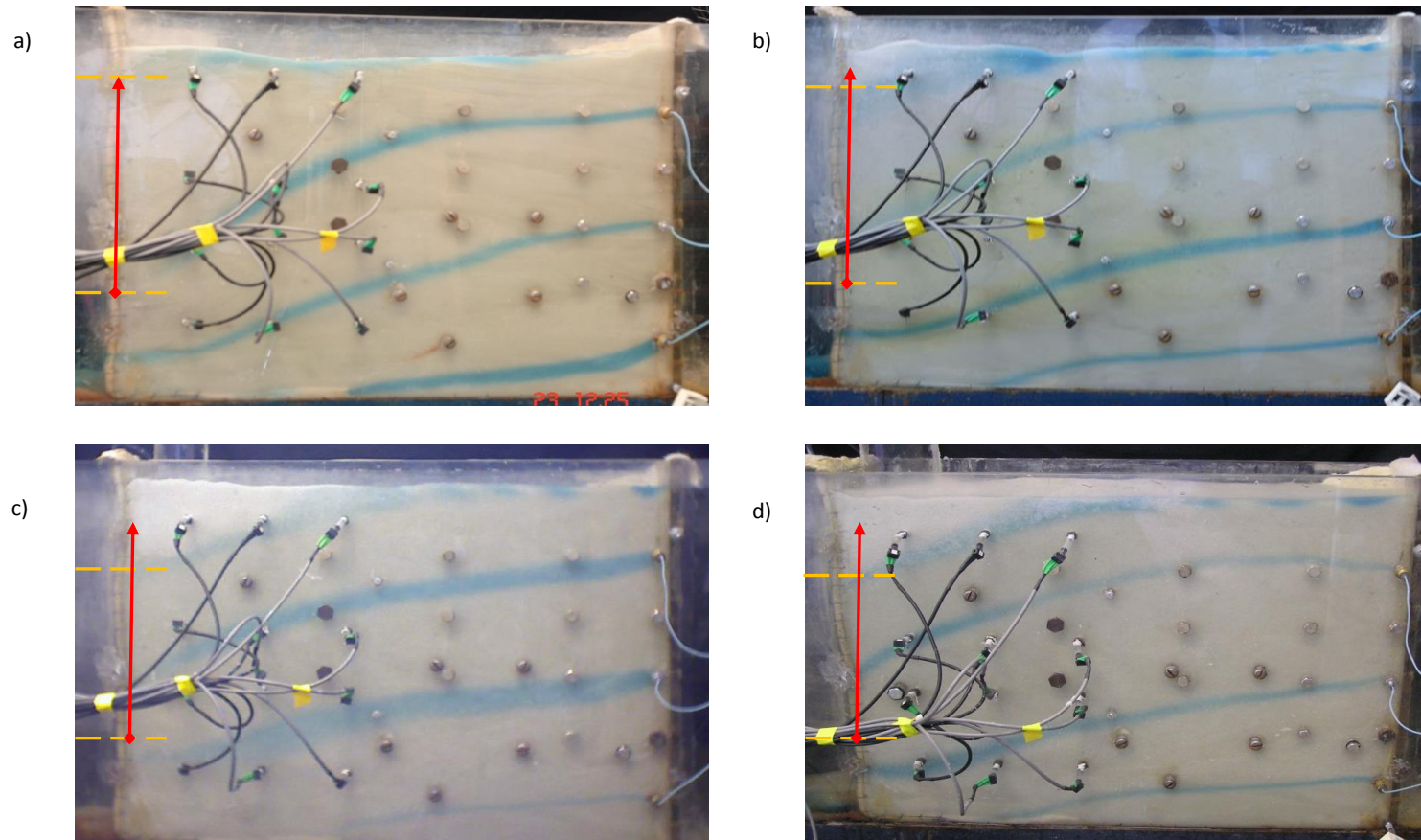
Figure 4.23: Seepage face lengths for *x/d*=a) 0.11, b) 0.25, c) 0.67 and d) 1.143. The arrows are of the same lengths and the distance between the dashed lines represent seepage face length, S_f.

Variation of seepage face length, S_f, with drawdown (h_0-h_i)

Seepage face length, S_f, from the flow tank experiments, were normalised with respect to the drawdown, h_0-h_i, of groundwater in front of the model wall from the original water level behind the wall. At x/d=0.0 there was no seepage face based on the definition by Sakthivadivel and Rushton (1989) due to the flow of water being around the model wall. Therefore, S_f was only measured once through-wall seepage was established. It is evident from Figure 4.24 that the normalised lengths of seepage face decrease with increasing pile gap width. This reduction in normalised S_f was most significant at small pile gaps and appeared to become constant as x/d increased. Normalised S_f values were consistent for x/d<0.4, after which significant increase in the spread of values occurred. The increased scatter of S_f was again consistent with changes in flow behaviour at higher x/d previously discussed. However, the trend in seepage face lengths was apparent throughout the investigation.
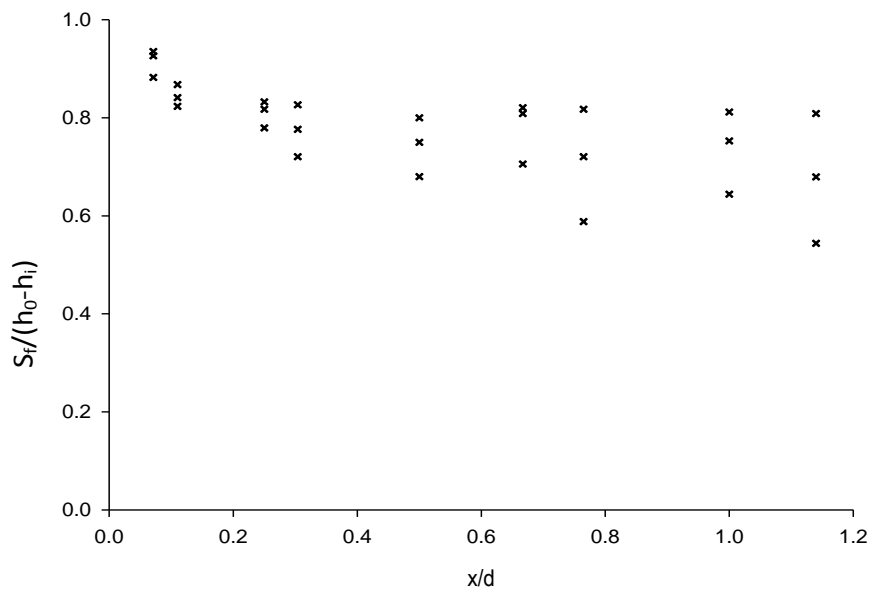
Figure 4.24: Variation of laboratory derived seepage face, S_f, with pile gap to diameter ratio, x/d.

The distance (y) from the ground surface to the top of the seepage face for saturated flow was normalised with respect to the hydraulic head (h) at the toe of the pile for a full tank. This was done for data from a best fit line through the experimental values in Figure 4.24. Only data from the stable portion of the graph, $0.0 \leq x/d \leq 0.3$ was used. Figure 4.25 shows that y increases with x/d. It is also evident that once through-wall seepage is allowed, the distance to the seepage face initially increased very rapidly. Further increase in x/d above about 0.2 however had negligible impact on the depth to the seepage face.
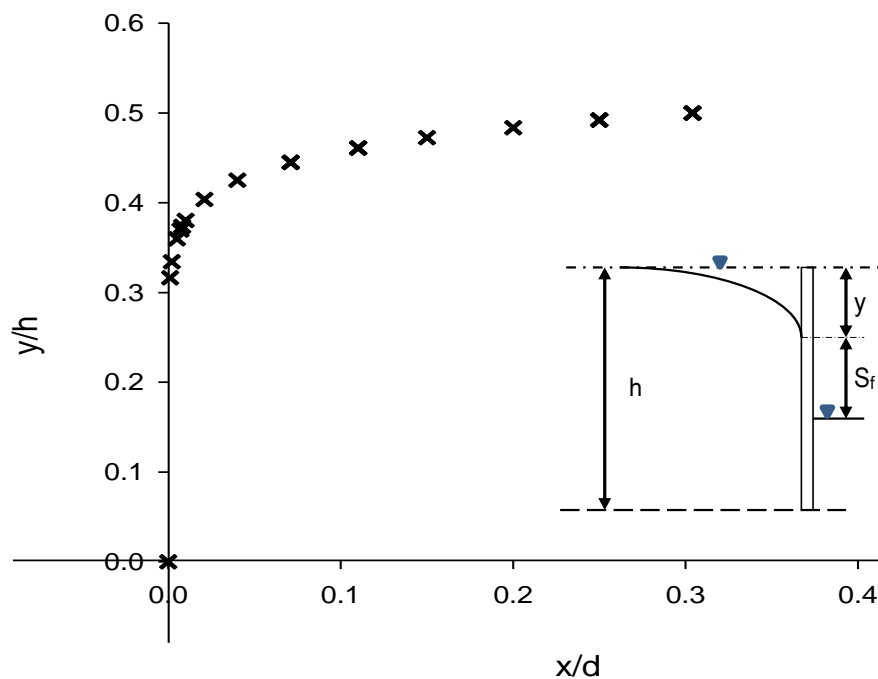
Figure 4.25: Best fit line of depth to seepage face normalised with respect to the original hydraulic head at the pile toe versus pile gap to diameter ratio.

Significance of *Sf*

The seepage face length, S_f, is indicative of the groundwater level behind the retaining walls formed from contiguous piles. This is useful in the design of retaining walls for which through-wall seepage is being considered as a means of reducing the hydraulic loads acting on the back of the wall. The dimensionless chart in Figure 4.25 can be used to estimate the groundwater level behind contiguous piles. For example, Figure 4.26 shows the wetted area at the lower end of a contiguous pile retaining wall, which indicates seepage through the pile gaps. The retaining wall is made of 1000 mm diameter piles with *x/d* = 0.286. The piles are 20 m long and the water table is 1 m below ground level giving h = 19 m. Using Figure 4.25, y/h = 0.48 which gives a depth to the seepage face, y of 9.12 m below ground level. This is similar to that observed in Figure 4.26 where the wetted areas are within 1-2 m above the base slab with an excavation depth of approximately 11 m.

In this example, a grout was used to prevent soil falling down through the pile gaps and not to exclude groundwater seepage. If the material used was of lower hydraulic conductivity than the soil it was meant to retain, then this would render the retaining wall impermeable and result in a loss of the efficiency gained by allowing through-wall seepage.
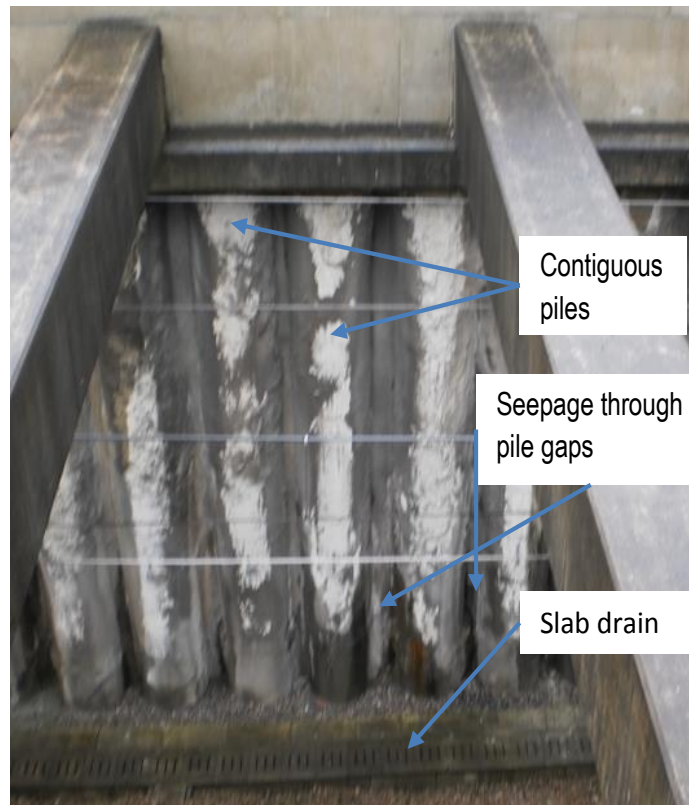
Figure 4.26: Seepage through a retaining wall formed from contiguous piles at CTRL, Ashford. Drainage of the trench is enhanced by the drain at the base of the excavation. Photo taken by Luca Montalti.

4.4.5 Impact of *x/d* on soil movement adjacent to the model pile

Soil displacement behind the model piles was monitored throughout the experiments to determine the influence of increasing pile gaps. This study focussed on vertical displacements owing to the constraint on horizontal movement caused by the fixed model piles. Consequently, it was not possible to evaluate adequately the development of instability at the face of the model wall. This was perhaps one of the greater drawbacks of the flow tank used in these experiments. Preliminary investigations, conducted to determine a suitable method of retaining the soil in the pile gaps, did however show that horizontal displacements increased with seepage particularly at higher pile gaps. Those investigations highlighted the difficulty of quantifying the amount of lateral displacement adjacent to the model pile due to instability of the

137

unrestrained soil in the pile gap. Based on these limitations, it was decided that only vertical displacements adjacent to the model piles would be measured for different pile gaps. The visual effect of increasing pile gaps on soil vertical displacement monitored during the investigation is illustrated in Figure 4.27. It is evident from Figure 4.27a that the amount of settlement behind the model pile was negligible for the impermeable wall, x/d=0.0. Surface settlement adjacent to the model piles increased with pile gaps as depicted by the diagrams for x/d=0.25, 0.667 and 1.143, in Figures 4.27b-d. Instability of the soil in the pile gaps meant that investigations into vertical displacements could not proceed accurately for larger pile gaps. This high level of soil instability around the model pile was consistent with the development of higher than expected flowrates and unrealistic pore pressures at larger values of x/d.
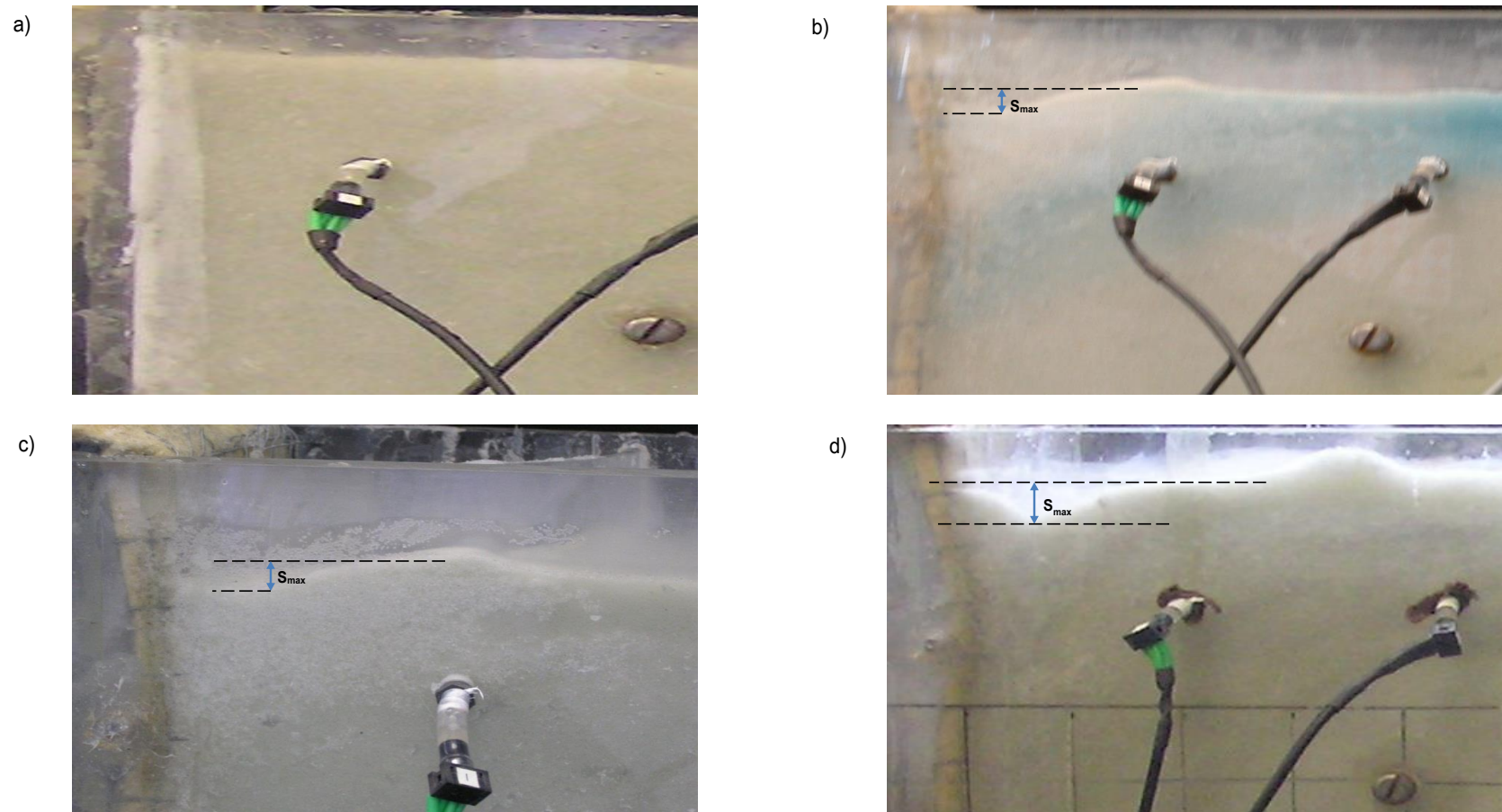
Figure 4.27: Comparison of vertical displacements behind the walls for pile gap to diameter ratios, $x/$d, of a) 0.0, b) 0.25, c) 0.667 and d) 1.143.

Vertical displacements at varying x/d were normalised with respect to displacements for the impermeable model wall, x/d=0.0. The results were plotted against pile gap to diameter ratios as shown in Figure 4.28. A general increase in normalised displacements adjacent to the model pile was observed. This is due to consolidation of the material as drawdown increased with increasing pile gaps. It was apparent from this increase that the soil settlement was proportional to the bulk permeability expressed in terms of the pile gap to diameter ratios, x/d. The normalised experimental results were compared with displacements from numerical simulations described in Chapter 3 and with those from one-dimensional stiffness modulus calculations. During this comparison the one-dimensional stiffness modulus, as explained by Preene *et al.* (2000), was adopted for the calculation of soil surface settlement. The thickness, D, of the soil layer and the average drawdown, S_{av} used in the analysis were taken as the height of soil in the flow tank and the difference in water levels between the front and back of the model wall respectively.
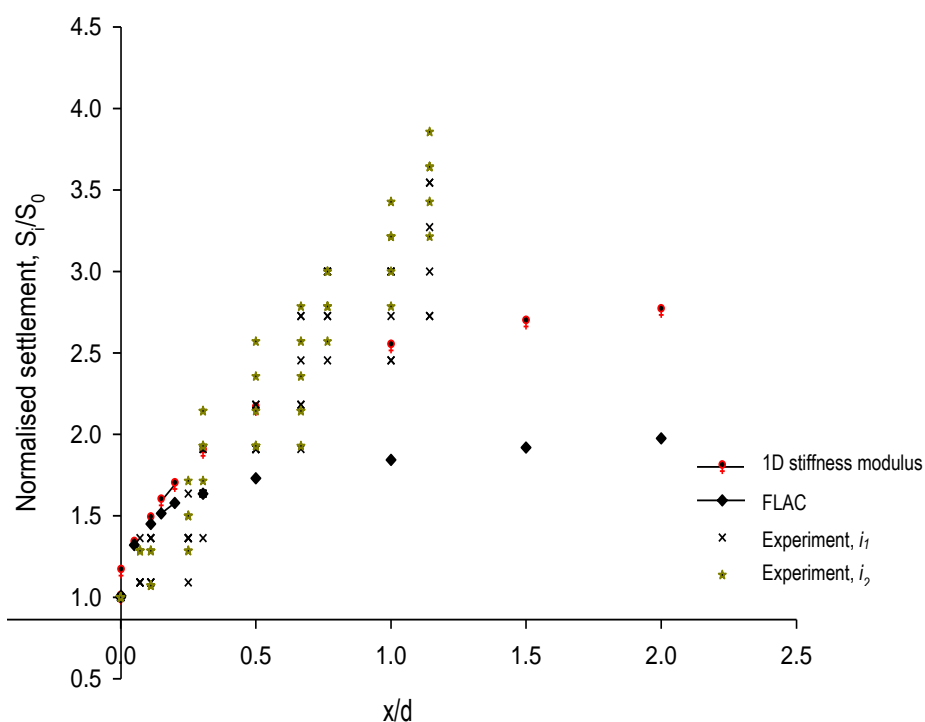
Figure 4.28: Normalised vertical displacement adjacent to the back of the model pile. Displacements are shown for normalised flow tank results at the two hydraulic gradients, i_1 and i_2 respectively.

Observations

The results from the experiments at *x/d<0.3* were consistent with, albeit slightly less than, those from the numerical and analytical solutions. The lower experimental values observed at *x/d*<0.3 may be attributed to the restraint on soil movements afforded by the fixed model piles. For *x/d* in the range 0.3 to about 0.9 the results from the experiments were noticeably higher than those predicted from numerical analysis but well encompassing those estimated using the 1D stiffness modulus. The higher settlement values are due to the difference in displacement mechanism between the experimental, analytical and numerical methods. During the flow tank experiment, soil displacement was due to the movement of soil towards the pile gap and to consolidation. Settlement values calculated using the one-dimensional stiffness modulus are only due to consolidation while the numerical simulations were conducted under ideal conditions. It would be expected therefore that soil settlement obtained from the experiment would be greater. This increase in settlement from the experiments continued at higher pile gaps whereas those from the numerical and analytical solutions became relatively constant as *x/d* increased. It was also noted that the displacement values from the experiments became increasingly scattered at greater pile gaps. This increase is consistent with previously observed changes in flow behaviour including flow quantities and pore pressures at higher *x/d*.

Further analyses showed that the results for the two hydraulic head differences investigated were similar at lower *x/d*. It was noted however, that as *x/d* increased, settlement at the higher head difference tend to be greater. This was particularly significant for *x/d* greater than about 0.4 and corresponded to the observed scattering of pore water pressure values and volumetric flowrates measured at higher *x/d* previously discussed.

Comparison of settlement profiles

Figures 4.29 and 4.30 show that the settlement troughs behind the piles, expressed as percentages of excavation depth, also increased with pile gaps. The larger than expected vertical movement adjacent to the piles may be due to the low wall friction between the Perspex pile section and the ballotini. The settlement profiles were otherwise consistent.
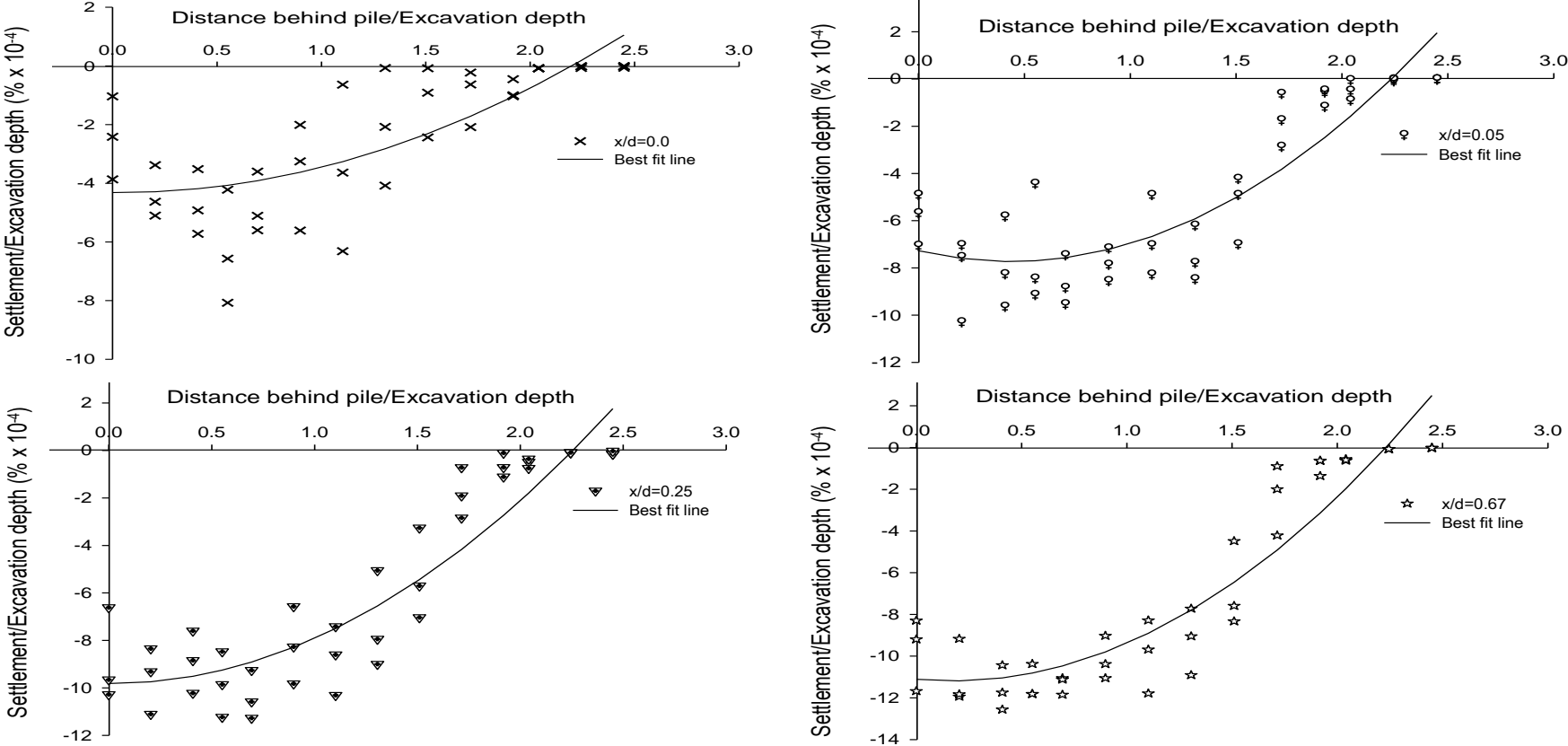
Figure 4.29: Settlement profiles for x/d=0.0, 0.05, 0.25 and 0.67. Profiles are shown as % of excavation depth.
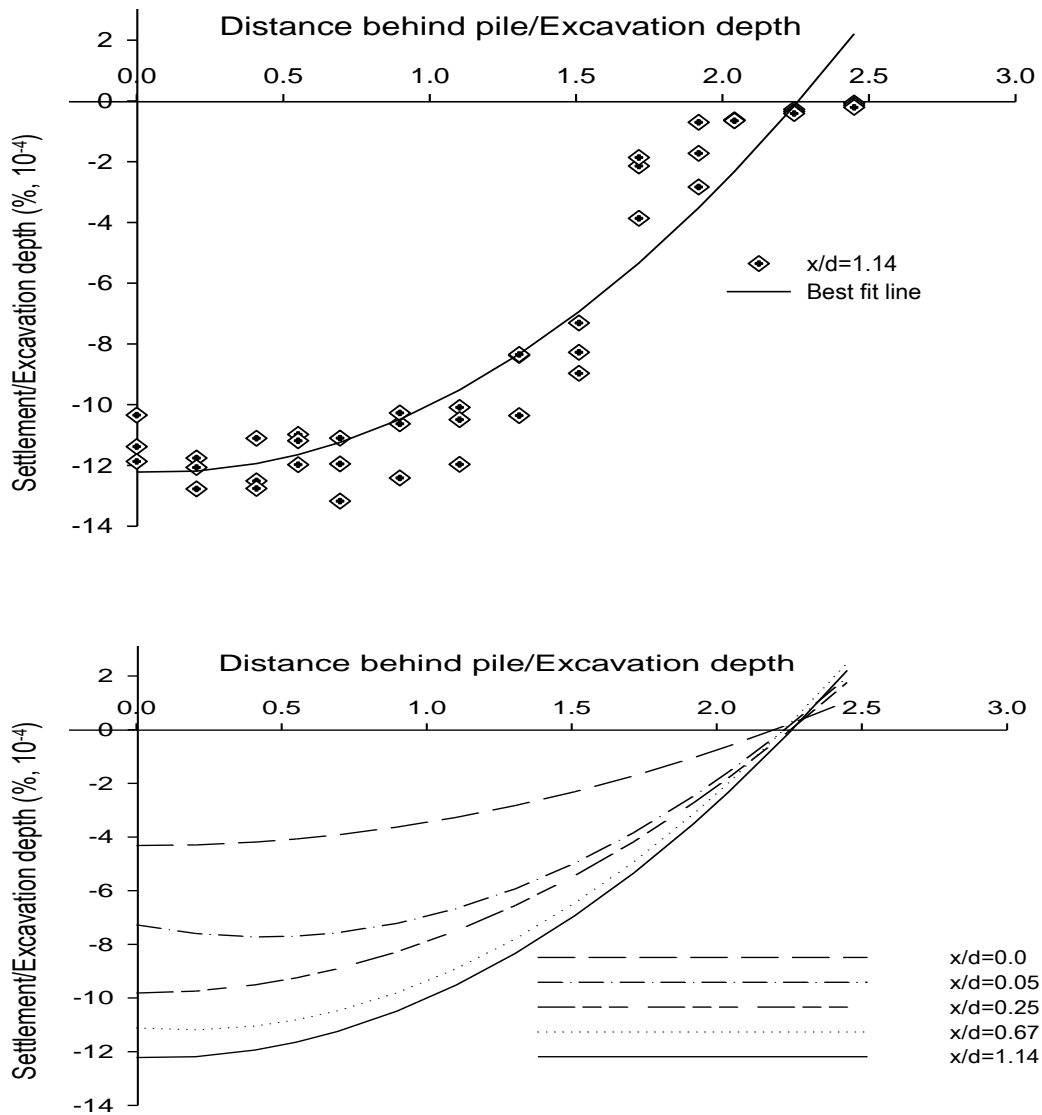
Figure 4.30: Settlement profiles for *x/d*=1.14 and best fit lines of settlement profiles from the flow tank experiments for *x/d*=0.0, 0.25, 0.67 and 1.14.

The increase in settlement, measured adjacent to the model pile, with wall permeability was also similar in trend to that observed by Zdravkovic *et al*. (2007) who conducted 2D numerical analysis of a deep excavation in London Clay. Zdravkovic *et al'*s (2007) results indicate an increase in soil surface settlement of about 25% more for a model wall in which the ratio $k_w/k_v=1$ relative to an impermeable wall in which $k_w/k_v=10^{-5}$. The soil and wall permeability was denoted by k_v and k_w respectively. It was not immediately clear from the analysis how the permeability values for the 2D wall in Zdravkovic *et al'*s (2007) analyses were derived or whether they were randomly selected. However, it was not possible during these experiments to conduct further direct comparison due to the large pile gaps required to achieve similar permeability ratios. Nonetheless, the trends are similar.

The dimensionless settlement charts may be used to estimate the amount of settlement as percentages of excavation depth behind contiguous piles at various pile gaps under similar conditions.

4.5 Summary

In this chapter, details of laboratory flow tank experiments conducted to investigate the groundwater flow regime around various model piles were presented and the results discussed. It is evident from the investigation that steady state flowrates increased as the pile gap to diameter ratio, x/d, increased. The back calculated values of the bulk permeability, k_p, using Darcy's law were consistent with Equation 3.6 derived in Chapter 3. Significantly, the bulk hydraulic conductivity, k_p, increased with x/d. The increase in steady state flowrates and k_p/k_s with x/d was consistent at lower pile gap to diameter ratios.

Pore water pressures measured at various distances behind the model piles however, decreased as the pile gaps increased. Pore pressures at the toe of the model piles were much less than estimated using linear seepage approximation at about 77% at x/d=0.3 which is representative of the pile gap at CTRL, Ashford.

A dye injection method was used to visualise the impact of increased pile gaps on different hydraulic parameters. Flow visualisation confirmed the development of flow patterns around the model wall, which were compared with the generally accepted distribution of flow paths for an impermeable wall. The direction of flow observed from the flow paths, in close proximity to the piles, appeared to become more horizontal at higher x/d indicating through-wall seepage (horizontal flow). Similarly, the combination of flow paths and total head distribution from the flow tank experiments compared well with those derived from numerical analysis in SEEP/W with those from the FLAC^{2D} simulations in Chapter 3. Divergence of hydraulic parameters, particularly volumetric flowrates and pore water pressure was observed at higher x/d. It was also evident that as x/d increased, the phreatic surface was pushed downwards. This caused the distance from the soil surface to the seepage face to increase and the seepage face length to decrease. A dimensionless chart was presented which can be used to estimate the depth of the groundwater behind the contiguous piles.

It was also observed that soil displacements increased with pile gap size. Dimensionless charts were also presented for estimating the soil settlement behind contiguous piles for various pile gaps.

It may be concluded therefore, that the flow regime established by numerical analysis in Chapter 3 and verified by laboratory experiments in this chapter, represents hydraulic conditions for the case of through-wall seepage and that this is definitively different from the conventional interpretation of groundwater flow around impermeable retaining walls.

Chapter 5

5.0 Case study: Field monitoring of the hydraulic conditions at CTRL, Ashford

5.1 Introduction

This chapter provides details of field monitoring of the hydraulic conditions from an instrumented section at the site of the construction of the Channel Tunnel Rail Link (CTRL), Ashford in Kent. The section under consideration is a cut and cover tunnel with propped embedded retaining walls formed from contiguous bored piles. Various reports provide details of the physical layout, construction sequence and method and the instrumentation of the retaining wall (Holmes *et al.*, 2005; Clark, 2006; Richards *et al.*, 2006; Richards *et al.*, 2007 and Roscoe and Twine, 2010). Clark (2006) presents a comprehensive description of the construction process, site geology and instrumentation of the construction site while Richards *et al.* (2007) elaborates on the development of long-term pore water pressures and horizontal total stresses. Holmes *et al.* (2005) describes the detailed site instrumentation and control processes for the entire

construction site and further illustrates the important contribution of the monitoring program towards building confidence in the design assumptions. Field data confirmed that the design assumptions were correct and that changes to the construction sequence were justified. Roscoe and Twine (2010) provides details on the redesign of approximately 1.8 km of the embedded retaining walls, which was carried out to improve the construction sequence and method and to enhance temporary propping.

The hydraulic conditions around the contiguous bored pile retaining walls at Ashford are presented and discussed in the following sections. Monitoring data of the long-term pore pressures in the soil strata at various depths below ground level and at different distances from the back and from the front of the retaining wall were analysed and the results discussed. During the analyses, comparisons were made between the hydraulic conditions around retaining walls in which there was through-wall seepage and the prevailing flow regimes for traditional impermeable retaining walls. Further assessments were made to determine the contribution of pore water pressure changes on horizontal total stresses and to resolve whether the observed reduction in lateral stresses can be attributed solely to variations in pore water pressures as indicated by Richards *et al.* (2007). These investigations were then used to recommend design assumptions for the groundwater flow regime associated with a contiguous pile retaining wall.

5.1.1 Site geology

The geological area of interest at CTRL, Ashford comprises a series of sandstones and clays of varying ages and states of weathering. This makes accurate determination of their geotechnical and hydraulic properties particularly difficult. The geology in the Ashford area is dominated by an aquifer confined below by low permeability clays and overlain by various deposits as illustrated in the idealised profile of the geological section in Figure 5.1. The aquifer was formed from Lower Greensands. The Hythe Beds is one of the two main sandstones that forms part of the Lower Greensand aquifer according to Shand *et al.* (2003), the other being the Folkestone Formation. The nature of the sandstones causes the flow of groundwater to be inter-granular. Significant fissure flow is also evident and adds to the observed large variations in the soil *in situ* permeability. Roscoe (2003) notes that the Hythe Beds in the region of the tunnel at

CTRL, Ashford predominantly comprise silty and clayey fine to medium sands with occasional bands of sandstone and thin beds of limestone. This variability of soil strata has significant influence on the hydraulic properties and particularly on the drainage characteristics in the region. Additionally, the Hythe Beds near the instrumented section are bounded below by typically 12 m of the less permeable Atherfield Clay. Weathered Gault Clay and various deposits, including several metres of made ground, overlay the Hythe Beds in different locations. This diversity of the bounding strata causes the Hythe Beds aquifer, in different locations, to be characterised as either confined or semi-confined.
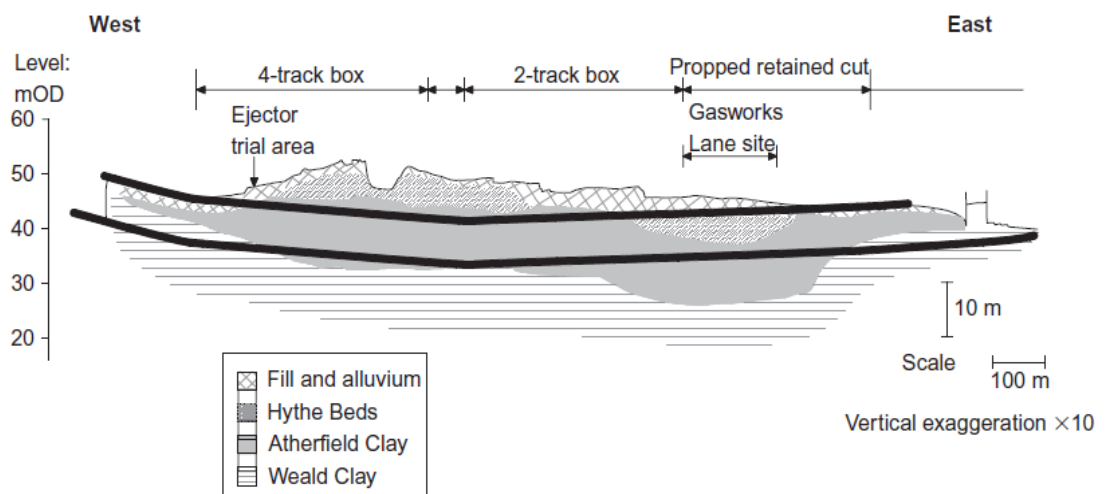
Figure 5.1: Idealised cross-section of the geology at the instrumented section at CTRL, Ashford (From Roberts *et al.*, 2007).

The Atherfield Clay is described by several authors as a stiff to very stiff clay which is heavily fissured and contains occasional lenses and silt/sand partings rendering the estimation of its hydraulic conductivity particularly difficult (Harris *et al*., 1996; Roscoe and Twine, 2001; Clark, 2006 and Roberts *et al*., 2007). This layer is comprised of two sub-layers, the Upper and the Lower Atherfield Clays. The lower Atherfield Clay is usually reddish brown and silty in nature while the upper Atherfield Clay is greyish blue to brown and of high plasticity (Roberts *et al*., 2007). The lower layer of the Atherfield Clay is also highly laminated in places.

The structure of the stiff to very stiff Weald Clay which extends to great depth (>100 m), in the vicinity of the CTRL, Ashford is dominated by silt laminations with thin bands of siltstone (Clark, 2006 and Roberts *et al*., 2007). The Weald Clay weathers to mottled orange-yellow or red clay. The distance between silt partings varies from less than 5 mm to about 100 mm in some areas while the vertical distance between silt lenses are 2-6 m. The many silt partings result in the permeability of the Weald Clay been usually of an order of magnitude greater than the overlying Atherfield Clay. The hydraulic conductivity is also highly anisotropic with the horizontal component of permeability, k_h, being much greater than the vertical, k_v ($k_h >> k_v$) (Roscoe and Twine, 2001). This further complicates efforts to characterise systematically the hydraulic properties of the various clays at Ashford.

5.1.2 Geotechnical properties

The high variability of the soil properties at the instrumented section at CTRL, Ashford may be attributed, in part, to the history and weathering of the soils at the particular location.

Hydraulic properties

The hydraulic properties of the various strata are even more difficult to quantify as illustrated by Roscoe and Twine (2010), who notes that the presence of numerous silt partings in the Weald Clay, for instance, causes inconclusive determination of its permeability. The hydraulic conductivity values of the soils were obtained by different researchers using *in situ* and laboratory tests. These have shown that the permeability

of the different soil strata and the Weald Clay in particular, depends on the testing method adopted. For example, Roberts *et al*. (2007) observed permeability in the range 1 to 2 x 10^{-6} m/s when ejector well pumping tests were carried out. These were in contrast to permeability of 1 x 10^{-8} m/s reported from borehole tests. Roberts *et al*. (2007) suggests however that borehole permeability tests are inaccurate and known to underestimate true permeability by up to an order of magnitude or more. The values from the ejector well pumping tests were also up to two orders of magnitude greater than reported by Roscoe and Twine (2001) from borehole permeability tests. Clark (2006) also reports that the permeability of the Weald Clay varied between 1 x 10^{-9} m/s and 3 x 10^{-7} m/s. The wide variation in permeability values for the Weald Clay can be attributed to the presence of the numerous horizontal silt laminations, which contributes to the anisotropic behaviour of the soil layer. The drain paths created by silt lenses also cause underdrainage of the less permeable Atherfield Clay by the Weald Clay. Therefore, the selection of a hydraulic conductivity value for the Weald Clay for geotechnical designs should take into consideration the most reliable results of large-scale permeability in the relevant direction.

Although the data on field permeability tests is scarce, the permeability of the Atherfield Clay appears to be better defined than that of the Weald Clay with values estimated to be in the range 2 x 10^{-9} m/s to 9 x 10^{-8} m/s. This low permeability meant that construction dewatering of the Atherfield Clays at Ashford by methods that depended on gravity was deemed impractical. This is despite the recommendation during the geotechnical engineering design phase that the Atherfield Clays be treated as a drained material (Roscoe and Twine, 2001). The decision to treat the Atherfield Clay as being drained would also mean making the assumption that there was significant amount of underdrainage by the Weald Clay. However, the lack of reliable available data meant that it was not conservative to treat the Atherfield Clay as a drained material during construction.

The hydraulic conductivity of the Hythe Beds, being aquifers, was much higher than that of the Atherfield Clay with permeability as high as 1 x 10^{-7} m/s reported.

Soil strength

The soil strength parameters were, for design purposes, obtained from triaxial tests as illustrated by Roscoe and Twine (2001). The soil properties appear to vary, sometimes significantly, between layers as shown in Table 4.1. For instance, the plasticity index (PI) of the Weald Clay varied between 10% and 30% while those of the Atherfield Clay were 20-30% and approximately 50% for the Lower and Upper Atherfield Clay respectively. Soil effective friction angles also vary between the different strata. The design effective friction angles were taken as 25.7^o, 18°, 17.7^o and 19.5^o for the Hythe Beds, Upper and Lower Atherfield Clay and the Weald Clay respectively. Bulk densities are relatively consistent regardless of the location as demonstrated by Clark (2006). The effective cohesion, c', was taken as zero for all soil layers except the Lower and Upper Atherfield Clay for which c' were 4 and 10 kPa respectively. Bulk moduli were taken as 37.5 MPa, 13.5 MPa, 12.5 MPa and 22.5 MPa for the different soil layers respectively.

	Hythe Beds	Upper Atherfield Clay	Lower Atherfield Clay	Weald Clay
Permeability, k (m/s)	1×10^{-7}	3×10^{-8}	3×10^{-8}	$1\text{-}2 \times 10^{-6}$
Bulk Modulus, K (MPa)	37.5	13.5	12.5	22.5
Effective friction angle, ϕ' (deg)	25.7	18	17.7	19.5
Effective cohesion, c' (kPa)	0	10	4	0
Plasticity Index, PI (%)	32	50	20-30	10-30

Table 5.1: Soil parameters used for the back analysis of the retaining wall at Ashford.

5.1.3 Site Characterisation and Instrumentation

The retaining walls for the instrumented section of the cut and cover tunnel were formed from contiguous bored piles 1.05 m in diameter and 21.0 m long. Formation level was approximately 11.0 m below the original ground surface while the excavation was 12.0 m wide. Excavation for the installation of the bored piles was carried out in two phases. The first 8 m of soil was excavated and temporary casings inserted to support the sides of the bore. The remaining depth was subsequently excavated and supported under a bentonite slurry mixture. The prefabricated reinforcement cage was inserted with the relevant monitoring gauges attached. Concrete was then tremied in from the base of the bore while the bentonite slurry was removed at the same rate. The temporary casings were then recovered. The entire pile installation process at the instrumented section took approximately 24 days.

To reduce pore water pressures in the proposed cutting during construction, temporary vertical sand drains were installed in front of the retaining walls. These uncased sand drains were positioned at 3 m centres in two rows, 3 m from the faces of the retaining walls. All temporary sand drains were 150 mm in diameter and filled with 10 mm gravel. The sand drains, been temporary in nature, were not expected to last beyond about three years after installation, as the gravel was not graded to prevent clogging up by debris and soil particles.

Pile caps (capping beams) were constructed after installation of the sand drains. The capping beams were 1.5 m deep by 1.35 m wide with integrated corbels to support the permanent reinforced concrete props. Reinforced concrete props fitted with strain gauges were installed after sufficient excavation of the soil in front of the retaining wall was carried out. Backfill was then placed behind the capping beams. Excavation to a depth of 5.4 m below the soffit of the permanent props was carried out after which the temporary props were installed. The temporary props, which were made of hollow cylindrical steel sections with external diameter of 1016 mm, were instrumented with vibrating wire strain gauges as described by Holmes *et al*. (2005). Figure 5.2 shows the arrangement of various elements of the cut and cover tunnel.
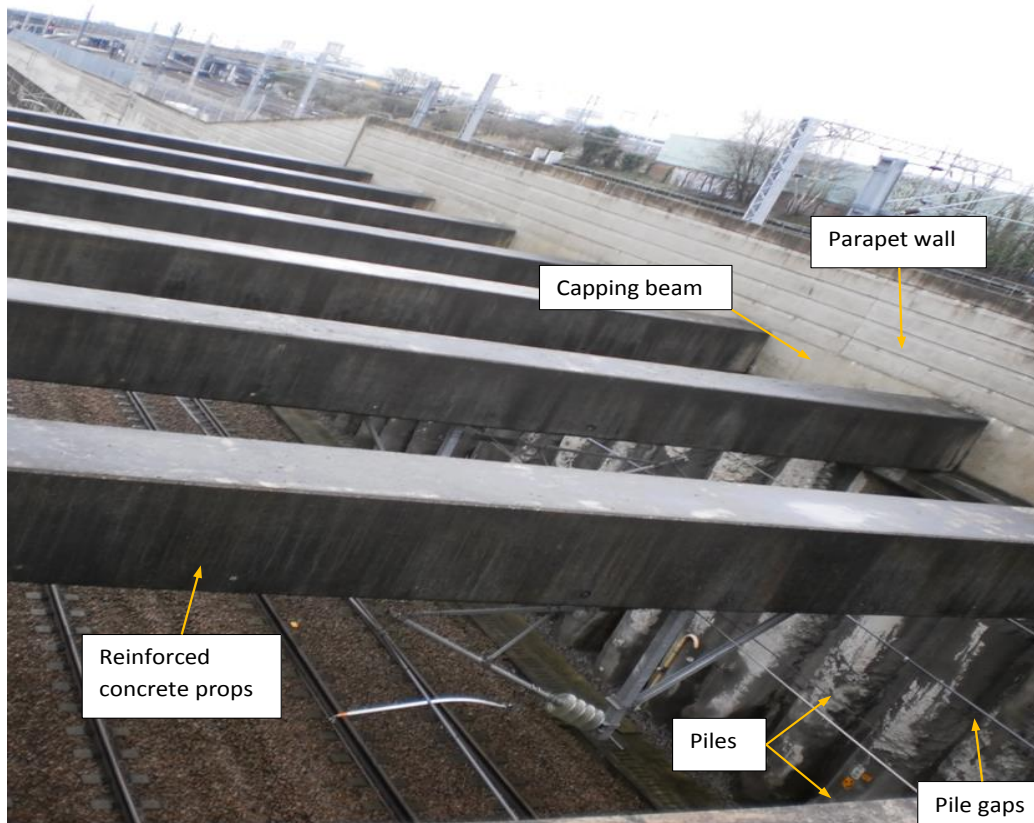
Figure 5.2: Layout of the cut and cover tunnel at CTRL, Ashford. Photo taken by Luca Montalti.

Excavation to formation level, a further 3.7 m below the temporary props, was carried out over a period of seven (7) days. Permanent vertical sand drains, which facilitated drainage of the Atherfield Clay into the Weald Clay, were installed. This was to prevent build-up of the pore water pressures in the Atherfield Clay beneath the base slab. The sand drains were further inter-connected by horizontal channels below the base slab. The base slab was constructed and vertical drains through the slab connected to those below. The temporary props were then removed over a period of fourteen days, starting three days after completion of the base slab.

Instrumentation

The instrumented section of the north wall of the cut and cover tunnel, described in this section, extended over a distance of approximately 12.0 m. The instruments used to collect the field data for these investigations were installed during the period prior to construction in 1999. Variations in horizontal total stresses was monitored using vibrating wire pushed-in pressure cells known as spade cells due to their shape. The spade cells, which were fairly simple in their design, consisted of two sheets of steel approximately 7 mm thick and 100 mm wide welded around the edges to leave a narrow gap between the plates as shown in Figure 5.3. The hydraulic system was completed by oil in the gap between the steel sheets and connected to a vibrating wire pressure transducer.
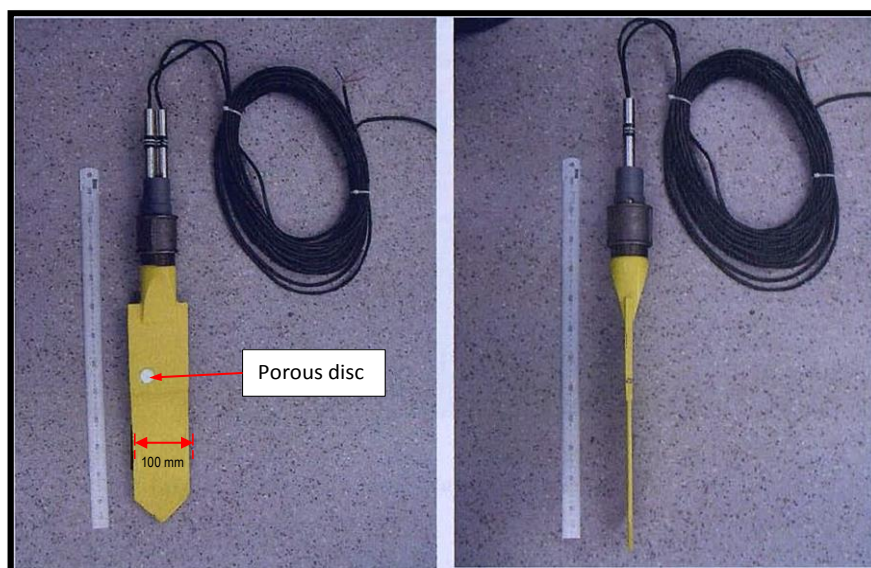
Figure 5.3: Pushed-in pressure cells (spade cells) used at CTRL, Ashford.

Pore pressure changes were recorded by way of integrated piezometers, incorporated into the spade cells, consisting of a circular porous ceramic filter disc connected to another vibrating wire pressure transducer. The procedures used to calibrate the spade cells and to correct over-read errors are described by Clark (2006). Calibration of the instruments was carried out by the supplier, Soil Instruments Ltd. The instruments were positioned in a pressure chamber with the porous disc covered by clamps during the calibration of the transducers used to measure horizontal total stresses. The pressure in the chamber was increased and the readings of the transducers recorded. The pore pressure transducers were calibrated by applying pressure at the outlet and the resulting pore pressures recorded. Subsequent calibration for over-read was conducted in the field. The difficulties associated with the installation of the spade cells and pore pressure transducers are explored by Clark (2006) and Richards *et al*. (2007). Richards *et al*. (2006) also presents and discusses the installation effects.

The pressure transducers used to measure changes in horizontal total stresses have a range of up to 1000 kPa while those for measuring pore pressure changes have a range of up to 500 kPa. The instruments could monitor data to an accuracy of within $\pm$ 0.1% of the *in situ* soil stresses and pore pressures at temperatures between -20°C and 80°C, according to the supplier.

The instruments were positioned as shown in Figures 5.4 and 5.5. The first line of instruments behind the retaining wall, *P1-P5* was located at a horizontal distance of 1.275 m and at depths of 3.3 m, 5.3 m, 8.3 m, 11.3 m and 15.3 m respectively. The second line of instruments, *P15* and *P16* was located 2.375 m behind the retaining wall at depths of 5.3 m and 8.3 m respectively. The third and last line of instruments behind the retaining wall comprising spade cells *P6 – P10* was located at a distance of 3.475 m and at depths of 3.3 m to 15.3 m similar to *P1-P5*. At the front of the retaining wall, the first line of instruments, *P11* and *P12* was at a distance of 1.275 m and depth of 11.3 m below the pre-construction ground level. One instrument, *P17* was located 2.375 m in front and at a depth of 15.3 m below the original ground level while *P13* was located 3.475 m in front of the retaining wall and at a depth of 11.3 m.
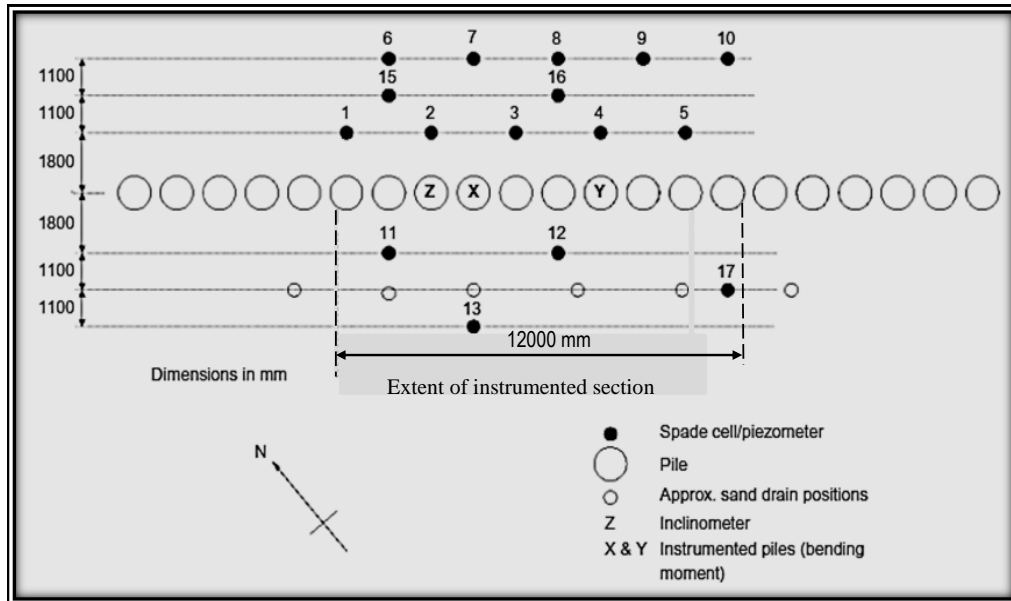
Figure 5.4: Plan of instrumented section at CTRL, Ashford (From Clark, 2006).
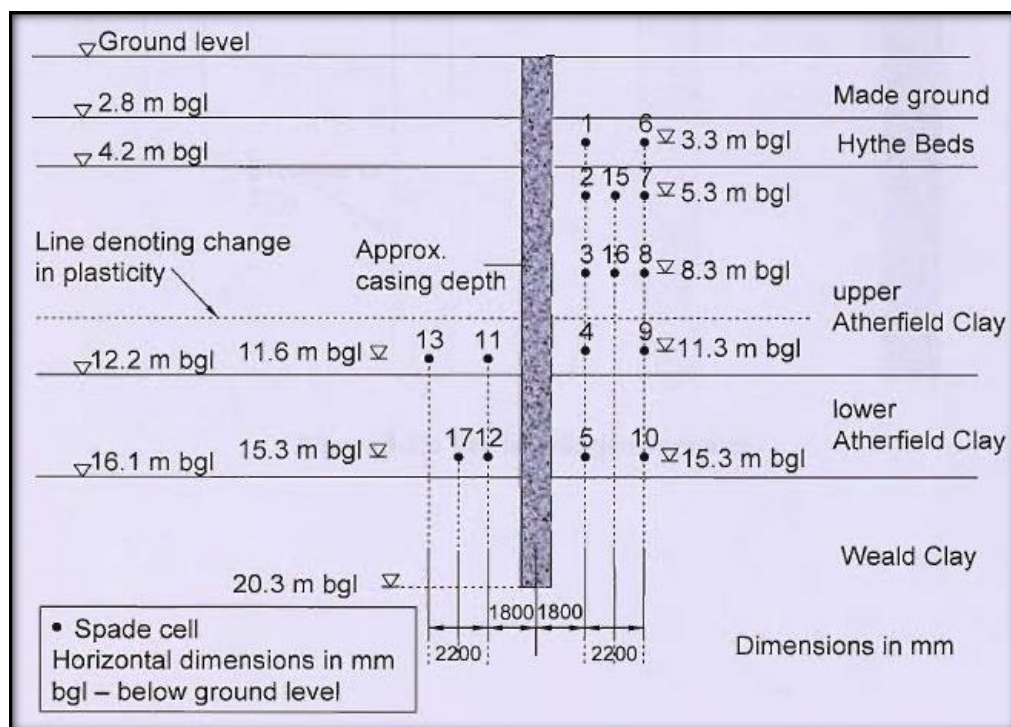
Figure 5.5: Elevation of instrumented section at CTRL, Ashford (From Clark, 2006).

5.2   Long-term pore water pressure distribution

The variation of pore water pressures around the contiguous pile retaining wall measured during the monitoring period was investigated to determine the impact of through-wall seepage on the long-term pressure distribution.   Pore pressure measurements were taken at various time intervals during the monitoring period, ranging from 15 minutes to 1 hour. The location of the pressure transducers relative to the retaining wall allowed various combinations of pore water pressure profiles and hydraulic head contours to be drawn around the retaining wall in order to visualize the groundwater flow regime at any particular time.   The distributions of pore water pressures behind and in front of the retaining wall and the resulting hydraulic head contours are presented and discussed in the following sections. These are compared for the short, medium and long-term conditions.   Further comparisons are made with retaining walls formed from secant piles in similar overconsolidated clays.

5.2.1 Pore water pressure distribution behind the retaining wall

Pore water pressures were compared at various distances behind the retaining wall at the locations of transducers *P1-P10* and *P15 & P16*. A general reduction in the pore pressures, measured at the various locations, was observed throughout the monitoring period as illustrated in Figures 5.6 to 5.8.
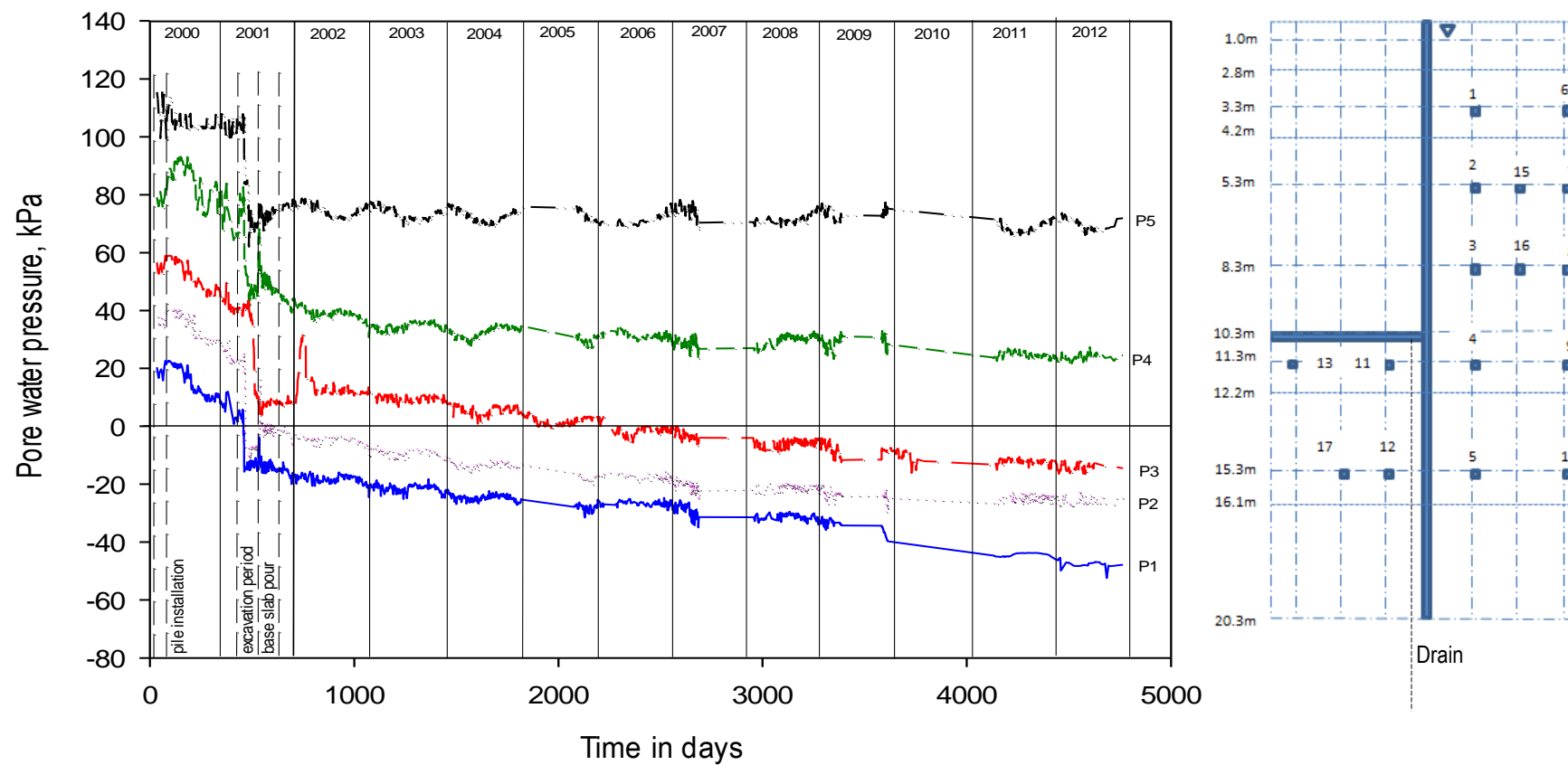
Figure 5.6: Pore water pressure distribution 1.275 m behind the retaining wall. The elevation through the instrumented section with the locations of the piezometers is shown inset.
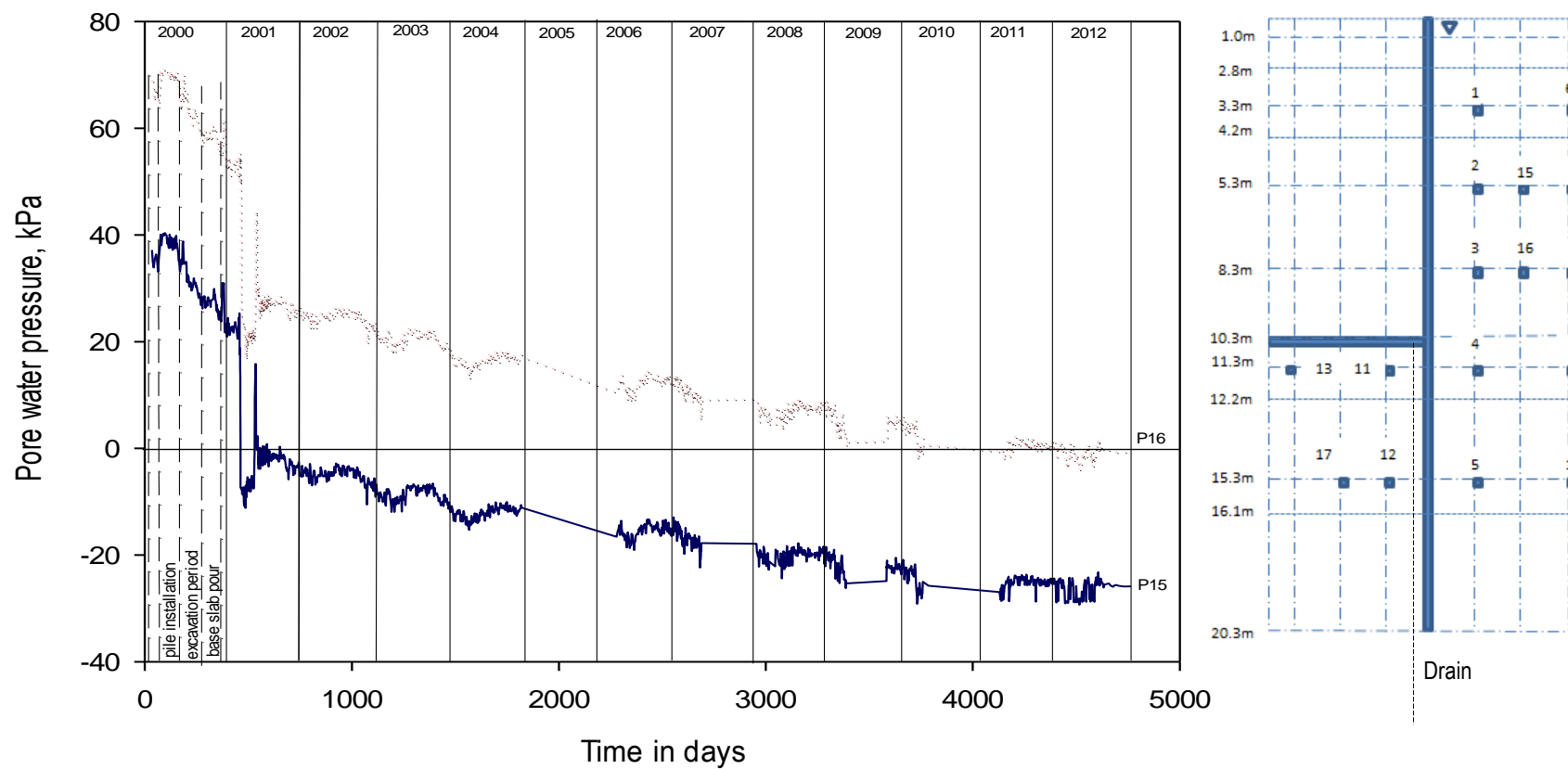
Figure 5.7: Variation of pore water pressures 2.375 m behind the retaining wall.
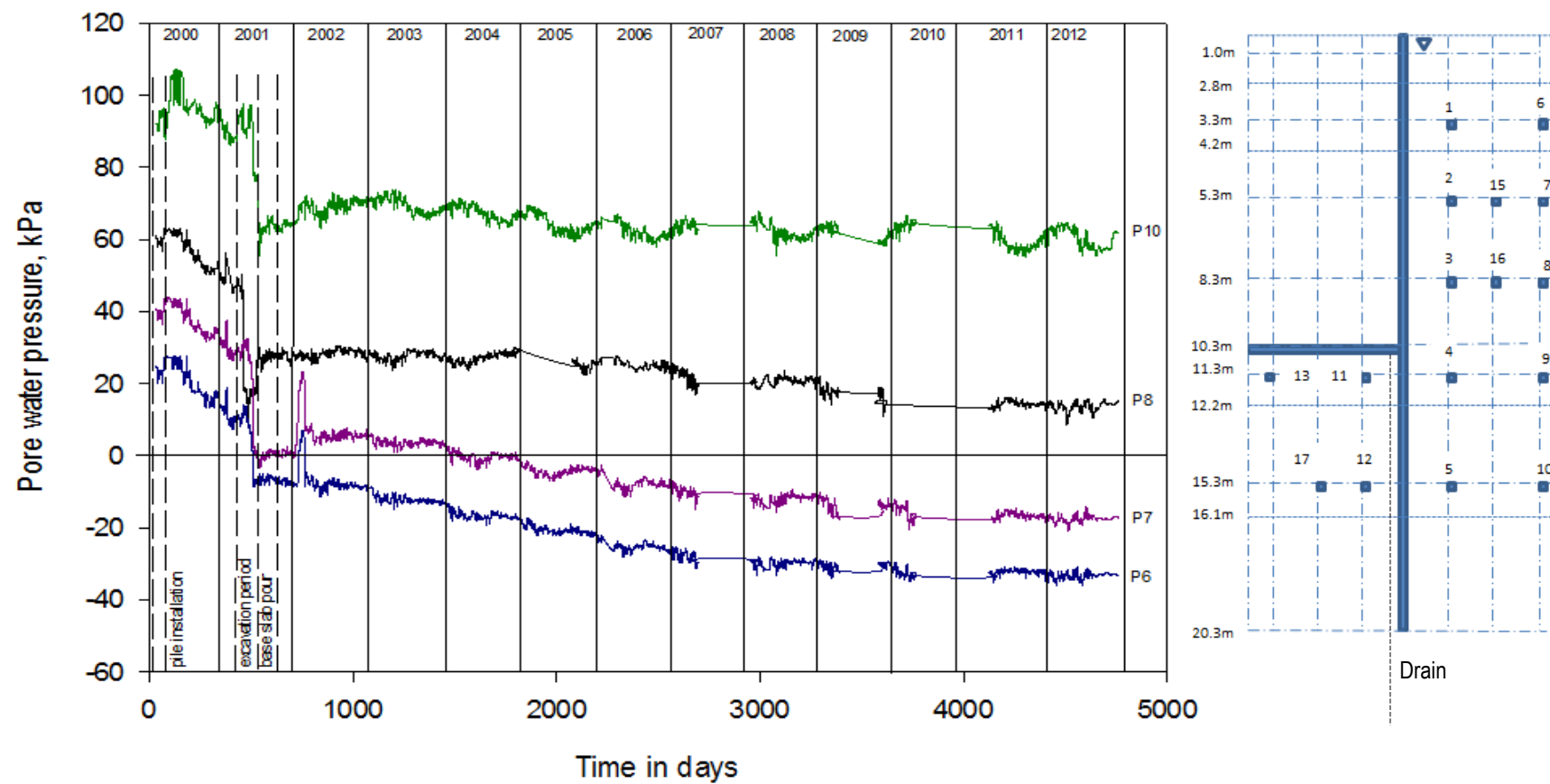
Figure 5.8: Pore water pressure distribution 3.475 m behind the retaining wall.

The variation of pore pressures behind the retaining wall during the construction period is typical of the behaviour encountered elsewhere in stiff soils. For instance, excavation for the installation of the contiguous bored piles, as seen in Figure 5.6, caused an initial decrease in pore pressure at piezometers *P1-P5* as would be expected. This initial reduction in pore pressures may be attributed to stress relief in the surrounding soil due to excavation for the piles during the installation process (Symons and Carder, 1993 and Gourvenec and Powrie, 1999). An immediate increase in pressure was then observed. This is possibly due to the placement of the support for the bore, in this instance a bentonite slurry mix, and later to the pressure exerted by the wet reinforced concrete for the piles (Gunn and Clayton, 1992). Dewatering and subsequent excavation of the soil in front of the retaining walls caused further reductions in pore water pressures. This was followed by a slight increase in pressure, particularly at the positions of piezometers *P4* and *P5* located below formation level, as the concrete for the base slab was poured. Pore pressure variations at corresponding depths at distances of 2.375 m and 3.475 m behind the retaining wall were consistent with those encountered at a distance of 1.275 m behind the retaining wall.

The pore pressures measured at distances of 1.275 m, 2.375 m and 3.475 m behind the retaining wall have fallen steadily following the completion of construction activities. This decrease in pore pressures is more significant at piezometers located closer to the soil surface. This is evident by the development of high suctions at piezometers *P1-P3*, *P6 & P7* and at *P15-P16*. Contrastingly, pore pressures measured at greater depths have attained steady state equilibrium conditions as can be seen from piezometers, *P4*, *P5* and *P10* in Figures 5.6 and 5.8. The pore pressures measured at these instruments have not changed significantly since about 2500 days after construction. While pore pressures at most piezometer locations have attained equilibrium states, those from instruments located closest to the ground surface and to the exposed face of the retaining wall continue to decrease.

It was also observed that pore pressures behind the retaining walls seemed to vary only slightly with changes in seasonal conditions. A gradual decrease in pore pressures occurred during the summer months with a slight increase in the spring and winter

months. These seasonal fluctuations in pore pressures were consistent and did not affect the trend of a general reduction in pore water pressure over the monitoring period.

Comparison with retaining walls formed from secant piles

Previous observations by Hubbard *et al.* (1983), of a retaining wall in overconsolidated London Clays at Bell Common, showed that pore pressures behind the retaining wall formed of secant bored piles followed a similar trend during construction. Installation effects were manifested as reduction in pore water pressures due to excavation of the bore followed by increased pressures during concreting. This was accompanied by subsequent reduction in pressure due to excavation of the soil in front of the retaining wall. For the retaining wall formed from secant piles, it was observed however that in the long-term, the pore pressures returned to near their pre-construction values despite the presence of a vertical drain behind the retaining wall. For the current investigation, of a retaining wall formed from contiguous bored piles in overconsolidated clays at Ashford, it was observed that the pore pressures behind the retaining wall did not return to anywhere near their pre-construction values. In fact, except for the piezometers located below formation (*P4, P5* and *P10*), pore pressures measured behind the retaining wall have continued to fall (*P1-P3, P6-P8* and *P15 & 16*) up to thirteen years following the start of construction.

It is also evident that the pore water pressures at piezometer *P15* located 2.475 m behind the retaining wall, and physically sandwiched between the vertical lines of instruments at a distance of 1.275 m and 3.475 m, were bracketed by those of piezometers *P2* and *P7* at a depth of 5.3 m below the ground level. A similar trend was observed at piezometer *P16* where the pore water pressures again stayed between those of piezometers *P3* and *P8*. The pore pressures at *P15* and *P16* continue to fall in value, which could indicate that a long-term equilibrium position has not yet been fully established at these locations.

Notwithstanding the continued decrease in pore water pressures observed behind the contiguous pile retaining wall, it is also evident that the rates of decrease of pore pressures at the piezometers closer to the soil surface and to the exposed face of the retaining wall are much higher than those further away. For instance, the pore pressures

measured 3.475 m behind the wall, although decreasing, are doing so to a lesser extent than those at 1.275 m. It can be concluded therefore from the data obtained at *P6-P10*, that equilibrium conditions have been achieved in those locations.

Pore pressure profiles behind the retaining wall

The long-term pore water pressure profiles were analysed for the two lines of instruments, *P1-P5* and *P6-P10*, located at distances of 1.275 m and 3.475 m behind the retaining wall respectively. These profiles are compared with the hydrostatic and the least conservative pore pressure profiles that were assumed during the design of the retaining wall at Ashford.

1.275 m behind the retaining wall

It is observed that the pore pressures adopted for the design of the retaining walls are slightly greater than hydrostatic to a depth of about 13 m below ground level, below which a hydrostatic distribution was adopted as shown in Figure 5.9. The water table was assumed to be approximately 1 m below ground level. During this investigation, the pore water pressure profiles were compared for the short, medium and long-term conditions corresponding to 100, 1100-2500 and 4600 days after construction of the retaining walls began.
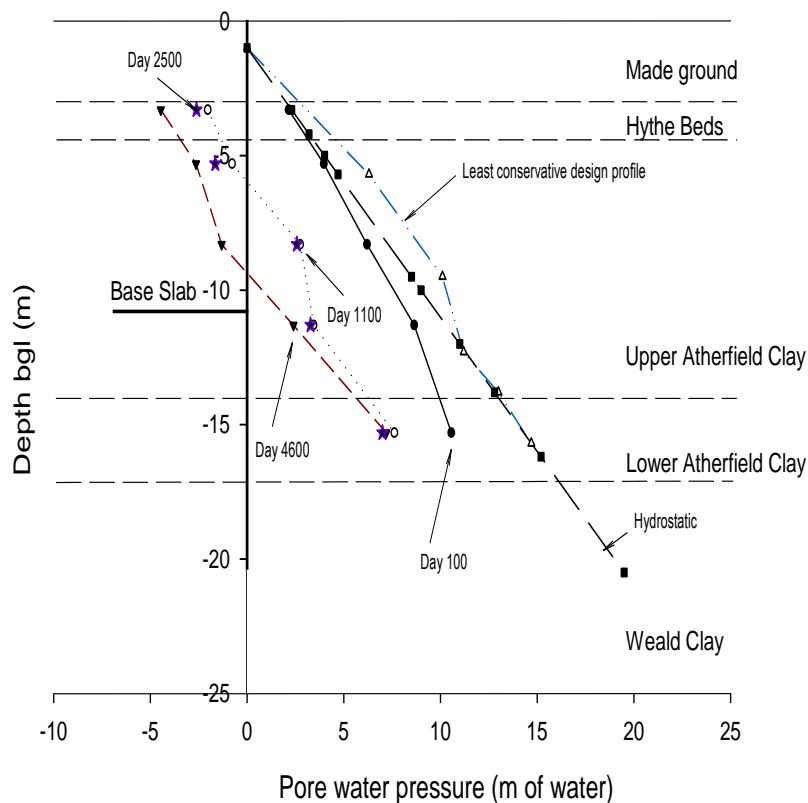
Figure 5.9: Pore water pressure profiles taken at different times at a distance of 1.275 m behind the retaining wall.

The profile of pore pressures measured at a distance of 1.275 m behind the retaining wall shows that there is a steady increase in pore pressure with depth. Figure 5.9 shows that the measured pore water pressures are less than those of the design least conservative profile and less than the hydrostatic profile, as would be expected in the presence of downward seepage. The measured pore pressures 100 days after construction commenced showed some divergence from the hydrostatic profile particularly at greater depths. This could be due to underdrainage of the Atherfield Clay into the more permeable Weald Clay. Additionally, this period included the installation of the contiguous bored piles and so any changes in pore pressures could also be attributed, perhaps in part, to mechanical actions. There were no significant pressure changes at lesser depths during this period. Similarly, the use of temporary casings to a depth of about 8 m could have resulted in less mechanically induced pore pressure change being observed at the locations of piezometers P1-P3, P6 and P8. In addition,

165

based on the low permeability of the Atherfield Clay, it would require a significantly longer time for changes in pore pressures to be detected and recorded. Therefore, it is fair to assume that there were no significant changes to the pore pressure distribution up to 100 days after construction began. By day 1100, when construction activities would have been completed, Figure 5.9 shows that the pore pressures had fallen significantly below hydrostatic and below those assumed in design. The development of a substantial amount of suction at depths to about 6 m is also apparent. Pressure profiles 2500 days after construction commenced did not deviate very much from those at 1100 days, except that the pore pressures were slightly lower at above approximately 6 m depth. The pore pressures for day 4600 were much less than at 2500 days as shown by the pressure profiles. This was consistent throughout the depth of the soil, particularly above formation level. At greater depths, the pore pressure profiles for day 2500 and 4600 were very much similar.

Pore pressures have continued to fall and the final equilibrium values, particularly those measured by the piezometers closer to the soil surface will be much less than assumed in the design and less than hydrostatic.

166

3.475 m behind the retaining wall

The general trend in pore pressure profiles observed at a distance of 3.475 m behind the retaining wall is similar to that at 1.275 m. The development of a region of high suction is again evident as Figure 5.10 shows. It is evident that the pore pressure profiles for the medium and long term hydraulic conditions are almost identical at depths greater than about 8 m. This indicates that pore pressure equilibrium conditions were achieved at positions further back from the wall and at greater depths over a shorter period of time.
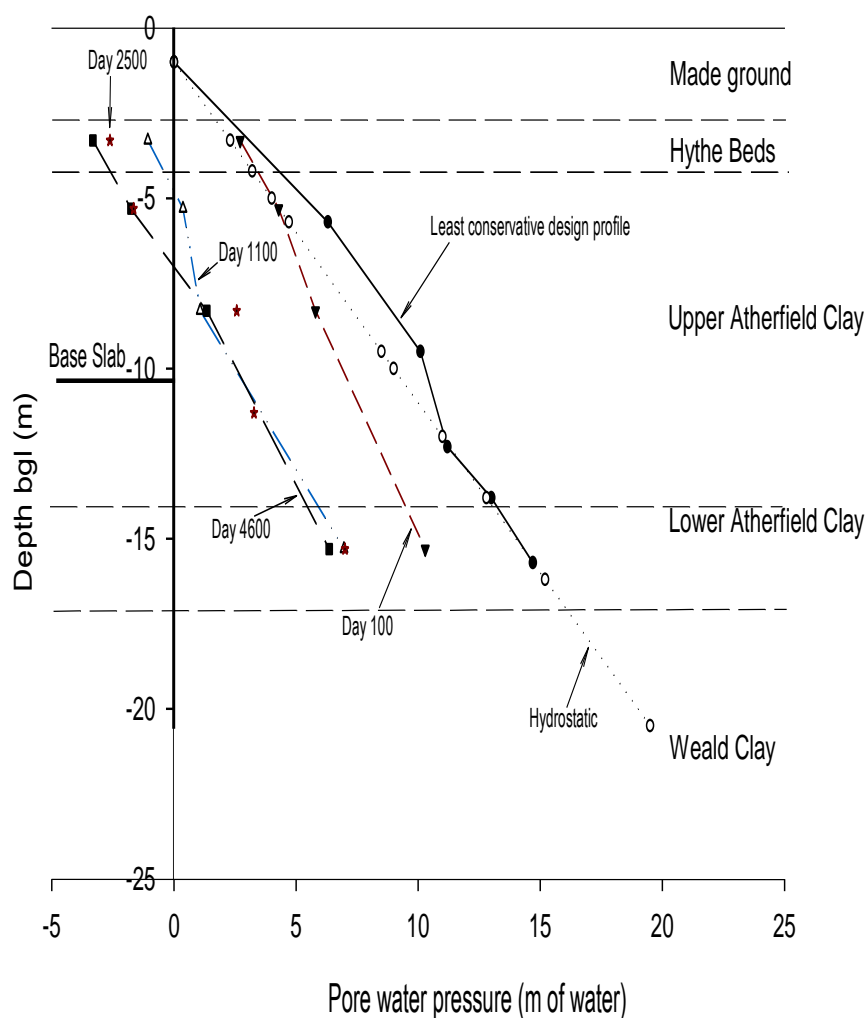
Figure 5.10: Pore water pressure profiles 3.475 m behind the retaining wall.

167

Combined profiles 1.275 m, 2.375 m and 3.475 m behind the retaining wall

Further comparisons were made between the long-term pore pressures measured at distances of 1.275 m, 2.375 m and 3.475 m behind the retaining wall. As Figure 5.11 shows, pore pressures closer to the face of the retaining wall (above base slab level) are consistently lower than those further back from the wall. It is also evident that the pore pressure trends at greater depths are less well defined. This is due, in part, to the paucity of field data at these locations.
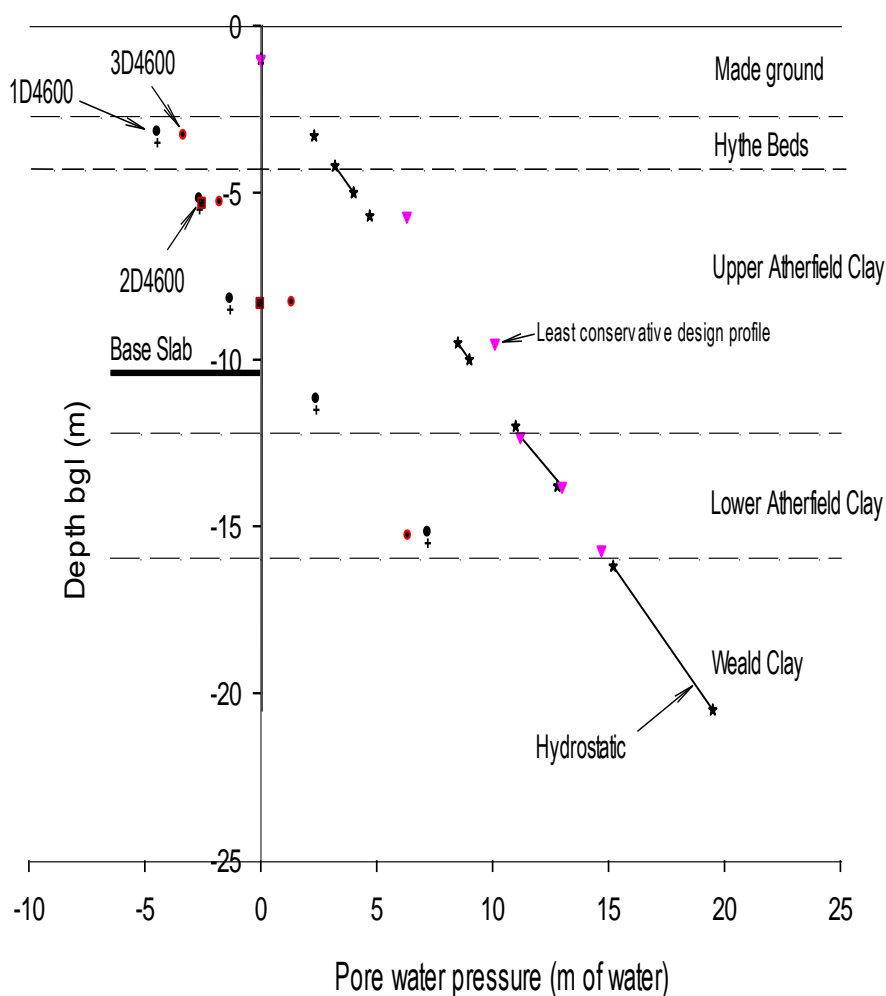
Figure 5.11: Comparison of pore pressure profiles at various distances behind the retaining wall. The designations 1D4600, 2D4600 and 3D4600 refer to pore pressure profiles day 4600 in the 1st, 2nd and 3rd lines of instruments behind the retaining wall respectively.

168

5.2.2 Pore pressure distribution in front of the retaining wall

Figure 5.12 shows the variation of pore pressures at P11 and P12. Only four instruments, *P11-P13* and *P17*, were positioned in front of the retaining wall. This meant that the availability of pore pressure measurements on the passive side was somewhat less than on the active side of the wall. Additionally, *P17* located at a distance of 2.375 m in front of the retaining wall and 15.3 m below the original ground level, encountered intermittent disruptions that limited the amount of useful data obtained at that location. Piezometers *P11* and *P12*, closest to the front of the wall, and located in a vertical line were expected to give an indication of how the pore pressures vary relative to the hydrostatic profile. Measured pore pressures at *P12* were however inconsistent with the general results. For instance, although *P12* was located at greater depth than *P11*, the initial gauge pressure observed at *P12* was much lower than at *P11* as Figure 5.12 illustrates.
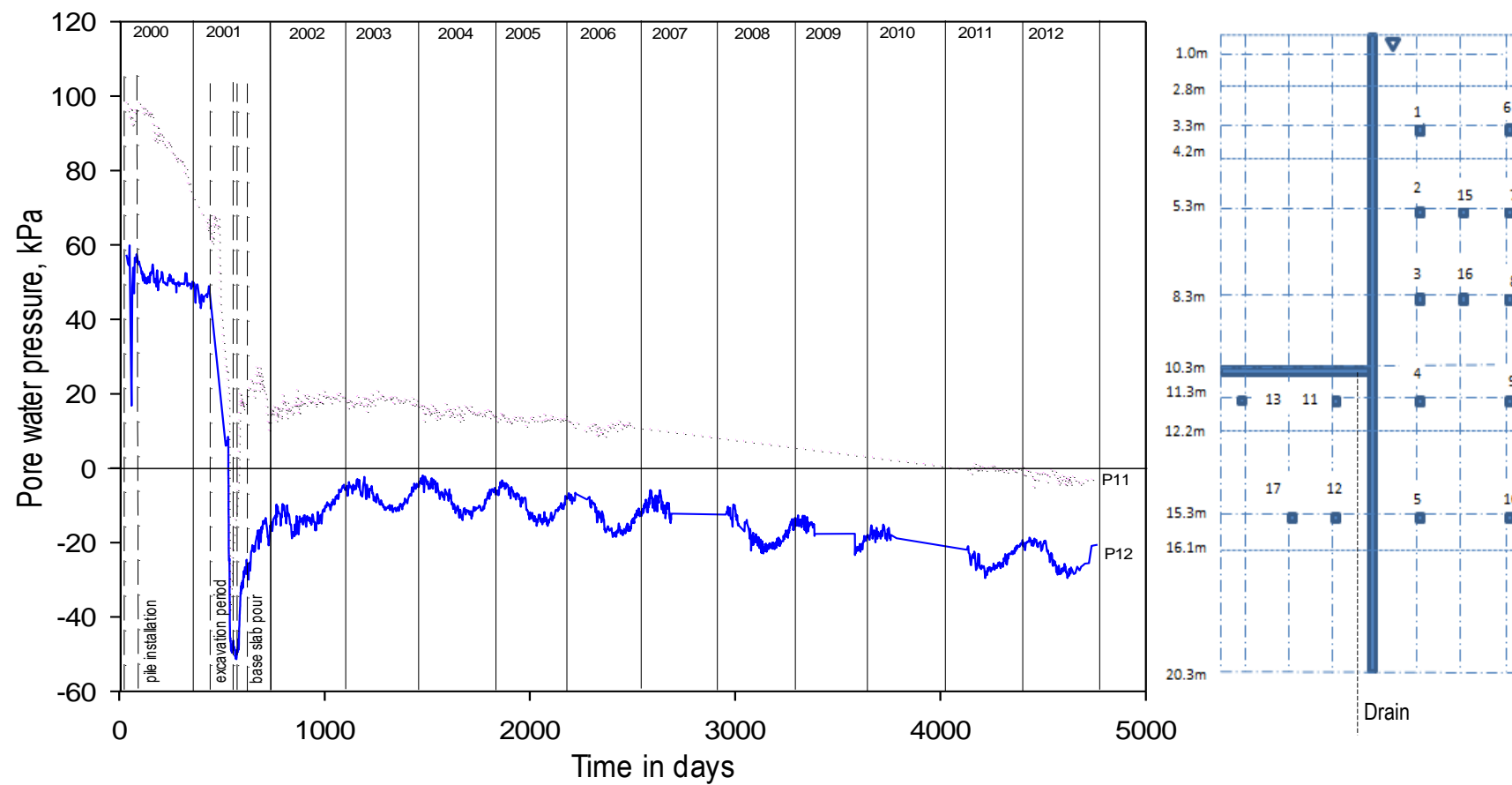
Figure 5.12: Long-term pore water pressures 1.275 m in front of the retaining wall.

This indicates a general decrease in gauge pore pressure with depth, which is improbable in this instance. Consideration was given to the possibility of the instrument numbers having been swapped; however, a comparison between the initial pore pressures at *P11* and *P13* at the same depth shows that both are similar. Subsequent activities show similar changes in pore pressures at *P11* and *P13*, thus ruling out any transcription error between *P11* and *P12*.

Notwithstanding the anomaly of the readings at *P12*, the general trends in pore pressures are apparent. The changes in pore pressures at *P12* due to the installation of the piles were inexplicably larger than those at *P11*, which were similar to the observed values at other piezometers. This large change in pressure was unexpected due to the pile being bored, which causes less mechanical influence on pore pressures than a driven pile (Gunn and Clayton, 1992). The higher than expected pressures might somehow give credence to the possibility of *P12* being located in the Weald Clay. Excavation of the soil in front of the retaining wall, as would be expected, produced significant drop in pore pressures for the two piezometers located below the excavated area. This is attributable to stress relief due to the removal of overburden. Subsequent construction of the base slab caused increased pore pressures similar to those observed behind the retaining wall.

Measured pore pressures at *P11* and *P12* have continued to decrease albeit at much slower rates. Large seasonal variations were observed for pore pressures measured at *P12* although equilibrium conditions are being approached. Pore pressures measured at *P11*, however, continue to decrease.

Pore pressures at *P13* and *P17* show similar trends to those at *P11* and *P12*. A general decrease in pore pressures due to boring for the piles was followed by an increase due to concreting as seen in Figures 5.13 and 5.14. A subsequent reduction in pressures due to excavation of the soil in front of the retaining walls was followed by a sudden increase due to the construction of the base slab. The long-term pore pressures are much less than the pre-construction values. Although the measurements from *P17* stopped just prior to day 4000, the development of suction similar to that at *P12* and *P11* was apparent. The pore pressures at *P13* are approaching equilibrium conditions with relatively low values being recorded.

171
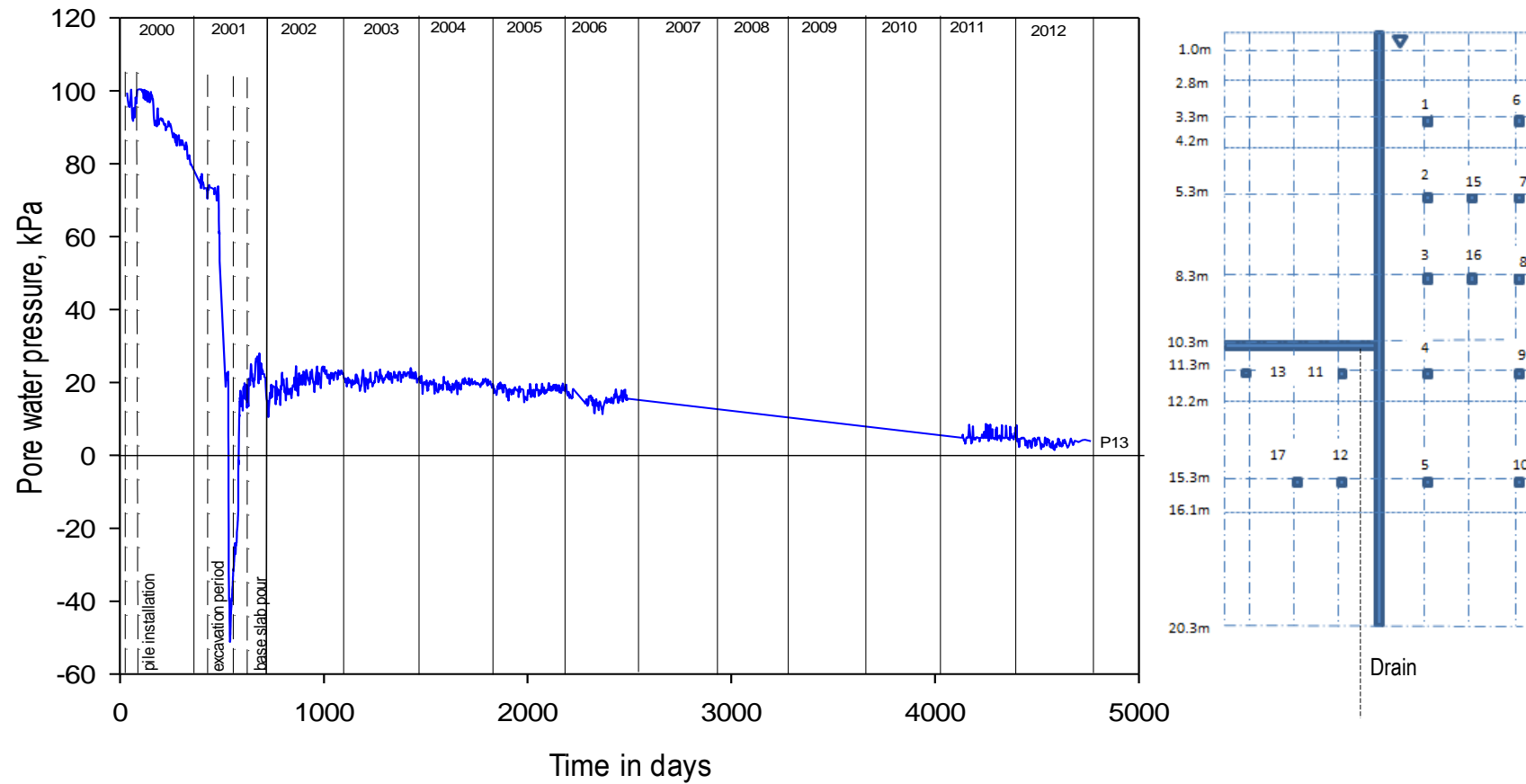
Figure 5.13: Long-term pore water pressure distribution 3.475 m in front of the retaining wall.
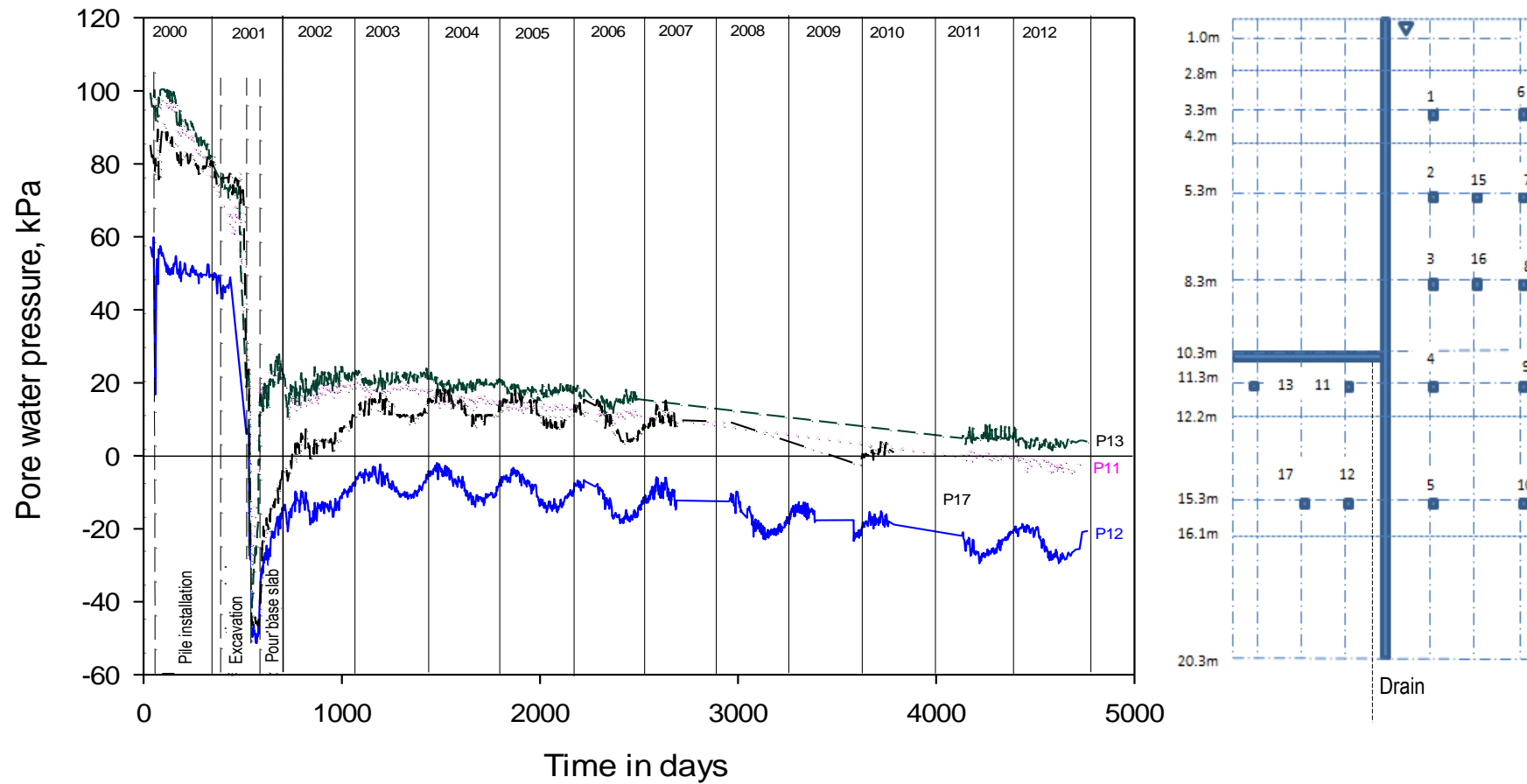
Figure 5.14: Comparison of long-term pore water pressures in front of the retaining wall.

173

5.2.3 Pore pressure at various depths below ground level

Pore pressures at the same depths and at various distances behind and in front of the retaining wall were compared to determine whether the variation of hydraulic heads would give an indication of the flow behaviour around the wall. This was analysed using the general rule that groundwater flows from a region of high to one of low hydraulic head.

3.3 m below ground level

Figure 5.15 shows pore water pressures for piezometers *P1* and *P6* located at a depth of 3.3 m below ground level. Long-term pore pressures measured at *P1*, which was closer to the exposed face of the contiguous pile wall, are much less than at *P6*. The hydraulic behaviour at both locations, however, follows a similar trend. For instance, pile installation, excavation of the soil in front of the walls and construction of the base slab caused almost identical variation in pore water pressures. Dewatering and subsequent excavation also resulted in the pore pressures in both instances falling to below zero. This decrease in pressures continued for a prolonged period after construction activities had ceased. It is also evident that long-term equilibrium conditions were achieved at approximately 4000 days after construction as illustrated by the pore pressures at *P6,* which have been relatively constant except for seasonal fluctuations. The pore pressure at piezometer *P1* however has continued to decrease with an almost linear reduction since the time the base slab was constructed.
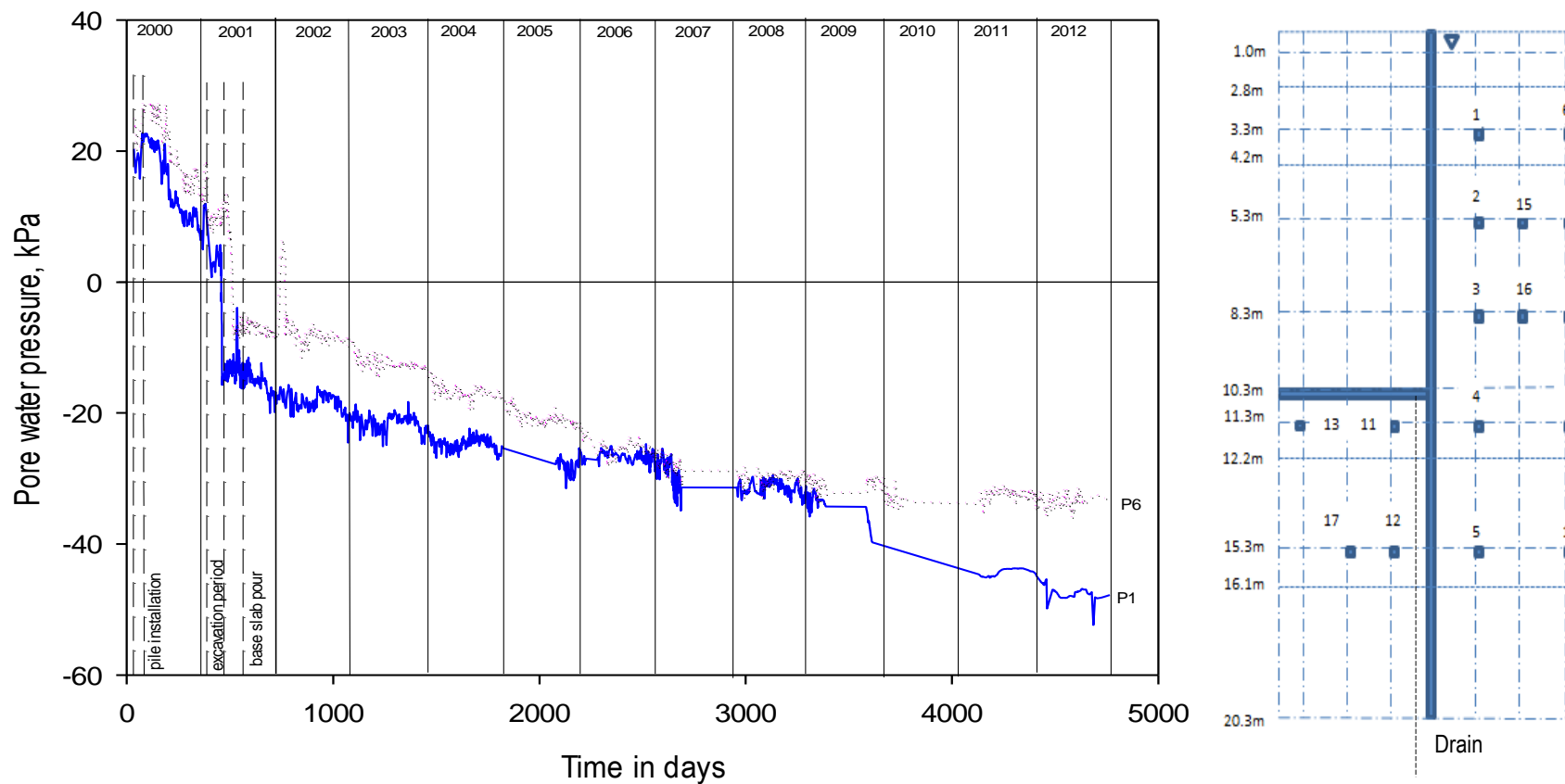
Figure 5.15: Pore water pressures measured at a depth of 3.3 m below ground level.

175

5.3 m below ground level

Pore pressures at the position of piezometers *P2*, *P7* and *P15*, located at distances of 1.275 m, 3.475 m and 2.375 m behind the retaining wall and at a depth of 5.3 m, showed similar trends with almost identical pressure changes due to installation of the piles. This was followed by a decrease induced by dewatering and excavation of the soil in front of the wall. The pore pressures have continued to fall since the construction of the base slab with all three piezometers recording relatively high suctions as shown in Figure 5.16. It is also evident that the pore pressures generally reduced towards the retaining wall. Consequently, measured pressures at *P2* are less than those at *P7*. Similarly, pore pressures at *P15* are less than those at *P7* while those at *P2* and *P15* are approximately equal. It is also apparent that the pore pressures behind the retaining wall at this depth have still not attained long-term equilibrium conditions and are continuing to decrease.
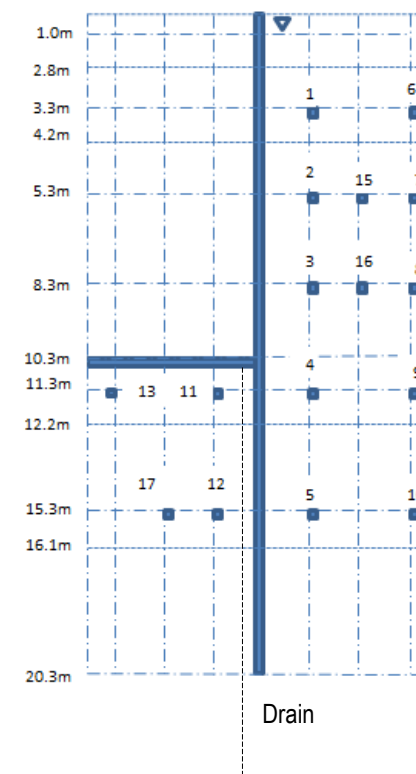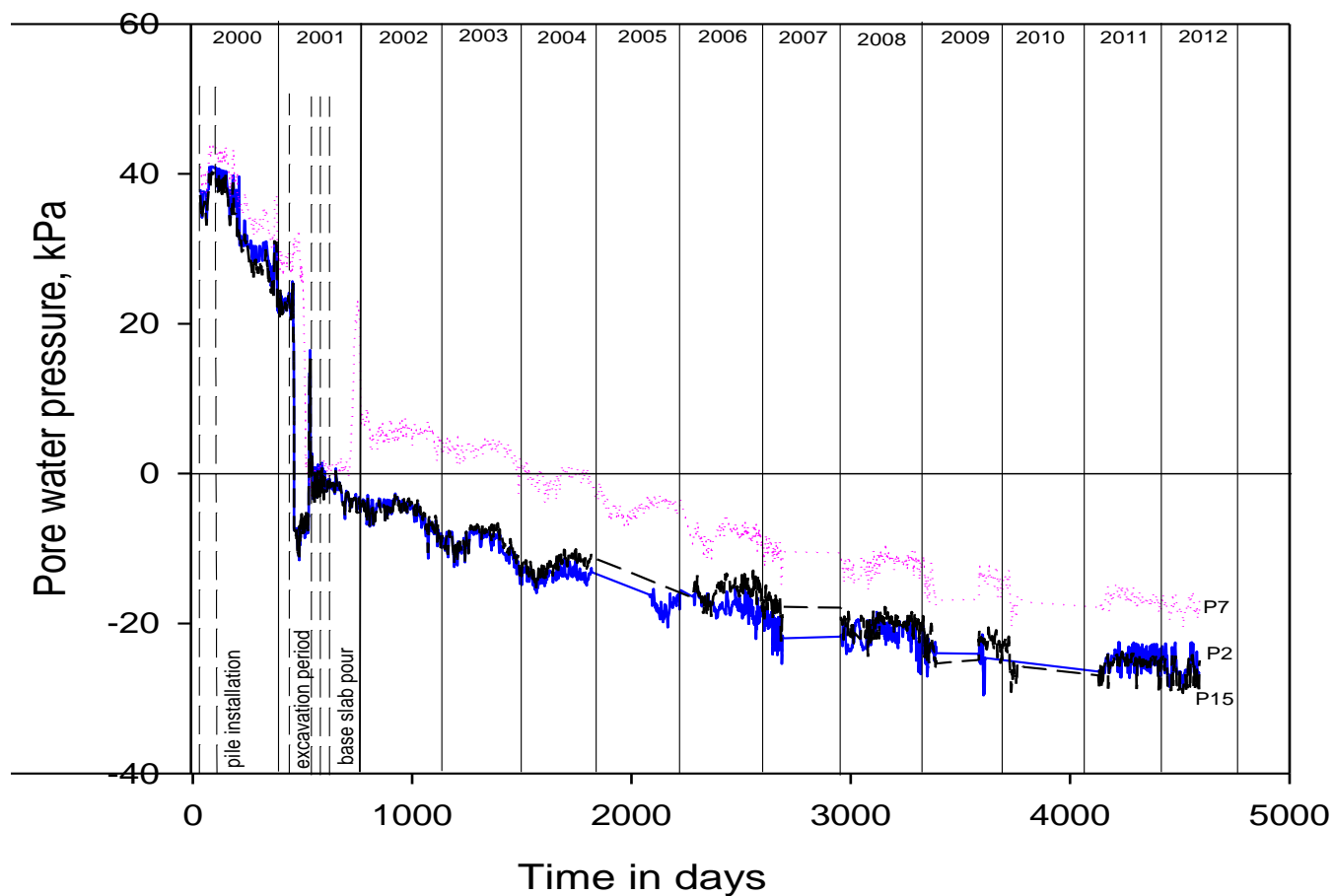
Figure 5.16: Pore water pressures measured at a depth of 5.3 m below ground level.

8.3 m below ground level

The pore pressure distribution behind the retaining wall at a depth of 8.3 m is better defined than those at 5.3 m.   Although the initial pore pressures measures at each distance behind the retaining wall were slightly different, the effects of pile installation on water pressures were identical.   As expected, the pore pressures continued to decrease after the construction of the base slab. Long-term equilibrium conditions were achieved after a period of about 4000 days after construction began as illustrated in Figure 5.17.   It is observed however, that the piezometers closer to the wall, *P3* and *P16* are both recording suctions in the long-term.   It is also apparent that there was a reduction in pore pressures towards the retaining wall with those measured at *P8* being highest and those at *P3* being lowest.
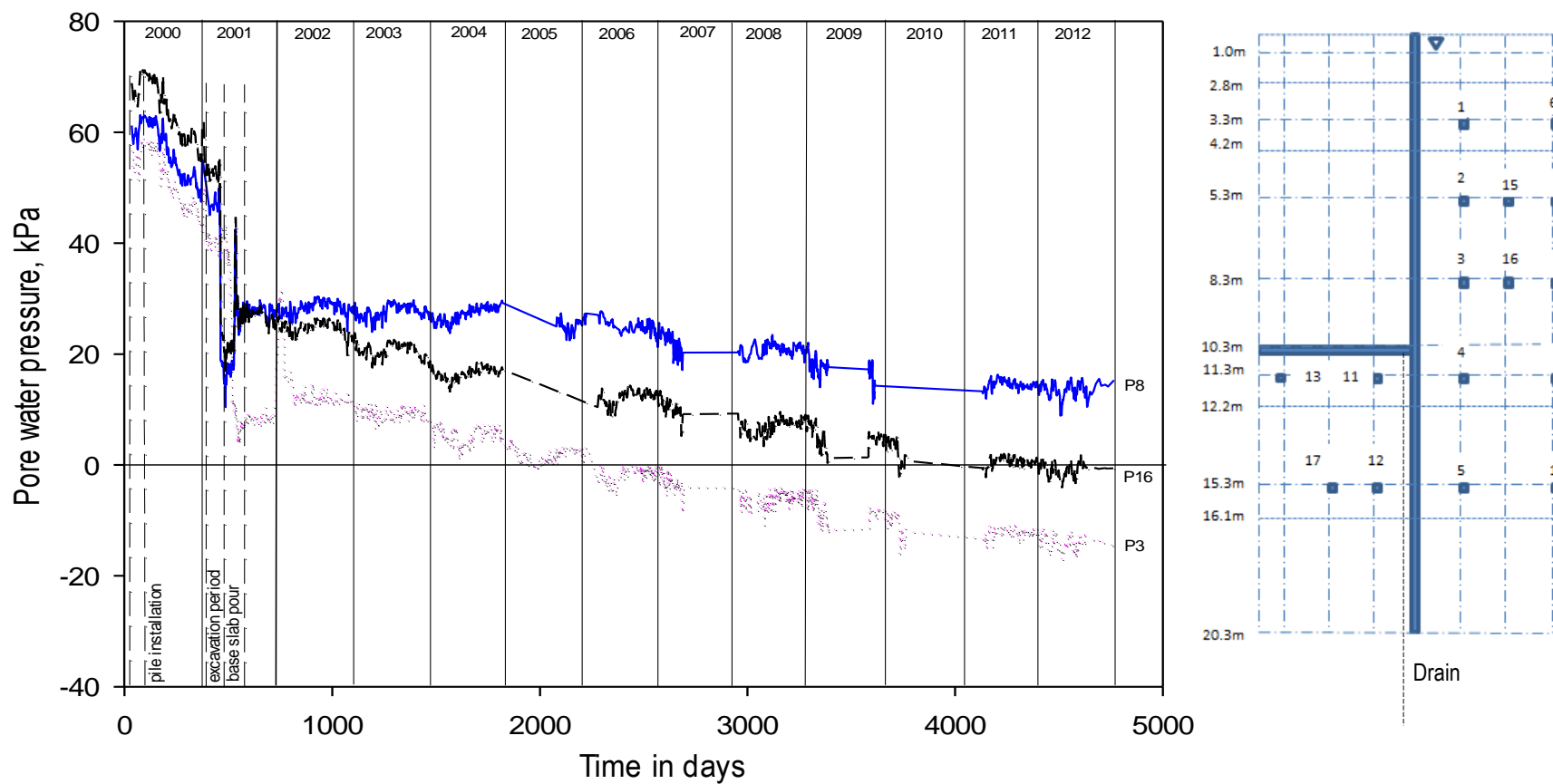
Figure 5.17: Pore water pressure measured at a depth of 8.3 m below ground level.

179

11.3 m below ground level

Piezometers *P4* and *P9* were located behind the retaining wall while *P11* & *P13* were in front of the wall at a depth of 11.3 m. Piezometer *P9* malfunctioned early in the monitoring process making determination of a flow pattern at this location more difficult. However, installation of the retaining wall caused comparable pore pressure changes at *P11* and *P13* although the value at *P4* differs slightly. The trends are however similar as illustrated in Figure 5.18. Dewatering and excavation of the soil in front of the retaining wall produced significant reduction in pressures at this depth. As expected, this reduction was more pronounced for piezometers *P11* and *P13* located directly below the excavated region. Dewatering and subsequent excavation also caused the development of large suction at *P11* and *P13* located just below the position of the base slab. Pouring of the concrete for the base slab resulted in considerable increase in pore pressures particularly at *P11* and *P13*. A comparatively small increase in pore pressures was recorded at the location of piezometer *P4*. Dissipation of mechanically induced pore pressures at *P4* commenced fairly quickly and continued at a relatively slow rate over the monitoring period. At *P11* and *P13*, the pressure induced by the base slab remained relatively constant over a period of about 4-5 years after which dissipation commenced albeit at a slow rate as might be expected based on their locations below the base slab. Pore pressures at *P11* and *P13* are still reducing and a region of negative pressure is developing at the location of *P11*. This is not surprising, as the regional water level is believed to be at about 1 m below ground level on either side of the retaining wall. Additionally underdrainage by the Weald Clay, enhanced by the presence of numerous vertical lenses, continues to cause a reduction in pore pressures in the overlying Atherfield Clay layers. It is not however clear why the pore pressures measured at *P13* are much less than those at *P11*.
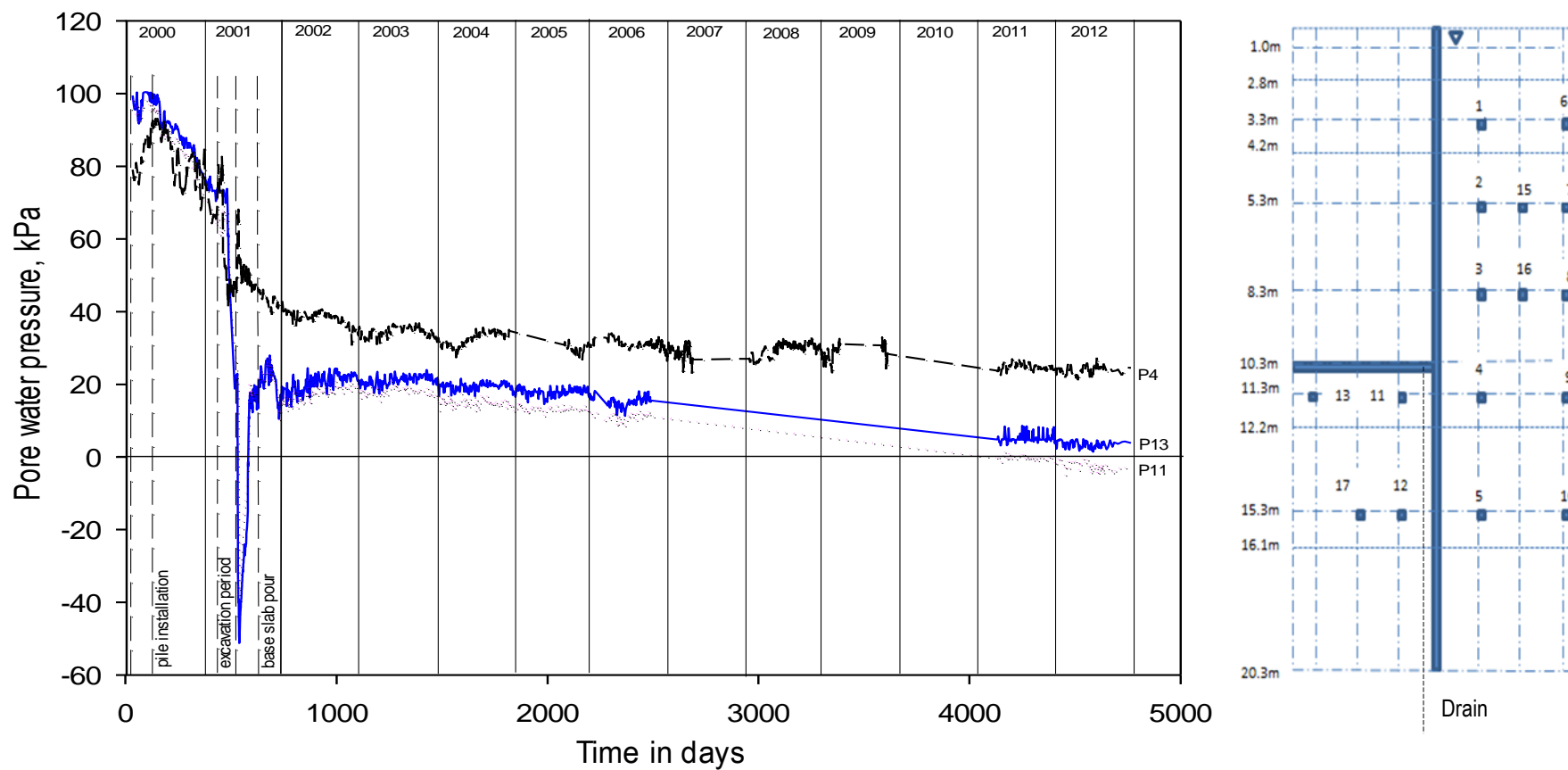
Figure 5.18: Pore water pressures measured at a depth of 11.3 m below ground level.

15.3 m below ground level

The piezometers located behind the retaining wall at a depth of 15.3 m below ground level, *P5* and *P10*, initially recorded almost identical pore water pressures. Installation of the retaining wall caused a decrease followed by an increase in pore pressures as seen in Figure 5.19. Pore pressures recorded at *P12* are inexplicably lower than those at *P17*, while those at *P5* and *P10* are fairly similar. Dissipation of excess mechanically induced pressures seemed to occur much more quickly for *P10* and *P17* located furthest from the wall. Dewatering and excavation produced a substantial reduction in pore pressures on the excavated side of the wall, as would be expected. Contrastingly, the changes in pore pressures were less significant behind the retaining wall. Likewise, the increase in pressures caused by pouring the concrete was more pronounced at locations in front of the wall. The pore pressures at this depth tended to be constant with only seasonal fluctuations observed.

It was further observed that pore pressures measured at *P5* were consistently higher than those at *P10* throughout the monitoring period. A possible explanation is that at some stage, particularly during the installation of the piles and the pouring of the concrete for the base slab, it might be plausible that increased lateral pressures caused an increase in the pore pressure at piezometer 5 to above that at 10. It would have been expected however that as these dissipate, the pore water pressures at piezometer 5 would have fallen to or below those at 10.

Although two of the instruments malfunctioned at some point during the monitoring period, sufficient information was gathered to present a clear picture of the development of the hydraulic regime at similar depths and various distances behind the retaining wall. It is apparent from the above discussion that pore pressures behind the retaining wall at each level decreased towards the wall. It was also shown that the influence of various construction activities on the hydraulic conditions around the retaining wall varied according to the location of instrument. It is however, apparent that instruments at the same depth and on the retained side of the wall generally recorded similar influence on pore pressure.
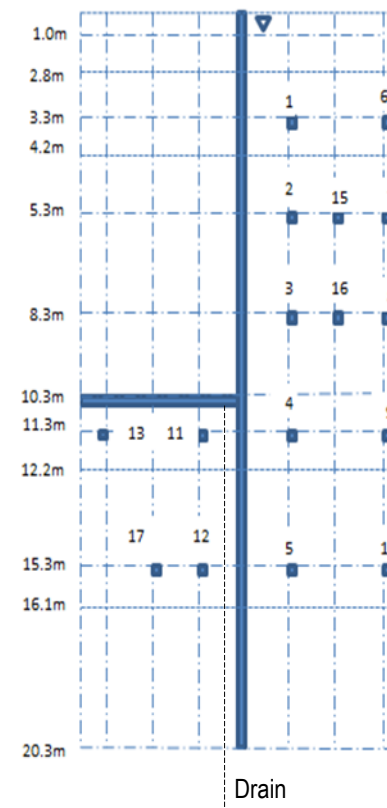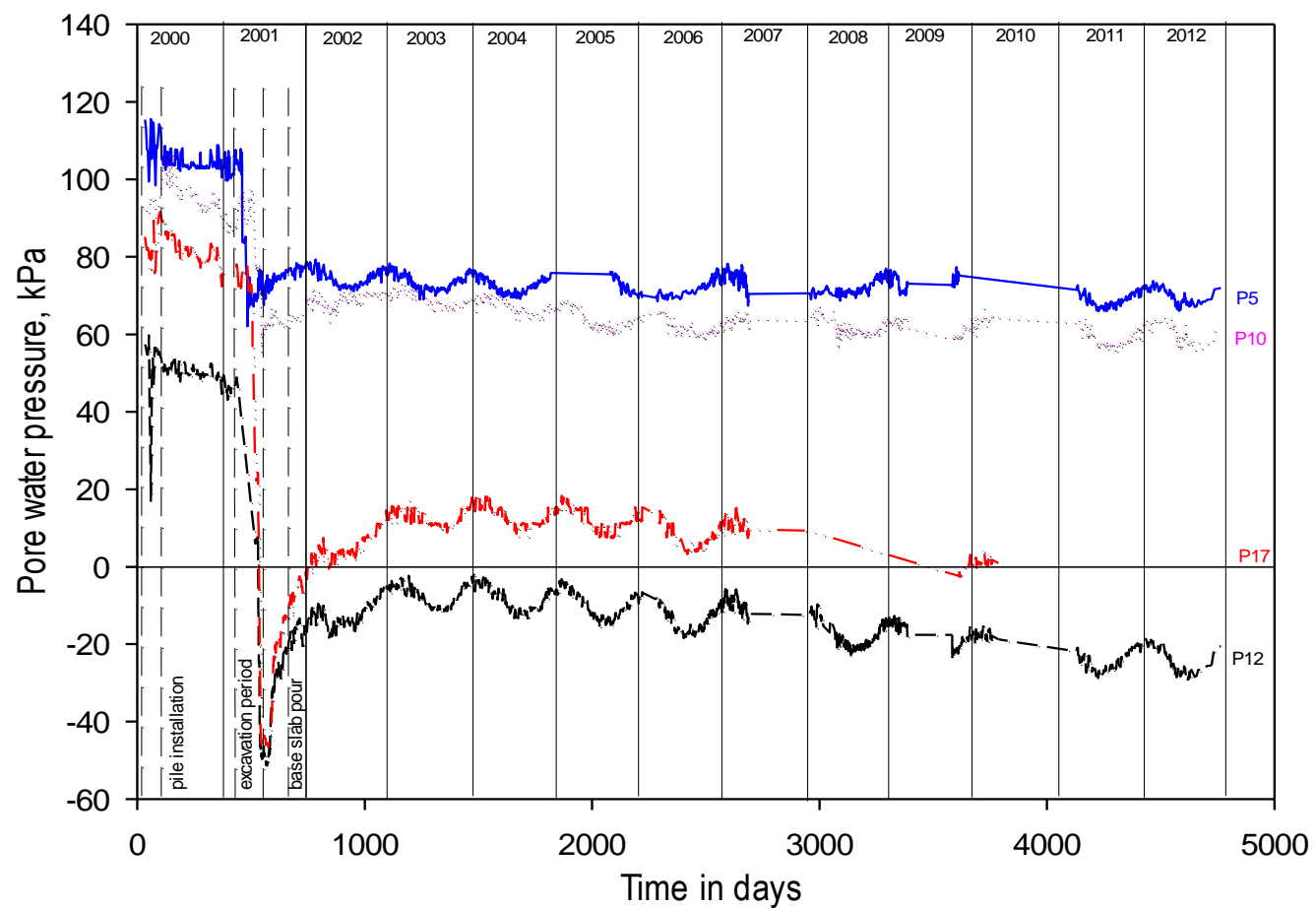
Figure 5.19: Pore water pressures measured at a depth of 15.3 m below ground level.

183

5.3 Hydraulic head distribution around the retaining wall

The total head values calculated from the pore water pressure data were analysed to determine how the flow regime developed during the period between installation of the retaining wall and the establishment of steady state long-term equilibrium conditions. The short, medium and long-term conditions corresponding to 33 & 100, 1100 & 2100 and 3100 & 4600 days after construction started were compared. The reference datum for the calculation of the hydraulic heads throughout the analyses was taken as the top of the base slab, which was approximately 10.3 m below ground surface level.

5.3.1 Short-term hydraulic head distribution - day 33 & 100

The contour plots of total head 33 and 100 days after the installation of the contiguous piles, shown in Figure 5.20, confirm the existence of some amount of under-drainage of the less permeable Atherfield Clay by the Weald Clay. This is similar to underdrainage of London Clay to the more permeable Chalk layer inferred by Powrie *et al*. (1999) and Carder *et al*. (1999). The low permeability of the Atherfield Clays meant that undrained conditions persisted during construction (short-term), as Richards *et al.* (2007) demonstrates. This assertion was supported by the pore pressure distribution, which did not change significantly during the first 100 days except for mechanically induced pore pressures caused by the installation of the contiguous piles. It can be confirmed therefore that the short-term hydraulic conditions were dominated by underdrainage of the Atherfield Clay by the Weald Clay as previously assumed in design.
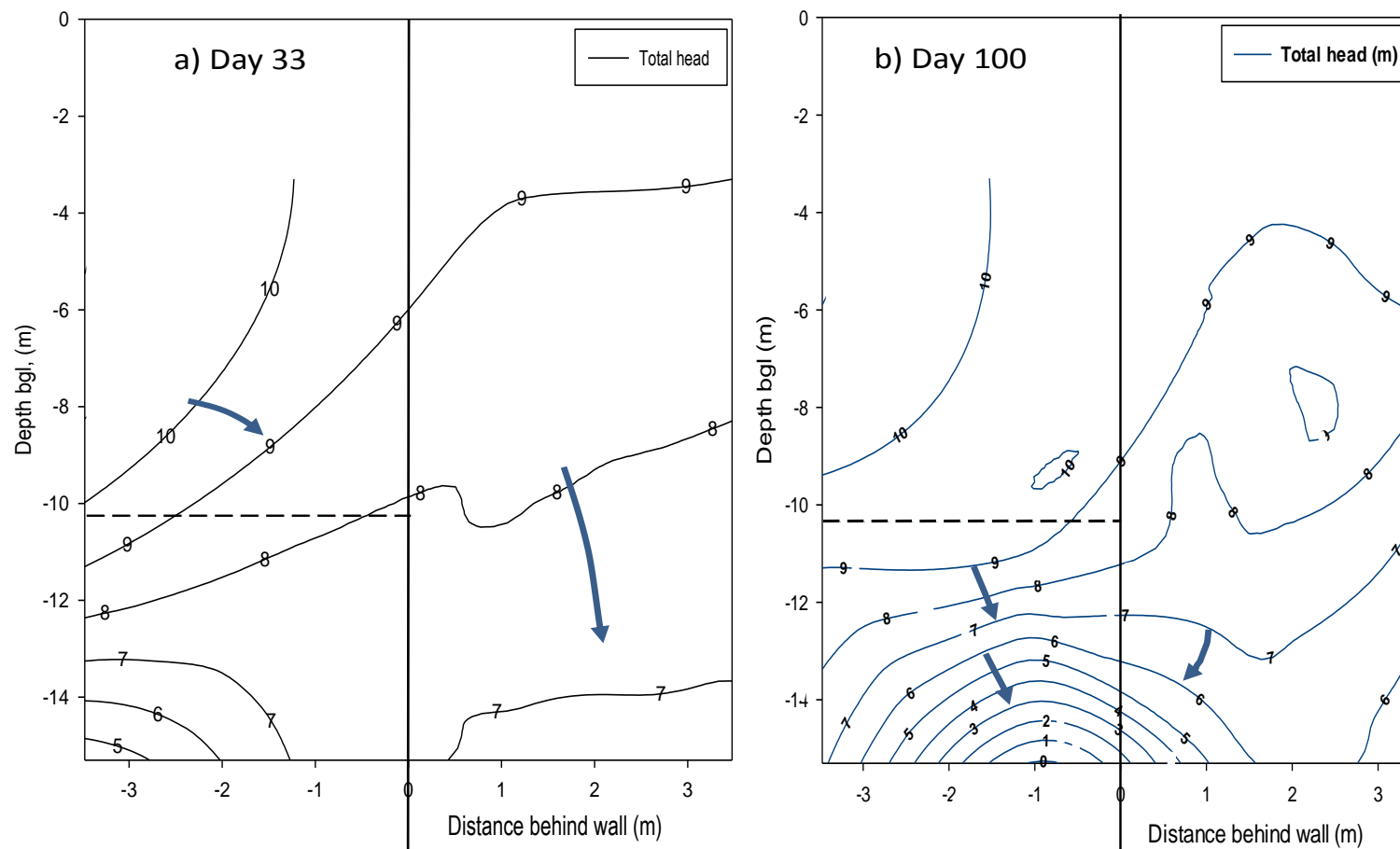
Figure 5.20: Short-term hydraulic head contour distribution for a) 33 and b) 100 days after installation of the contiguous piles.

5.3.2 Medium-term hydraulic head distribution - day 1100 & 1500

Figure 5.21a shows the hydraulic head contours 1100 days after the installation of the contiguous pile retaining wall. It is evident that, by this time, the installation of the retaining walls and the subsequent excavation of the soil between them affected significantly the groundwater flow regime. Consequently, adjustment of the hydraulic head contours, particularly behind the retaining wall, is observed. However, groundwater flow in front of the retaining wall was still dominated by underdrainage to the Weald Clay layer although there were noticeable changes to the flow direction as Figure 5.21b shows. Flow conditions at the back of the retaining wall have changed significantly with some amount of flow towards the excavated side of the wall. Due to the low permeability of the Atherfield Clay in particular it was difficult, even up to 1500 days after construction, to confirm definitively that the hydraulic regime around the contiguous pile retaining wall was fully established. The trends in flow direction however were well defined.
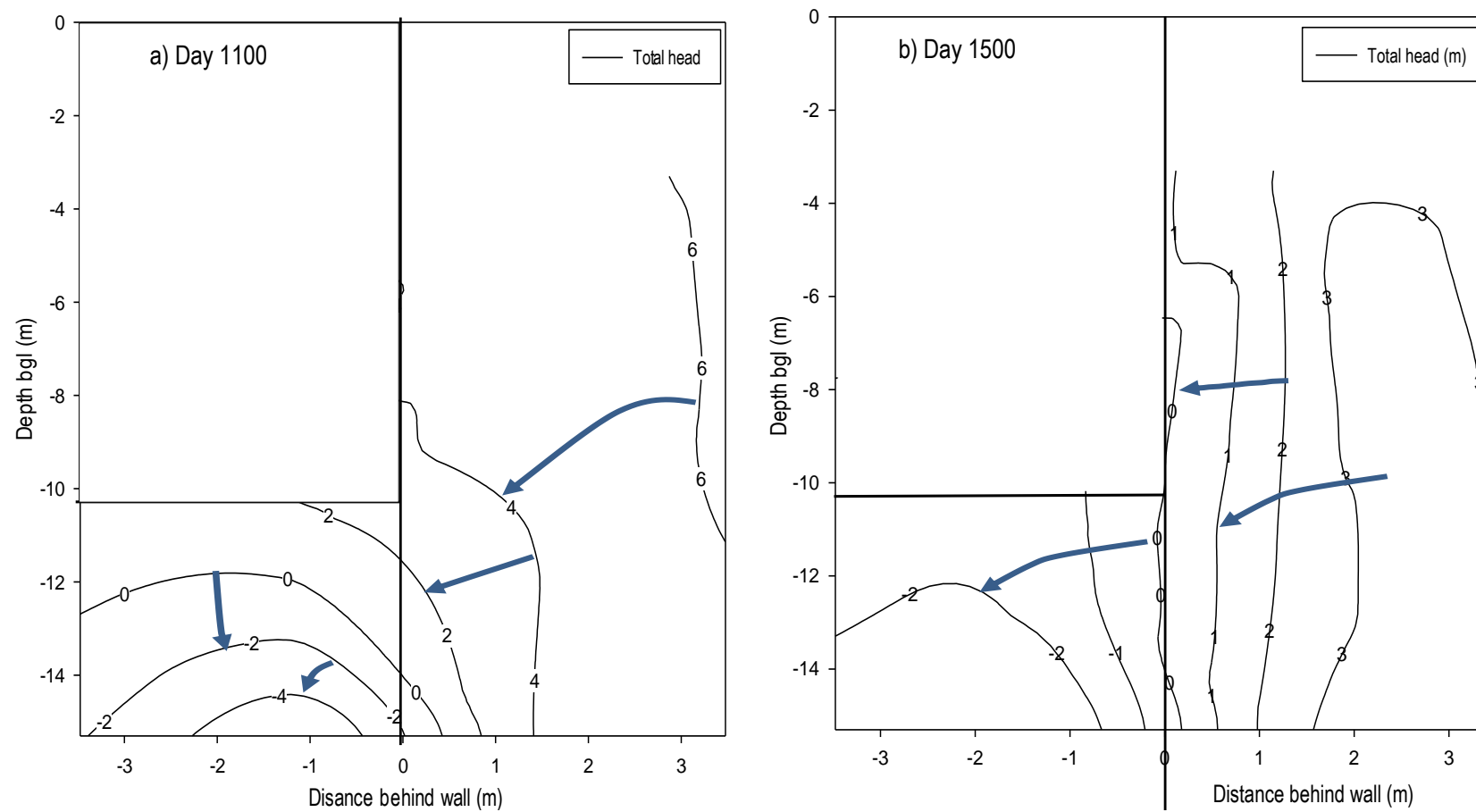
Figure 5.21: Medium-term hydraulic head contour distribution for a) 1100 and b) 1500 days after installation of the contiguous bored piles.

5.3.3 Long-term hydraulic head distribution - day 2100 & 4600

The total head contour plot shown in Figure 5.22, for an observation period corresponding to 2100 days after installation of the retaining wall, illustrates that significant changes to the groundwater flow regime have occurred. Specifically, although there were not enough monitoring points to establish a detailed hydraulic head contour map, the amount of data obtained from the available instruments was sufficient to show that groundwater flow was influenced by the presence of the contiguous pile retaining wall. Seepage from the back to the front of the retaining wall is taking place through the pile gaps. It is also apparent that there was still significant underdrainage, particularly in front of the retaining walls.

It is also evident from Figures 5.22a, 5.22b and 5.22c, representing day 2100, 3100 and 3600 that there were still some changes taking place in the hydraulic conditions around the retaining wall at those times. However, by 4600 days after installation of the contiguous piles, the groundwater flow regime had mostly attained its equilibrium position and flow behind the wall above the base slab level was dominated by seepage through contiguous piles as shown in Figure 5.22d. As would be expected, there was still a significant amount of underdrainage of the lower Atherfield Clay by the Weald Clay as evident by the hydraulic head contours in front of the retaining wall. Notwithstanding the influence of underdrainage, it may be deduced therefore that the flow of groundwater from behind the retaining wall is predominantly through the gaps between the contiguous piles.
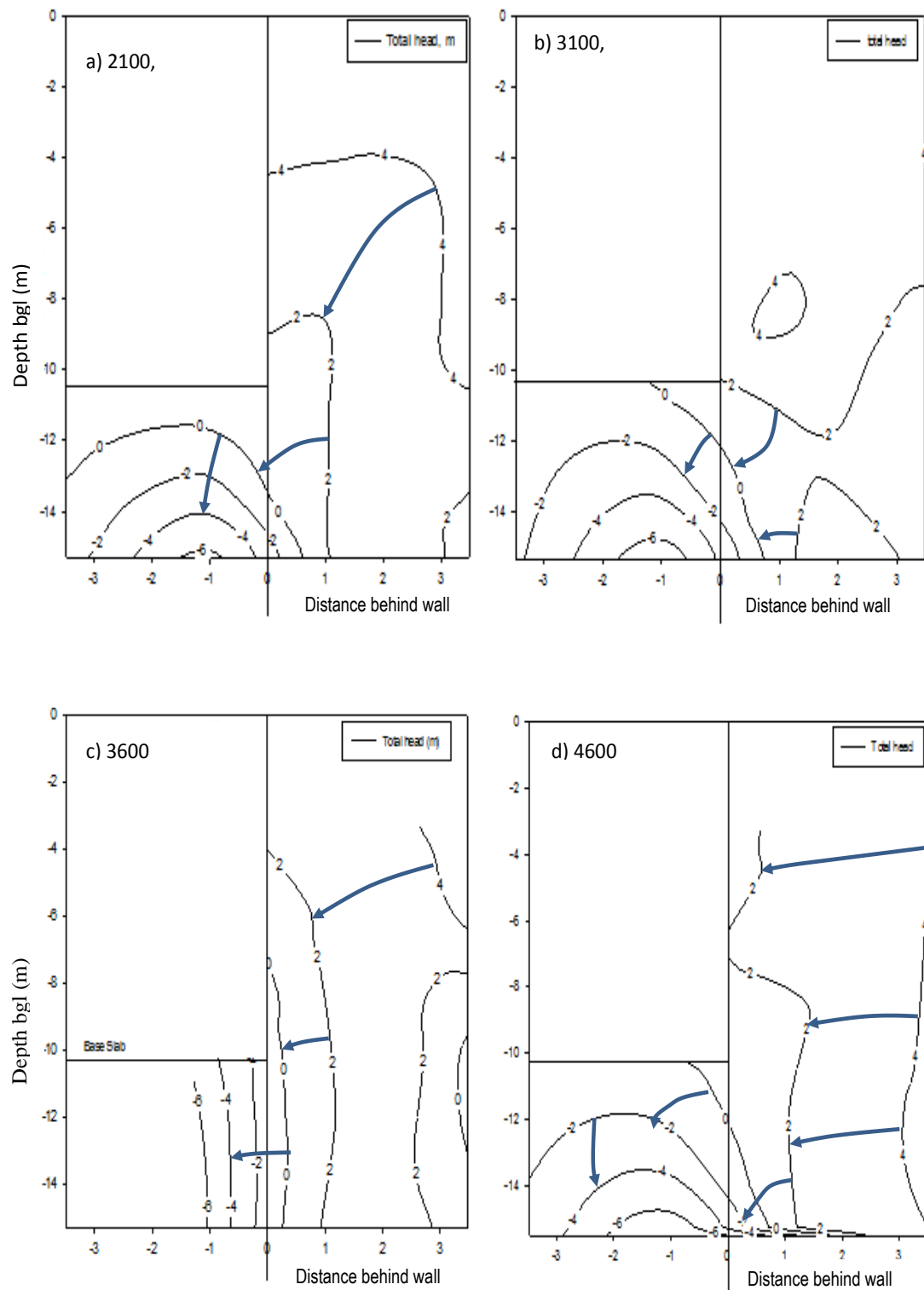
Figure 5.22: Long-term hydraulic head distribution for a) 2100, b) 3100, c) 3600 and d) 4600 days after installation of the contiguous bored piles.

189

5.3.4 Impact of pile gaps on lateral loads on the retaining wall

Long-term horizontal total stresses, σ_h, and pore water pressures, U, were compared at distances of 1.275 m and 3.475 m behind, and at a distance of 1.275 m in front of the retaining wall. This was to determine the correlation between changes in pore pressures and lateral stresses with respect to their *in situ* values (σ_{h0}).

The *in situ* horizontal total stresses were obtained from a best-fit line through field data presented by Clark (2006) who explained that the spade cell measurements, from pre-construction tests, were corrected for over-read and temperature fluctuations. The best-fit line for σ_{h0} is given by Equation 5.1, where Z is the depth below the pre-construction ground level. Horizontal total stresses, σ_h, measured over the monitoring period, were normalised with respect to the *in situ*, (σ_h/σ_{h0}) and compared.

$$\sigma_{h0} = 20.6Z + 0.8 \hspace{4cm} \text{Equation 5.1}$$

The *in situ* pore pressures, U_0, were also calculated from a best-fit line, through field data, which is shown in Equation 5.2.

$$U_0 = 8.6Z - 10.5 \hspace{4cm} \text{Equation 5.2}$$

It is evident that Equation 5.2 does not represent a hydrostatic distribution of pore water pressures below the water table, which was located approximately 1.2 m below ground level. A hydrostatic distribution would have given a gradient of 9.81 m^2/s rather than 8.6 in Equation 5.2. This slight variation of pore pressures from the hydrostatic profile may be attributed to underdrainage of the Atherfield Clay to the more permeable Weald Clay. The long-term pore pressures at each observation point were normalised with respect to *in situ*, (U/U_0) and the variation over the monitoring period observed.

Comparison of long term horizontal stresses and pore pressures with *in situ*

1.275 m behind the retaining wall

Figure 5.23 shows is a general reduction in horizontal total stresses measured 1.275 m behind the retaining wall over the monitoring period. The long-term stresses, (σ_h/σ_{h0}), are less than the *in situ* values.
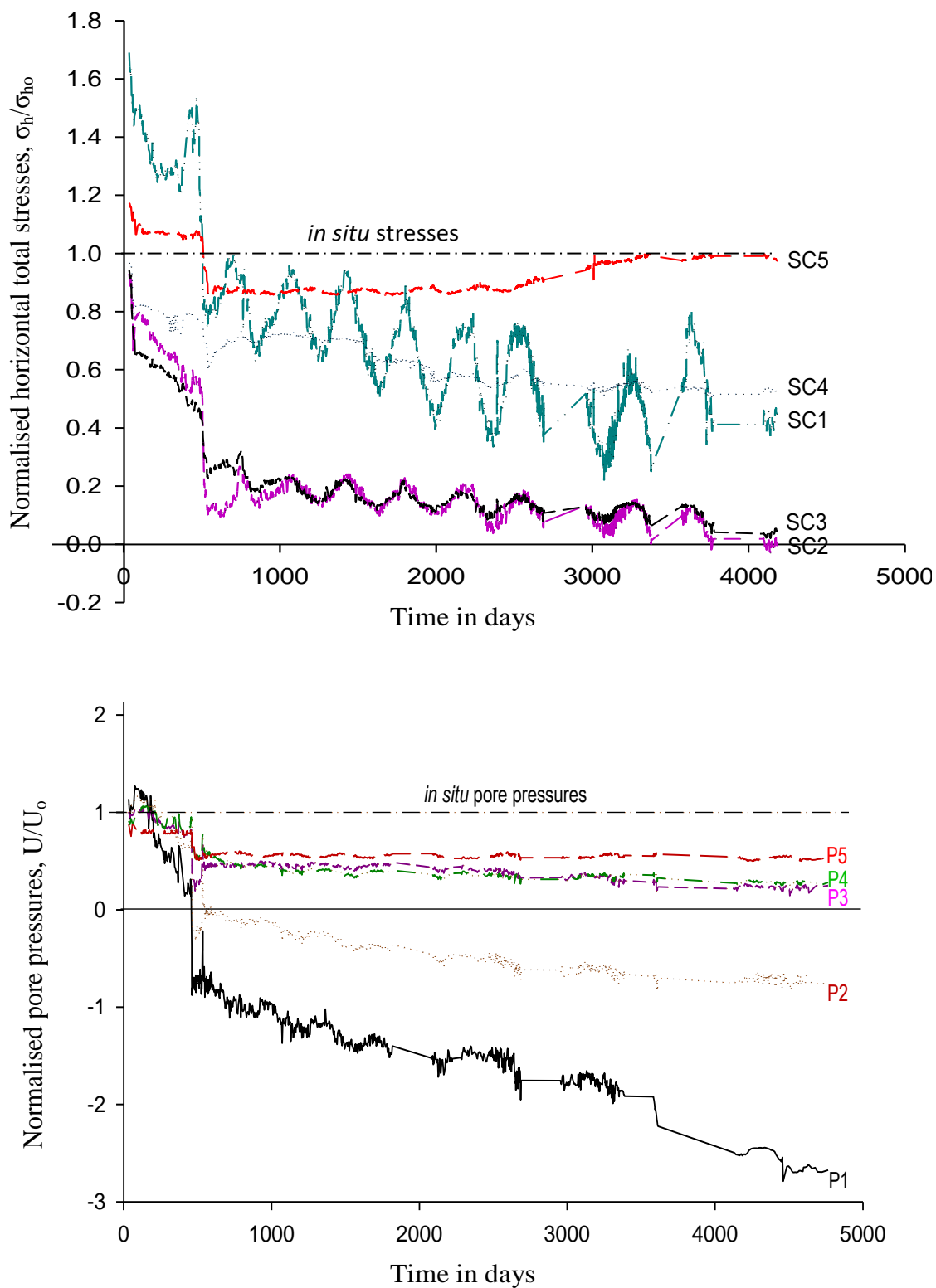
Figure 5.23: Normalised horizontal total stresses and pore pressures 1.275 m behind the contiguous pile retaining wall.

The magnitudes of the normalised stresses, however vary depending on the position of the spade cell. For example, during the pile installation period, stresses at SC1 located closest to the soil surface increased by approximately 70% above the *in situ* values. Long-term stresses at SC1 are however only about 40% of *in situ*. There was an unexplained increase in normalised stresses at SC1 above those at the other spade cells. This could perhaps be attributed to the effect of thermal expansion of the reinforced concrete props, which were located just above the position of SC1. Contrastingly, the initial stress changes at SC2 – SC5 are only within 10-20% of their *in situ* values.

The long-term stresses at SC2 and SC3 are less than 10 % of their *in situ* values while those at SC4 are about 50%. The long-term stresses at SC5, measured 15.3 m below ground level, have stabilised at about *in situ* values although this is mainly due to unexplained increases over the last 5 years. It is however evident that, apart from the anomaly at SC1, there is a general trend of horizontal stresses measured closer to the soil surface becoming increasingly less than *in situ*. Contrastingly, pore pressure variation with respect to *in situ*, (U/U_0) appears better defined. All long-term pressure transducer readings are less than *in situ*. Those closer to the soil surfaces are much less than *in situ* with P1 and P2 being almost 4 and 2 times less respectively. Pore pressures at P3, P4 and P5 have stabilised to within 20-60% of their *in situ* values as expected.

3.475 m behind the retaining wall

Long-term horizontal stresses and pore pressures 3.475 m behind the retaining wall show similar trend to those measured 1.275 m behind as seen in Figure 5.24. The influence on lateral stresses at SC6, located 3.3 m below ground level is similar to that observed at SC1, with a generally large (50%) increase above *in situ* during installation of the bored piles. However, the long-term stresses at SC6, 7 and 9 are within 20-50% of *in situ*. Normalised stresses at the location of SC8 seem to be much lower than would be expected, especially when compared with those from SC3 at the same depth and SC7 & SC9 located above and below respectively. This could be due to malfunctioning of SC8. In comparison, the long-term pore pressures are again fairly well defined. P6 located closer to the soil surface are about three times lower than *in*

situ while P7 and P8 are within a range of 1-2 times less than their *in situ* values. The pressure measurement from P10, located 15.3 m below ground level are about 50% less than *in situ*.
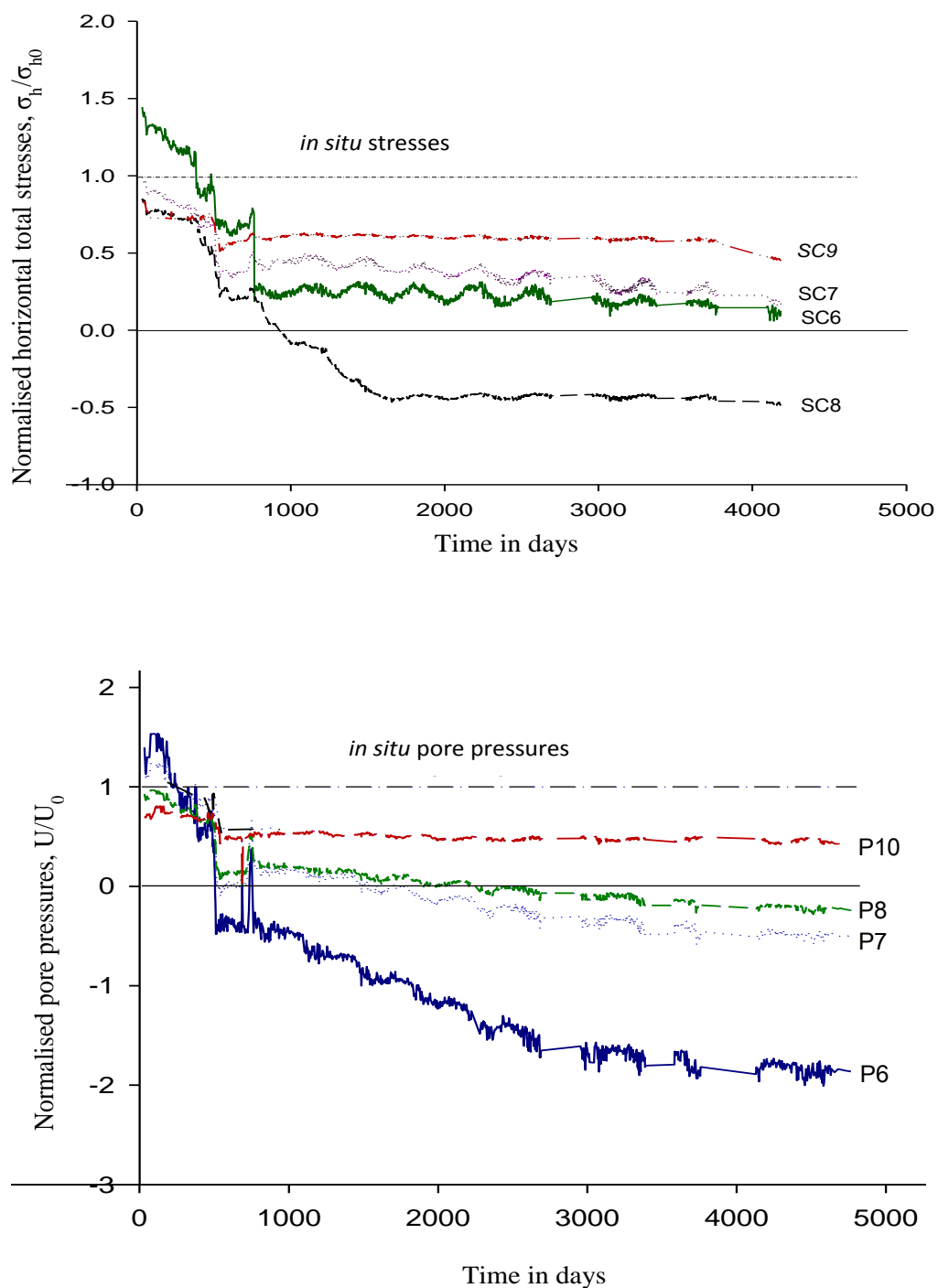
Figure 5.24: Long-term changes in horizontal total stresses and pore pressures 3.475 m behind the contiguous pile retaining wall.

193

1.275 m in front of the retaining wall

Long-term horizontal total stresses and pore water pressures measured in front of the retaining wall show no discernible trend between those at SC11 and SC12 as demonstrated in Figure 5.25. Horizontal total stresses, as would be expected due to the removal of the overburden are much less than *in situ*. Normalised long-term stresses, σ_h, at SC11 and SC12 are about 25 and 40% of their *in situ* values respectively. This again contrasts with the pore pressures at the same locations which are about 1 to 2 times less than the *in situ* pressures.
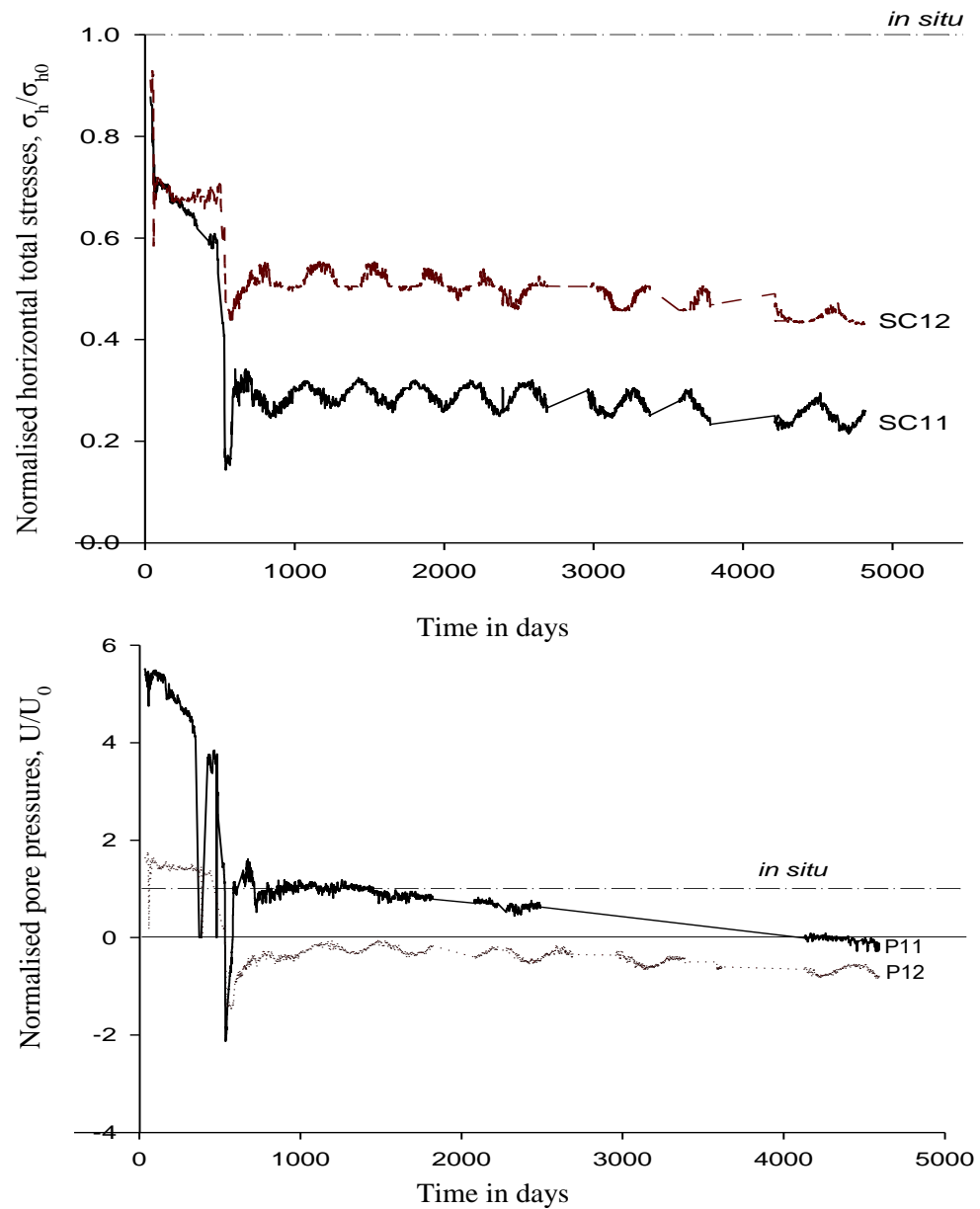
Figure 5.25: Long-term changes in horizontal total stresses and pore pressures 1.275 m in front of the contiguous pile retaining wall.

Comparison of short and long-term horizontal total stresses and pore pressures

Changes between the long and short-term pore pressures and horizontal total stresses, at distances of 1.275 m, 2.375 m and 3.475 m behind the retaining wall, are shown in Figure 5.26. The stress and pressure changes were calculated using Equation 5.3 and 5.4 respectively where ST and LT are the short and long-term conditions respectively. The pore pressure profiles are very similar for the three positions. Further analyses of the horizontal total stress changes, $\Delta\sigma_h$, was however restricted by insufficient data due to malfunctioning of the instruments, SC8 and SC10, located 3.475 m behind the retaining wall. Nonetheless, it is evident that there is some amount of proportionality between the changes in pore pressures and changes in horizontal stresses at the same depth. This relationship is consistent at the three locations behind the retaining wall.

$$\Delta\sigma_h = \sigma_{ST} - \sigma_{LT} \qquad\qquad \text{Equation 5.3}$$

$$\Delta U = U_{ST} - U_{LT} \qquad\qquad \text{Equation 5.4}$$
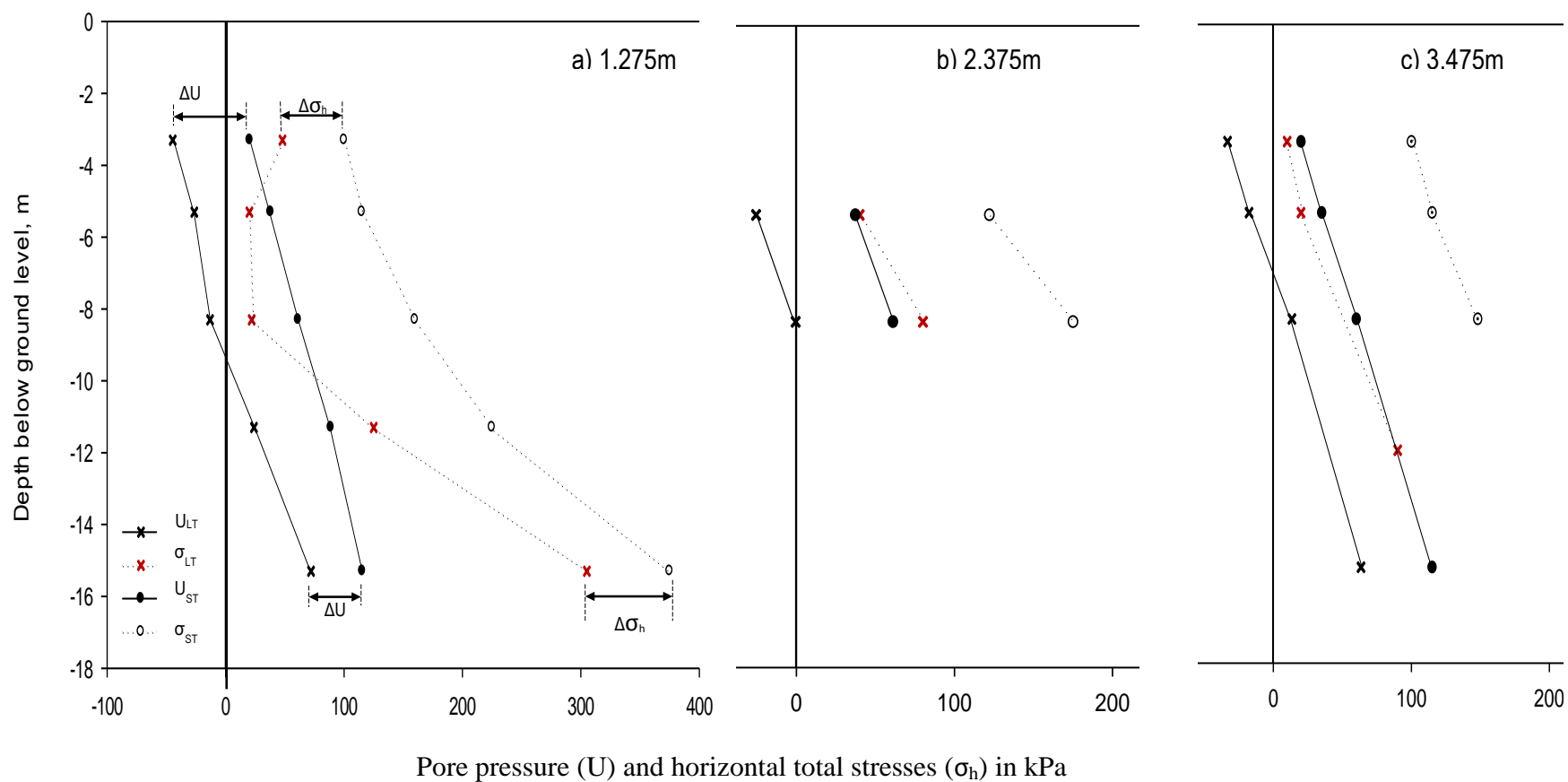
Figure 5.26: Comparison of pore pressure (U) and horizontal total stress (σ) profiles for short term (ST) and long-term (LT) conditions at distances of 1.275 m, 2.375 m and 3.475 m behind the retaining wall. The differences between the short and long-term pore pressures, ΔU at various depths and the corresponding differences in horizontal stresses, ΔSC are also shown for comparison.

Plotting $\Delta\sigma_h$ and ΔU at various depths in Figure 5.27 confirms that the changes in pore pressure at distances of 1.275 m and 3.475 m behind the retaining wall are similar. Changes in pore pressures and horizontal total stresses are inexplicably higher further from the wall with the exception of those measured at positions closer to the soil surface.
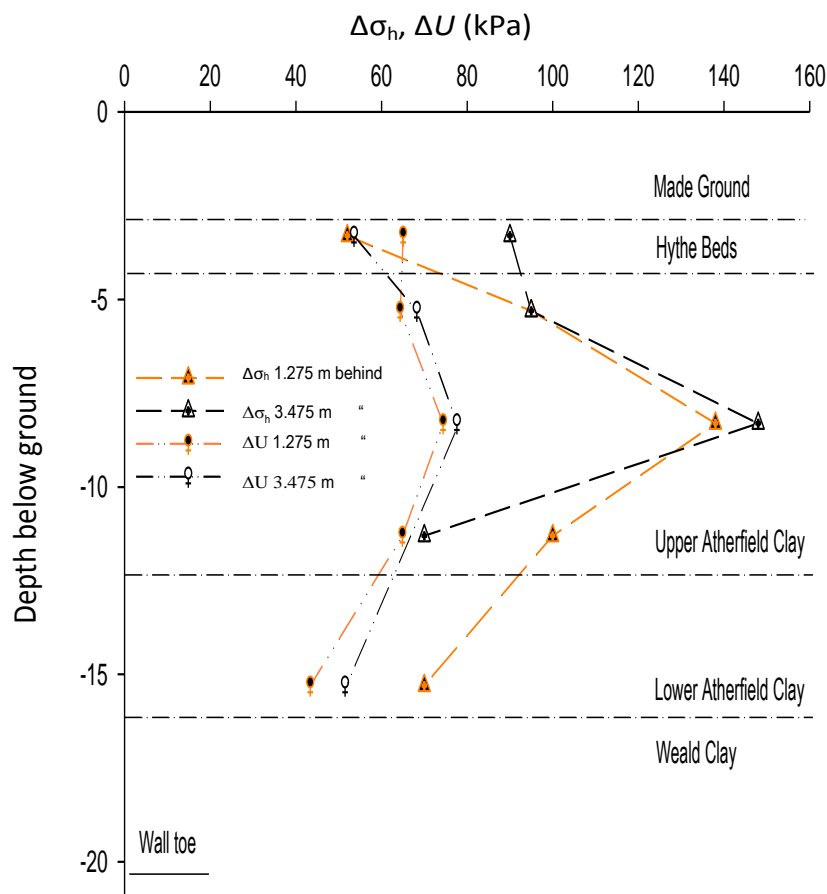
Figure 5.27: Variation of horizontal total stresses and pore pressures from the short-term (*ST*) to long-term (*LT*) conditions.

Stress changes normalised with respect to pore pressure changes, $\Delta\sigma_h/\Delta U$, at a distance of 1.275m behind the retaining wall are shown in Figure 5.28. It is evident that changes in horizontal total stresses from the short to the long-term conditions are much more significant than changes in pore pressures except closer to the soil surface. At depths greater than about 10 m, $\Delta\sigma_h/\Delta U$ is constant at about 1.5. This trend indicates that although there is a direct relationship between ΔU and $\Delta\sigma_h$, other factors, such as the thermal expansion of the reinforced concrete props, might have contributed to the stress changes.

Additionally, the changes in U and σ_h seem to be similar in trend to the horizontal displacement profile for a retaining wall propped at the crest and with stabilising base. This suggests that movement of the retaining wall also contributes to the change in lateral stresses.
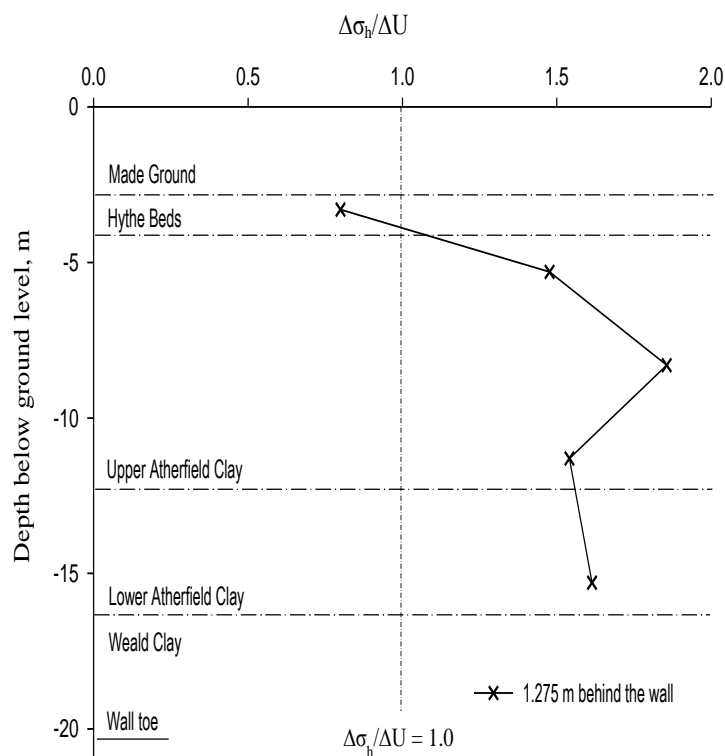
Figure 5.28: Changes between the short and long-term (ST-LT) horizontal total stresses, $\Delta\sigma_h$ normalised with respect to changes in pore pressure, ΔU.

Comparison of *in situ* and long-term profiles

Long-term changes in pore pressures and horizontal total stresses, at distances of 1.275 and 3.475 m behind the retaining wall, are compared with the *in situ* values in Figure 5.29. Large pressure changes relative to the in situ values occurred at locations closer to the soil surface. These changes reduce with depth. Normalised changes in pore pressures are fairly similar at distances of 1.275 m and 3.475 m behind the retaining wall. Changes in lateral stresses seem to coincide more with wall movement, with the greatest changes occurring in the middle of the wall and small to negligible changes at the propped crest and towards the wall toe. The profiles of changes in horizontal stresses and pore pressures relative to *in situ* diverge closer to the soil surface but converge at greater depths.
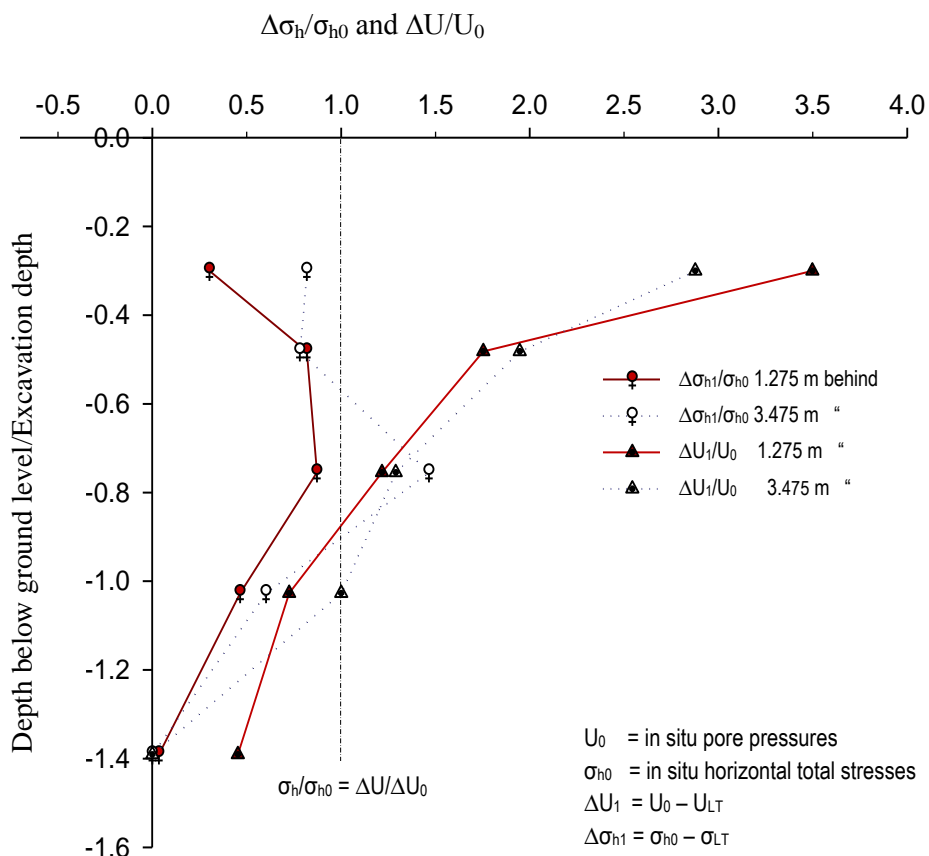
Figure 5.29: Changes in horizontal total stresses (σ_{h0}-$\Delta\sigma_h$) and pore pressures (U_0-U) normalised with respect to *in situ* values at distances of 1.275 m and 3.475 m behind the retaining wall.

From the preceding discussion, it is apparent that changes to the horizontal total stresses are attributable in part to changes in pore water pressures measured at similar locations. Other factors such as thermal expansion of the reinforced concrete props and base slab and consequent movement of the retaining wall could have also contributed to changes in horizontal total stresses.

5.4 Implication for the design of contiguous pile retaining walls

Practising and research geotechnical engineers are always looking for ways to improve the efficiency of the design for in-ground structures. Most efforts have concentrated on making small long-term gains, as it is believed that major improvements will not be achieved overnight. The designers of the cut and cover tunnel at CTRL Ashford recognised that the use of the contiguous piles would allow the seepage of groundwater through the pile gaps. The seepage of groundwater through the pile gaps was not however investigated as a possible means of reducing the pore pressures behind the retaining walls. It was acknowledged however that through-wall seepage could cause an increase in pore water pressure in front of the wall. This lead to concerns about the resulting reduced passive resistance or support for the wall.

It was also recognised that through-wall seepage could influence the pore pressures in the Weald Clay. The corresponding pore pressure increase in the soil on the excavated side of the retaining walls could cause the plug of Atherfield Clay above the Weald Clay and between the retaining walls to heave or fail by uplift during the short-term construction period. Thus, temporary sand drains were installed in front of the retaining walls.

The activities at CTRL, Ashford illustrate that although it was not intended or designed to have an impact on the pore water pressures, the use of the contiguous piles influenced significantly the long-term hydraulic regime around the retaining walls. This also introduced an accompanying drawback of allowing through-wall seepage in terms of the effect on hydraulic stability in front of the wall. The observations from Ashford suggest that significant amount of economic benefits could be realised if retaining walls formed

from contiguous piles were treated as permeable. However, it is necessary to consider methods to reduce the build-up of pore pressures in the soil in front of the retaining wall. Additionally, water exclusion techniques would also have to be designed so that they do not interfere with or impede through-wall seepage, which is the basis of the reduced pore pressures for contiguous piles.

It is also necessary to consider other water management techniques to prevent the deleterious effects of water induced settlement on the surrounding buildings and infrastructure. For example, water recharge could be used where the short-term drainage of groundwater through pile gaps is likely to contribute to increased surface settlement. These actions should be taken into consideration whilst conducting risk analyses for the construction of the retaining structure.

5.5 Summary

The results and analyses of the long-term field measurements from CTRL, Ashford were presented in this chapter. Pore water pressures at various positions behind the retaining wall formed of contiguous bored piles have decreased over a period of about 4600 days. High levels of suction have developed closer to the soil surface and near the exposed face of the retaining wall. The pore pressures measured at greater depths have achieved equilibrium. Pore pressures were less than hydrostatic behind the retaining wall. The pore pressure distribution in front of the retaining wall was less well defined.

Hydraulic heads were calculated using the pore pressures from the field data and the elevation heads with formation level as reference datum. The resulting contour plots demonstrated progressive changes in flow conditions between the short, medium and long-term. The plots of total head contours show negligible short-term changes to the hydraulic regime. Short-term flow conditions were therefore dominated by underdrainage, which was assumed pre-construction. Minor medium-term changes of the hydraulic head contours were observed. The low permeability of the Atherfield Clay in particular resulted in the establishment of pore pressure equilibrium taking much longer than expected. Long-term conditions however indicate that groundwater flow was predominantly through the pile gaps although there was still some residual

underdrainage in front of the retaining walls. It is also evident from the preceding analyses that the pore water pressures have not returned to near their pre-construction values as would be expected for an impermeable retaining wall.

Horizontal total stresses, measured at the same locations as the pore pressures, have generally decreased significantly over the monitoring period. The observed reduction in lateral stresses can be directly attributed, in some instances, to the corresponding changes in pore pressures. There are however, other factors contributing to the reduction in horizontal total stresses. These include the possible thermal expansion of the reinforced concrete props and base slab.

Chapter 6

_____

6.0 Back analysis of the contiguous pile retaining wall at CTRL, Ashford

_____

6.1 Introduction

Numerical investigations of the contiguous bored pile retaining wall at CTRL, Ashford were conducted to investigate the long-term hydraulic conditions around the wall. The results of the numerical analyses were then compared with field measurements from the instrumented section at the site of the construction of the retaining wall at Ashford reported in Chapter 5. Results from the numerical simulations were also compared with published reports on pore water pressures around retaining walls formed from contiguous piles in similar overconsolidated soils. Numerical analyses of conventional

impermeable retaining walls, in the form of secant piles, were also carried out and comparisons made with retaining walls in which there was through-wall seepage. Parametric studies were also conducted to compare the influence of the retaining wall and base slab geometries with and without seepage on:

- The hydraulic conditions of the soil in front of, and behind, the retaining wall,

- The vertical displacement of the soil behind the wall and

- Lateral wall movements.

The numerical simulations described in this chapter were conducted using the explicit finite difference numerical code in two dimensional plane strain mode FLAC^{2D}, described in Chapter 3.

6.2   Methodology

The numerical grid used in these investigations modelled a cross section of the ground 96 m in length by 62 m high as shown in the typical FLAC^{2D} grid in Figure 6.1.   The soil and retaining wall were represented by rectangular grid elements.   The grid elements that represented the continuous retaining wall were attached directly to the soil elements.   This is the recommended approach to facilitate the flow of groundwater between grid elements representing two different materials (Itasca, 2012).   To quantify the effect of groundwater flow on vertical soil displacement behind the retaining wall interface elements, of similar stiffness, were installed between the soil and the wall elements.
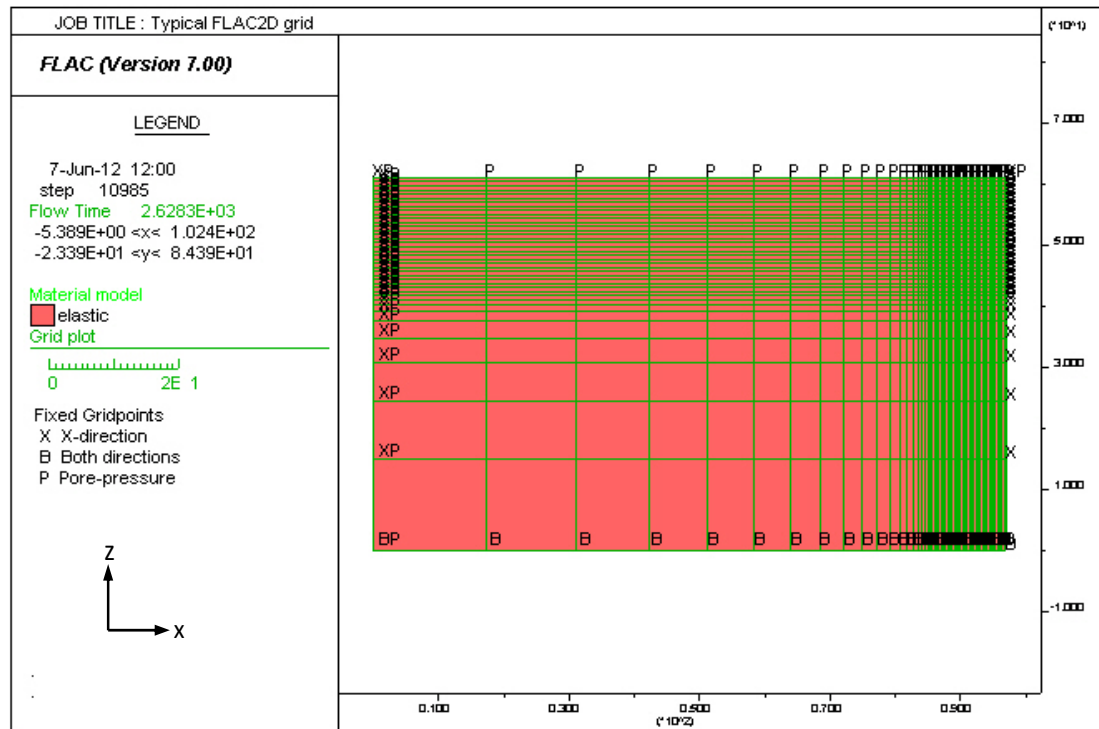
Figure 6.1: Typical numerical grid for FLAC^{2D} plane strain analyses.

Conditions of symmetry were assumed for the retained cutting. This allowed only one half of the cross-section of the cut and cover tunnel to be modelled thus reducing the amount of computational resources required. During the investigations, the regional groundwater level was maintained at 1 m below the soil surface by the far field hydraulic boundary conditions. The lateral boundaries were restrained from movement in the horizontal (x) direction and the lower boundary from movement in the vertical (z) and horizontal directions.

The contiguous pile retaining wall was represented in two dimensional plane strain analyses by a continuous wall of uniform cross section. This is the accepted norm for numerical simulation of retaining walls made of circular piles.   The equivalent wall thickness was therefore calculated and assigned to the model wall using the approaches adopted by Day and Potts (1983) and Powrie *et al.* (1999), described in Chapter 3.   The method used by Powrie *et al.* (1999) to determine the equivalent wall thickness made use of the second moment of area, *I* of the field and model retaining wall section. Day and Potts (1983) used the stiffness method to calculate the equivalent thickness. For a

pile diameter of 1050 mm, the equivalent thickness calculated was approximately 920 mm.

The bulk permeability (k_p) of the equivalent structure for the 2D plane strain wall was calculated using the expression derived in Chapter 3 (Equation 3.6) along with published data for the hydraulic parameters of the soils at Ashford (Roscoe *et al.*, 2003; Clark, 2006 and Richards *et al.*, 2007). The derived relationship gives the bulk permeability, k_p, from the *in situ* soil hydraulic conductivity, k_s and the pile gap to diameter ratio, *x/d*. A pile gap to diameter ratio of 0.286 (300/1050) was chosen for the analyses based on the existing pile and gap sizes at the construction site.

6.3 Soil and retaining wall properties

Throughout the investigations, the soil model used for each layer represented was assumed to be a homogeneous, isotropic continuous material with linear stress/strain behaviour. A plot of the soil strata with positions at which hydraulic parameters were calculated is shown in Figure 6.2.

1.0 m	Made Ground (MG)
2.8 m	Hythe Beds (HB)
3.3 m	P1 P6
4.2 m	B1
5.3 m	P2 P15 P7
	B2
	Upper Atherfield
8.3 m	P3 P16 P8
	Clay (UA)
	B3
	Base slab
10.3 m	
11.3 m	P13 P11 F1 P4 P9
	B4
12.2 m	
	Lower Atherfield
15.3 m	P17 P12 F2 P5 P10
	Clay (LA)
16.1 m	B5
	Weald
	Clay (WC)
20.3 m	
	Drain
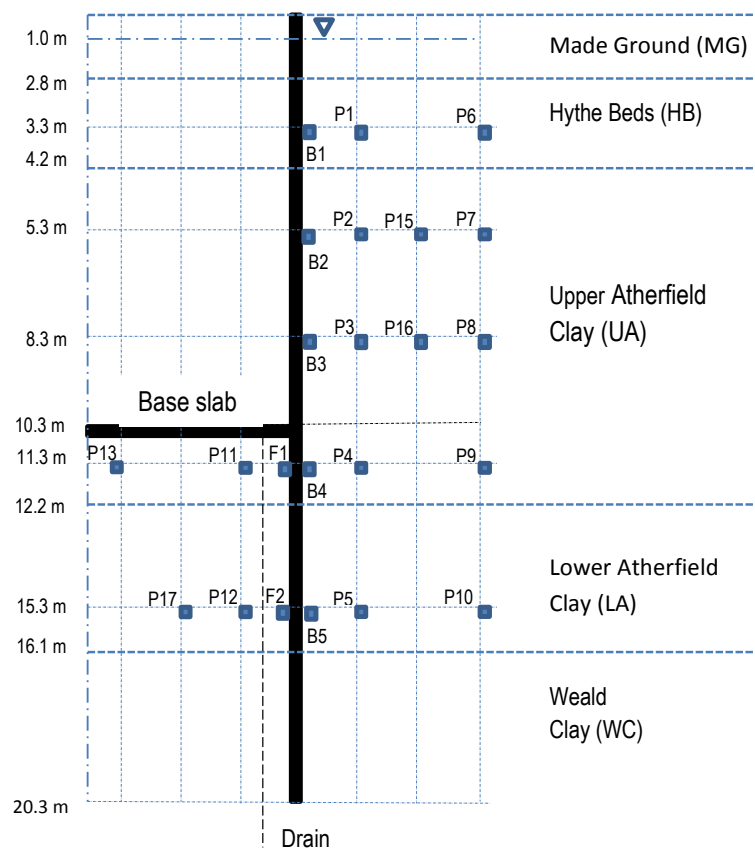
P   = monitoring locations corresponding to piezometer/spadecell positions at CTRL, Ashford

B, F = additional positions for calculating pore pressures and stresses in the numerical model (Back and Front)

Figure 6.2: Elevation of soil strata used in the numerical model.

An elastic, isotropic constitutive soil model, with the properties shown in Table 6.1, was used to characterise the soil. The soil properties are based on published data (Holmes *et al.,* 2005; Clark, 2006; Richards *et al.*, 2006 and Richards *et al.*, 2007) and site investigation records.   Clark (2006) notes that the geotechnical engineers at the construction site at CTRL, Ashford used a value for the *in situ* lateral earth pressure coefficient, K_0 of 1.2. This was considered reasonable for a slightly overconsolidated soil. This value is similar to those reported by Richards *et al.* (2006) who suggests that the *in situ* horizontal earth pressure coefficient was within the range 0.7 to 1.5 with typical values of $K_0=1.04$ used extensively.   These K_0 values are particularly low because soils of similar stiffness and overconsolidation history are known to have

209

$K_0 > 2.0$ in some instances. For example, Hubbard *et al*. (1984) measured K_0 of up to 2.5 for London Clays of similar stiffness. The differences in K_0 values could perhaps be attributed to more recent geological activities such as landslip at the Ashford construction site area as posited by Clark (2006). Notwithstanding the reported difficulties in determining consistent K_0 values, in order to compare the results from the numerical simulations with those from the instrumented section at Ashford K_0 values, which are known to vary according to the soil layer, were adopted as indicated in Table 6.1.

Soil parameters	Made Ground	Hythe Beds	Upper Atherfield Clay	Lower Atherfield Clay	Weald Clay	Units
Dry density, ρ_{dry}	1757	1510	1580	1723	1750	Kg/m^3
Permeability, k	1x10^{-6}	1x10^{-7}	2x10^{-8}	2x10^{-8}	3x10^{-7}	m/s
Porosity, n	0.3	0.3	0.25	0.25	0.25	-
Poissons' Ratio, v	0.3	0.3	0.25	0.25	0.2	-
Effective friction angle, ϕ'	26.0	30.0	24.0	21.0	23.0	Deg
Bulk modulus, K'	16.7	17.5	24	38.7	111.1	MPa
Shear modulus, G	1.7	8.1	14.4	23.2	83.3	MPa
Average thickness of layer	2.8	1.4	8.0	3.9	100.0	m
Coefficient of earth pressure at rest, K_0	0.6	1.5-1.1	1.5-1.0	1.5-1.2	1.5-1.1	-

Table 6.1: Soil properties from the site of the construction of the retaining wall at CTRL, Ashford.

Throughout the analyses, the values of the stiffness parameter for each soil layer were assumed to be constant with depth. The elastic properties of bulk, K and shear, G moduli were used instead of Young's modulus, E and Poisson's ratio, v. As discussed in Section 3.3, bulk and shear moduli are related to the stiffness modulus and Poisson's ratio by Equations 6.1 and 6.2.

$$K = \frac{E}{3(1-2v')}$$
Equation 6.1

$$G = \frac{E}{2(1+v')}$$
Equation 6.2

The literature on the hydraulic properties of the soils at the site of CTRL, Ashford indicates that there is a large variability in the values of the soil hydraulic conductivity. The apparent differences in permeability values may be attributed, in part, to the suitability of the method used to determine *in situ* permeability. For example, Roberts *et al.* (2007) notes that borehole tests are particularly unreliable and can underestimate soil permeability by an order of magnitude or more. For the numerical simulations described herein, the hydraulic conductivity values shown in Table 6.1 for each soil layer were used

The retaining wall was modelled as an elastic isotropic material with the properties listed in Table 6.2.

Pile properties	Value
Dry density (ρ), Kg/m^3	2500
Young's modulus (E), GPa	28
Poisson's ratio (v),	0.15
Second moment of area (I), m^4	0.0597

Table 6.2: Elastic properties for the continuous retaining wall of uniform cross section representing the contiguous piles in 2D plane strain analyses.

In the absence of measured values of Young's modulus, for the reinforced concrete contiguous piles at Ashford, it was decided to use a value of 28 GPa, which is the same as that at Bell Common (Hubbard *et al.*, 1984). Ellis *et al.* (2010) also recommended 30 GPa as being a typical value for the stiffness parameter for the type of contiguous piles under consideration. As the structural performance of the retaining wall was not being assessed and since the strength of the wall would not impact the groundwater flow regime, it was decided that more detailed consideration of the stiffness parameters was not necessary for these simulations.

6.4   Modelling procedure

The analysis commenced with the soil being brought to a state of equilibrium. This was achieved by applying gravitational acceleration of 10 m/s to the soil mass in the numerical grid and allowing the developing gravitational stresses to equilibrate as recommended by Itasca (2012). Uncoupled analyses were conducted during the equilibrium stage. These uncoupled simulations were divided into hydraulic and mechanical phases. During the mechanical phase, the hydraulic properties of water bulk modulus, K_w, and density, ρ_w, were set to zero and the model cycled to mechanical equilibrium. The hydraulic phase was then undertaken with the mechanical properties switched off and K_w and ρ_w assigned their correct values.

The ratio of the unbalanced forces to the applied forces was used to determine when the initial mechanical and hydraulic equilibrium were achieved. This equilibrium condition is based on the principle that the numerical steps taken in FLAC^{2D} ensure that the forces generated by the applied stresses and boundary displacements are evenly distributed between the nodes. The unbalanced force is therefore calculated as the sum of the net forces at the nodes. The ratio of the unbalanced forces to the applied forces continuously reduces during the numerical procedure and should approach zero as shown in Figure 6.3. Equilibrium is also achieved when this ratio approaches a constant value, which is not necessarily zero. A constant non-zero unbalanced force ratio usually indicates that plastic flow or failure of the soil is taking place within the numerical grid. The default unbalanced force ratio used in FLAC^{2D} is 1 x 10^{-5} (Itasca, 2012).
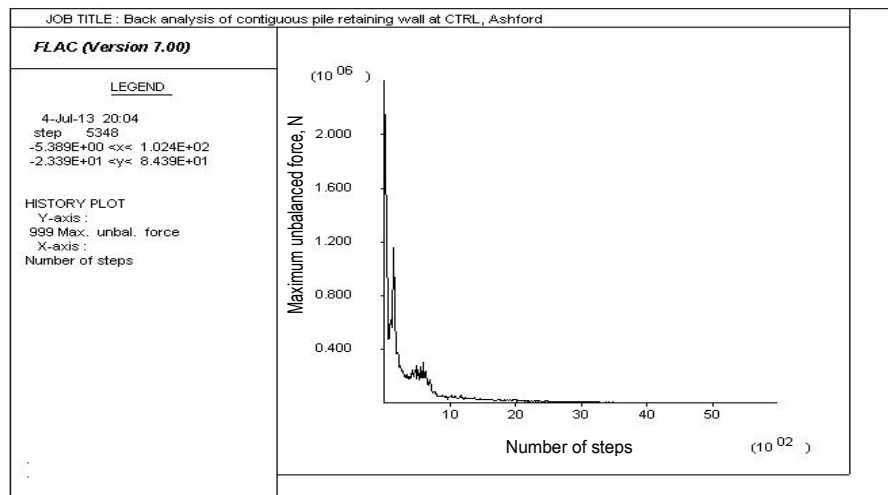
Figure 6.3: FLAC^{2D} history plot of maximum unbalanced force.

The construction sequence is summarized in Table 6.3. During the numerical analyses, node displacements and velocities were initialised to zero to observe the impact on the hydraulic properties during each phase of the analysis. Separate simulations were also conducted without initialising displacements and velocities at each stage so that the magnitude of the total soil and wall movements could be determined.

As the focus of this study was on the long-term hydraulic conditions, construction steps were mostly simulated as instantaneous events. This is obviously not realistic but should suffice for the study of long-term hydraulic conditions. Most construction events were therefore simulated for the duration between each activity shown in Table 6.3.

213
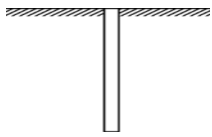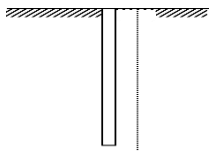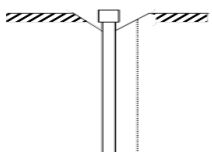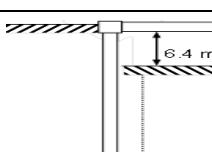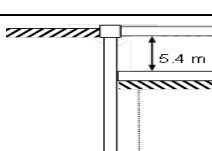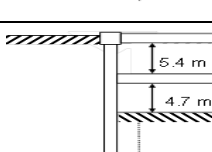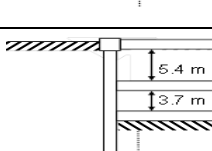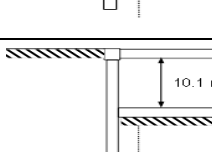
Modelling stage	Name	Duration (days)	Time to next stage (days)	Schematic
1	Install piles	24	278	
2	Install sand drain to 30 m below ground level	3	90	
3	Construct capping beam	2	25	
4	Excavate for and install permanent props	2	15	
5	Excavate to 6.4m below ground level	26	3	6.4 m
6	Install temporary props	10	8	5.4 m
7	Excavate to formation level	7	42	5.4 m / 4.7 m
8	Construct base slab	2	2	5.4 m / 3.7 m
9	Remove temporary props and simulation of long-term conditions	14		10.1 m

Table 6.3: Construction timeline for the instrumented section at CTRL, Ashford.

The construction of the retaining wall was modelled in nine stages as follows:

1. The piles were installed by assigning the material properties, in Table 6.2, to the grid elements representing the retaining wall. No attempts were made to model accurately the installation effects as these were being investigated elsewhere.

2. Dewatering was simulated by fixing the pore water pressures in front of the retaining wall to zero from the ground surface to a depth of approximately 30 m below ground level. This corresponded to the depth of the temporary sand drains (Clark, 2006).

3. Construction of the capping beam was simulated by applying a distributed load, vertically downward, to the top of the retaining wall.

4. The permanent reinforced concrete (RC) props were applied using the FLAC^{2D} built-in logic for structural beam elements. The props were fixed from rotation and translation at the boundary of symmetry (Itasca, 2012) and were assigned the properties indicated in Table 6.4.

5. Phase 1 excavation, to a depth of 6.4 m below the soffit of the permanent props, was modelled by switching the soil model from elastic isotropic to null model for the grid elements representing the excavated region.

6. Installation of the temporary circular hollow (CHS) steel section props was modelled using built-in structural beam elements. The temporary props were then fixed from rotation and translation at the boundary of symmetry and assigned the properties in Table 6.4.

7. Final excavation to formation level, a further 4.7 m below the soffit of the temporary props, was carried out as previously described.

8. The base slab was constructed by assigning the reinforced concrete properties to the grid elements at formation level. In order to simplify the analyses, a uniform cross-section was assumed for the reinforced concrete base slab.

9. The temporary props were then removed by assigning zero values to the parameters in Table 6.4. Long-term conditions were then simulated by applying the boundary conditions explained in the following paragraph.

Property	Permanent props	Temporary props
Cross-sectional area, A (m²)	1	0.032
Spacing (m)	4.5	4.5
Young's modulus, E (GPa)	25.0	205.0
Second moment of area, I (m⁴)	0.083	0.004

Table 6.4: Structural properties of the permanent reinforced concrete and the temporary circular steel props.

Simulation of long-term hydraulic conditions

This was done by setting the initial pore pressures at the exposed surface of the retaining wall and top of the base slab to zero. This condition facilitated seepage if the soil and wall permeability allowed. The phreatic surface behind the retaining wall was allowed to develop freely as the groundwater levels changed. The regional groundwater level was maintained by far field infiltration, which was simulated by fixing the water level at 1 m below ground level at the left hand boundary as recommended by Itasca (2012). It is recognized that surface infiltration from precipitation and human activities such as broken water mains local to an earth retaining structure, especially in fine soils, can be significant. Similarly, the presence of urban activities such as paved areas might also have an impact on the percolation rate in the soil surrounding a subsurface structure. Maintaining the far field boundary water level in the model at the level of the regional water level in the Ashford area ensured that the groundwater model more than adequately represented infiltration in the area. Additionally there were no reported cases of significant amount of ponding in the area of the retaining walls at Ashford during the construction.

6.4.1 Calculating hydraulic parameters

During the numerical analyses, pore water pressures, horizontal total stresses and volumetric flowrates were calculated in front of and behind the retaining wall, at positions numbered P1-P13, P15-P17, B1-B5 and F1 & F2 shown on the idealised cross-section in Figure 6.2. Vertical movement of the soil behind the retaining walls was also calculated to compare the resulting displacement profiles for a permeable and an impermeable retaining wall in similar conditions. Lateral displacements of the retaining walls were also calculated to determine the influence of wall permeability.

6.4.2 Investigation into the effect of wall geometric properties

Parametric studies were conducted to determine the differences in hydraulic conditions around a permeable and an impermeable retaining wall caused by varying the retaining wall and base slab geometric properties. The comparison between permeable and impermeable retaining wall geometry was calculated in terms of:

- The pore water pressures in front of and behind the model walls,
- Vertical displacement of the soil behind the walls and
- The lateral movement of the model retaining walls.

The selection of a constitutive soil model, which would give reliable and consistent results, was conducted by referring to published literature. The difficulties associated with the selection of constitutive soil models are well researched (Bolton *et al*., 1994; Addenbrooke *et al*., 1997 and Masin and Herle, 2005). For instance, it is acknowledged that an elastic perfectly plastic soil model, with a Mohr Coulomb (MC) failure criterion, can provide useful information on some aspects of soil behaviour. However its efficacy in predicting soil vertical displacement is questionable. Similarly, the linear elastic Mohr Coulomb plastic model does not represent reductions in soil stiffness that occurs with increasing strain although reasonable results can be obtained if the soil stiffness profile is carefully selected (Hicher and Shao, 2008 and Powrie *et al*., 1999). It was decided therefore that an elastic soil model would be used for these simulations. The parametric studies were conducted for two main retaining wall geometries:

i)   A permeable retaining wall in which there was through-wall seepage typical of retaining walls formed from contiguous piles and

ii) An impermeable retaining wall, typical of secant pile walls.

To reiterate, the purpose of the parametric studies was to determine the impact of through-wall seepage on the hydraulic parameters under varying retaining wall and base slab geometries.

6.5   Results and discussion

Results from the numerical analyses of the permeable and impermeable retaining walls were compared with field measurements from the contiguous pile retaining wall at CTRL, Ashford. It is ac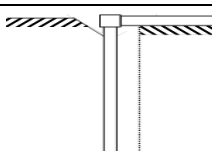knowledged that several factors could have contributed to differences between the results from numerical simulations and those from field measurements. For instance, estimating the initial soil stresses for the numerical model sets the 'start point' for the analyses. Thus it is important to have reliable information about the soil stress history and groundwater conditions. Similarly, there are reported difficulties associated with measuring *in situ* pore pressures. This can be compounded by reduced reliability as data is recorded over long periods. Additionally high negative pore pressures are difficult to measure and the pressure transducers can be affected by, for instance the desaturation of the porous tips or the ceramic disks used in most instruments (Ridley *et al*., 2003). This means that *in situ* measurements have to be carefully selected and the results viewed in light of the method used. It is for these reasons that the results in the following sections were analysed with emphasis on the general trends in long-term results. Thus the absolute values are regarded as not being as important as the long-term trends.

6.5.1 Results of parametric studies

In the following sections, the influence of the retaining wall and base slab geometric properties on the hydraulic conditions, around the permeable and impermeable retaining walls, and on the vertical displacement of the soil behind the walls is presented and discussed. Differences in horizontal displacements of the permeable and impermeable retaining walls are also considered.

The effect of base slab permeability

As noted in Chapter 5, the geotechnical engineers at the site of the construction of the retaining walls at CTRL, Ashford were concerned that seepage through the contiguous piles could cause a build-up of pore water pressures underneath the Lower Atherfield Clay. Consequently, vertical drains were installed to reduce the water pressures in the

Atherfield Clay by enhancing the existing underdrainage afforded by the Weald Clay. Further vertical drains were installed through the base slab and connected to the underlying drainage system. For the parametric studies described herein, numerical simulations were undertaken to compare the pore water pressures, soil vertical displacement and wall horizontal movement for the permeable and impermeable model walls with and without drainage through the base slab.

Pore pressures

The impact on pore pressures of drainage through the base slab is shown in Figure 6.4.
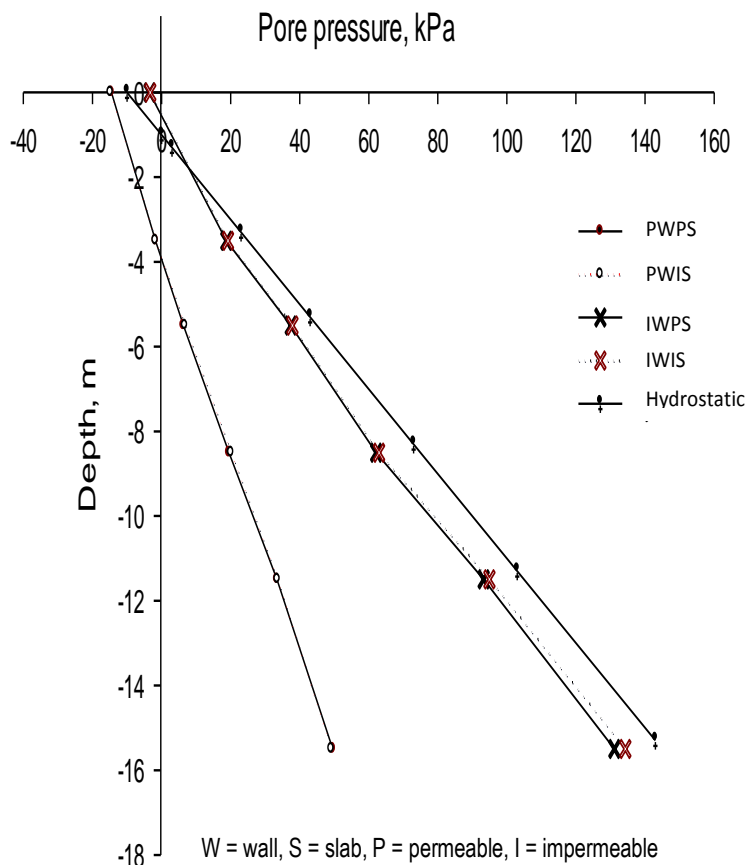
Figure 6.4: Pore pressure profiles measured at a distance of 1.3 m behind the retaining walls for the permeable and impermeable base slab.

The presence of the vertical drains through the reinforced concrete base slab does not seem to affect significantly the distribution of pore water pressures with depth behind the permeable and impermeable retaining walls. Nonetheless, allowing seepage through the base slab caused a slight decrease in pore pressures at greater depths behind the impermeable wall. This behaviour is consistent at various distances behind the retaining walls. It is also evident that the pore pressure profiles for the permeable and impermeable retaining walls, with and without seepage through the base slab, were less than hydrostatic at depths greater than approximately 2 m below ground level.

The impact of base slab permeability on pore pressures in front of the permeable and the impermeable retaining walls is shown in Figure 6.5.
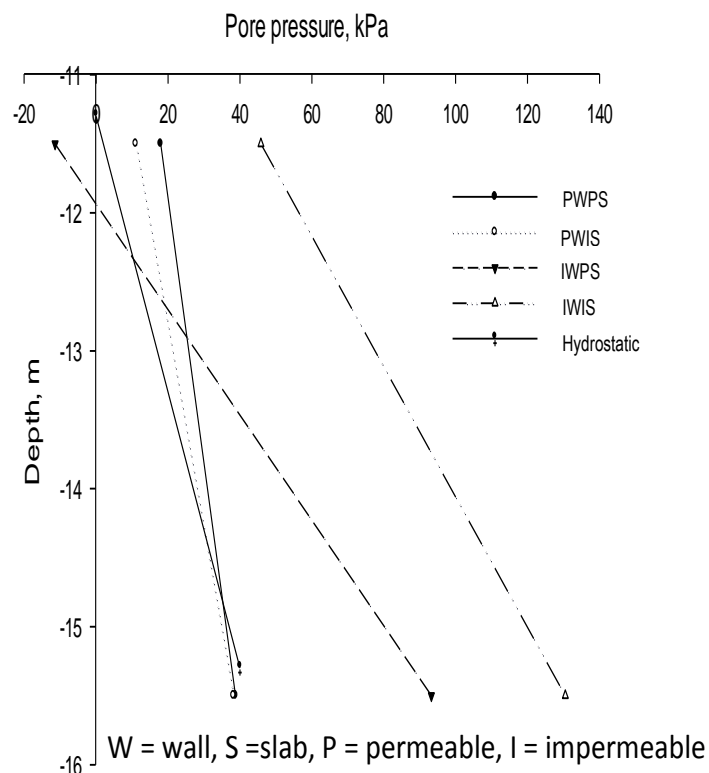
Figure 6.5: Pore pressure profiles measured at a distance of 1.3 m in front of the retaining walls for the permeable and impermeable base slab.

Pore water pressures in front of the permeable retaining wall inexplicably increased, albeit only slightly, when drainage through the base slab was allowed. Pore pressures however tended to converge with depth as would be expected. The effect of base slab permeability on pore water distribution for the permeable wall is therefore negligible at greater depths. Contrastingly, there is a substantial reduction in pore pressures in front of the impermeable wall when seepage through the base slab is allowed. This reduction in pore pressures is due to drainage through the base slab and is particularly significant for design purposes as it demonstrates that the presence of the drains through the base slab not only causes reduced water pressures under the slab but also results in a slight decrease in hydraulic loads on the back of the retaining wall. The pore water pressures in front of the impermeable wall for the permeable and impermeable base slab are converging with depth albeit at a much slower rate than for the permeable wall.

Vertical displacement

In contrast to the pore pressure distribution, the influence of base slab permeability on soil settlement behind the retaining walls is more noticeable as illustrated in Figure 6.6.
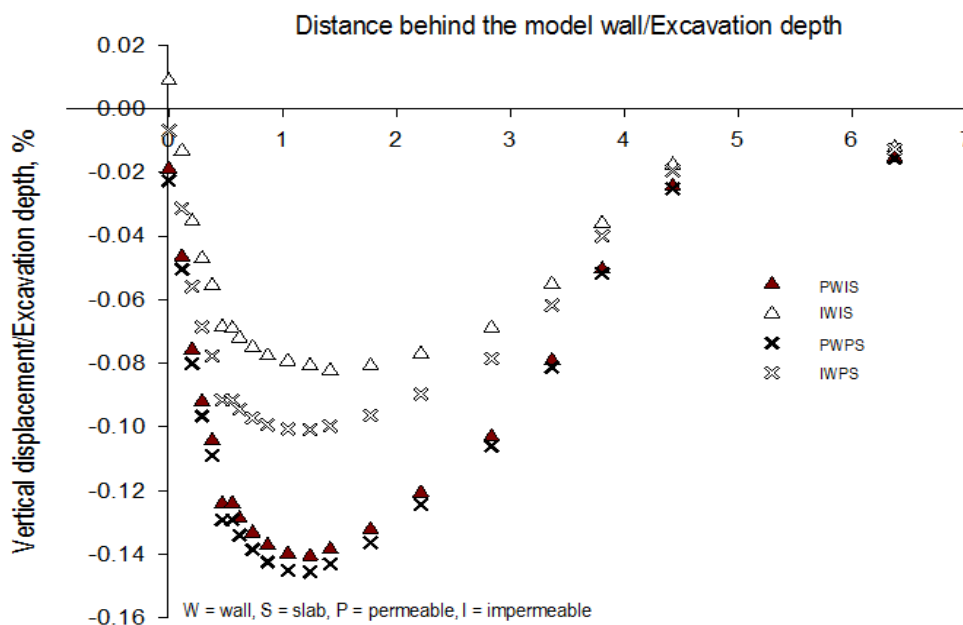
Figure 6.6: Comparison of vertical displacement for various slab permeability.

Through-wall seepage has a greater impact on soil settlement behind the wall than does the permeability of the base slab. This is evident by the more than 60% increase in settlement for the permeable retaining wall relative to the impermeable. Contrastingly, allowing drainage through the base slab caused only a slight increase in settlement for the permeable retaining wall because most of the one-dimensional consolidation of the soil already occurred due to through-wall seepage. Drainage through the base slab caused a 25% increase in settlement for the impermeable wall. Again, this is due to 1D consolidation of the soil.

Lateral wall movement

Figure 6.7 shows the variation of lateral wall movements of the permeable and impermeable retaining model walls with and without groundwater flow through the base slab.
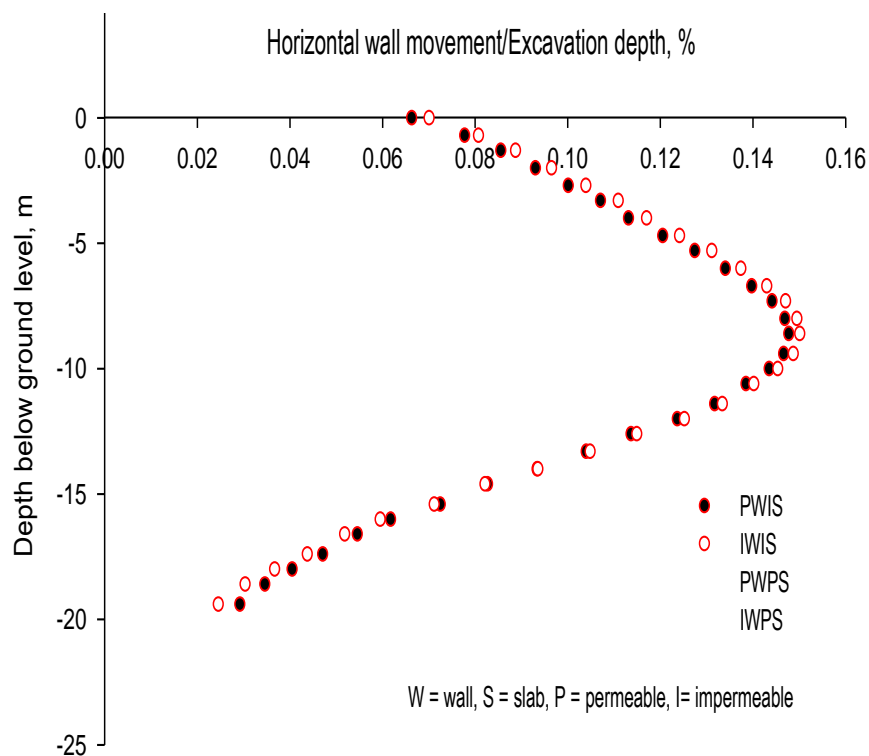
Figure 6.7: Variation of horizontal displacement for permeable and impermeable base slab.

The impact on horizontal wall movement in both cases is negligible. Nonetheless, it is evident from Figure 6.7 that there is slightly greater movement of the impermeable wall for the permeable and impermeable base slab relative to that observed for the permeable wall. Similarly there seems to be an unexplained slight increase in lateral movement of the impermeable wall when flow was allowed through the base slab.

It seems therefore that the impact of base slab permeability on the horizontal displacement of the impermeable retaining wall is more than that on the permeable wall.

6.5.2 Long-term pore pressures behind the retaining walls

Consolidation analyses were carried out to determine the long-term pore pressures behind and in front of the retaining walls. The results were compared with field measurements at distances and depths corresponding to the locations of the piezometers at CTRL, Ashford described in Chapter 5.

Pore pressure changes at the back of the retaining wall

The variation of pore pressures at the back of the permeable and impermeable retaining walls is shown in Figure 6.8. No field data was available for the pore pressures directly behind the wall. Pore pressures, as expected, generally decreased due to construction activities. In both cases, permeable and impermeable retaining walls, the pore pressures increased following construction and have since attained a state of equilibrium. The pore pressures adjacent to the permeable wall stabilised at values significantly less than the pre-construction pressures while those behind the impermeable wall have recovered to just below their pre-construction values and are noticeably higher than those behind the permeable wall. The pore pressures closer to the soil surface were fairly similar (B1), however those behind the impermeable wall seem to increase at a higher rate with depth than those behind the permeable retaining wall. The recovery of the pore water pressures behind the impermeable wall is similar to observations made by Hubbard *et al*. (1984) during studies of the behaviour of the hydraulic conditions around secant pile retaining walls at Bell Common.
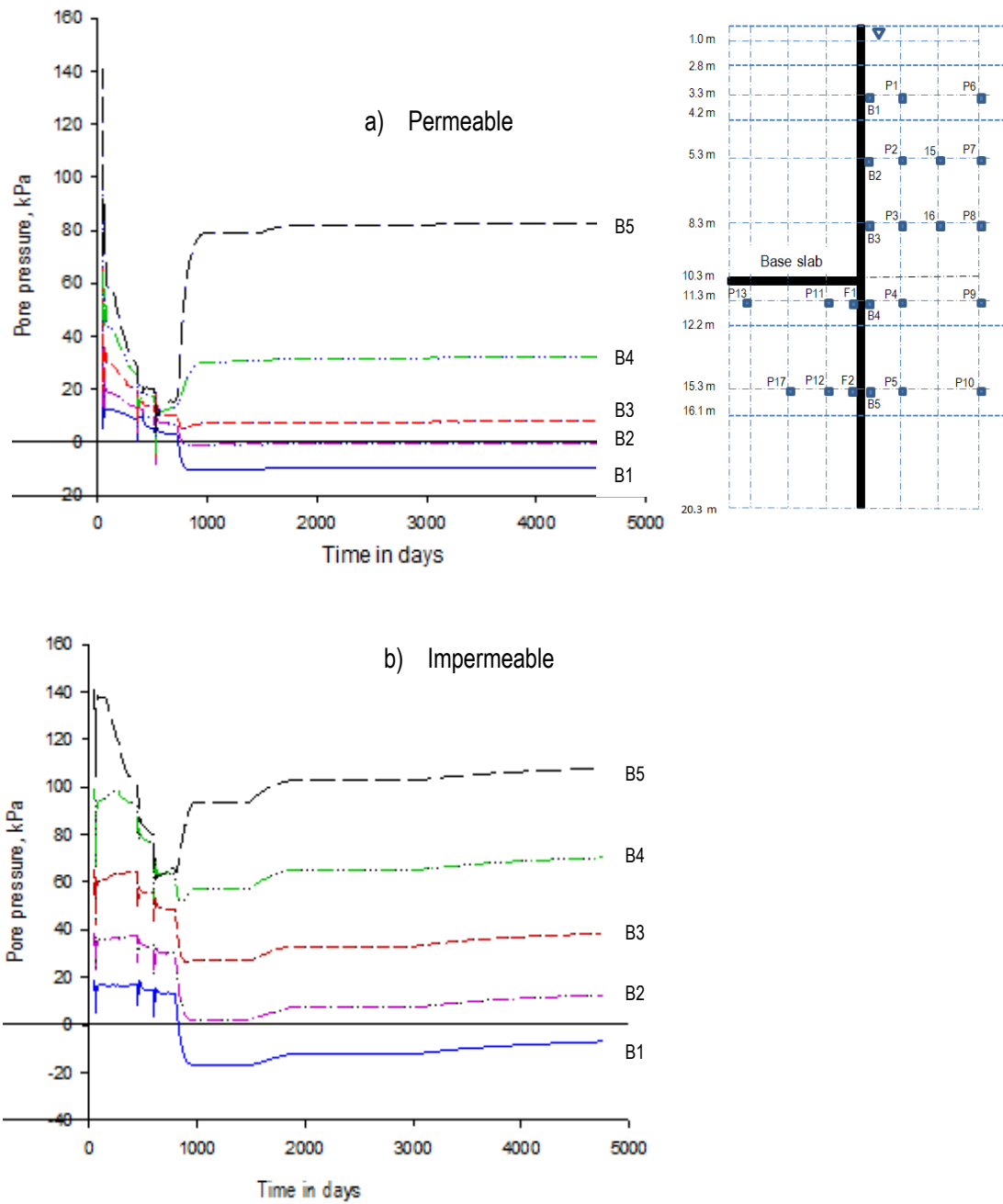
Figure 6.8: Pore pressure distribution adjacent to the back of the a) permeable and b) impermeable retaining walls.

Pore pressure changes 1.3 m behind the retaining wall

The distribution of pore pressures at a distance of 1.3 m behind the model retaining wall shows a similar trend to that observed adjacent to the wall as shown in Figure 6.9. Once again the long-term pore pressures for the impermeable wall are noticeably higher than those for the permeable wall at all locations except nearest to the soil surface. The pore pressures closer to the soil surface, *P1*, appear to be similar with relatively high levels of suction displayed for the permeable and impermeable walls. The short-term changes in pore pressures were very similar, as would be expected. This is due to the low permeability of the soils causing long equilibration times. Further comparisons were made with the measured pore pressures at similar locations at the instrumented section of the retaining wall at CTRL, Ashford discussed in Chapter 5. It is evident that, whereas the absolute values of the pore water pressure differ slightly, the general trends are similar for the results from the numerical analysis of the permeable wall and those from the field measurements.

The pre-construction pore water pressures from the site measurements appear to be consistently lower, than those assumed in the numerical investigation, by about 20 kPa at each depth. This was although the initial groundwater level was assumed to be 1.0 m below ground level during the numerical simulations adopting the published values from CTRL, Ashford (Holmes *et al.*, 2005; Clark, 2006 and Richards *et al.*, 2007). It is possible that other pre-construction dewatering might have resulted in a lowering of the water table in the area of the instruments. Notwithstanding the differences in pore pressure values, the similarities in trends between the numerical results for the permeable wall and those from the field measurement of the contiguous piles are evident.
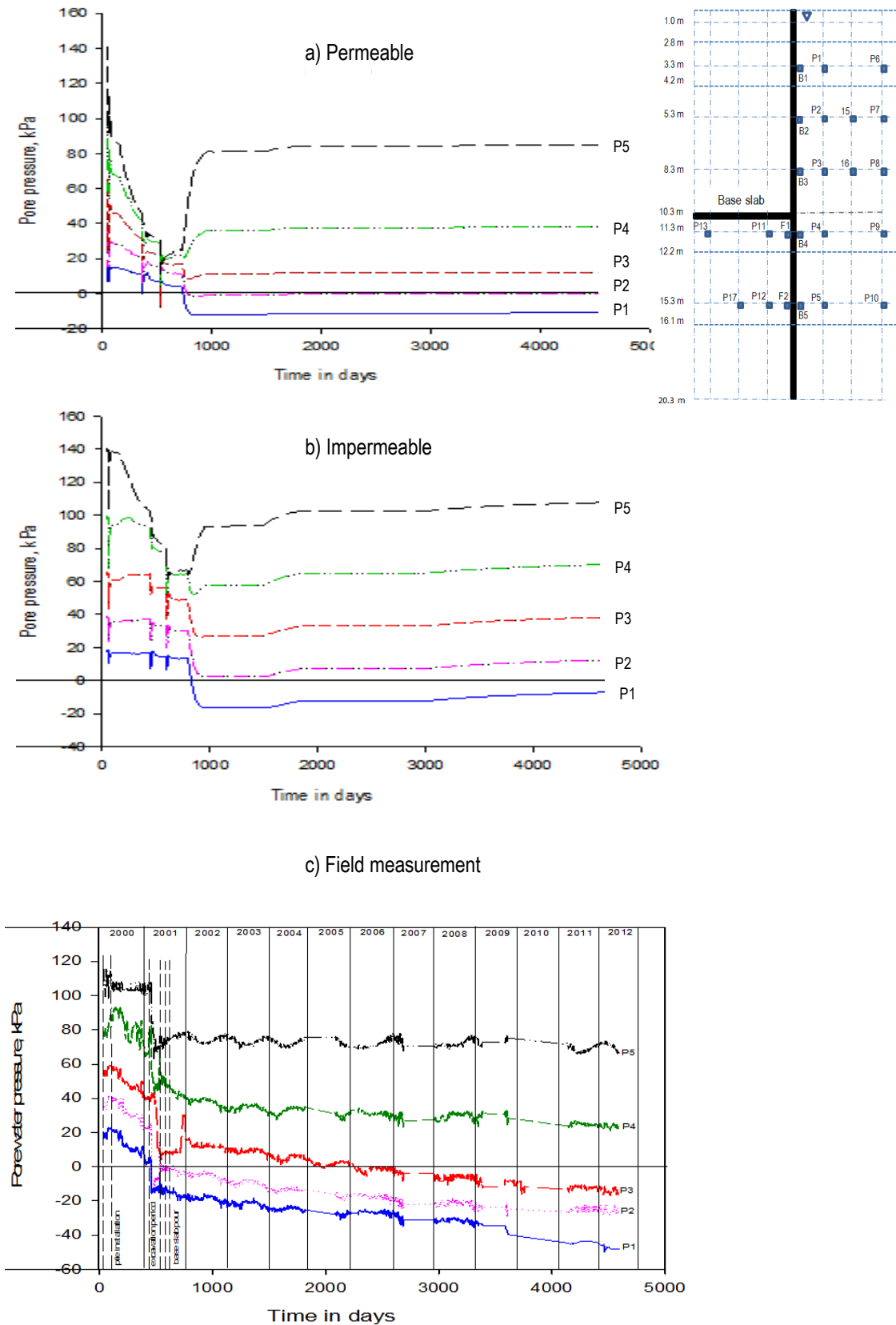
Figure 6.9: Pore pressure distribution 1.3 m behind a) a permeable retaining wall, b) an impermeable retaining wall and c) field measurements.

Pore pressure changes 2.3 m and 3.4 m behind the retaining walls

Figure 6.10 shows the comparison between the field measurements and numerical results at a distance of 2.3 m behind the permeable and impermeable retaining wall. Again, there is good correlation of the results from the numerical simulation of the permeable wall and those from the field monitoring.   The pore water pressures at the similar locations are slightly higher for the numerical results however the general trends are apparent.   The long-term equilibrium pore pressures around the impermeable wall were again much higher than those around the permeable wall.

228
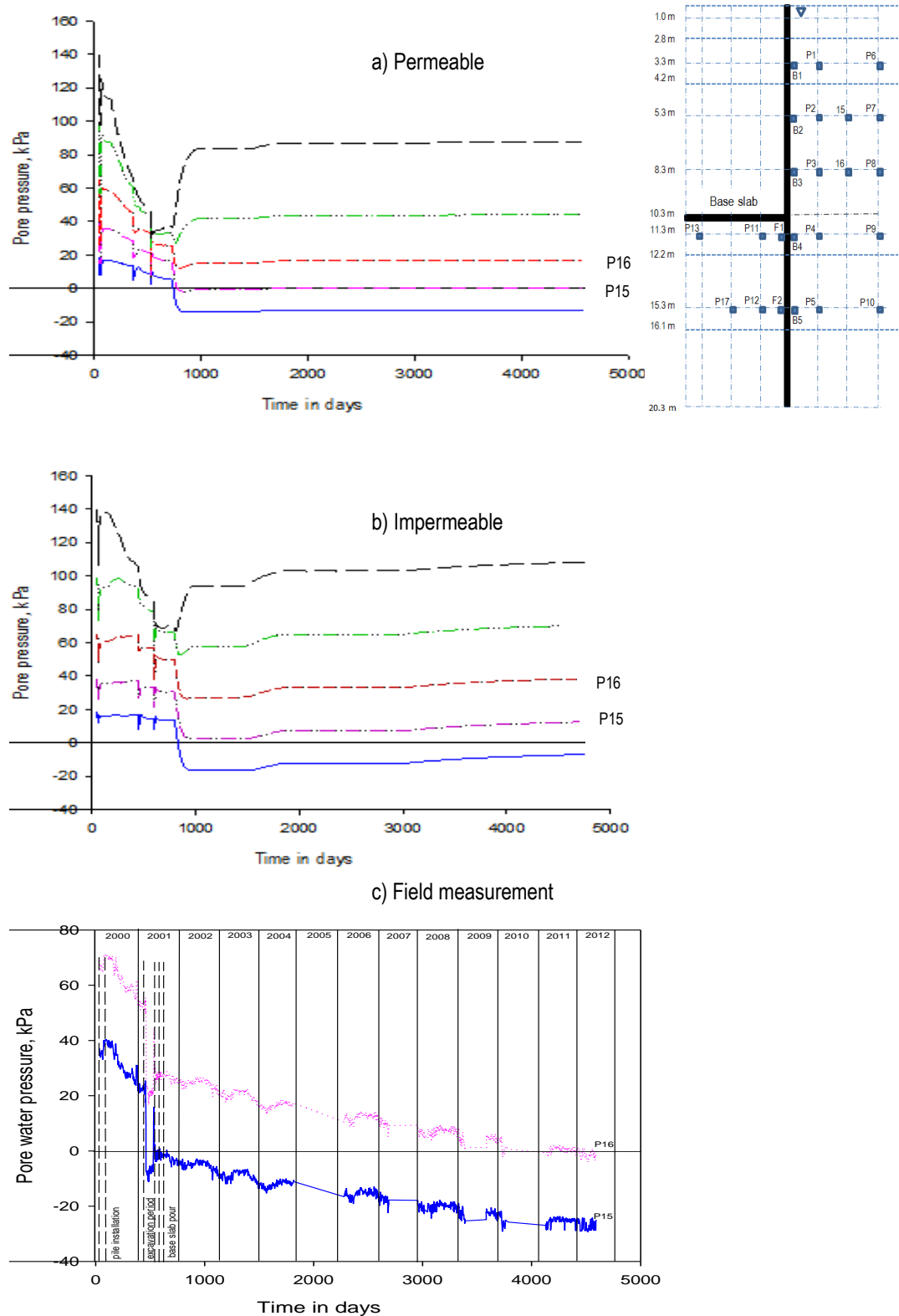
Figure 6.10: Pore pressure distribution 2.3 m behind a) a permeable retaining wall, b) an impermeable retaining wall and c) field measurement.

The pore pressure changes observed at a distance of 3.4 m behind the retaining walls are very similar in trend to that noted closer to the wall as illustrated in Figure 6.11. Again it is evident that the general results for the permeable retaining wall compare well with those from the site monitoring data at similar locations. Pore pressures for the impermeable retaining wall have also recovered to just below their pre-construction values.
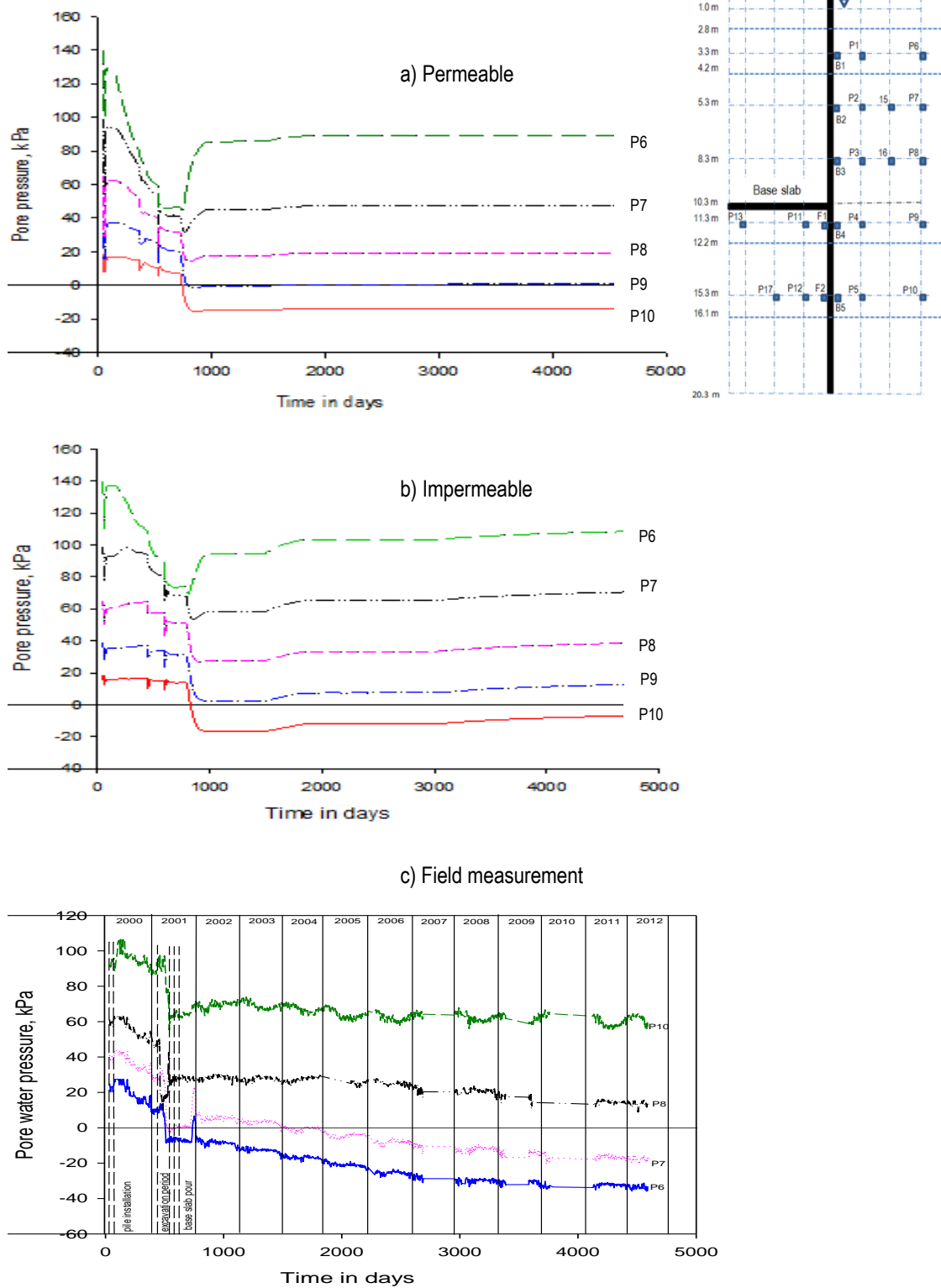
Figure 6.11: Pore pressure distribution 3.4 m behind a) impermeable retaining wall,
b) permeable retaining and c) field measurement.

231

Pore pressures 20 m behind the retaining wall

To complete the analysis behind the retaining wall, pore pressure changes were calculated at a distance of 20 m from the back of the wall at identical depths below ground level. The results are plotted in Figure 6.12. It is evident that the differences in pore pressures are significantly less than at distances closer to the retaining walls as would be expected as the distance of influence is approached. Construction activities induced the largest changes in pore pressure albeit recorded at a much later period. This later recording of pore pressures is due to the amount of time it takes for the induced changes to be calculated 20 m away in fine soil. It is however evident that the pore pressures at 20 m behind the impermeable wall are still increasing, although very slowly as seen on the plot at 3.3 m below ground level. Pore pressures at similar depths behind the permeable wall have attained equilibrium conditions. It is likely therefore that the equilibrium pore pressures, particularly closer to the soil surface, for the impermeable wall will be higher than those for the permeable retaining wall. No field data was available to compare pore pressure changes at this location.
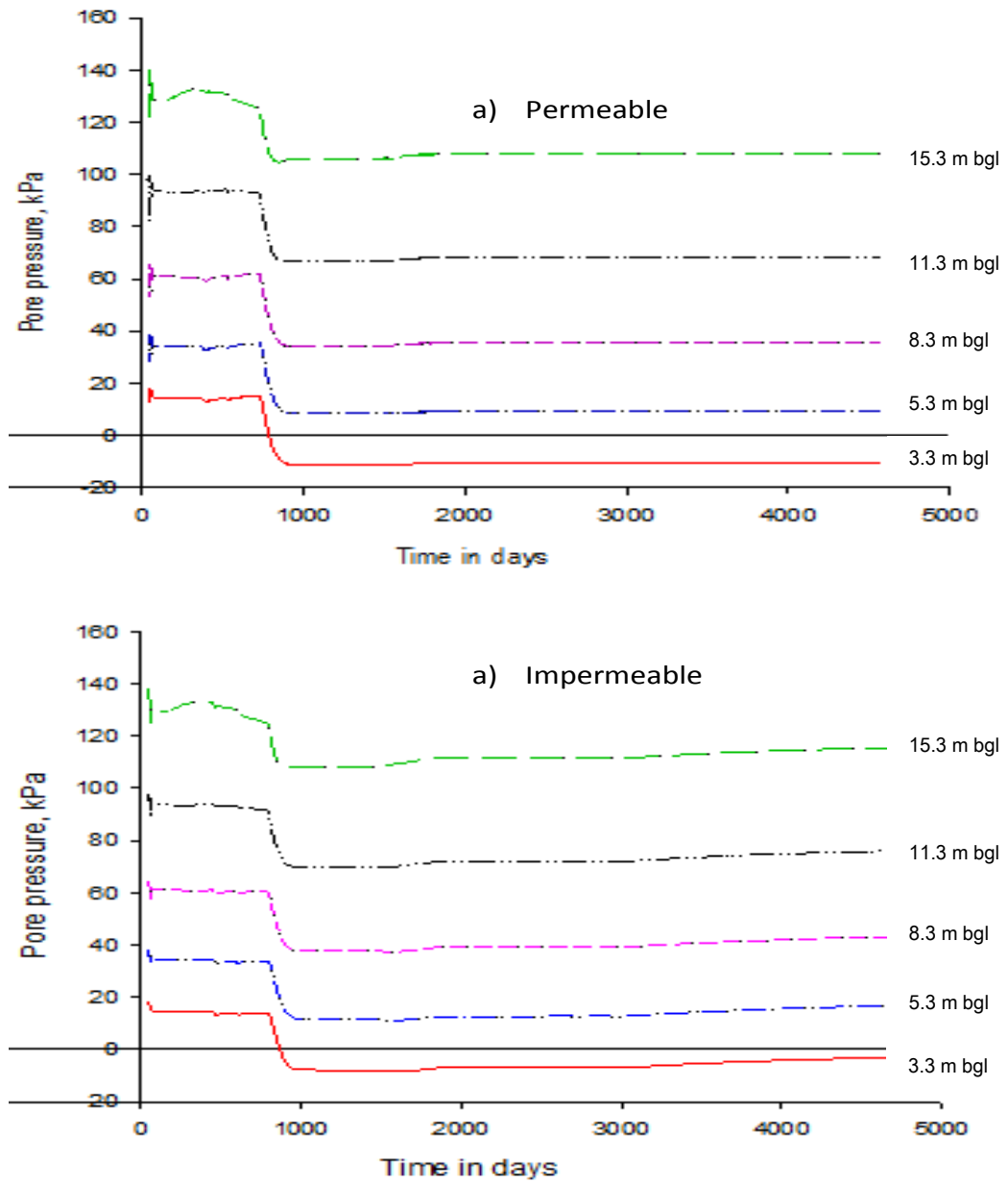
Figure 6.12: Pore pressure distribution 20 m behind a) impermeable and b) permeable retaining wall model.

6.5.3 Pore pressure variation in front of the retaining wall

Pore water pressures at various positions in front of the permeable and impermeable retaining walls were compared during the simulations and are shown in Figure 6.13. The impact of the wall permeability on pore pressures in front of the two walls in the numerical simulations is less than at the back. Pore pressures in front of the permeable wall are slightly higher than those for the impermeable wall. This trend is consistent at each location in front of the retaining walls. Further comparison of the calculated pore pressures and field measurements in front of the retaining walls did not provide any useful information.
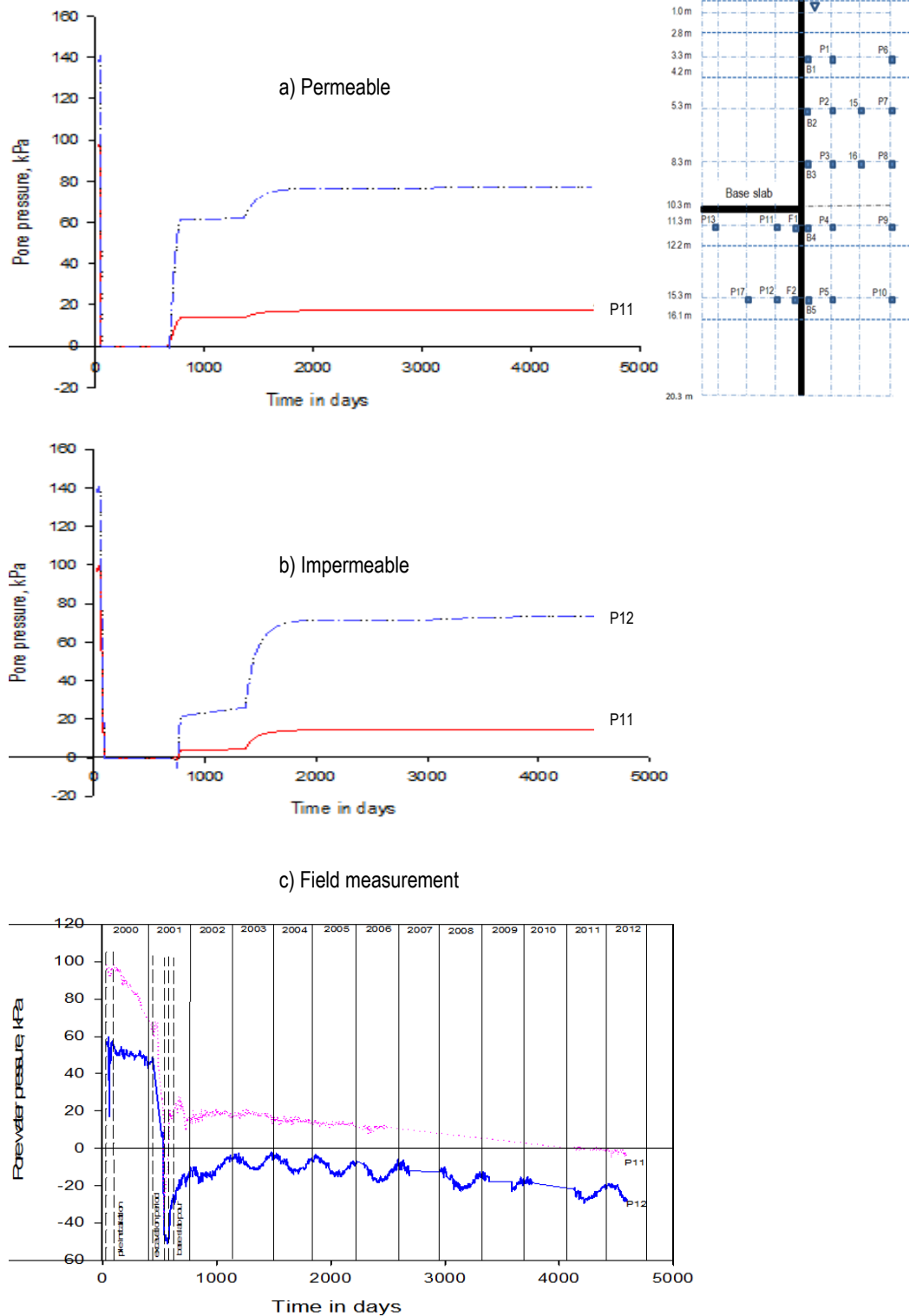
Figure 6.13: Pore pressure distribution 1.3 m in front of a) a permeable wall, b) an impermeable retaining wall and c) field measurement.

6.5.4 Pore pressure profiles

Pore pressure profiles at distances of 1.3 m in front of and behind the model walls were compared for the permeable and impermeable retaining wall. Further comparisons were made with the long-term profiles from the field measurements. Hydrostatic pressure distribution, assuming a groundwater level of 1.0 m below ground level, was also plotted as shown in Figure 6.14.
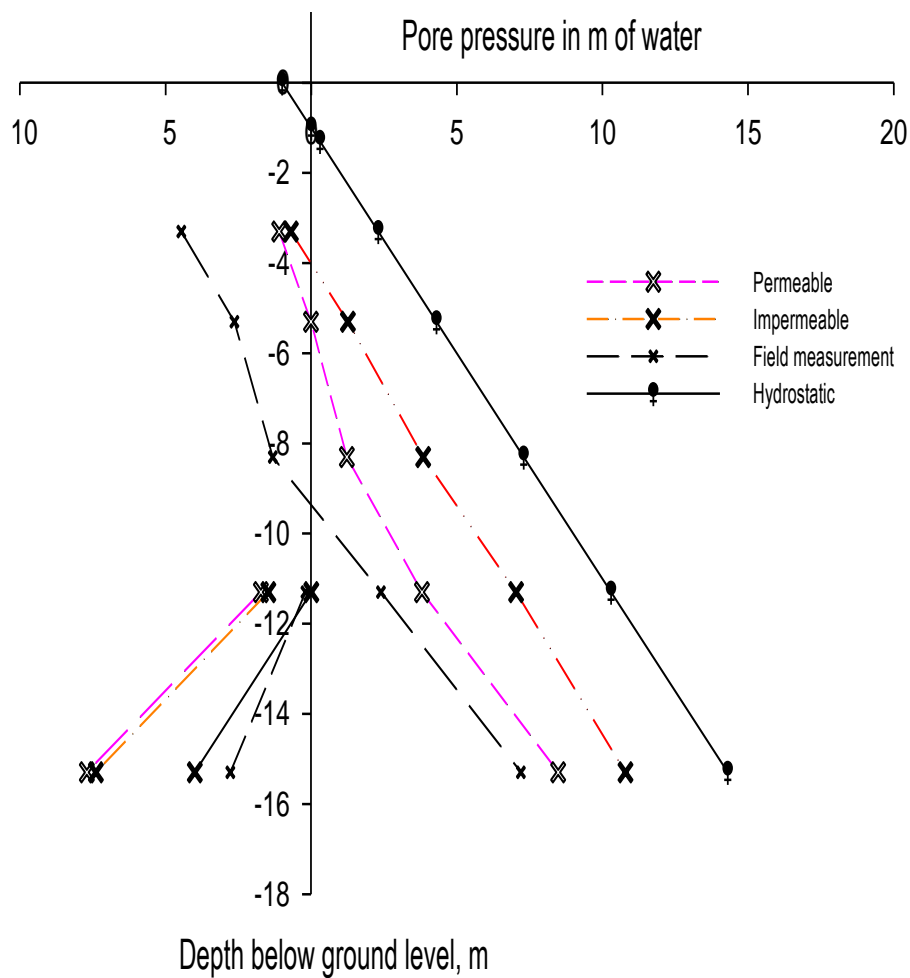
Figure 6.14: Comparison of pore pressure profiles calculated for the permeable and impermeable retaining walls and long-term field measurement.

The field and numerically calculated pore water pressures behind the retaining walls are less than hydrostatic as would be expected in the presence of groundwater seepage from the retained soil. Pore pressures for the impermeable wall are significantly higher than those of the permeable wall and higher than those from field measurement. There are remarkable similarities between the pore pressure profile for the permeable wall and that from the field measurements. Pore pressures for the permeable wall and those from field measurements seem to be converging at depths greater than 8.3 m. Pore pressure values diverge at lesser depths. The pore pressure trend in front of the retaining wall is less well defined. It is apparent, however that pore pressures from the field measurement are less than hydrostatic while those from the numerical analyses are both greater. Pore pressures calculated in front of the permeable retaining wall are greater than those in front of the impermeable wall.

It is evident from the above that there is significant reduction in pore pressures behind when groundwater flow is allowed through the retaining wall and that a permeable retaining wall more realistically characterise the retaining walls at CTRL, Ashford which are formed from contiguous piles.

6.5.5 Distribution of total head contours and flow paths

The distribution of total head contours illustrates that there are significant differences between the flow regimes surrounding the permeable and impermeable retaining walls as shown in Figure 6.15. Far field hydraulic heads, as expected, are identical for the permeable and impermeable walls. However the influence of through-wall seepage becomes more significant at a distance of approximately 30 m behind the wall. This seems to be the approximate distance of influence, in this instance, for through-wall seepage as indicated by the reduced impact on pore pressures observed 20 m behind the wall as discussed in Section 6.5.3. One of the drawbacks of these analyses is that there are not sufficient monitoring locations from the field measurements to give a more detailed estimation of the hydraulic conditions beyond about 3.4 m behind the retaining wall. Notwithstanding, if the flow of groundwater is taken as perpendicular to the contours representing equipotential drops, then it is evident that there is significantly

more horizontal flow towards the permeable wall than towards the impermeable wall. Detailed analyses of the total head contours for the permeable wall showed that flow was predominantly through the wall. However, for the impermeable wall, the equipotential lines are perpendicular to the wall. This indicates the dominance of vertical flow near the impermeable retaining wall.
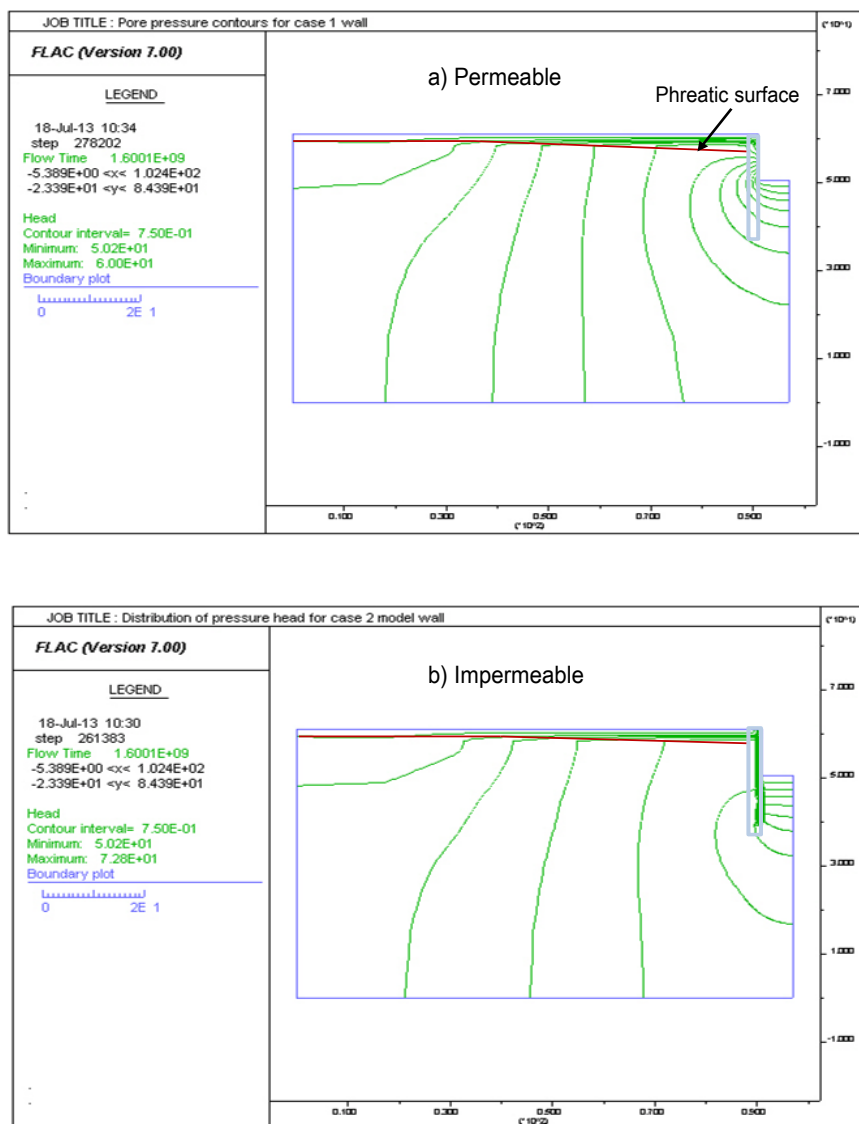
Figure 6.15: Distribution of pressure heads around a) a permeable and b) an impermeable retaining wall. Position of the phreatic surface indicated.

Comparison of flow paths

Fluid particles were also tracked from a distance of approximately 50 m behind the retaining walls as shown in Figure 6.16. There is greater amount of groundwater flow towards the permeable wall than towards the impermeable retaining wall. The classically accepted flow pattern around the retaining wall is evident for the impermeable wall. Similarly, there is significant vertical flow adjacent to the model wall. This is again in contrast to the predominantly horizontal flow behind the permeable wall, particularly above formation level. Since the geometry and mechanical properties of both retaining walls are similar then it is reasonable to assume therefore that the differences in flow patterns are due to the influence of the bulk permeability of the equivalent structure.
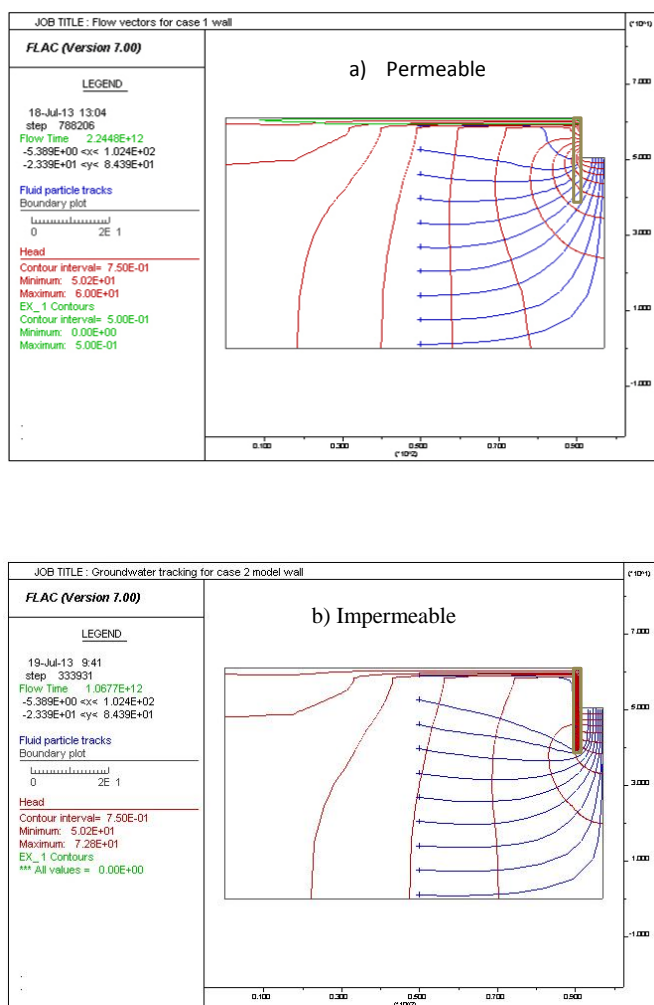
Figure 6.16: Comparison of fluid flow paths around a) a permeable and b) an impermeable retaining wall.

6.5.6 Comparison of soil and retaining wall displacement

It is acknowledged that the calculation of soil displacements using an elastic perfectly plastic constitutive soil model can sometimes lead to unrealistic simulation results and will not always give reliable displacement magnitudes (Bolton *et al*., 1994; Addenbrooke *et al*., 1997; Masin and Herle, 2005 and Hejazi *et al*., 2009). It was thought however, that the general displacement trends may be compared using a simple soil model for which the required parameters are readily available. Soil vertical displacements and lateral wall movements were therefore calculated for the permeable and impermeable retaining walls and, where applicable, comparisons made with field measurements. The results are discussed below.

Soil vertical displacement

Vertical displacement of the soil behind the permeable and impermeable wall, normalised with respect to excavation depth, were plotted against normalised distances behind the retaining walls to illustrate the development of the settlement troughs with distance away from the walls. The displacement profiles shown in Figure 6.17 are fairly similar with negligible soil movement observed adjacent to the model walls. This was particularly evident for the impermeable wall.
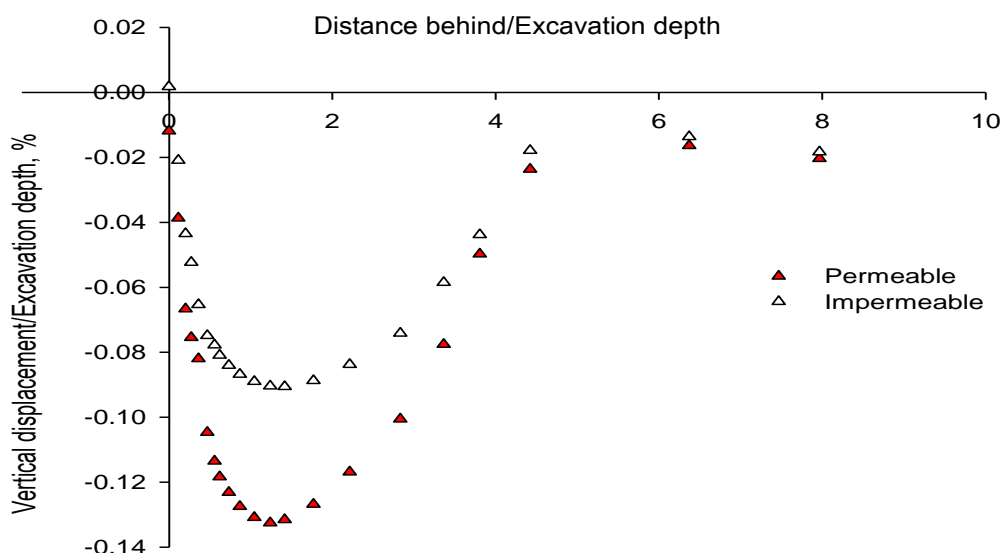
Figure 6.17: Comparison of vertical displacement behind a permeable and an impermeable retaining wall.

Soil settlement increased initially going away from the wall. This was more pronounced for the permeable wall. Maximum soil settlement was calculated within a distance of less than two excavation depths from the back of the walls. Soil settlement then decreased with distance away from the walls in both cases resulting in the typically observed settlement trough behind retaining walls. The results from the simulation of the impermeable wall compare well with the observed maximum displacement occurring at a distance of about 23 m from the secant pile retaining walls at Bell Common as reported by Higgins *et al*., (1989). The distance of 12 m at which maximum settlement was calculated behind the permeable retaining wall is also similar to the approximately 15 m reported by Zdravkovic *et al*. (2007) who conducted 2D numerical simulations of a retaining wall, with varying permeability, for a deep foundation in London Clay. The calculated vertical displacement profiles also conformed to the theoretical pattern of long-term global movements around an excavation as suggested by Burland *et al*. (1979). This long-term pattern posits the development of a settlement trough behind the wall with significant amount of heaving of the soil in front of the retaining wall.

Retaining wall lateral movement

The variation of horizontal displacements with depth (as percentage of excavation depth) for the permeable and impermeable retaining walls was calculated during the numerical simulations and the results presented in the plots of normalised displacement shown in Figure 6.18.
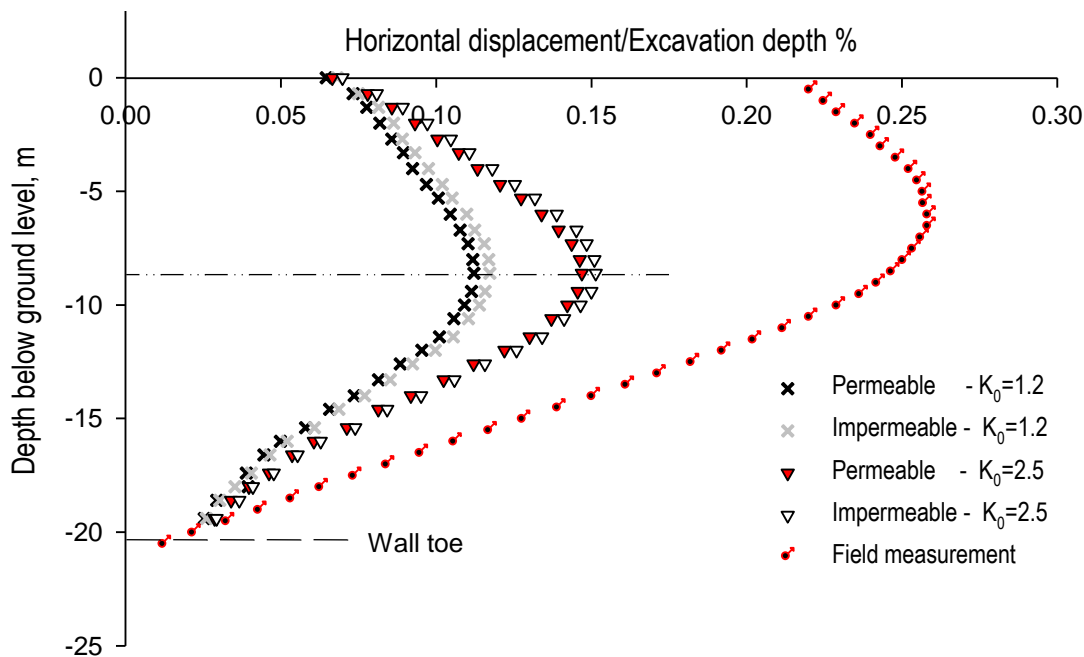
Figure 6.18: Comparison of horizontal displacement at various depths for a permeable and an impermeable retaining wall with K_0=1.2 and 2.5. Field measurements are included for comparison.

The results indicate similar trends for the permeable and impermeable walls with the location of the maximum wall movement located just above base slab level in both cases. The displacement profiles are very similar in shape for both the permeable and the impermeable retaining walls and are also of the general profile expected of a propped retaining wall with a berm as demonstrated by Burland *et al*. (1979). The similarities in the calculated lateral movement for the permeable and impermeable walls also extend to the location of the maximum displacements. The maximum displacements of approximately 0.1% and 0.12% of the excavation depth for the

permeable and impermeable walls respectively occurred at a depth 8 m below the top to the walls and just over 2 m above the reinforced concrete base slab. These results were obtained from simulations in which the at rest coefficient of lateral earth pressure, K_0 was 1.2. Increasing K_0 to 2.5, which represents the soil in its overconsolidated state, resulted in an approximately 30% increase in lateral displacement for both retaining walls which is similar to the trends observed by Osman and Bolton (2004). This also confirms the influence of K_0 as suggested by Franzius *et al*. (2005). The magnitude of the lateral wall movement for the impermeable retaining wall is consistently higher than that for the permeable wall even though all other mechanical and hydraulic conditions were the same.

The horizontal movement of the walls with high and low K_0 values, and the location of the maxima, were significantly less than those obtained from field measurements. The results from the contiguous pile retaining wall at CTRL, Ashford indicate that a maximum horizontal displacement of approximately 0.25% of excavation depth occurred at a depth of about 6 m below the top of the wall. These displacement measurements were taken about 2 years after the removal of the temporary props. Notwithstanding the locations and magnitude of the maximum displacements for the simulated and field conditions, the results so far show that there was general agreement in the displacement profiles for the numerical analysis and field studies.

It is noted that the large deflection measured at the top of the retaining wall at Ashford seemed unrealistic for a propped retaining wall in stiff clay. In fact, Clark (2006) suggested that this observed discrepancy in wall movement was possibly due to the swaying of the cutting. This may be attributed to differences in the ground levels between the north and south retaining walls forming the cut and cover tunnel. Access to the southern wall was restricted due to construction of another rail line hence it was impossible to verify this assumption through field measurements. It is also plausible that the deflection of the retaining wall could have been caused by the contraction of the reinforced concrete props due to thermal effects. There was however insufficient data to determine the true reasons for the excessive wall movement.

The combined soil vertical and retaining wall lateral displacements are shown in Figure 6.19. The displacements are magnified by ten times the calculated values to visualise more clearly the long-term conditions.
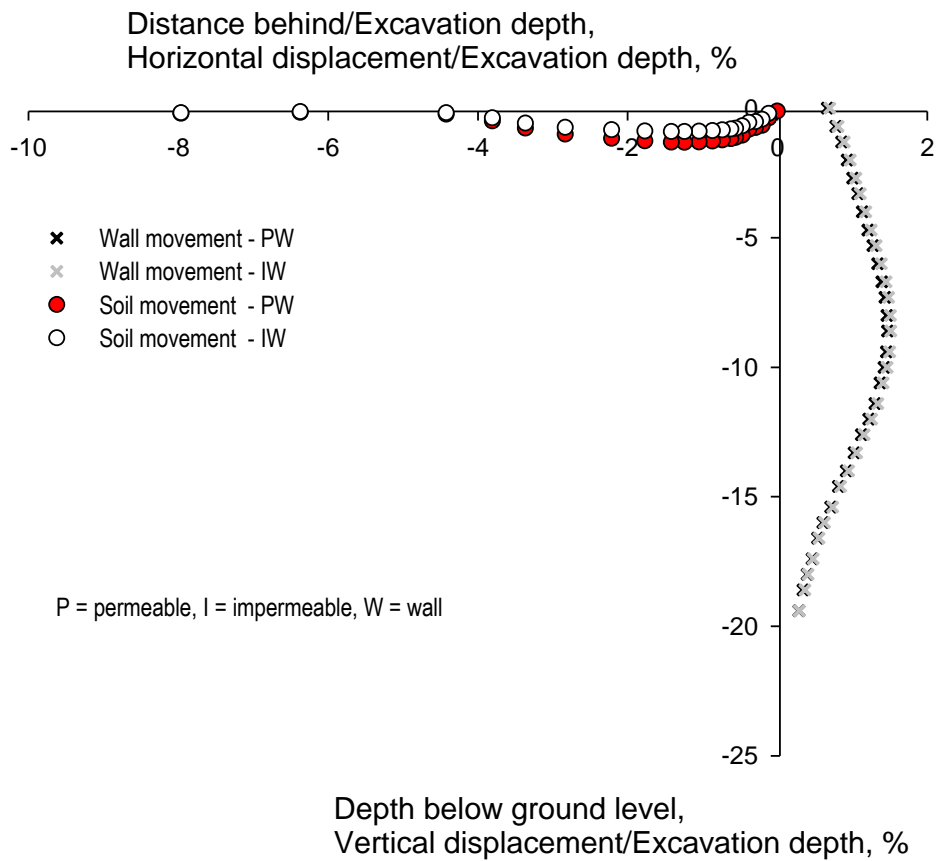
Figure 6.19: Comparison of soil vertical movement and retaining wall lateral displacement. Displacements shown are scaled by 10x.

6.6   Limitations of 2D analyses of retaining walls

It is acknowledged that groundwater flow problems are essentially three dimensional in nature. Therefore a purely two-dimensional analyses, although providing very useful information, is better augmented by 3D groundwater modelling. Equation 3.6 was derived from 2D simulations of the impact of pile gap sizes on groundwater flow. The phreatic surface effects adequately provided validation of the groundwater model. It is still thought however, that to complete the understanding of the groundwater flow problem, 3D simulations of flow around contiguous piles is necessary.

Similarly, the difficulties in deriving a reliable estimate for local surface infiltration meant that recharge was restricted to the far field boundary. Some might argue that infiltration from broken mains and localised high intensity rainfall is not adequately represented. This approach is however recommended by various geotechnical applications including Itasca (2012) as it is recognised that maintaining the far field groundwater level is usually sufficient to provide acceptable levels of accuracy. Thus the groundwater flow trends are acceptably represented.

Additionally, Potts *et al*., (2002) noted that immediately following excavation the pore fluid pressure in the soil adjacent to a retaining wall could be tensile. This condition would cause the improbable situation of water from the excavation going into the retained soil during the numerical simulations. Shin *et al*. (2010) made similar observations while analysing the hydraulic conditions around shallow tunnels. Both reports suggest approaches in which flow was restricted if the pore pressure fell below a pre-defined value. Preliminary investigations demonstrated similar tendencies for the plane strain analyses of the retaining walls. The air entry value was therefore selected as the cut-off switch to prevent water migrating from the excavation into the retaining wall. This is similar to the technique suggested by Shin *et al*. (2010).

Whilst the results of the 2D numerical analyses were generally of the trends observed from field measurements of a contiguous pile retaining wall, it is still believed that a larger three-dimensional model would therefore enhance the understanding of the hydraulic conditions around the contiguous piles especially in light of the observed limitations of the 2D simulations.

6.7 Summary

The hydraulic regime around the contiguous pile retaining wall at CTRL, Ashford was investigated by numerical simulation using the commercially available finite difference code FLAC^{2D}. The bored pile retaining walls were represented in 2D analyses by continuous retaining walls of uniform cross sections. The bulk soil/structure permeability of the wall was assigned using Equation 3.6 derived in Chapter 3. The analyses were conducted using a permeable and an impermeable retaining wall. Parametric studies of the retaining wall and base slab geometries were conducted to determine the influence on:

i)   the distribution of pore pressures,
ii)   soil vertical displacement and
iii) the lateral wall movements.

The results showed that allowing drainage through the reinforced concrete base slab did not affect the pore pressures behind the permeable and impermeable retaining walls. As expected, pore pressures in front of the impermeable model wall however reduced once drainage through the base slab was allowed. The effect of base slab permeability on pore pressures in front of the permeable wall was negligible.

The influence of wall permeability on soil settlement behind the retaining walls was more significant than the effect of base slab permeability. Nonetheless, soil settlement behind the impermeable wall was more sensitive to base slab permeability. The influence of base slab permeability on horizontal wall movement was insignificant for the propped retaining walls

The results for pore pressures calculated at various distances and depths behind the permeable retaining wall were consistent with field measurements from the contiguous pile retaining wall at CTRL, Ashford. These contrasted with the results for the impermeable wall in which pore pressures in particular were much higher than field measurements. It was also evident that up to the simulated period corresponding to days after construction, pore water pressures closer to the soil surface and to the face of the permeable model wall were still decreasing. Those at greater depths seemed to have attained long-term equilibrium conditions. These trends are similar to those from field measurements.

It was also noted that the long-term pore pressures from the numerical results at each monitoring point were, in some instances, approximately 20-30 kPa greater than the corresponding field measurement. This seemed to be due to the initial stresses and pore pressures. Initialisation of the pore water pressures and soil stresses were conducted using the built-in facility in the numerical code, which converted soil densities to initial stresses due to gravitational effect. The initial pore pressure distribution was calculated in similar manner using the supplied regional groundwater level, which was assumed to be 1.0 m below ground level as published. The initial pore pressures measured at the construction site did not seem to correspond and were 20-30 kPa lower at various locations. This suggests that the local groundwater level was lower than the approximately 1 m depth assumed by various studies.

Groundwater flow problems are essentially three dimensional in nature. The limitations of the two dimensional plane strain model were therefore acknowledged. Three-dimensional numerical analyses of the seepage problem are therefore necessary to complete the understanding of the groundwater flow through retaining walls made from contiguous piles.

Chapter 7

7.0   Conclusions and Recommendations

Investigations were carried out to determine the groundwater flow regime around permeable retaining structures. Particular emphasis was placed on the impact on the hydraulic conditions around retaining walls formed from contiguous piles. Previous investigations conducted using advanced numerical techniques have demonstrated the usefulness of allowing groundwater flow through the segmented linings of shallow tunnels. These reports showed that the pore water pressures, axial stresses and bending moments on the tunnel linings through which groundwater seepage was allowed were much less than those observed for fully water-proofed tunnel linings. There is however limited research into the effect of through-wall seepage on the hydraulic conditions around retaining walls. This paucity of data is in spite of the recognition that retaining walls formed from contiguous piles, based on their geometry, allow the flow of

249

groundwater through the pile gaps. Similarly, although there is some research into the effect of retaining wall permeability, there are no guidelines for the treatment of the resulting bulk permeability of the equivalent retaining wall representing contiguous piles in 2D simulations. Consequently, selection of the usually assigned permeability ratios, k_p/k_s, appears to be arbitrary.

Two-dimensional numerical plane strain analyses were conducted to investigate the impact of pile gaps on pore water pressures and on steady state flowrates during groundwater flow simulations. A relationship between the resulting bulk permeability, k_p, of the region impacted by the pile, the soil hydraulic conductivity, k_s, and the pile gap to diameter ratio, x/d, was derived (Equation 3.6). This relationship is very useful in calculating k_p, based on pile gaps, for continuous retaining walls representing contiguous piles in 2D plane strain simulations. The phreatic effects of the pile gaps on the hydraulic regime were investigated by applying values of k_p to an equivalent retaining wall in 2D groundwater flow simulations. Laboratory flow tank experiments were used to verify the results from the numerical investigation.

Field data, gathered over a period of 13 years from the site of the construction of the contiguous pile retaining walls at CTRL, Ashford shows a reduction in pore water pressures and lateral stresses to below those for comparable impermeable retaining walls. Back analysis of the field measurements, using 2D numerical simulations in which values of k_p were calculated using Equation 3.6, confirmed that the hydraulic regime was different from that expected of a conventional impermeable retaining wall.

Chapter specific detailed results were summarized at the end of Chapters 2-6; this chapter therefore presents the general conclusions arising from the research and the implication for practice. Recommendations are made towards further investigations into the hydraulic conditions around permeable retaining walls.

7.1 Conclusions

The charts presented were derived from controlled laboratory experiments and numerical simulations and are therefore only suitable for investigating general trends in groundwater flow regime.

- The field monitoring of the hydraulic conditions around contiguous piles in overconsolidated soils contributed significantly to the understanding of the long-term pore water pressures and horizontal total stresses behind retaining walls through which there is groundwater seepage.

- Replacing *in situ* soil with structures made from materials of lower permeability, significantly alter the bulk hydraulic conductivity of the affected region. Consequently, the presence of the reinforced concrete piles reduced the hydraulic conductivity of the ground near the piles. For retaining walls formed from contiguous piles, the resulting bulk permeability (k_p) of the equivalent structure (soil and piles) is directly proportional to the pile gap to diameter ratio, *x/d*, according to Equation 3.6. A plot of Equation 3.6 asymptotes to one as pile gap size increases.

- For propped retaining walls formed from contiguous piles, once through-wall seepage is established, changing the length of the piles do not alter significantly the pore water pressures and horizontal total stresses behind the retaining wall. Neither is the soil displacement affected.

- The long-term pore water pressures and horizontal total stresses behind contiguous pile retaining walls are much less than those behind secant pile retaining walls under similar conditions. The pore pressures behind traditional impermeable retaining walls tend to increase to near their pre-construction values in the long-term. However, the long-term pore water pressures behind contiguous pile retaining walls do not recovery to near, and are in fact much less than, their pre-construction values. The decrease in horizontal total stresses, in some instances, may be directly attributed to the reduction in pore water

251

pressures at similar locations. Other changes in horizontal total stresses are due to thermal expansion of the reinforced concrete props.

- Lateral movement of propped retaining walls towards an excavation, while not large, reduced with through-wall seepage. This is consistent with the reduced horizontal loads on permeable retaining walls.

- High negative pore pressures tend to develop more rapidly and to a larger extent when through-wall seepage is allowed. This is more prevalent closer to the soil surface and nearer to the exposed face of the wall. Hydraulic heads increased away from contiguous pile retaining walls indicating flow towards and through the structure. The magnitude and long-term reliability of the high negative pore pressures behind contiguous piles are not well understood and are therefore not relied on in the design of retaining walls.

- Pore pressures calculated at the toe of a contiguous pile retaining wall with x/d=0.3, which is comparable to that at CTRL, Ashford are only about 77% of those estimated using the linear seepage approximation method for an impermeable wall.

- There are some accompanying drawbacks to allowing groundwater seepage through earth retaining structures. For example, vertical displacement of the soil behind the retaining walls increases when through-wall seepage is allowed. This increase in settlement in fine soils is due to one-dimensional consolidation of the soil behind the wall induced by groundwater seepage through the pile gaps. The amount of settlement is proportional to the bulk permeability of the equivalent structure.

Notwithstanding the observed drawbacks, it is thought however, that the economic benefits of allowing through-wall seepage far outweigh the disadvantages.

7.2 Implications for practice

The implications of the results for application to geotechnical engineering designs are outlined below:

- Equation 3.6 can be used to calculate the bulk permeability of a continuous wall of uniform cross-section representing contiguous piles in 2D numerical simulations. This ensures consistency in applying permeability values to 2D simulations of retaining walls formed from piles.

- The trend of pore pressure reduction due to base slab permeability is very useful for design purposes as the analyses demonstrated that the presence of the drains through the base slab not only caused reduced water pressures under the slab but also causes a slight decrease in hydraulic loads on the back of the retaining wall.

- The hydraulic conditions at any point behind contiguous piles are not affected by the pile length. This is because once a wall is defined as permeable ($k_p/k_s>=0.001$) the pore pressure changes with pile length are negligible.

- The pore pressures at the toe of a contiguous pile retaining wall, at different pile gaps, can be estimated as a percentage of those calculated from the linear seepage approximation method using the dimensionless chart in Figure 4.11.

- The groundwater level behind contiguous piles, for different pile gaps, can be estimated using Figure 4.25.

- Soil settlement behind contiguous piles at different pile gaps can be estimated using the dimensionless settlement charts presented in Figures 4.29 and 4.30.

7.3 Recommendations for future work

The results of the numerical simulations, laboratory experiments and field monitoring and analyses of the hydraulic conditions around contiguous pile retaining walls provided in this report have presented areas for which further research is possible. Some recommendations concerning future research are listed below.

- Acknowledging that groundwater flow is essentially a three dimensional phenomenon, further investigation of the hydraulic conditions around retaining walls made from contiguous piles using 3D numerical modelling is necessary to fully exploit the reduction in hydraulic loadings caused by through-wall seepage.

- Further studies of the influence of through-wall seepage on the structural behaviour of the retaining wall including the development of bending and axial stresses in the contiguous piles and the impact on prop loads is also recommended.

- The results of laboratory permeability measurements can be influenced by the amount of air entrapment and the texture of the soil particles. There is a requirement to investigate fully the impact of existing laboratory de-airing methods and soil texture on the estimated permeability of fine soils. This would contribute to improved confidence in the accuracy of groundwater flow modelling.

- More case studies of the monitoring of the hydraulic conditions around retaining walls are also necessary. These are necessary particularly in built-up areas where attempts are made to mitigate the impact of the construction of underground structures on the groundwater flow regime.

- Further investigations into the long-term reliability of negative pore pressures developed as a result of flow through contiguous piles are necessary to develop reliable design guidelines for pore pressure reduction methods due to through-wall seepage.

- Further investigation of the contribution that unsaturated flow makes to the length of the seepage face is necessary.

This research has demonstrated that the hydraulic regime around retaining walls formed from contiguous piles is different from that around traditional impermeable retaining walls such as those formed from secant piles. Pore water pressures and horizontal total stresses were shown to decrease when groundwater is allowed to seep through the pile gaps. The results of the investigations can be used to determine the trends in groundwater flow parameters around contiguous piles at various pile gaps during field investigation and geotechnical designs.

List of References

Addenbrooke, T.I., Potts, D.M., & Puzrin, A.M., 1997. The influence of pre-failure soil stiffness on the numerical analysis of tunnel construction. *Geotechnique*, 47, (3) 693-712.

Ahmed, A.A. & Bazaraa, A.S., 2009. Three-Dimensional Analysis of Seepage below and around Hydraulic Structures, *ASCE.*

Arjnoi, P., Jeong, J.H., Kim, C.Y., & Park, K.H., 2009. Effect of drainage conditions on porewater pressure distributions and lining stresses in drained tunnels. *Tunnelling and Underground Space Technology*, 24, (4) 376-389.

Asche, H. R,. 1999. The choice of mesh size for accuracy in elastoplastic tunnel FLAC analyses, *In International FLAC Symposium on Numerical Modelling in Geomechanics*, C. &. H. R. Detournay, ed., Rotterdam: A.A. Balkema/Brookfield.

Atkinson, J.H. & Mair, R.J., 1983. Loads on Leaking and Watertight Tunnel Linings, Sewers and Buried Pipes Due to Groundwater. *Geotechnique*, 33, (3) 341-344.

Barros, P.L.A. 2006. A Coulomb-type solution for active earth thrust with seepage. *Geotechnique*, 56, (3) 159-164.

Benmebarek, N., Benmebarek, S., Kastner, R., & Soubra, A.H., 2006. Passive and active earth pressures in the presence of groundwater flow. *Geotechnique*, 56, (7) 521-522.

Benmebarek, S., Khelifa, T., Benmebarek, N., & Kastner, R., 2008. Numerical evaluation of 3D passive earth pressure coefficients for retaining wall subjected to translation. *Computers and Geotechnics*, 35, (1) 47-60.

Bobet, A., 2003. Effect of pore water pressure on tunnel support during static and seismic loading. *Tunnelling and Underground Space Technology*, 18, (4) 377-393.

Bobet, A. & Nam, S.W., 2007. Stresses around Pressure Tunnels with Semi-permeable Liners. *Rock Mechanics and Rock Engineering*, 40, (3) 287-315.

Bolton, M. D., Dasari, G. R., & Britto, A. M., 1994. Putting small strain non-linearity into Modified Cam Clay model, *In 8th International conference on computer methods and advances in geomechanics.*, Siriwadane & Zaman, eds., Balkema, Rotterdam: pp. 537-542.

British Standards Institution, 2004. Eurocode 7: Geotechnical Design Part 1, General Rules. EN1997-1. 2004.

British Standards Institution, 1990. BS 1377: Part 4. British Standard Methods of Tests for Soils of Civil Engineering: Classification Tests.

Bryson, L.S. & Salehian, A., 2011. Performance of constitutive models in predicting behavior of remolded clay. *Acta Geotechnica*, 6, (143) 154.

Burland, J.B. & Karla, J.C., 1986. Queen Elizabeth II Conference Centre: geotechnical aspects. *Proceedings of the Institution of Civil Engineers, Part 1*, 80, 1479-1503.

Burland, J. B., Simpson, B., & St John, H. D., 1979. Movements around excavation in London Clay. Proceedings of the 7th European Conference on Soil Mechanics and Foundations Engineering, Brighton, Vol. 1, 13-29.

Carder, D.D. & Symons, I.F., 1989. Long-term performance of an embedded cantilever retaining wall in stiff clay. *Geotechnique*, 39, (1) 55-76.

Carder, D.R., Watson, G.V.R., Chandler, R.J., & Powrie, W., 1999. Long-term performance of an embedded retaining wall with a stabilizing base slab. *Proceedings of the Institution of Civil Engineers-Geotechnical Engineering*, 137, (2) 63-74.

Cedergren, H.R., 1989. *Seepage, Drainage and Flow nets*, 3rd ed. New York, John Wiley & Sons.

Chapman, T.G., 1957. Two-dimensional groundwater flow through a bank with vertical faces. *Geotechnique*, 7, (1) 35-40.

Chu-Agor, M.l., Fox, G.A., Cancienne, R., & Wilson, G.V. 2008. Seepage caused tension failures and erosion undersutting of hillslopes. *Journal of Hydrology*, 359, (3) 247-259.

Clark, J., 2006. *Performance of a propped retaining wall at the Channel Tunnel Rail Link, Ashford.* PhD University of Southampton.

Clausen, B., Heimli, P., & Jensen, A. K., 1987, Groundwater effects from an excavation in soft, marine clay, *In Groundwater effects in geotechnical engineering*, E. T. Hanrahan, T. L. L. Orr, & T. F. Widdis, eds., Dublin: pp. 665-668.

Conti, R. & Sanctis, L., 2012. Numerical modelling of installation effects of diaphragm walls in sand. *Acta Geotechnica*, 7, 219-237.

Darcy, H., 1856. *Les Fontaines Publiques de la Ville de Dijon*.

Day, R.A. & Potts, D.M., 1993. Modeling Sheet Pile Retaining Walls. *Computers and Geotechnics*, 15, (3) 125-143.

De Moor, E.K., 1994. An analysis of bored pile/diaphragm wall installation effects. *Geotechnique*, 44, (2) 341-347.

Dolezalova, M., 2002. Approaches to numerical modelling of ground movements due to shallow tunnelling. *Soil Interaction in Urban Civil Engineering*, Zurich: Vol 2, pp. 365-373.

Dolezalova, M., Havlena, V., Karhanek, J., Hamza, P., & Stavicek, J., 1991. Numerical analysis of staged excavation of a sewer tunnel. *Proceeding, Underground Structures* 16-25.

Ellis, E.A., Durrant, I.K., & Reddish, D.J., 2010. Numerical modelling of discrete pile rows for slope stability and generic guidance for design. *Geotechnique*, 60, (3) 185-195.

Fahimifar, A. & Zareifard, M.R., 2009. A theoretical solution for analysis of tunnels below groundwater considering the hydraulic-mechanical coupling. *Tunnelling and Underground Space Technology*, 24, (6) 634-646.

Fernandez, G. & Alvarez, T.A., 1994. Seepage-Induced Effective Stresses and Water Pressures Around Pressure Tunnels. *Journal of Geotechnical Engineering*.

Forth, R.A., 2004. Groundwater and geotechnical aspects of deep excavations in Hong Kong. *Engineering Geology*, 72, (3-4) 253-260.

Fourie, A.B. & Potts, D.M., 1989. Comparison of finite element and limiting equilibrium analyses for an embedded cantilever retaining wall. *Geotechnique*, 39, (2) 175-188.

Fox, G.A., Heeren, D.M., Wilson, G.V., Langendoen, E.J., Fox, A.K., & Chu-Agor, M.l., 2010. Numerically predicting seepage gradient forces and erosion: Sensitivity to soil hydraulic properties. *Journal of Hydrology*.

Franzius, J.N., Potts, D.M., & Burland, J.B., 2005. The influence of soil anisotropy and K0 on ground surface movements resulting from tunnel excavation. *Geotechnique*, 55, (3) 189-199.

Gaba, A. R., Simpson, B., Powrie, W., & Beadman, D. R., 2003, *Embedded retaining walls: guidance for more economic design*, Construction Industry Research and Information Association, CIRIA, London, C580.

Geo-Slope International Ltd, 2007. Seepage Modelling with SEEP/W. An Engineering methodology, 4th edition.

Ghaboussi, J., Ranken, R. E., & Karshenas, M., 1978, Analysis of subsidence over soft-ground tunnels, *In International Conference on Evaluation and Prediction of Subsidence*, ASCE, pp. 182-196.

Gourvenec, S., Powrie, W., & De Moor, E.K., 2002. Three-dimensional effects in the construction of a long retaining wall. *Proceedings of the Institution of Civil Engineers-Geotechnical Engineering*, 155, (3) 163-173.

Gourvenec, S.M., Mair, R.J., Bolton, M.D., & Soga, K., 2005. Ground conditions around an old tunnel in London Clay. *Proceedings of the Institution of Civil Engineers-Geotechnical Engineering*, 158, (1) 25-33.

Gourvenec, S.M. & Powrie, W., 1999. Three-dimensional finite-element analysis of diaphragm wall installation. *Geotechnique*, 49, (6) 801-823.

Griffiths, D.V. & Fenton, G.A., 1995. Observations on two- and three-dimensional seepage through a spatially random soil. *JOURNAL OF GEOTECHNICAL AND GEOENVIRONMENTAL ENGINEERING*, 123, (2) 153-160.

Guedes, R. J. & Pereira, C., 2002. The role of soil K0 value in numerical analysis of shallow tunnels, *In International Symposium on Geotechnical Aspects of Underground Construction in Soft Ground*, 379 edn, IS-Tokyo: p. 384.

Guilloux, A., 1994. A French National Report on Tunneling in Soft Ground, *In International Symposium on Underground Construction in Soft Ground*, New Delhi.

Gunn, M.J. & Clayton, C.R.I., 1992. Installation effects and their importance in the design of earth-retaining structures. *Geotechnique*, 42, (1) 137-141.

Gunn, M.J., Satkunananthan, A., & Clayton, C.R.I., 1992. Finite element modelling of installation effects. *Proc ICE Retain Struct* 46-55.

Guoping, D., Jiao, J., & Dongxiao, Z., 2008. Modelling study on the impact of deep building foundations on the groundwater system. *Hydrological Processes* 1857-1865.

Harr, M.E., 1962. *Groundwater and seepage.* New York, McGraw-Hill.

Harris, C. S., Hart, M. B., Varley, P. M., & Warren, C. D., 1996. Engineering Geology of the Channel Tunnel. Thomas Telford Publishing.

Hazen, A., 1892, *Physical properties of sands and gravels with reference to their use in filtration. Report to the Massachusetts State Board of Health.*

Head, K. H., 1992. Manual of Soil Laboratory testing.

Hejazi, Y., Dias, D., & Kastner, R., 2009. Impact of constitutive models on the numerical analysis of underground constructions. *Acta Geotechnica*, 3, (4).

Hicher, P.Y. & Shao, J.F., 2008. *Constitutive modeling of soils and rocks.* ISTE Ltd and Wiley.

Higgins, K. G., Potts, D. M., & Symons, I. F., 1989, *Comparison of Predicted and Measured Performance of the Retaining Walls of the Bell Common Tunnel.*, TRRL, 124.

Hofle, R., Fillibeck, J., & Vogt, N., 2009. Time dependent deformations during tunnelling and stability of tunnel faces in fine-grained soils under groundwater. *Acta Geotechnica*, 3, (4) 309-316.

Holmes, G., Roscoe, H. and Chodorowski, A., 2005. Construction monitioring of cut and cover tunnels. Proceedings of the ICE, Geotechnical Engineering,158 (4).

Hubbard, H.W., Potts, D.M., & Miller, D., 1984. Design of the retaining walls for the M25 cut and cover tunnel at Bell Common. *Geotechnique*, 34, (4) 495-512.

ITASCA., 2012. Fast Langrangian Analysis of Continua in 2 Dimensions. User Manual. Itasca Consulting Group[7.0]. Minneapolis, USA.

Jardine, R.J., Potts, D.M., Fourie, A.B., & Burland, J.B., 1986. Studies of the influence of non-linear stress-strain charactieristics in soil-structure interaction. *Geotechnique*, 36, (3) 377-396.

Jiao J.J., Wang X.S., & Nandy, S., 2006. Preliminary assessment of the impacts of deep foundations and land reclamation on groundwater flow in a coastal area in Hong Kong, China. *Hydrogeology*, 14, 100-114.

Kolymbas, D. & Wagner, P., 2007. Groundwater ingress to tunnels - The exact analytical solution. *Tunnelling and Underground Space Technology*, 22, (1) 23-27.

Kulhawy, F.H., 1974. Finite element modelling criteria for underground openings in rock. *International Journal of Rock Mechanics and Mineral Sciences*, 11, 465-472.

Kutmen, G., 1986. *The influence of the construction process on bored piles and diaphragm walls: a numerical study.* MPhil University of Surrey.

Lacasse, S. & Berre, T., 1988, "Triaxial testing methods for soils," *In Advanced Triaxial Testing of Soil and Rock*, ASTM STP 977, pp. 264-289.

Lee, G. T. K. & Ng, C. W. W., 2007. Three-dimensional analysis of ground settlements due to tunnelling: Role of K_0 and stiffness anisotropy., Lyon: pp. 617-622.

Lee, G.T.K. & Rowe, R.K., 1989. Deformations caused by surfaace loading and tunnelling. *Geotechnique*, 39, (1) 125-140.

Lee, I. M. & Nam, S. W., 2006, Seepage Force Considerations in Tunnelling, *In International Symposium on Underground Excavation and Tunnelling*.

Lee, I.M., Nam, S.W., & Ahn, J.H., 2003. Effect of seepage forces on tunnel face stability. *Canadian Geotechnical Journal*, 40, (2) 342-350.

Lee, I.M. & Nam, S.W., 2001. The study of seepage forces acting on the tunnel lining and tunnel face in shallow tunnels. *Tunnelling and Underground Space Technology*, 16, (1) 31-40.

Lee, K.M. & Rowe, R.K., 1991. An analysis of three-dimensional ground movements: the Thunder Bay tunnel. *Canadian Geotechnical Journal*, 28, 25-41.

Lee, Y. J., Kim, S. B., & Yoo, C., 2009, Characteristics of tunneling induced ground settlement in groundwater drawdown environment, *In 6th International Symposium on Geotechnical Aspects of Underground Construction in Soft Ground*.

Lei, S., 1999. An analytical solution for steady flow into a tunnel. *Ground Water*, 37, 23-26.

Liu, G., Houlsby, G.T., & Augarde, C.E., 2000. 2-Dimensional analysis of settlement damage to masonry buildings caused by tunnelling. *The Structural Engineer*, 79, (1) 19-25.

Lobkovsky, A.E., Jensen, B., Kudrolli, A., & Rothman, D.H., 2004. Threshold phenomena in erosion driven by subsurface flow. *Journal of Geophysical Research-Earth*, 109, (F4, F04010).

Lopez-Fernandez, C., Prieto, D.A., ernandez-Viejo, G., Pando, L., & Fernandez, E.C., 2013. Surface Subsidence Induced by Groundwater Drainage Tunneling in Granite Residual Soils (Burata Railway Tunnel, Spain). *Journal of Geotechnical & Geoenvironmental Engineering*, 139, (5) 841-4.

Mair, R.J., 1993. Unwin Memorial Lecture 1992 Developments in Geotechnical Engineering Research - Application to Tunnels and Deep Excavations. *Proceedings of the Institution of Civil Engineers-Civil Engineering*, 97, (1) 27-41.

Mair, R.J., Taylor, R.N. and Bracegirdle, A., 1993. Subsurface settlement profiles above tunnels in clays. Geotechnique, Vol. 43, No. 2, pp 315-320.

Masin, D. & Herle, I., 2005. Numerical analyses of a tunnel in London clay using different constituitive models, pp. 595-600.

Mayer, P.M. & Gudehus, G., 2002. Prediction of soil movements due to diaphragm wall construction. *Geotechnique Special Publication*, 1, (16) 696-712.

Miura, S. & Tuki, S., 1982. A sample preparation method and its effect on static and cyclic deformation-strength properties of sand. *Soils and Foundations*, 22, (1).

Muskat, T.G., 1935. The seepage of water through dams with vertical faces. *Physics*, 6, (402).

Nam, S.W. & Bobet, A. 2006. Liner stresses in deep tunnels below the water table. *Tunnelling and Underground Space Technology*, 21, (6) 626-635.

Ng, C. W. W., 1994. Effects of modelling wall installation on multi-staged excavations in stiff clays., pp. 595-600.

Ng, C.W.W., Lings, M.L., Simpson, B. and Nash, D.F.T., 1995. An approximate analysis of the three-dimensional effects of diaphragm wall installation. *Geotechnique*, 45 (3) 497-507.

O'Reilly, M.P and New, B.M., 1982. Settlement above tunnels in the United Kingdom Their magnitude and prediction. Tunneling 82, London, IMM, pp. 173-181.

Orr, T. L. L., 1987. Effect of uncertainty in the groundwater level on safety in geotechnical design, *In Groundwater Effects in Geotechnical Engineering*, E. T. Hanrahan, T. L. L. Orr, & T. F. Widdis, eds., Rotterdam: pp. 841-844.

Osman , A.S. and Bolton, M.D., 2004. A new design method for retaining walls in clay. Canadian Journal of Geotechnical Engineering, 41 (3) 451-466.

Ou, C.Y., Liao, J.T., & Lin, H.D., 1998. Performance of diaphragm wall constructed using top-down method. *Journal of Geotechnical and Geoenvironmental Engineering*, 124, (9) 798-808.

Padfield, C.J., and Mair, R.J., 1984. Design of retaining walls embedded in stiff clay. Construction Industry Research and Information Association, CIRIA Report R104.

Palmer, J.H.L. and Belshaw, D.J., 1980. Deformations and pore pressures in the vicinity of a precast, segmented, concrete-lined tunnel in clay. Canadian Geotechnical Journal, 17 (2), 174-184.

Panet, M., 1979, Time-Dependent Deformations in Underground Works, *In 4th ISRM Congress (Montreux)*, A. A. Balkema and the Swiss Society for Soil and Rock Mechanics, pp. 279-289.

Park, K.H., Lee, J.G., & Owatsiriwong, A., 2008. Seepage force in a drained circular tunnel: An analytical approach. *Canadian Geotechnical Journal*, 45, (3) 432-436.

Park, K.H., Owatsiriwong, A., & Lee, J.G., 2007. Analytical solution for steady-state groundwater inflow into a drained circular tunnel in a semi-infinite aquifer: a revisit. *Tunnelling and Underground Space Technology*, 23, (2) 206-209.

Peck, R.B., 1969. Deep excavation and tunneling in soft ground. Proc. of the 7th International Conference on SMFE (Mexicao), pp 225-290.

Polubarinova-Kochina, P.Y.A., 1962. *Theory of ground water movement,* Princeton, New Jersey, Princeton University Press.

Potts, D. M., Axelsson, K., Grande, L., Schweiger, H., & Long, M., 2002. Guidelines for the use of advanced numerical analysis. Thomas Telford Publishing.

Potts, D.M. & Zdravkovic, L., 1999. *Finite element analysis in geotechnical engineering: theory* London, Thomas Telford.

Powers, J.P., 1985. Dewatering-Avoiding its Unwanted Side Effects. *American Society of Civil Engineers.*

Powrie, W., 1994. Ground movements due to construction dewatering. *Groundwater Problems in Urban Areas* 237-250.

Powrie, W., 2013. Private communications.

Powrie, W., 2004. *Soil Mechanics Concepts and Applications*, Second ed. Spon Press, Taylor & Francis Group, London and New York.

Powrie, W., 2008. Contributions to *Geotechnique* 1948-2008: Groundwater. *Geotechnique*, 58, (5) 435-439.

Powrie, W., Chandler, R.J., Carder, D.R., & Watson, G.V.R., 1999. Back-analysis of an embedded retaining wall with a stabilizing base slab. *Proceedings of the Institution of Civil Engineers-Geotechnical Engineering*, 137, (2) 75-86.

Powrie, W. & Kantartzi, C., 1996. Ground response during diaphragm wall installation in clay: Centrifuge model tests. *Geotechnique*, 46, (4) 725-739.

Powrie, W. & Li, E.S.F., 1991. Finite-Element Analysis of An Insitu Wall Propped at Formation Level. *Geotechnique*, 41, (4) 499-514.

Powrie, W. & Preene, M., 1994. Time-Drawdown Behavior of Construction Dewatering Systems in Fine Soils. *Geotechnique*, 44, (1) 83-100.

Preene, M., Roberts T.O.L, Powrie, W., & Dyer, M. R., 2000, *Groundwater control - design and practice*, Construction Industry Research and Information Association.

Rampello, S., Stallebrass, S. E., & Viggiani, G. M. B., 1998. Ground movements associated with excavations in stiff clays: current prediction capability., 1527 edn, Naples: p. 1540.

Richards, D.J., Clark, J., & Powrie, W. 2006. Installation effects of a bored pile wall in overconsolidated clay. *Geotechnique*, 56, (6) 411-425.

Richards, D.J., Clark, J., Powrie, W., & Heymann, G. 2007a. Performance of push-in pressure cells in overconsolidated day. *Proceedings of the Institution of Civil Engineers-Geotechnical Engineering*, 160, (1) 31-41.

Richards, D.J., Powrie, W., & Page, J.R.T., 1998. Investigation of retaining wall installation and performance using centrifuge modelling techniques. *Proc.ICE, Geotech.Eng.,* 131, (3) 163-170.

Richards, D.J., Powrie, W., Roscoe, H., & Clark, J., 2007b. Pore water pressure and horizontal stress changes measured during construction of a contiguous bored pile multi-propped retaining wall in Lower Cretaceous clays. *Geotechnique*, 57, (2) 197-205.

Ridley, A., Brady, K. C., & Vaughan, P. R., 2003, *Field Measurement of Pore Water Pressures*, TRL, TRL555.

Rizkallah, V. & Cunze, G., 1987. Effects of pile driving on excess pore pressure, *In Groundwater effects in Geotechnical Engineering*, E. T. Hanrahan, T. L. L. Orr, & T. F. Widdis, eds., pp. 627-631.

Roberts, T.O.L., Roscoe, H., Powrie, W., & Butcher, D.J.E., 2007. Controlling clay pore pressures for cut-and-cover tunnelling. *Proceedings of the Institution of Civil Engineers-Geotechnical Engineering*, 160, (4) 227-236.

Roscoe, H., 2003. Retaining wall movements, CTRL Contract 430 - Ashford Tunnels, T. A. Newson, ed.

Roscoe, H. & Twine, D., 2001. Design collaboration speeds Ashford tunnels. *World Tunnelling*, 14, (5) 237-241.

Roscoe, H. & Twine, D., 2010. Design and performance of retaining walls. *Proceedings of the Institution of Civil Engineers-Geotechnical Engineering*, 163, (5) 279-290.

Rowe, R.K., Lo, K.Y., & Kack, G.J., 1983. A method of estimating surface settlement above tunnels constructed in soft ground. *Canadian Geotechnical Journal*, 20.

Rulon, J.J. & Freeze, R.A., 1985. Multiple seepage faces on layered slopes and their implications for slope-stability analysis. *Canadian Geotechnical Journal*, 22, 347-356.

Rushton, K.R. 2006. Significance of a seepage face on flows to wells in unconfined aquifers. *Quarterly Journal of Engineering Geology and Hydrogeology*, 39, 323-331.

Sakthivadivel, R. & Rushton, K.R., 1989. Numerical analysis of large diameter wells with a seepage face. *Journal of Hydrology*, 107, 43-55.

Sakurai, S., 1978. Approximate time dependent analysis of tunnel support structure considering progress of tunnel face. *International Journal for Numerical and Analytical Methods in Geomechanics*, 2, 159-175.

Schafer, R. & Triantafyllidis, T., 2004. Modelling of earth and water pressure development during diaphragm wall construction in soft clay. *International Journal for Numerical and Analytical Methods in Geomechanics*, 28, (13) 1305-1326.

Schanz, T., Vermeer, P. A., & Bonnier, P. G., 1999. Formulation and verification of the Hardening-Soil Model, Balkema, Rotterdam: pp. 281-290.

Schleiss, A., 1986. Design of previous pressure tunnels. *International Water Power and Dam Construction*, 38, 21-26.

Schofield, A.N., 1980. Cambridge geotechnical centrifuge operations. 20th Rankine Lecture. *Geotechnique*, 30, (3) 227-268.

Schweiger, H., Pottler, T.K., & Steiner, H., 1991. Effect of seepage forces on the shotcrete lining of a large undersea cavern. *Computer Methods and Advances in Geomechanics,* 1503-1508.

Shamsai A. & Narasimhan T.N., 1991. A numerical investigation of free surface-seepage face relationship under steady state flow conditions. *Water Resource*, 27, (3) 409-421.

Shand, P., Cobbing, J., Tyler-Whittle, R., Tooth, A. F., & Lancaster, A., 2003, *The Lower Greensand of Southern England*, British Geological Survey, Environment Agency, 9.

Shin, H.S., Youn, D.J., Chae, S.E., & Shin, J.H., 2009. Effective control of pore water pressures on tunnel linings using pin-hole drain method. *Tunnelling and Underground Space Technology*, 24, (5) 555-561.

Shin, J.H., 2008. Numerical modeling of coupled structural and hydraulic interactions in tunnel linings. *Structural Engineering and Mechanics*, 29, (1) 1-16.

Shin, J.H., 2010. Analytical and combined numerical methods evaluating pore water pressure on tunnels. *Geotechnique*, 60, (2) 141-145.

Shin, J.H., Addenbrooke, T.I., & Potts, D.M., 2002. A numerical study of the effect of groundwater movement on long-term tunnel behaviour. *Geotechnique*, 52, (6) 391-403.

Shin, Y.J., Kim, B.M., Shin, J.H., & Lee, I.M., 2010. The ground reaction curve of underwater tunnels considering seepage forces. *Tunnelling and Underground Space Technology*, 25, (4) 315-324.

Simpson, B. 1992. Retaining structures: displacement and design, 32nd Rankine Lecture. *Geotechnique*, 42, (4) 541-576.

Sinclair, T. J. E. & Norfolk, P. D., 2001. Settlements over close-proximity tunnels in saturated sands: Prediction and Performance, *In Geotechnical Engineering Meeting on Society' Needs*, K. K. S. Ho & K. S. Li, eds., London: Taylor & Francis Group, pp. 431-436.

Symons, I.F. & Carder, D.R., 1993. *Stress changes in stiff clay caused by the installation of embedded retaining walls.* London, Thomas Telford.

Tedd, P., Chard, B.M., Charles, J.A., & Symons, I.F., 1984. Behaviour of a propped embedded retaining wall in stiff clay at Bell Common. *Geotechnique*, 34, (4).

Terzaghi, K., and Peck, R. B., 1964. Soil mechanics in engineering practice, Wiley, New York.

Trudeep, N., Dasaka, S., & Hemant, D., 2011. Universal calibration device for pressure transducer calibration, *In Geo-Frontiers: Advances in Geotechnical Engineering*.

Vaughan, P.R. & Walbancke, H.J., 1973. Pore pressure changes and the delayed failure of cutting slopes in overconsolidated clay. *Geotechnique*, 23, (4) 531-539.

Vermeer, P. A., Bonnier, P. G., & Moller, S. C., 2002. On a smart use of 3D-FEM in tunnelling., *In 8th International Symposium on Numerical Models in Geomechanics*, pp. 361-366.

Vrecl-Kojc, H. & Skrabl, S., 2009. Limit analysis of cantilever retaining walls with spaced piles. *Proceedings of the Institution of Civil Engineers-Geotechnical Engineering*, 162, (6) 311-322.

Wang, Y.Z., 2000. Distribution of earth pressures on retaining walls. *Geotechnique*, 50, (1) 83-88.

Ward, W. H. & Pender, M. J., 1981. Tunnelling in soft ground: general report, *In 10th International Conference on Soil Mechanics and Foundation Engineering*, pp. 261-275.

Ward, W. H. & Thomas (1965). The development of earth loading and deformation in tunnel linings in London Clay. *Proceedings of the 6th Conference in Soil Mechanics and Foundation Engineering,* Toronto.

Watson, G.V.R. & Carder, D.R., 1994. Comparison of the measured and computed performance of a propped bored pile retaining wall at Walthamstow. *Proc.ICE, Geotech.Eng.,* 107, 127-133.

Wolfgang, M., 1987. *Flow Visualization*, Second ed. London, Academic Press, INC.

Wong, I.H., 2001. Methods of resisting hydrostatic uplift in substructures. *Tunnelling and Underground Space Technology*, 16, (2) 77-86.

Wongsaroj, J., Soga, K., & Mair, R.J., 2007. Modelling of long-term ground response to tunnelling under St James's Park, London. *Geotechnique*, 57, (1) 75-90.

Yoo, C., Kim, S. B., & Kim, J. T., 2008, Influencing factors on groundwater drawdown induced settlement during tunnelling, *In World Tunnelling Congress*, New Delhi, India: Central Board of Irrigation & Power, pp. 863-871.

Yoo, C.S., 2005. Interaction between tunneling and groundwater - Numerical investigation using three dimensional stress-pore pressure coupled analysis. *Journal of Geotechnical and Geoenvironmental Engineering*, 131, (2) 240-250.

Zdravkovic, L., Potts, D.M., & St John, H.D., 2005. Modelling of a 3D excavation in finite element analysis. *Geotechnique*, 55, (7) 497-513.

Zdravkovic, L., Tsiarnpousi, A., & Potts, D.M., 2007. Effect of wall and soil permeability on the long-term ground movements adjacent to a deep excavation. *Numerical Models in Geomechanics: Numog X* 589-594.

266